JASI

JOURNAL OF THE ANATOMICAL SOCIETY OF INDIA

An International Journal

An Official Publication of Anatomical Society of India

Full text online at **https://journals.lww.com/joai**
Submit articles online at **https://review.jow.medknow.com/jasi**

Editor-in-Chief
Dr. Vishram Singh

Journal of the Anatomical Society of India

GENERAL INFORMATION

About the Journal

Journal of the Anatomical Society of India (ISSN: Print 0003-2778) is peer-reviewed journal. The journal is owned and run by Anatomical Society of India. The journal publishes research articles related to all aspects of Anatomy and allied medical/surgical sciences. Pre-Publication Peer Review and Post-Publication Peer Review Online Manuscript Submission System Selection of articles on the basis of MRS system Eminent academicians across the globe as the Editorial board members Electronic Table of Contents alerts Available in both online and print form. The journal is published quarterly in the months of January, April, July and October.

Scope of the Journal

The aim of the *Journal of the Anatomical Society of India* is to enhance and upgrade the research work in the field of anatomy and allied clinical subjects. It provides an integrative forum for anatomists across the globe to exchange their knowledge and views. It also helps to promote communication among fellow academicians and researchers worldwide. The Journal is devoted to publish recent original research work and recent advances in the field of Anatomical Sciences and allied clinical subjects. It provides an opportunity to academicians to disseminate their knowledge that is directly relevant to all domains of health sciences.

The Editorial Board comprises of academicians across the globe.

JASI is indexed in Scopus, available in Science Direct.

Abstracting and Indexing Information

The journal is registered with the following abstracting partners:

Baidu Scholar, CNKI (China National Knowledge Infrastructure), EBSCO Publishing's Electronic Databases, Ex Libris – Primo Central, Google Scholar, Hinari, Infotrieve, Netherlands ISSN center, ProQuest, TdNet, Wanfang Data

The journal is indexed with, or included in, the following:

SCOPUS, Science Citation Index Expanded, IndMed, MedInd, Scimago Journal Ranking, Emerging Sources Citation Index.

Impact Factor® as reported in the 2022 Journal Citation Reports® (Clarivate Analytics, 2023): 0.4

Information for Authors

Article processing and publication charges will be communicated by the editorial office. All manuscripts must be submitted online at https://review.jow.medknow.com/jasi.

Subscription Information

A subscription to JASI comprises 4 issues. Prices include postage. Annual Subscription Rate for non-members-		
Rates of Membership (with effect from 1.1.2022)		
	India	**International**
Ordinary membership	INR 1500	US $ 100
Couple membership	INR 2250	
Life membership	INR 8000	US $ 900
Subscription Rates (till 31ˢᵗ August)		
Individual	INR 6000	US $ 650
Library/Institutional	INR 12000	US $ 1000
Trade discount of 10% for agencies only		
Subscription Rates (after 31ˢᵗ August)		
Individual	INR 6500	US $ 700
Library/Institutional	INR 12500	US $ 1050

The Journal of Anatomical Society of India (ISSN: 0003-2778) is published quarterly **Subscriptions** are accepted on a prepaid basis only and are entered on a calendar year basis. Issues are sent by standard mail Priority rates are available upon request.

Information to Members/Subscribers

All members and existing subscribers of the Anatomical Society of India are requested to send their membership/existing subscription fee for the current year to the Treasurer of the Society on the following address: Prof (Dr.) Punit Manik, Treasurer, ASI, Department of Anatomy, KGMU, Lucknow - 226003. Email: punitamanik@yahoo.co.in. All payments should be made through an account payee bank draft drawn in favor of the **Treasurer, Anatomical Society of India,** payable at **Lucknow** only, preferably for **Allahabad Bank, Medical College Branch, Lucknow.** Outstation cheques/drafts must include INR 70 extra as bank collection charges.

All complaints regarding non-receipt of journal issues should be addressed to the Editor-in-Chief, JASI at editorjasi@gmail.com. The new subscribers may, please contact wkhlrpmedknow_subscriptions@wolterskluwer.com.

Requests of any general information like travel concession forms, venue of next annual conference, etc. should be addressed to the General Secretary of the Anatomical Society of India.

For mode of payment and other details, please visit www.medknow.com/subscribe.asp Claims for missing issues will be serviced at no charge if received within 60 days of the cover date for domestic subscribers, and 3 months for subscribers outside India. Duplicate copies cannot be sent to replace issues not delivered because of failure to notify publisher of change of address. The journal is published and distributed by Wolters Kluwer India Pvt. Ltd. Copies are sent to subscribers directly from the publisher's address. It is illegal to acquire copies from any other source. If a copy is received for personal use as a member of the association/society, one cannot resale or give-away the copy for commercial or library use.

The copies of the journal to the subscribers are sent by ordinary post. The editorial board, association or publisher will not be responsible for non receipt of copies. If any subscriber wishes to receive the copies by registered post or courier, kindly contact the publisher's office. If a copy returns due to incomplete, incorrect or changed address of a subscriber on two consecutive occasions, the names of such subscribers will be deleted from the mailing list of the journal. Providing complete, correct and up-to-date address is the responsibility of the subscriber.

Nonmembers: Please send change of address information to subscriptions@medknow.com.

Advertising Policies

The journal accepts display and classified advertising. Frequency discounts and special positions are available. Inquiries about advertising should be sent to Wolters Kluwer India Pvt. Ltd, advertise@medknow. com.

The journal reserves the right to reject any advertisement considered unsuitable according to the set policies of the journal.

The appearance of advertising or product information in the various sections in the journal does not constitute an endorsement or approval by the journal and/or its publisher of the quality or value of the said product or of claims made for it by its manufacturer.

Copyright

Permissions

For information on how to request permissions to reproduce articles/information from this journal, please visit https://journals.lww.com/joai.

Disclaimer

The information and opinions presented in the Journal reflect the views of the authors and not of the Journal or its Editorial Board or the Publisher. Publication does not constitute endorsement by the journal. Neither the JASI nor its publishers nor anyone else involved in creating, producing or delivering the JASI or the materials contained therein, assumes any liability or responsibility for the accuracy, completeness, or usefulness of any information provided in the JASI, nor shall they be liable for any direct, indirect, incidental, special, consequential or punitive damages arising out of the use of the JASI. The JASI, nor its publishers, nor any other party involved in the preparation of material contained in the JASI represents or warrants that the information contained herein is in every respect accurate or complete, and they are not responsible for any errors or omissions or for the results obtained from the use of such material. Readers are encouraged to confirm the information contained herein with other sources.

Addresses

Journal of the Anatomical Society of India

EDITORIAL BOARD

▌▌ CONTENTS ▌▌

continued...

Alzheimer's Disease: A Neuroanatomical Basis

Alzheimer's disease (AD) is a progressive brain disorder. It is the most common cause of dementia in the elderly involving parts of the brain that control thoughts, memory, and language, limiting a person's ability to carry out simple daily tasks.

Recently, the incidence of AD has increased worldwide. The prevalence of its onset is about 5%–7% in people aged 70 years and over 20% in people aged over 80 years. At present, there are about 50 million people suffering from AD, around the world, and this number is projected to double every 5 years and will increase to reach about 150 million by 2050.[1]

The brain consists of a network of about 100 billion neurons. They communicate with each other through synapses. The brain performs a wide variety of sensory and motor functions. In addition, it also plays a key role in cognitive functions such as memory, decision-making, motivation, problem-solving, and conceptual thinking.

In AD, there is a gradual decline in memory, thinking, behavior, and social skills. These changes affect a person's ability to function properly. The signs and symptoms can be categorized into three types:
- Cognitive such as forgetfulness of recent events, difficulty in thinking and creating new memories, confusion, wandering, and falling not to return home after an evening walk
- Mood variations such as anger, apathy, loneliness, and general disconnect
- Psychological such as depression, hallucinations, jumbled speech, paranoia, and delusion.[2]

The exact cause of AD is not known. However, it is believed that in most people, AD is caused by a combination of age-related changes, along with genetic, environmental, and lifestyle factors.
- **The age -related changes,** are associated with neuronal degeneration and loss of synapses. Here, it is important to know that the brain is made up of a network of neurons which communicate with each other by neurotransmitters through synapses. It is believed that the memory is stored in synapses.[3]

In AD, there is a loss of excitatory cholinergic pathways in the basal forebrain and excitatory glutaminergic pathways in the hippocampus.

Two theories have been given regarding age-related changes in the brain:

Formation of Intracellular Neurofibrillary Tangles

These are formed by small proteins called tau proteins, which are associated with microtubules. These tubules not only maintain the shape of nerve cell bodies and dendrites but also play an important role in the transport of nutrition across the neuron.

The small tau proteins are separated from microtubules and form helical thread-like tangles, which affect the transport of nutrition by microtubules and the production of energy from mitochondria.

Formation of Amyloid Plaques

Formation of extracellular amyloid plaques of beta-amyloid protein, which destroys neurites and synapses. The beta-amyloid protein is normally present in the interstitial fluid of the brain and usually cleared up during sleep. However, these plaques are also found, albeit at a lower frequency in normal elderly people.

As a result of the formation of tangles and plaques, there is degeneration of neurons, neurites, and synapses at the cortical and subcortical levels of the brain.

This leads to atrophy of the brain. The weight of the brain is reduced by 40%. The sulci are widened, and the ventricles are abnormally enlarged.
- **The genetic factors** may play some role. In most cases of AD, there is no single genetic cause. The research has found several genetic variants which are associated with AD, which may either increase or decrease the risk of AD
- **The environmental factors** included air pollution, Vitamin D deficiency, exposure to some pesticides, food born poisons, and viruses[3]
- **The lifestyle factors** include smoking, obesity, diabetes, high blood pressure, lack of physical activity, use of alcohol, and improper/incomplete sleep.

As of now, there is no curable treatment for AD. However, some medicines are given which may change the progression of the disease. These are acetylcholinesterase and N-methyl-D-aspartate inhibitors.

Both these medicines increase the amount of acetylcholine and glutamate neurotransmitters in the brain. Thus, these drugs compensate for the death of cholinergic and glutaminergic neurons in AD. In this way, they help alleviate the signs and symptoms of the disease.

AD is a classic example where "prevention is better than cure."

This is possible by bringing some lifestyle changes in life as under:
- Daily morning walks and light physical exercises in fresh air
- Involving in reading, writing, and solving mathematical problems (intellectual activities)

- Playing musical instruments and listening to soothing songs
- Living active social life and volunteering in local community work (active socialization)
- Avoiding any kind of stress in life as far as possible and doing yogic activities.

By adopting the above-mentioned lifestyle changes, one will not only escape from the occurrence of AD and related diseases such as parkinsonism and depression but will also increase their life span.

Vishram Singh, Rashi Singh[1], Gaurav Singh[2]

Department of Anatomy, Kasturba Medical College, Mangalore, Manipal Academy of Higher Education, Manipal, Karnataka, [1]Department of Pediatric and Preventive Dentistry, Santosh Dental College and Hospital, Ghaziabad, [2]British Medical Journal, Noida, NCR, Delhi, India

Address for correspondence: *Prof. Vishram Singh, B5/3 Hahnemann Enclave, Plot No. 40, Sector 6, Dwarka Phase – 2, New Delhi - 110 075, India. E-mail: drvishramsingh@gmail.com*

References

1. Michael-Titus AT, Shortland P. The Nervous System, E-Book: Systems of the Body Series. Elsevier Health Sciences; 2022.
2. Available from: https://www.mayoclinic.org/diseases-conditions/alzheimers-disease/symptoms-causes/syc-20350447. [Last accessed on 2023 May 29].
3. Breijyeh Z, Karaman R. Comprehensive review on Alzheimer's disease: Causes and treatment. Molecules 2020;25:5789.

Access this article online	
Quick Response Code:	**Website:** https://journals.lww.com/joai
	DOI: 10.4103/jasi.jasi_57_23

How to cite this article: Singh V, Singh R, Singh G. Alzheimer's disease: A neuroanatomical basis. J Anat Soc India 2023;72:91-2.

Immuno Histological Evidence of Ormocarpum Sennoides DC Extract in the Expression of Bax and Bcl2 in Wister Rats with Glucocorticoid induced Osteoporosis

Abstract

Introduction: Glucocorticoid therapy is the most common cause for secondary osteoporosis leading to a resurgence of interest in traditional medicine that could have bone sparing effects by naturally occurring bioactive molecules. Therefore, this study was done to evaluate the effect of Ormocarpum sennoides DC through immunohistological evidence in the expression of Bax and Bcl_2 in glucocorticoid-induced Osteoporosis in Wister albino rats. **Materials and Methods:** Rats were divided into five groups (Control, MPA (Osteoporosis), Alendronate (2 mg/kg), 100 mg (EOS), and 200 mg (EOS). The treatment was conducted for 45 days the Bax and Bcl_2 expressions were evaluated in osteoclast of distal femur diaphysis. **Results:** When compared the MPA to control group ($P < 0.05$) Bax increased and Bcl_2 reduced, when compared with MPA ($P < 0.05$) Alendronate, EOS 100 mg and EOS 200 mg increased the Bcl_2 expressions, Alendronate, EOS 100 mg, and EOS 200 mg reduced the Bax expression. **Discussion and Conclusion:** EOS 100 mg and EOS 200 mg increased Bcl_2 expression and reduced the Bax expression Ormocarpum sennoides prevents glucocorticoid-induced Apoptosis of preosteoblast; therefore, Bcl_2 may be an important regulator of bone growth thus reporting antiapoptotic property of Ormocarpum sennoides DC.

Keywords: *Bax, Bcl2, glucocorticoid-induced osteoporosis, Ormocarpum sennoides DC*

Bhuvaneswari C. Srinivasan, Radhika Krishnan[1]

Department of Anatomy, Faculty of Medicine, Panimalar Medical College Hospital and Research Institute, [1]Department of Anatomy, Faculty of Medicine, SRM Medical College Hospital and Research Centre, Chennai, Tamil Nadu, India

Introduction

Glucocorticoids have been used as a treatment of chronic diseases because of their anti-inflammatory, immunomodulatory and anti-proliferative properties.

The deleterious effects of prolonged exposure to an excess of cortisol on the skeleton were first recognized and described by Cushing in 1932[1] glucocorticoid therapy is the most common cause of secondary osteoporosis and the leading iatrogenic cause of the disease[2] it affects the region that has abundant cancellous bones such as the lumbar spine and proximal femur the reduced bone formation rather than increased bone resorption is thought to be the predominant effect of glucocorticoid on the bone which directly affects bone cells by stimulating osteoclast genesis decreasing osteoblast function and life span, increasing osteoblast apoptosis and impairing preosteoclast formation.[3-5]

Apoptosis is regulated by an intrinsic process involving activation of genes that can promote cell death[6] likewise the Bcl2 gene family encodes a large number of proteins including Bax and Bcl2 which proapoptotic and antiapoptotic members of the Bcl2 gene family respectively.[7] Thus, one of the best-characterized mechanisms to induce cell death is the release of the proapoptotic protein such as Bax which causes permeabilizations of the mitochondrial membrane, freeing pro-apoptogenic factors such as cytochrome C, which promote activation of the caspases that mediate cellular death.[8,9] However, the expression of Bcl2 protein can prevent cell death induced by a variety of stimuli including stress, chemotherapeutic agents, and glucocorticoids.[10-12]

In the traditional treatment of osteoporosis, one of the most used medications is bisphosphonates, adverse clinical events associated are osteonecrosis of the jaw, atrial fibrillation gastrointestinal intolerance.[13,14]

Currently, the alternative system of medicine sought to design strategies to prevent and

Access this article online

Website: https://journals.lww.com/joai

DOI: 10.4103/jasi.jasi_19_22

Quick Response Code:

How to cite this article: Srinivasan BC, Krishnan R. Immuno histological evidence of Ormocarpum sennoides DC extract in the expression of Bax and Bcl2 in Wister rats with glucocorticoid induced osteoporosis. J Anat Soc India 2023;72:93-7.
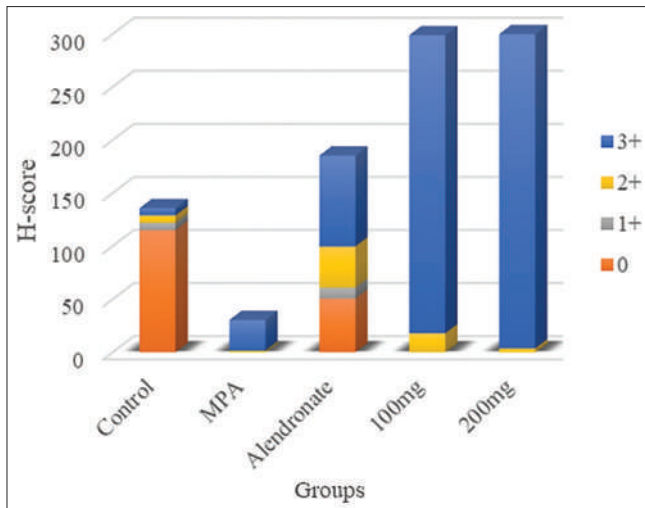
Graph 1: Expression of Bcl2 in control and various treatment groups. Values expressed as mean ± SEM. Different alphabet between groups denotes significant ($P < 0.05$) at 5% level using Turkey HSD test, $P < 0.001$. SEM: Standard error of the mean, HSD: Honestly significant difference

Graph 2: Expression of Bax in control and various treatment groups. Values expressed as mean ± SEM. Different alphabet between groups denotes significant ($P < 0.05$) at 5% level using Turkey HSD test, $P < 0.001$. SEM: Standard error of the mean, HSD: Honestly significant difference

cure this devastating ailment. Ayurveda an ancient system of Indian medicine cited several plants which are useful in treating bone disorders including bone fractures and metabolic disorders with no adverse effects.[15] This resurgence of interest in traditional medicine could also arise from the bone-sparing effects of phytoestrogen and another naturally occurring bioactive molecule.[16]

Ormocarpum sennoides DC is traditionally used for healing bone fracture (external application) by Irula Tribes in southern regions of India. Commonly known as Elumbotti (Bone knit). It is a leguminous shrub with membranous leaflets, yellow flowers, and moniliform pods, the leaves are used in curing bone-related problems, bone fracture setting, and nerve pain.[17]

Ormocarpum sennoides has the highest antioxidant activity (0.1155 μL to 1.3076 μL) DPPH radical assay ranges from 245.53 μL to 1015 μL showing the free radical scavenging activity potential of Ormocarpum sennoides,[18] these findings of EOS could be a possible alternative in the treatment of osteoporosis.

This study aimed to evaluate the effect of EOS on the BAX and Bcl$_2$ expressions by bone cells in distal femur diaphysis thus providing the antiapoptotic property of Ormocarpum sennoides DC.

Materials and Methods

The methodology of this work was approved by the Institutional animal ethical clearance committee (Letter No. 32/IAEC/10-19, 10.10) SRM University which follows the principles in ethics for animal experimentations.

Plant materials

The leaves of Ormocarpum sennoides DC were collected from the Irula Tribal Women's Welfare Society (1113/2011)

and authenticated by the Botanical Survey of India (BSI/SRC/5/2013-14ech/550).

The powder was soaked in n-hexane for defatting and then successively extracted in 80% ethanol. The filtrate was evaporated using a Rota evaporator, a dark green viscous mass of the extract was collected and stored at 0°C–4°C and acquired 20% to yield.

Animals

In the present study 30 female growing rats were used to create the rodent model of osteoporosis, animals weighing (150–200 g) were obtained from the lab animal maintenance unit, King institute, Guindy, Tamilnadu, India. The animals were housed in sanitized polypropylene cages in a room with controlled environmental conditions (12 h light/12 h dark cycle temperature 22°C) and were fed with commercially available pelleted food (Proximi Animal Nutrition India Pvt Ltd.,) and ac libitum water.

Osteoporosis induction

The osteoporosis induction was done through the subcutaneous administration of methylprednisolone acetate 10 mg/kg body weight alternate days for 42 days in all groups except in the control group.[19]

Bioassay

In this experiment after the end of osteoporosis induction 30 animals were selected and divided evenly into five groups ($n = 6$), the control group was not submitted to osteoporosis induction and any treatment. MPA group (osteoporosis) methylprednisolone acetate only. EOS 100 mg group (extract of Ormocarpum sennoides 100 mg/kg) EOS 200 mg group (extract of Ormocarpum sennoides 200 mg/kg) Alendronate group (Sodium alendronate 2 mg/kg).[20]

The Alendronate, EOS 100 mg, and EOS 200 mg were treated intragastrically once a day for 45 days after induction of osteoporosis. The choice of EOS doses was based on an Acute toxicity study the rats were anesthetized with ether, and sacrificed, the right femur was removed and fixed in 4% formaldehyde solution, and were decalcified in formic acid for 10 days and then processed for paraffin embedding.[21]

Immunohistochemistry

Five microns tissue sections were taken and treated in xylene for dewaxing followed by 100% alcohol twice for dehydration. The slides were washed in a tap of water and treated with 0.3% hydrogen peroxide for 30 min to quench the endogenous peroxides activity in the tissue.

Antigen retrieval was done using 10 mm citrate buffer (pH 6.0) and washed with Phosphate-buffered saline (PBS) for 5 min. The slides were kept in a moist chamber to prevent drying, 100 μL of 2% BSA added, followed by the primary antibody (75 μL Bax, Bcl$_2$) in appropriate dilutions and kept overnight, slides washed thrice with PBS. Secondary antibody (75 μL) and incubated for 45 min and washed in PBS thrice for 5 min each followed by addition of Horseradish Peroxidase (HRP) conjugate (Avidin Biotin complex - 75 μL) and incubated for 45 min; the slides washed in PBS thrice, 2 drops of 3, 3' Diaminobenzidine (DAB) solution added and excess was washed and counterstained in hematoxylin for 2 min slides treated with 2 changes of alcohol followed by xylene treatment and mounted using DPX.[22]

Semi-quantitative analysis of BAX and Bcl$_2$ expressions immunostaining results for Bcl$_2$ and Bax were scored semi-quantitatively on basis of the visually estimated percentage of positively stained cell nuclei the semi-quantitative intensity scale ranging from O for no staining to 3f form the most intense staining is used. At × 100, the number of cells in each field was counted with different staining intensities. Ten random fields in six sections per group were counted; H score (Histo score) using the following formula was generated H score = (% at 0) × 0 + (% at 1+) × 1 + (%at2+) × 2 + (%at 3+) × 3.

Statistical analysis

The data were expressed as mean ± standard error, and were analyzed for statistical significance using one-way analysis of variance, values are expressed as mean ± standard error of the mean for every six rats. Different alphabet between groups denotes significance at ($P < 0.05$) 5% level using Tukey HSD test, here all the $P < 0.001$.

Results

In the present study, the Bcl$_2$ expression reduced significantly in the methylprednisolone treated group [Figure 1b] compared to the control group [Figures 1a and 2a] and rising Bax expression may promote the apoptosis in bone cells in methylprednisolone treated group [Figure 2b] whereas Bcl$_2$ expression increased significantly in Ormocarpum sennoides DC treated group thus, the Ormocarpum sennoides DC prevents glucocorticoid-induced apoptosis of preosteoblast, therefore, Bcl$_2$ may be an important regulator of bone growth this reporting the antiapoptotic of Ormocarpum sennoides DC. Alendronate had a reduction in the expression of Bax [Figure 2a and c] and a significant increase in the expression of Bcl$_2$ [Figure 1c] by osteoblast cells probably reducing the apoptosis of these cells. The Osteoclast activity improves their apoptosis due to the direct antiresorptive act of the Alendronate drug.
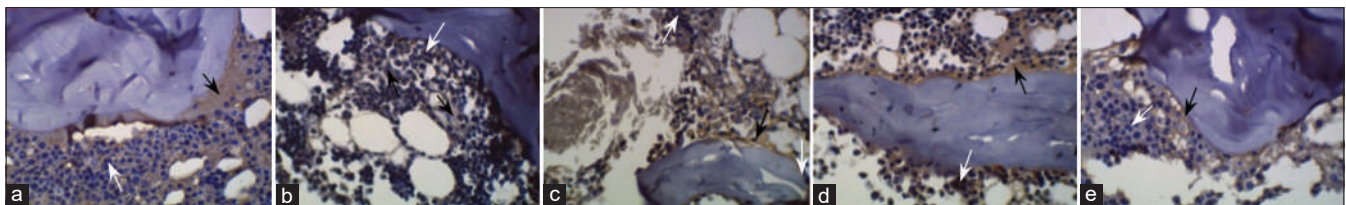
Figure 1: Photomicrograph of Bcl2 expression by osteoblasts in the trabecular bone tissue of the proximal epiphysis of the femur (×400); (a) Control group, (b) MPA group; (c) Alendronate group; (d) 100 mg group; (e) 200 mg group. The white arrow shows the positive osteoblast and the black arrow shows the negative osteoblast
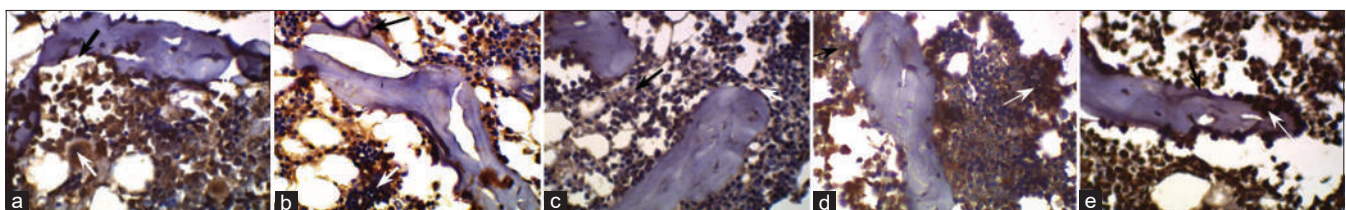
Figure 2: Photomicrograph of Bax expression by osteoblasts in the trabecular bone of epiphysis of the femur in control and various treatment groups (a-e) (×400); (a) control group, (b) MPA group; (c) alendronate group; (d) 100 mg group; (e) 200 mg group. The white arrow shows the positive osteoblast and the black arrow shows the negative osteoblast

Discussion and Conclusion

Glucocorticoid therapy induces osteoporosis through th decrease in calcium intestinal absorption, the increase in renal calcium excretion and the stimulated osteoclast activity as well as suppression of bone formation.

The Bcl_2 gene family encodes a large number of protein that participate in programmed cell death including the proapoptotic protein Bax and the antiapoptotic protein Bcl_2.[7]

In the present study Bax expression was significantly higher and the expression of Bcl_2 decreased significantly in the femur Bone in the osteoporosis group[26] showed similar results without findings. A fall in Bcl_2 expression and a rise in Bax expression showed that the osteoblast are responsive to the glucocorticoid treatment.[24] These finding suggest that osteoblasts have a critical role in the mechanism of bone loss induces by glucocorticoids;[23] thus, the increase in osteoblasts apoptosis together with reduction in their replication differentiation and bone formation can result in low bone mass.[5]

The result in the present study is that the alendronate had as significant reduction in the expression of Bax and significant increase in the expression of Bcl_2 by the osteoblast cells of the Tibia probably reducing the apoptosis of these cells.

Alendronate is an antiresorptive drug that acts directly in the osteoclast activity improving their apoptosis.[26,27]

Furthermore, alternative treatment with EOS was effective in decreasing the expression of the proapoptoic protein Bax [Figure 2d and e] and in increasing the expression of antiapoptotic protein Bcl_2 [Figure 1d and e] giving credence to the hypothesis that EOS and alendronate increase the survival of osteoblast and also may contribute to the therapy of glucocorticoid-induced osteoporosis (GIO).[25]

As a result, the treatment with EOS increased the bone mineral content in the proximal femur epiphysis preserving not only the osteoblast cells from death but also their function in the same way that anabolic therapies improve bone formation by increasing the umber of mature osteoblasts or by preventing their apoptosis.[28]

To our knowledge, the present study is the first on to evaluate the effect of the Ormocarpum sennoides DC in the expression of Bax and Bcl_2 proteins by osteoblast of the proximal femur epiphysis after the GIO. EOS was effective in decreasing the expression of the antiapoptotic Bcl_2. This study could form the basis for further clinical trials with EOS in the GIO [Graphs 1 and 2].

Financial support and sponsorship

Nil.

Conflicts of interest

There are no conflicts of interest.

References

1. Cushing H. The basophil adenomas of the pituitary body and their clinical manifestations (pituitary basophilism). 1932. Obes Res 1994;2:486-508.
2. Weinstein RS. Clinical practice. Glucocorticoid-induced bone disease. N Engl J Med 2011;365:62-70.
3. Deal C. Potential new drug targets for osteoporosis. Nat Clin Pract Rheumatol 2009;5:20-7.
4. Hock JM, Krishnan V, Onyia JE, Bidwell JP, Milas J, Stanislaus D. Osteoblast apoptosis and bone turnover. J Bone Miner Res 2001;16:975-84.
5. Chang JK, Li CJ, Liao HJ, Wang CK, Wang GJ, Ho ML. Anti-inflammatory drugs suppress proliferation and induce apoptosis through altering expressions of cell cycle regulators and pro-apoptotic factors in cultured human osteoblasts. Toxicology 2009;258:148-56.
6. Bras M, Queenan B, Susin SA. Programmed cell death via mitochondria: Different modes of dying. Biochemistry (Mosc) 2005;70:231-9.
7. Verborgt O, Tatton NA, Majeska RJ, Schaffler MB. Spatial distribution of Bax and Bcl-2 in osteocytes after bone fatigue: Complementary roles in bone remodeling regulation? J Bone Miner Res 2002;17:907-14.
8. Tsujimoto Y. Role of Bcl-2 family proteins in apoptosis: Apoptosomes or mitochondria? Genes Cells 1998;3:697-707.
9. Willis SN, Fletcher JI, Kaufmann T, van Delft MF, Chen L, Czabotar PE, et al. Apoptosis initiated when BH3 ligands engage multiple Bcl-2 homologs, not Bax or Bak. Science 2007;315:856-9.
10. Memon SA, Moreno MB, Petrak D, Zacharchuk CM. Bcl-2 blocks glucocorticoid- but not Fas- or activation-induced apoptosis in a T cell hybridoma. J Immunol 1995;155:4644-52.
11. Adams JM, Cory S. The Bcl-2 protein family: Arbiters of cell survival. Science 1998;281:1322-6.
12. Gohel A, McCarthy MB, Gronowicz G. Estrogen prevents glucocorticoid-induced apoptosis in osteoblasts in vivo and in vitro. Endocrinology 1999;140:5339-47.
13. Khan A. Bisphosphonate-associated osteonecrosis of the jaw. Can Fam Physician 2008;54:1019-21.
14. Chang JT, Green L, Beitz J. Renal failure with the use of zoledronic acid. N Engl J Med 2003;349:1676-9.
15. Mitra SK, Venkataranganna MV, Udupa UV, Gopumadhavan S, Seshadri SJ, Rafiq M, et al. The beneficial effect of OST-6 (OsteoCare), a herbomineral formulation, in experimental osteoporosis. Phytomedicine 2001;8:195-201.
16. Reddy NP, Lakshmana M, Udupa UV. Antiosteoporotic activity of OST-6(osteocare), a herbomineral preparation in calcium deficient ovariectomized rats. Phytother Res 2004;18:25-9.
17. Thamacin Arulappan M, John Britto S. Some important medicinal plants used in Gingee Taluk of Villupuram District of Tamil Nadu, India. J Nat Prod Plant Resour 2014;4:13-9.
18. Thamacin Arulappan M, John Britto S, Thomas S, George M, Kindo I. Screening of the endangered medicinal plant extracts for antioxidant activity. Pharma Innov J 2014;3:38-43.
19. Wang Y, Ohtsuka-Isoya M, Shao P, Sakamoto S, Shinoda H. Effects of methylprednisolone on bone formation and resorption in rats. Jpn J Pharmacol 2002;90:236-46.
20. Salazar M, Hernandes L, Ramos AL, Salazar Bde O,

Micheletti KR, Paranhos LR, *et al.* Effect of alendronate sodium on tooth movement in ovariectomized rats. Arch Oral Biol 2015;60:776-81.

21. Bancroft JD, Gamble M. Theory and Practice of Histological Techniques. 6th ed. China: Churchil Livingston (Elsevier); 2008. p. 56,339,340.

22. Wang G, Zhu Z, Lei C, Li M, Liu F, Mao Y, *et al.* Low-dose risedronate sodium protects bone cells after abrupt oestrogen withdrawal. J Int Med Res 2012;40:1761-74.

23. Longui CA, Santos MC, Formiga CB, Oliveira DV, Rocha MN, Faria CD, *et al.* Antiproliferative and apoptotic potencies of glucocorticoids: Nonconcordance with their antiinflammatory and immunosuppressive properties. Arq Bras Endocrinol Metabol 2005;49:378-83.

24. Mocetti P, Silvestrini G, Ballanti P, Patacchioli FR, Di Grezia R, Angelucci L, *et al.* Bcl-2 and Bax expression in cartilage and bone cells after high-dose corticosterone treatment in rats. Tissue Cell 2001;33:1-7.

25. Lafage-Proust MH, Boudignon B, Thomas T. Glucocorticoidinduced osteoporosis: pathophysiological data and recent treatments. Joint Bone Spine 2003;70:109-18.

26. Lucinda LMF, Aarestrup BJV, Peters VM, de Paula Reis JE, de Oliveira RSMF, de Oliveira Guerra M. The Effect of theGinkgo bilobaExtract in the Expression of Bax, Bcl-2 and Bone Mineral Content of Wistar Rats with Glucocorticoid-Induced Osteoporosis. Phytotherapy Research 2012;27:515-20. doi:10.1002/ptr.4747.

27. Duque G, Rivas D. Alendronate has an anabolic effect on bone through the differentiation of mesenchymal stem cells. Journal of Bone and Mineral Research 2007;22:1603-11.

28. Marie PJ, Kassem M. Osteoblasts in osteoporosis: past, emerging, and future anabolic targets. Eur J Endocrinol 2011;165:1-10.

Evaluating the Renal Toxicity Profile of *Moringa oleifera* Seed: Associating its Wide Consumption with Renal Failure – Subacute *In vivo* Study

Abstract

Background: The alarming rate of kidney failure in Africa and Asia could be associated with wide levels of consumption of *Moringa oleifera* seed preparations in the continent. **Objectives:** The study aims to ascertain the phytochemicals in aqueous and ethanol extracts of *M. oleifera* seed and determine how its consumption affects the histopathology and function of the kidney. **Materials and Methods:** Albino rats (32) about 7 weeks old and weight, 120 g each, were divided into Groups 1–8, using nonprobability sampling technique. The rats in Groups 2–8 were fed daily, 100 mg, 200 mg, 400 mg, 800 mg, 1600 mg, 3200 mg, and 6400 mg/kg body weight of *M. oleifera* seed powder dissolved in 2 mL of distilled water, respectively, for 9 days, with the aid of a syringe and cannula. Group 1 (control) received 2 mL of distilled water daily. On the 8th day, two rats were randomly selected from Group 8 and fed with 15,000 mg/kg body weight (Group 9). **Results:** The seed has moderate alkaloids, saponins, glycosides, and terpenoids concentrations, and it is rich in carbohydrates, protein (aromatic amino acids), and oil. The renal tissues of rats in Groups 3–9 were distorted and necrosed. The rats in Groups 6–9 had an appreciable reduction in concentrations of blood creatinine and urea, and mortality was recorded in Groups 8 and 9. **Discussion and Conclusion:** Although subacute consumption of 100 mg/kg body weight daily of *M. oleifera* seed could not distort the renal architecture, blood electrolytes, creatinine, or urea concentration of the rats, relatively high-grade level of consumption could precipitate renal failure. An urgent need to standardize the consumption of the seed preparations of the "miracle plant" is required.

Keywords: *Aromatic amino acids, kidney failure, medicinal plant, saponin glycosides, water purification*

Uchenna Kenneth Ezemagu[1,2], Chiagozie C. Okafor[1], Chike P. Anibeze[1], Chioma M. Ojobo[1], Getrude N. Okechukwu[2], Eunice I. Ezemagu[3]

[1]Department of Anatomy, Enugu State University of Science and Technology, [3]Department of Animal Science and Production, University of Nigeria, Enugu, [2]Department of Anatomy, Faculty of Basic Medical Sciences, Alex Ekwueme Federal University Ndufu-Alike Ikwo, Ebonyi, Nigeria

Introduction

A solution to the alarming rate of kidney failure in Africa and Asia requires a multidimensional approach. Fourteen percentage of adults in the Southeast geopolitical zone of Nigeria are battling with different stages of kidney diseases which were attributed to dehydration and toxic herb consumption (31st Conference, National Association of Nephrology, Nigeria; January 14, 2019, Abakaliki; Vanguard Newspaper, January 15, 2019, Pg 1). *Moringa oleifera* seed consumption could be a target, because of its abundance and recent overwhelming use as a food and biological coagulant,[1-3] and purification of drinking water in Java, rural villages in Africa, and Asia.[4,5] Although the so-called "miracle plant" has been widely assumed to cure a plethora of diseases and infections, its chronic consumption as food or in water treated with seed preparations might constitute a problem to the kidney.

Meanwhile, proof of efficacy or safety of *M. oleifera* seed has not been fully established through an evidence-based approach. This study may provide a preliminary step to address the above proposal. Nonetheless, the administration of an aqueous extract of *M. oleifera* seed (500 and 200 mg/kg) for 14 days had no signs of systemic toxicity in mice, and there were no significant changes in organs and hematological indices between treatment and control groups.[6] Methanol extract of seeds of *M. oleifera* is safe for nutritional use in mice.[7] However, the chemical and physical qualities of an herb depend on its environment.[8-10] Moreover, it is not clear

Address for correspondence:
Dr. Uchenna Kenneth Ezemagu,
Department of Anatomy, Faculty of Basic Medical Sciences, Alex Ekwueme Federal University Ndufu Alike Ikwo, P. M. B. 1010, Abakaliki, Ebonyi State, Nigeria.
E-mail: uchennaezemagu@ gmail.com

Access this article online

Website: https://journals.lww. com/joai

DOI: 10.4103/jasi.jasi_22_22

Quick Response Code:

How to cite this article: Ezemagu UK, Okafor CC, Anibeze CP, Ojobo CM, Okechukwu GN, Ezemagu EI. Evaluating the renal toxicity profile of *Moringa oleifera* seed: Associating its wide consumption with renal failure – subacute *in vivo* study. J Anat Soc India 2023;72:98-104.

as to what extent the various constituents present in the seed preparations interrelate through additive, synergistic, and inhibitory effects.

Hence, we orally administered aqueous mixtures of the seed powder to albino rats, aiming to determine the level of its consumption that is safe or toxic to the kidney. Furthermore, ascertain the different concentrations of the basic phytochemicals in aqueous and ethanol extracts of *M. oleifera* seed found in our locality.

Materials and Methods

Seed preparation and extraction

The seeds of *M. oleifera* were harvested from three plants in different compounds that were located within Enugu metropolis, Nigeria. The seeds ($n = 1970$) were authenticated by a taxonomist in the Department of Botany, University of Nigeria, and shade dried for 2 weeks. The husks were removed and the seeds were blended into a fine powder (weight, 351.54 g) using a Qlink Electric Blender (Model QBL-18 L40) and stored in airtight containers. The seed powder (2 g) was assayed for proximate composition. Two grams of the powder was measured into a Soxhlet extractor – glass flask of size suitable for the extraction thimble was fitted with a condenser. Ethanol/distilled water (500 mL) in a round/flat bottom flask was placed on a heating mantle fixed with the extractor and the condenser connected to a water tank. The system was allowed to oscillate six times in 4–5 h per sample load. The extracts were concentrated in water bath at 60°C and 90°C for ethanol and aqueous extracts, respectively. The concentrations of constituent phytochemicals in the extracts were qualitatively and quantitatively analyzed with specific reagents. The study was approved by the institutional review board in line with the requirements of the Medical Research Ethics Committee.

Experimental animals

Thirty-two albino rats (age, 5 weeks) were purchased and housed in the Department of Animal Husbandry, University of Nigeria Enugu Campus. They were maintained under standard laboratory conditions (22°C–28°C, 60%–70% relative humidity, 12:12 h light and dark cycle) and fed with standard grower mash (vital feed) and water *ad libitum*. The rats were acclimatized for 2 weeks before the experiment.

Experimental design

The thirty-two adult albino rats (7 weeks old; weight, 75–130 g) were randomly divided into 8 groups of four each. With the aid of syringe and cannula, the rats in Groups 2–8 were fed 100 mg, 200 mg, 400 mg, 800 mg, 1600 mg, 3200 mg, and 6400 mg/kg body weight of the seed powder mixed in 2 mL of distilled water, respectively. The rats in Group 1 (control) received 2 mL of distilled

water each, daily. On the 8th day, the rats in the test groups had an appreciable increase in body weight, when compared with the control group. Therefore, we randomly selected two rats from Group 8 and fed each of the rats with 15,000 mg/kg body weight (Group 9), all at once to know whether the seed could be classified as a relatively harmless substance, as shown in Table 1.

Collection of tissues for histology

The rats were isolated in an airtight container containing chloroform, to keep them unconscious. Each unconscious rat was placed in a supine position and pinned firmly by its four limbs to the dissecting board. The abdominal region was incised using a surgical blade. The kidneys were harvested, processed, and stained with H and E, and their photomicrographs were taken.

Renal function tests

An assay of creatinine, urea, sodium, potassium, and chloride concentrations in the blood of the rats was done using a spectrophotometer (model, 752 – U – Clear, England) and Randox test kit (BT294QY, United Kingdom).

Statistical analysis

All data were expressed as mean ± standard deviation of the number of rats in each group. The level of homogeneity among groups was tested using a one-way analysis of variance and two sample test statistics. Where heterogeneity occurred, the groups were separated using Duncan multiple-range test. A value of $P < 0.05$ was considered to indicate a statistically significant difference between groups. The null hypothesis, $H_0{:}\mu = \mu_0$ _There is no significant mean difference/effect of *M. oleifera* seed consumption on renal function tests between treatment and control groups.

Results

The seed extract has moderate alkaloids, saponins, glycosides, and terpenoids concentrations, and it is rich in carbohydrates, protein (aromatic amino acids), and oil [Tables 2-5]. The proximate analysis of the seed reveals

Table 1: Experimental protocol and treatment				
Groups	Number of rats per cage	Single daily dose of MS (mg/kg BWT)	Duration (days)	Number of death
1	4	2 mL distill water	9	0
2	4	100	9	0
3	4	200	9	0
4	4	400	9	0
5	4	800	9	0
6	4	1600	9	0
7	4	3200	9	0
8	4*	6400	9	1**
9	2	15,000	1	1

*Reduced to 2 on 8th day, **Mortality on 8th day. MS: Moringa seed, BWT: Body weight

Table 2: Qualitative analyses of the basic phytochemicals of *Moringa oleifera* seed

Constituent	Method	Aqueous extract	Ethanol extract
Carbohydrates	Molisch test	++	+
Polysacch and reducing sugar	Iodine and Benedict's tests	–	–
Monosacch, pentose and ketose sugar	Barfoed's, Bial's and Seliwanoff's tests	–	–
Protein	Biuret test	++	++
Amino acid	Ninhydrin test	–	–
Aromatic amino acid	Xantheoprotein	+	+
Oil	Filter paper	++	++
Saponins	Frothing test	++	+
Tannin (catecholic)	Ferric chloride test	–	–
Flavonoids	Ammonium test	–	–
Glycosides	Keller–Kiliani test	++	+
Alkaloids	Picric acid test	+	+
	Wagner's test	++	+
Steroids	Salkowski test	–	–
Terpenoids	Salkowski test	++	++
Phenol	Ellagic acid test	–	–
Resin	Ferric chloride test	–	–

+: Present in trace concentration, ++: Present in moderate concentration, −: Absent

Table 3: Glycoside concentration in aqueous extract of *Moringa oleifera* seed

Weight of sample (g)	Absorbance				Concentration (g/mL)
	A	B	C	Average	
5.042	1.701	1.701	1.701	1.701	0.0337
5.042	1.717	1.717	1.717	1.717	0.0340
5.042	1.694	1.694	1.694	1.694	0.0335
Average					0.0337

$$\text{Glycoside concentration} = \frac{\text{Average absorbance} \times \text{volume of extract} \times 100}{1000 \times \text{weight of sample}}$$

Table 4: Alkaloid concentration in aqueous extract of *Moringa oleifera* seed*

Weight of sample (g)	Weight of empty filter paper (g)	Weight of filter paper + residue after oven drying (g)	Percentage alkaloid
5.047	1.033	1.168	2.675
5.039	1.041	1.140	1.965

*Method adopted by Harborne[12]

Table 5: Saponin concentration in aqueous extract of *Moringa oleifera* seed*

Weight of sample (g)	Weight of empty crucible (g)	Weight of crucible + residue after oven drying (g)	Percentage saponin
10.087	49.697	49.784	0.863
10.055	50.962	51.087	1.243

*Methods of Obdoni and Ochuko[13]

that it contains 27.50% and 7.80% of oil and protein, respectively [Table 6]. The rats in Groups 8–9 and 6–9 had a significant reduction in the concentration of blood urea and creatinine, respectively, when compared with that of rats in Group 1 (control), which was dependent on grade levels of seed consumption [Table 7]. The rats in Groups 3–9 showed varying degrees of distortion and necrosis of renal tubules and glomeruli [Figures 1-7], and mortality was recorded in Groups 8 and 9. The results are further summarized in Tables 2-7 and Figures 1-9 below.

Phytochemical analysis

Result in Table 2 shows that Moringa oleifera seed has moderate concentration of carbohydrates, protein, oil, saponins, glycosides and terpenoids.

Quantitative analysis

The rats in Groups 3, 6, 8, 9, and 6–9 had a significant reduction in the concentration of blood urea and creatinine, respectively, when compared with that of rats in Group 1 (control).

Discussion

Many drugs and poisons were derived from plant glycosides and alkaloids. Most compounds of triterpenes in plants are saponin glycosides. The categories of oral lethal dose 50 of a toxic substance for small animals such as rats are as follows: extremely toxic (<1 mg/kg body weight); highly toxic (1–50 mg/kg body weight); moderately toxic (50–500 mg/kg body weight); slightly toxic (500–5000 mg/kg body weight); practically nontoxic (5000–15,000 mg/kg body weight); and relatively harmless (≥15,000 mg/kg body weight). Based on assumption that *M. oleifera* seed could be nontoxic, and the observed appreciable increase in body weight of rats in test groups, the study attempted to classify

Figure 1: Photomicrograph of a cross-section of the kidney of a rat in Group 3, showing renal tissue with PPC, clump of glomeruli (CG), and DRT (H and E, ×400). PPC: Poor perfuse cytoplasm, DRT: Distortion of renal tissue
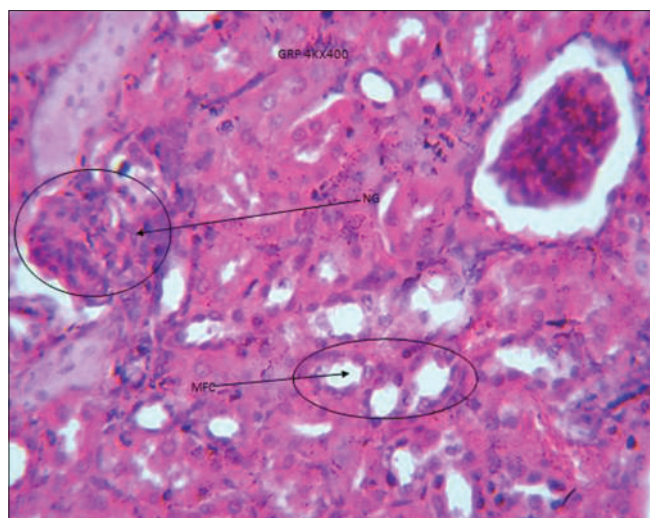
Figure 2: Photomicrograph of a cross-section of the kidney of a rat in Group 4, showing renal tissue with moderate fatty (MFC) and NG (H and E, ×400). NG: Necrotic glomeruli
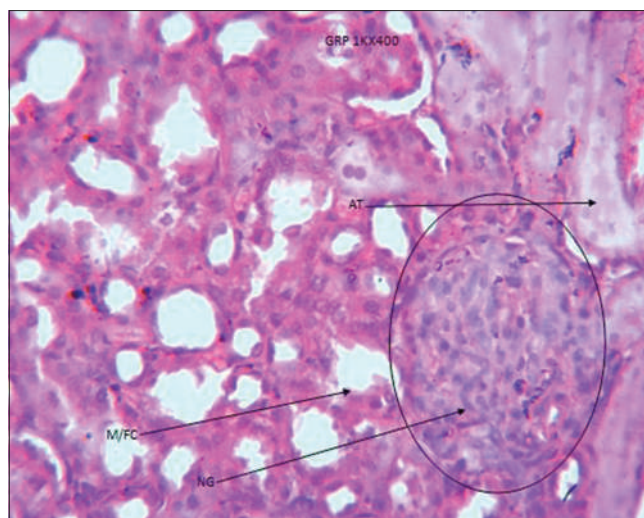
Figure 3: Photomicrograph of a cross-section of the kidney of a rat in Group 5, showing renal tissue with moderate-to-severe fatty changes (MFC) NG and ATs (H and E, ×400). NG: Necrotic glomeruli, AT: Atrophic tubule
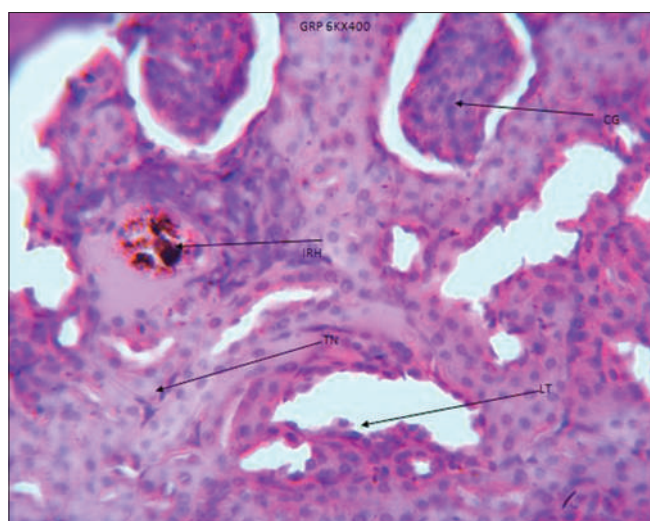
Figure 4: Photomicrograph of a cross-section of the kidney of a rat in Group 6, showing renal tissue with moderate to STN, and LTs in some areas and clumping of glomeruli (CG) with intrarenal hemorrhage, IRH (H and E, ×400). STN: Severe tubular necrosis, LT: Loss of tubule
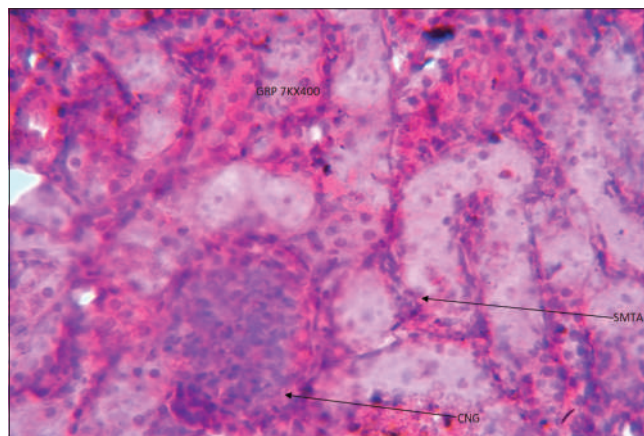
Figure 5: Photomicrograph of a cross-section of the kidney of a rat in Group 7, showing renal tissue with SMTA and CNG (H and E, ×400). SMTA: Severe marked tubular atrophy, CNG: Coagulating necrosis of glomeruli

Table 6: Proximate composition of *Moringa oleifera* seed*

	Percentage
Moisture	7.50
Crude fiber	5.00
Oil	27.50
Ash	2.50
Protein	7.80

*M. oleifera seed has relatively high concentration of oil and protein. AOAC: Association of Official Analytical Chemists

the seed as a relatively harmless substance [Table 1]. Aja *et al*.[14] isolated oleic acid (84.6%), L-(+)-ascorbic acid-2, 6-dihexadecanoate-9-octadecenoic acid, methyl ester-hexadecanoic acid, and 9-octadecenamide as main

constituents of methanol extract of *M. oleifera* seed found in our locality.

Furthermore, Oluduro and Aderiye[15] reported that *M. oleifera* seed contains protein (37.8%), fat (36.2%), crude fiber (3.67%), and ash (9.48%). It is also rich in magnesium (129.6 mg/L), potassium (103.5 mg/L), sodium (70.1 mg/L), calcium (34.6 mg/L), and iron (5.4 mg/L). Similarly, the proximate and phytochemical analyses of the seed revealed a relatively low moisture content, large proportion of oil and protein (aromatic amino acids), and glycosides, alkaloid, and saponin using Association of Official Analytical Chemists' guidelines (AOAC) [Tables 3-6].[11] The whole seed meal was used in the experiment; since it is not clear as to what extent the various constituents present in the seed preparations interrelate through additive, synergistic, and inhibitory effects. The interactions of the basic phytochemicals [Table 2] and their metabolites could introduce new classes of therapeutics.[16,17]
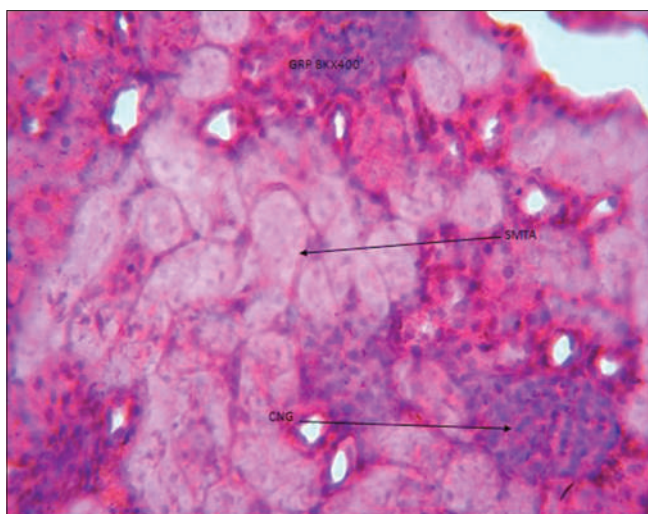
Figure 6: Photomicrograph of a cross-section of the kidney of a rat in Group 8, showing pale proximal tubules with SMTA, and CNG (H and E, ×400). SMTA: Severe marked tubular atrophy, CNG: Coagulating necrosis of glomeruli
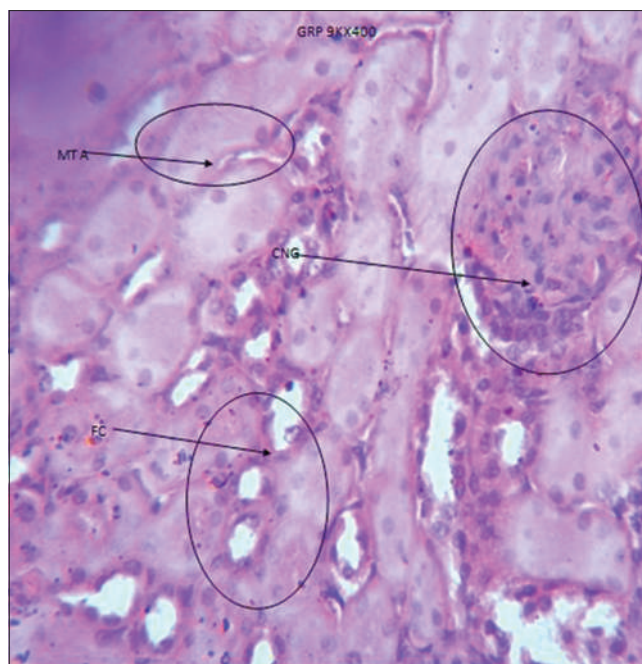
Figure 7: Photomicrograph of a cross-section of the kidney of a rat in Group 9, showing pale proximal tubules with SMTA, CNG, and FC (H and E, ×400). SMTA: Severe marked tubular atrophy, CNG: Coagulating necrosis of glomeruli, FC: Fatty change
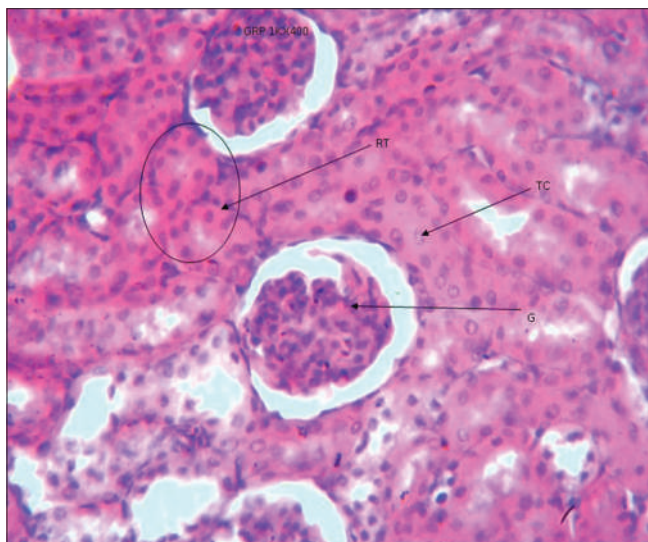
Figure 8: Histopathology results Figures 1-9 showed the effects of graded levels of consumption of *Moringa oleifera* seed on histology of the kidney of albino rats Figure 1: Photomicrograph of a cross-section of the kidney of a rat in Group 1 (control) showing normal renal architecture, well perfuse glomeruli (G) and RT lined with TCs (H and E, ×400). RT: Renal tubule, TC: Tubular cell, G: Glomeruli
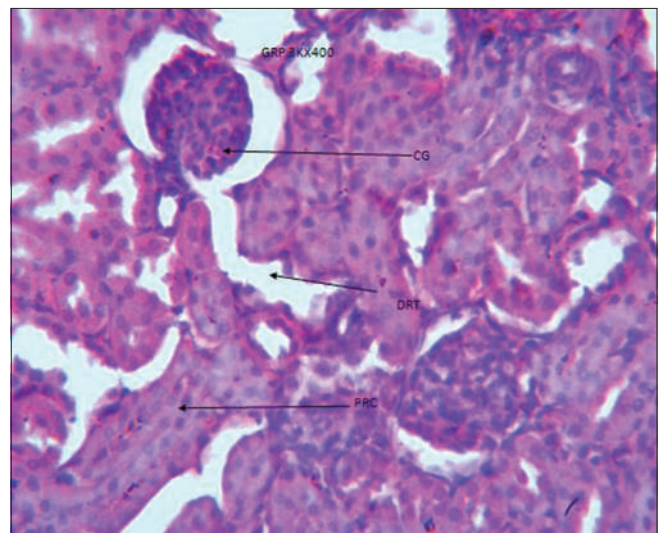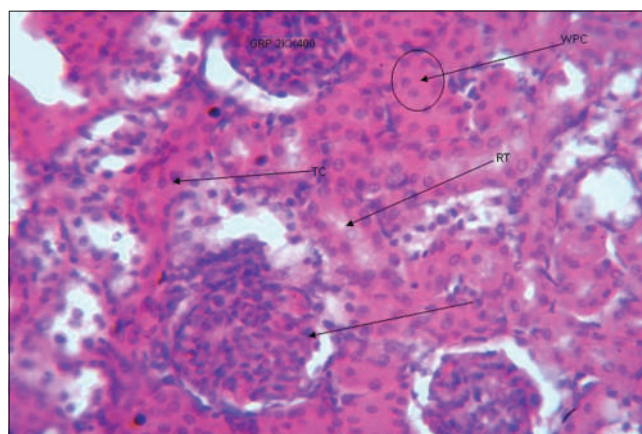

Figure 9: Photomicrograph of a cross-section of the kidney of a rat in Group 2, showing normal renal tissue with WPC, glomeruli (G) normal filtering units of the kidney and RTs lined with TCs (H and E, ×400). RT: Renal tubule, TC: Tubular cell, WPC: Well perfuse cytoplasm

Notably, aminoglycoside antibiotics contain as a portion of the molecule an amino-modified glycoside, which inhibits protein synthesis,[18,19] and in recommended dosages could cause systemic hypertension and renal toxicity.

The blood electrolytes; sodium, potassium, and chloride concentration of the rats in test groups failed to correlate with grade levels of consumption of the seed, but that of creatinine and urea did. Based on the assertion that *M. oleifera* seed consumption was safe for nutritional use in mice,[7] we could not assess intermittently, the alterations in other predictors of renal failure. However, there could be some clinical correlates, since the rats in Groups 3–9

showed varying degrees of distortion and necrosis of renal tubules and glomeruli [Figures 1-7], and mortality was recorded in Groups 8 and 9. Specifically, the histopathology revealed the following features; poorly perfuse cells and clumps of glomeruli, atrophy, and necrosis of the renal tubules and glomeruli, when the grade level of consumption of an aqueous mixture of the seed powder range from 200 to 15,000 mg/kg body weight. Notably, the features of the renal tissues of the rats in Groups 6–9, depict that of renal failure. We could not observe any adverse effect at 100 mg/kg body weight grade level of consumption [Figure 9] when compared with the control [Figure 8].

Parameter	Sodium (mmol/L)	Potassium (mmol/L)	Chloride (mmol/L)	Urea (mmol/L)	Creatinine (µmol/L)
Group 1	136.5±2.121	8.80±0.56	98.50±0.70	2.00±0.70	154.1±4.10
Group 2	136.5±2.12	9.35±0.91	96.0±2.82	2.4±0.14	161.0±6.22
Group 3	139.50±3.53	8.75±0.63	101.0±1.41	1.06±0.33*	150.80±5.93
Group 4	135.50±2.12	7.75±0.49	93.0±4.24	1.95±0.21	145.95±4.17
Group 5	140.0±4.24	7.50±1.13	98.0±0.00	1.75±0.35	147.40±3.11
Group 6	133.0±1.41	7.15±1.06	95.00±4.24	1.25±1.06*	115.45±5.30*
Group 7	138.00±4.24	6.60±1.27	100.50±6.36	1.95±1.06	107.75±4.03*
Group 8	138.00±1.41	7.55±0.07	98.50±2.12	0.75±0.35*	102.33±3.62*
Group 9	129.00±0.00	8.80±0.00	94.00±0.00	0.50±0.00*	58.40±0.00*

Table 7: Test of mean difference in the renal function analyses of the control and test groups

*Significant mean difference $P<0.05$. The rats in Group 3, 6, 8, 9, and 6–9 had a significant reduction in the concentration of blood urea and creatinine, respectively, when compared with that of rats in Group 1 (control)

Furthermore, the rats in Groups 3, 6, 8 and 9, and 6–9 had an appreciable reduction in the concentration of blood urea and creatinine, respectively, when compared with that of rats in Group 1 (control), which was dependent on grade levels of the seed consumption [Table 7]. Abnormal creatinine concentration was linked to chronic kidney disease or damage. Notably, most alkaloids and glycosides potentially inhibit histamine release and CD 40 ligand expression by mast cells and basophils; and saponins have hemolytic properties.[20,21] For instance, tomato saponin and alpha-tomatine could potentiate apoptosis and eliminate cells that are abnormal and potentially dangerous.[22,23] Most likely, the interaction of saponins and other constituent phytochemicals in *M. oleifera* seed or their metabolites could be toxic to the kidney of albino rats at certain level of consumption. Thus, the mechanisms of actions of alkaloids, glycosides, and saponins in *M. oleifera* seed could explain the changes in blood electrolytes, creatinine, and urea concentration when compared with that of control group.

Conversely, Jahn and Mangale *et al*.[4,24] found *M. oleifera* seed to be nontoxic at a dose <800 mg/kg body weight. Hence, they recommended its use as a water coagulant in developing countries. On the other hand, the population of some infectious microorganisms increased when they were exposed to the seed extract.[2,25] Second, *M. oleifera* seed extract (200 mg/kg body weight) had genetic effects on fish guppies, protozoan, and bacteria.[26] There is a dearth of works on the effect of *M. oleifera* seed consumption on renal architecture. Therefore, the above findings might be a unique contribution to the knowledge of renal toxicity of the so-called miracle plant.

Conclusion

The seed of *M. oleifera* plant found in Enugu State-Nigeria has a relatively low moisture content, large proportion of oil and protein (aromatic amino acids), glycosides, alkaloids, and saponins. Although the blood electrolytes; sodium, potassium, and chloride concentration failed to correlate with grade levels of the seed consumption, reduction in blood creatinine and urea concentration did. We could not observe an adverse effect with subacute consumption of 100 mg/kg body weight daily of *M. oleifera* seed, but above this level of consumption, there were distortion and necroses of renal tubules and glomeruli. The above changes could precipitate renal failure.

Recommendation

A detailed study of *M. oleifera* seed is recommended considering the interactions and metabolism of the constituent phytochemicals, especially, the saponin glycosides, alkaloids, and aromatic amino acids, and the pivotal roles they play in the safety and intoxication of the kidney. The study also suggests that there is an urgent need to discourage the wide levels of consumption of *M. oleifera* seed and standardize its use in purifying water; given that it is toxic to the kidney and could pose a health risk.

Conflicts of interest

There are no conflicts of interest.

References

1. Farooq F, Rai M, Tiwari A, Khan A, Farooq S. Medicinal properties of *Moringa oleifera*; an overview of promising healer. J Med Plants Res 2012;6:4368-74.

2. Oluduro AO, Aderiye BI. Impact of moringa seed extract the physiochemical properties of surface and underground water. Int J Biol Chem 2007;1:244-9.

3. Anwar F, Latif S, Ashraf M, Gilani AH. *Moringa oleifera*: A food plant with multiple medicinal uses. Phytother Res 2007;21:17-25.

4. Jahn SA. Using Moringa seed as coagulants in developing countries. J Am Water Works Assoc 1988;80:43-50.

5. Olayemi AB, Alabi RO. Studies on traditional water purification using *Moringa oleifera* seed. Afr Study Monogr 1994;15:135-42.

6. Araújo LC, Aguiar JS, Napoleão TH, Mota FV, Barros AL, Moura MC, *et al.* Evaluation of cytotoxic and anti-inflammatory activities of extracts and lectins from *Moringa oleifera* seeds. PLoS One 2013;8:e81973.

7. Ajibade TO, Arowolo R, Olayemi FO. PhytochemicalScreening and toxicity studies on the methanol extract of the seeds of Moriga oleifera. J Complement Integr Med 2013: 10. doi:10.1515/jcim-2012-0015.

8. Awang DV. Quality control and good manufacturing practices: Safety and efficacy of commercial herbals. Food Drug Law J 1997;52:341-4.

9. Fong HH. Integration of herbal medicine into modern medical practices: Issues and prospects. Integr Cancer Ther 2002;1:287-93.

10. Brinker F. Managing and interpreting the complexities of botanical research. Herbal Gram 2009;82:42-9.

11. AOAC Association of Official Analytical Chemists. Official Methods of Analysis. 21st ed. Washington D. C. USA: Association of Official Analytical Chemists; 2006.

12. Harborne JB. Phytochemical Methods: A Guide to Modern Techniques of Plant Analysis. London: Chapman A & Hall; 1973. p. 279.

13. Obdoni B, Ochuko P. Phytochemical studies and comparative efficacy of the crude extracts of some homostatic plants in Edo and Delta States of Nigeria. Global J Pure Appl Sci 2001;8:203-8.

14. Aja PM, Nwachukwu N, Ibiam UA, Igwenyi IO, Offor CE, Orji UO. Chemical constituents of *Moringa oleifera* leaves and seeds from Abakaliki, Nigeria. Am J Phytomed Clin Ther 2014;2:310-21.

15. Oluduro AO, Aderiye BI. Efficacy of *Moringa oleifera* seed extract on the Microflora of surface and underground water. J Plant Sci 2007;2:453-8.

16. Dougherty DA. Cation-pi interactions involving aromatic amino acids. J Nutr 2007;137:1504S-8S.

17. Gallivan JP, Dougherty DA. Cation-pi interactions in structural biology. Proc Natl Acad Sci U S A 1999;96:9459-64.

18. Hudson KL, Bartlett GJ, Diehl RC, Agirre J, Gallagher T, Kiessling LL, *et al.* Carbohydrate-aromatic interactions in proteins. J Am Chem Soc 2015;137:15152-60.

19. Zhang X, Wang S, Wu X, Lui S, Li D, Wang L, *et al.* Sub site-specific contributions of different aromatic residues in the active site architecture of glycoside hydrolase family 12. Sci Rep 2015;5:18357.

20. Arabski M, Węgierek-Ciuk A, Czerwonka G, Lankoff A, Kaca W. Effects of saponins against clinical *E. coli* strains and eukaryotic cell line. J Biomed Biotechnol 2012;2012:286216.

21. Alsaudi BH, AlHarbi SH, Ibrahim SR, El-Kholy AA, El-Agamy DS, Mohamed GA. Hepatoprotective activity of *Costus speciosus* (KOEN. EX. RETZ) against Paracetamol-induced liver injury in mice. Afr J Tradit Complement Altern Med 2018;15:35-41.

22. Kudelova J, Seifrtova M, Sucha L, Tomsik P, Havelek R, Rezacova M. Alpha-tomatine activates cell cycle checkpoints in the absence of DNA damage in human leukemic MOLT-4 cells. J Appl Biomed 2013;11:93-103.

23. Ezemagu UK, Uzomba C, Akunna GO, Egwu OA, Nwite KN. Comparing *Ficus vogelli* extract and Omeprazole as therapy and prophylaxis of aspirin-induced gastric ulcer in Wistar rat. Biomed Res 2019;30:697-70.

24. Mangale SM, Chonde SG, Jadhav AS, Raut PD. Study of *Moringa oleifera* (Drum stick) seed as natural absorbent antimicrobial agent for river water treatment. J Nat Prod Plant Resour 2012;2:89-100.

25. Olsen SJ, Miller G, Breuer T, Kennedy M, Higgins C, Walford J, *et al.* A waterborne outbreak of *Escherichia coli* O157:H7 infections and hemolytic uremic syndrome: Implications for rural water systems. Emerg Infect Dis 2002;8:370-5.

26. Ndabigengesere A, Narasiah KS, Talbot BE. Active agents and mechanism of coagulation of turbid waters using *Moringa oleifera*. Water Res 1995;29:703-10.

Embryogenesis and Histogenesis of the Human Fetal Liver at Various Stages of Gestation

Abstract

Background of Study: To assess the prenatal development of the human liver at gestation ages (GAs) 12–36 weeks using microscopic parameters and their correlation to predict the GA. The observation of microscopic features such as Kupffer cells (KCs), hematopoietic activity, stellate cells, glycogen granules, central vein (CV), and portal triad (PT) carries immense importance for its use in the estimation of fetal GA, detection of anatomical variations, and identification of congenital anomalies concerning branches such as anatomy, surgery, forensic sciences, radiology, pediatrics, and phytopathology. **Materials and Methods:** The present study was conducted in the department of anatomy on 33 normal fetuses of GA 12–36 weeks and classified them into 5 groups as A (12–16 weeks), B (17–21 weeks), C (22–26 weeks), D (27–31 weeks), and E (32–36 weeks). The general parameters were measured. Slides were prepared as per standard protocol and observed under a light microscope. **Results:** Microscopic observation reveals CV and PT in 15 weeks, dominant hematopoiesis till 21 weeks and then declines gradually, KC in 16 weeks, sinusoids in 19 weeks, glycogen granules deposition from 36 weeks, and hepatic lobule and portal lobule appears at 31 weeks. **Conclusion:** The knowledge of morphological features with respect to gestational age is a reliable reference help to prevent misdiagnosis of various pathological conditions of the liver such as cirrhosis, hepatomegaly, fetal anemia, intrauterine growth retardation, and congenital anomalies.

Keywords: *Embryology, fetal liver, gestation age, histogenesis, morphology*

Pooja Bhadoria,
Kavita Modi,
Brijendra Singh,
Jaya Chaturvedi[1],
Amarjyoti
Chaturvedi,
Bhavaniprasad
Mahindrakar[2]

Departments of Anatomy and [1]Obstetrics and Gynecology, All India Institute of Medical Sciences, Rishikesh, [2]Department of General Surgery, Himalayan Institute of Medical Sciences, Dehradun, Uttarakhand, India

Introduction

The liver is a highly precocious organ**,** diseases such as cirrhosis, hepatitis, and hepatic fibrosis are the four leading causes of death in middle-aged adults. Three percent of pregnant women are diagnosed with liver diseases making it the most frequent cause of significant morbidity and mortality for both mother and infant. In the embryonic period, it appears in 3rd week of intrauterine life and grows rapidly from 5 to 10 weeks of gestation, occupying a large portion of the abdominal cavity which represents 10% of total body weight at 10 weeks. Initially, both the right and left lobes are the same but then, the right lobe preferably becomes large as the morphological and physiological growth of the liver is accelerated after 32 weeks of gestation.[1] In postnatal life, it contributes to 4%–5% of infant body weight and then reduces to nearly 2% in puberty, approximately 1500 g in weight.[2] The liver acts as a principal hematopoietic

organ after 6 weeks of intrauterine life.[3] The first hematopoiesis, often referred to as primitive hematopoiesis, occurs in the yolk sac producing embryonic-type erythroblasts with large nuclei and expression of embryonic globin genes, as well as primitive macrophages.[4] Glycogen is absent in the embryonic liver. It appears around 30 weeks and then increases gradually. Histologically, the liver is completely developed during 8–9 months of gestation. Its phagocytic activity is performed by mononuclear macrophages known as Kupffer cells (KC).[5] The goal of the current study is to look at the comprehensive gross morphological aspects of the human fetal liver at gestation ages (GA) 12–36 weeks using microscopic examination and histotechniques, as well as the link between gestational ages. The observation of microscopic features about the time of appearance of KC, hematopoietic activity (HA), stellate cells (S), glycogen granules (G), central vein (CV), portal triad (PT) carries immense importance for

Access this article online

Website: https://journals.lww.com/joai

DOI:
10.4103/jasi.jasi_148_22

Quick Response Code:

How to cite this article: Bhadoria P, Modi K, Singh B, Chaturvedi J, Chaturvedi A, Mahindrakar B. Embryogenesis and histogenesis of the human fetal liver at various stages of gestation. J Anat Soc India 2023;72:105-13.

its use in estimation of fetal GA, detection of anatomical variations, and identification of congenital anomalies concerning branches such as anatomy, surgery, forensic sciences, medicine, radiology, pediatrics, obstetrics, and phytopathology.

Materials and Methods

The current study was an institutional-based, observational study conducted by the department of anatomy in collaboration with the department of obstetrics and gynecology. The present study was done on 33 legally aborted fetuses (male – 22, female – 11) without any gross congenital anomaly, which was collected immediately after delivery after receiving written consent from the mother and legal guardian. Ethical clearance was taken from the institutional ethical committee (Letter no.: AIIMS/IEC/20/551, date: August 22, 2020). The rules and standard guidelines for the disposal of human anatomical wastes were strictly followed.[6]

H and E stains were prepared by following standard protocol.[7] Slides were prepared followed by protocol given by Feldman and Wolfe 2014.[8] For fixation, a 5 mm thick tissue from the specimen was selected and fixed in 10% neutral buffered formalin for 24–48 h. Then, the tissue was dehydrated through ascending grades of alcohol (ethanol) for 8 h thrice. Clearing of the tissue was done by placing it in ascending grades of xylene for 8 h thrice to clear the residual alcohol since it is water-insoluble and acts as a lipid solvent. The tissue was left overnight in melted paraffin for paraffinization and embedding. The final block solidifies on the cold plate at −22°C. Microtomy was done manually on the rotary microtome to get thin ribbons of 5 microns, and then, it was transferred in a water flotation bath at 56°C. Albuminized slides were made by spreading a drop of Mayor's albumin (equal parts of egg albumin and glycerin) on a glass slide, the floating tissue was then transferred to these albumenized slides and then placed on slide warming plates for paraffin melting. The warm slides were processed in ascending grades of xylene for 30 min to remove paraffin. Hydration: it was hydrated by passing it through descending grades of alcohol (absolute alcohol, 75%, 50%) for 5 min each. Proper hydration facilitates better staining.

Method of analysis

The microscope used for the examination of slides was Olympus binocular microscope with Camera (DSS Imagetech (P). Ltd). Slides from each group of specimens of 12–36 weeks of GA were observed to assess the cellular development of the liver with advancement in GA by the presence of capsule, mesenchymal cells, hematopoietic activity, KC, stellate cells, hepatocytes (H), hepatic sinusoids (S), endothelial cells (E), bile ductule (BD), PT, portal vein (PV), hematopoietic activity (HA), glycogen deposition, and connective tissue (CT) elements.

Results

In Group A, a fibrous Glisson's capsule (C) made of flat cells of the endothelium (E) was observed [Figure 1]. Endothelial cells had fusiform cytoplasm, with a dense and elongated nucleus. PT appeared, formed of a large irregular portal venule (PV), internally lined endothelial cells, hepatic arterioles, and a bile ductule lined by cuboidal cells enclosed in thick fibrous CT and blood vessels were filled with primitive blood cells [Figure 2]. The hepatic sinusoids were characterized by discontinuous endothelial lining and were separated from nearby hepatocytes by perisinusoidal spaces or spaces of Disse. In sinusoids, nucleated red blood cells (RBCs) with a thin rim of cytoplasm were present representing hematopoietic activity, and cells with elongated pyknotic nuclei were mononuclear phagocytes and were marked as KC [Figure 3]. The CV was observed, lined internally by a fenestrated layer of endothelial cells surrounded by thick fibrous CT [Figure 4]. Iron deposits appeared as brown granules, like copper. Hepatic parenchyma showed a glycogenated nucleus and abundant mesenchyme which looked like a large cell with a centrally placed nucleus, having irregular anastomosis of cords of hepatocytes and separated by blood-filled hepatic sinusoids [Figures 5 and 6]. The fetal hepatocytes were characterized by a low-nuclear–cytoplasmic ratio, cytoplasm was foamy and abundant. Its nucleus was oval, basophilic, and pale.

In Group B, Glisson's capsule [Figure 7], well-arranged PT enclosed in thick fibrous CT [Figure 8]. This CT extends to form interlobular septum (IS). In the fetal liver, the presence of CT septum in between these portal tracts is well-known and species-specific [Figure 9]. The nucleated RBCs were present in well-marked sinusoids and marked by hematopoietic activity [Figure 9]. The
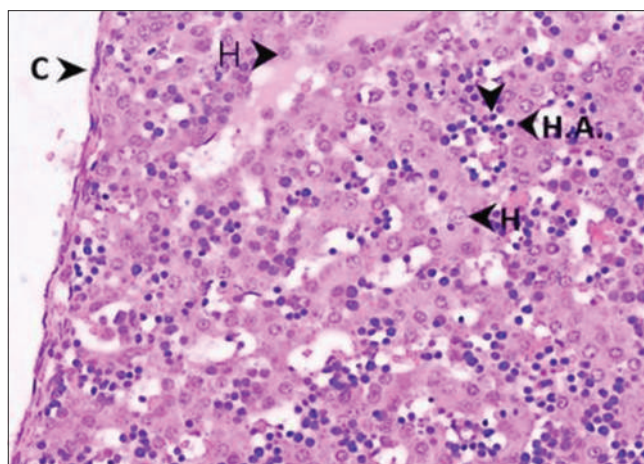
Figure 1: Photomicrograph of TS of 15 weeks human fetal liver showing capsule (C), Hepatocyte (H), (H and E, ×40). HA: Hematopoietic activity, H: Hepatocyte, C: Capsule, TS: Transverse section

plates of hepatocytes surrounding the CT which limits the PT was known as limiting plate. The parenchyma was formed by immature hepatocytes arranged in the form of thick anastomosing plates separated by one-cell thick sinusoids [Figure 10]. In sinusoids, KC and cluster of stellate cells were present. Binucleate hepatocyte was observed [Figure 10]. In developing a liver, the number of stellate cells increases with advancement in GA. A large well-defined CV is internally lined by a fenestrated layer of flattened endothelial cells. A portal lobule is defined as the orientation of the portal tract in the center and CVs around it. A classical hexagonal hepatic lobule is defined as the orientation of PV in the center and surrounded by six CVs at the periphery. Here, a portal lobule with a portal tract in the center and CV at the periphery was seen and classical signs of hepatic lobule were visible [Figure 11].

In Group C, thick Glisson's capsule [Figure 12] and well-defined CV with radiating cords of hepatocytes which form the hepatic parenchyma was present. These were separated by well-defined blood-filled sinusoids [Figure 13]. The PT was well arranged, formed of a large irregular PV, internally lined by a flat layer of endothelial cells, hepatic arteriole, lymphatic, and a bile ductule lined by cuboidal cells, enclosed in a sheath of thick fibrous CT. The limiting plates of hepatocytes surrounded the CT [Figure 14]. IS was present [Figure 15] Hematopoietic activity was focal and scanty in hepatic parenchyma, and the number of KC and stellate cells increased with an increase in GA [Figure 16]. Classical features of the hepatic lobule and portal lobule disappeared.

In Group D, with the advanced GA, the thickness of Glisson's capsule increased [Figure 17]. The CV became
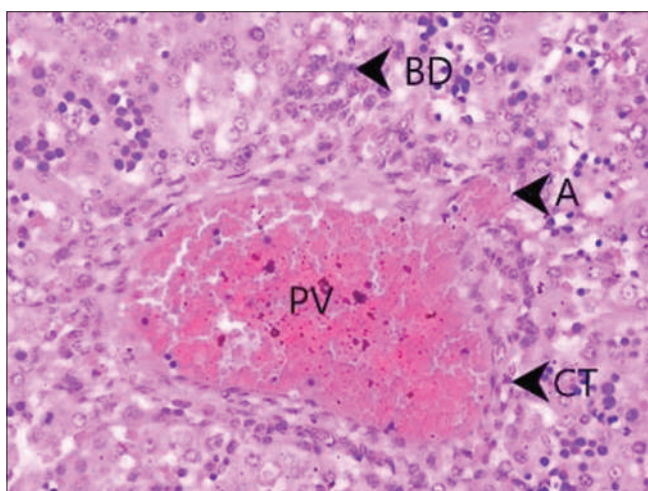
Figure 2: Photomicrograph of TS of 15 weeks of human fetal liver showing PT with a large PV, and hepatic arteriole (A), filled with blood cells, and developing BD lined by cuboidal cells. Portal triad is surrounded by thick fibrous CT (H and E, ×40). A: Arteriole, PV: Portal venule, BD: Bile ductile, CT: Connective tissue, PT: Portal triad
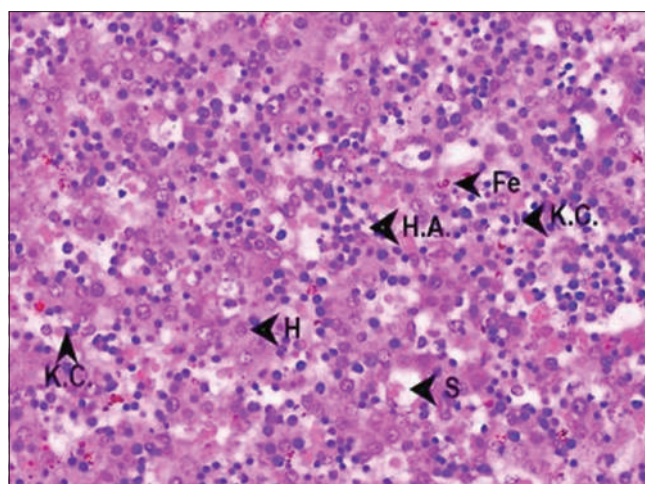
Figure 3: Photomicrograph of TS of 15 weeks of hepatic parenchyma showing brown granules of Fe, hematopoietic activity, blood-filled sinusoids (S), and KC (H and E, ×40). Fe: Iron, S: Sinusoids, KC: Kupffer cells, TS: Transverse section
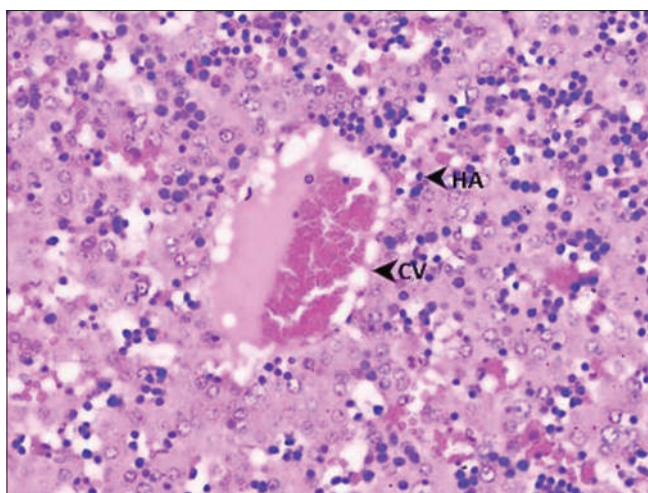
Figure 4: Photomicrograph of TS of 15 weeks fetal liver showing well-defined CV, endothelial cells (E), filled with blood cells (H and E, ×40). E: Endothelial cells, CV: Central vein, TS: Transverse section
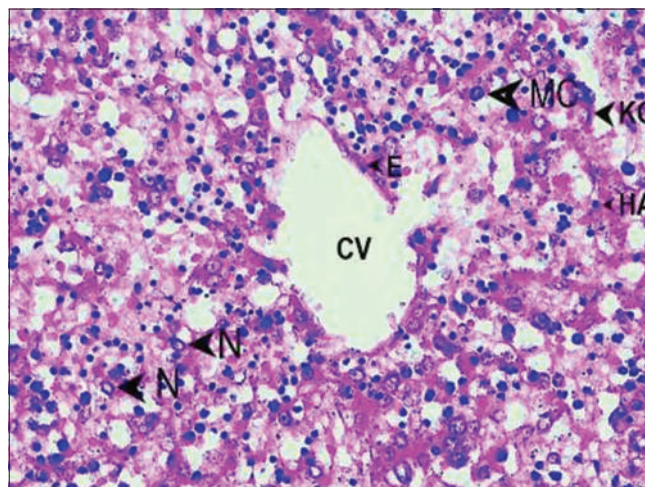
Figure 5: Photomicrograph of TS of 16 weeks fetal liver showing well-defined CV, endothelium (E), clear glycogenated nucleus (N), MC, and KC (H and E, ×40). E: Endothelial cells, N: Nucleus, CV: Central vein, MC: Mesenchymal cells, KC: Kupffer cells, TS: Transverse section
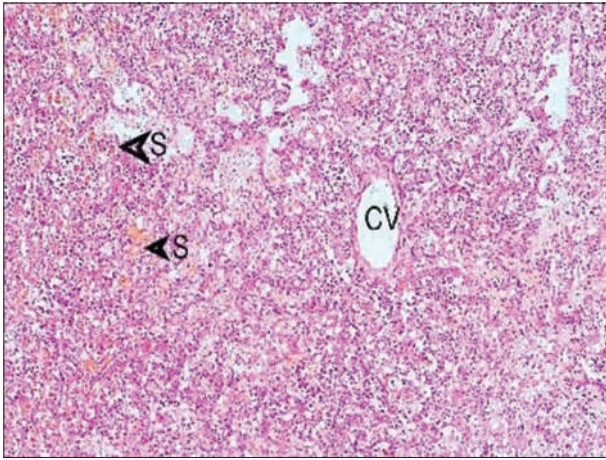
Figure 6: Photomicrograph of TS of 16 weeks fetal liver showing CV, and hepatic sinusoids (S) filled with blood (H and E, ×4). S: Sinusoids, CV: Central vein, TS: Transverse section

Figure 7: Photomicrograph of 18 weeks human fetal liver showing capsule (C), endothelial cells (E), hepatocytes (H), and KC (H and E, ×40). KC: Kupffer cells, E: Endothelial cells, H: Hepatocytes, C: Capsule

Figure 8: Photomicrograph of 18 weeks of human fetal liver showing PT with a large PV, lined by endothelial cells (E), developing BD lined by cuboidal cells, hepatic arteriole (A) and hepatic sinusoids (S), thick fibrous CT and presence of IS (H and E, ×10). PT: Portal triad, PV: Portal venule, CT: Connective tissue, IS: Interlobular septum, BD: Bile ductule
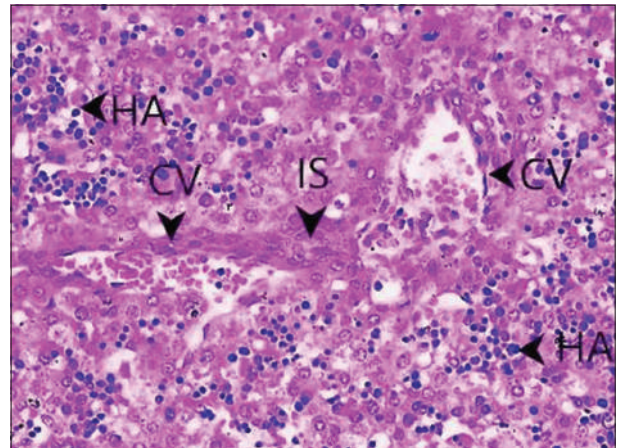
Figure 9: Photomicrograph of human fetal liver of 18 weeks hepatic parenchyma showing CV filled with blood, IS, cluster of HA (H and E, ×40). CV: Central vein. IS: Interlobular septum, HA: Hematopoietic activity
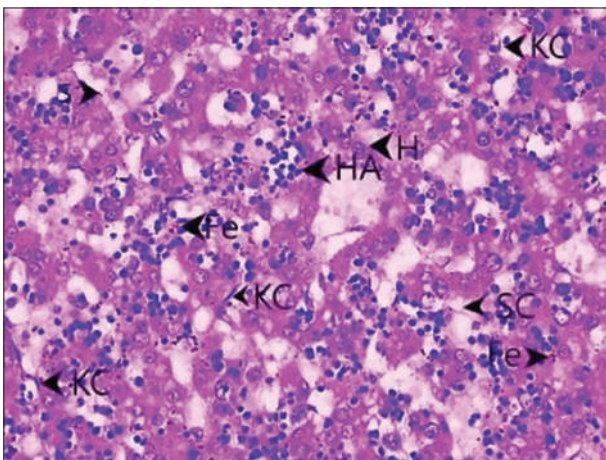
Figure 10: Photomicrograph of TS of 19 weeks of hepatic parenchyma showing brown granules of iron (Fe), blood-filled sinusoids (S), hepatocytes (H), HA, SC and KC (H and E, ×40), HA: Hematopoietic activity, SC: Stellate cells, KC: Kupffer cells, TS: Transverse section
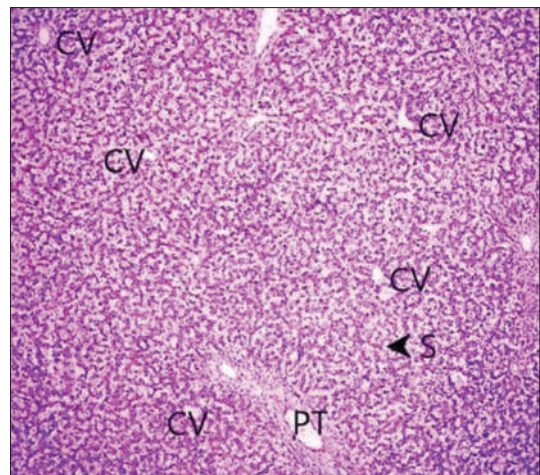
Figure 11: Photomicrograph of TS of 20 weeks human fetal liver showing CV, and radiating cords of hepatocytes, separated by sinusoids (S), PT surrounded by thick fibrous CT. It appears as a classical sign of portal lobule. (H and E, ×4). CV: Central vein, PT: Portal triad, CT: Connective tissue, TS: Transverse section
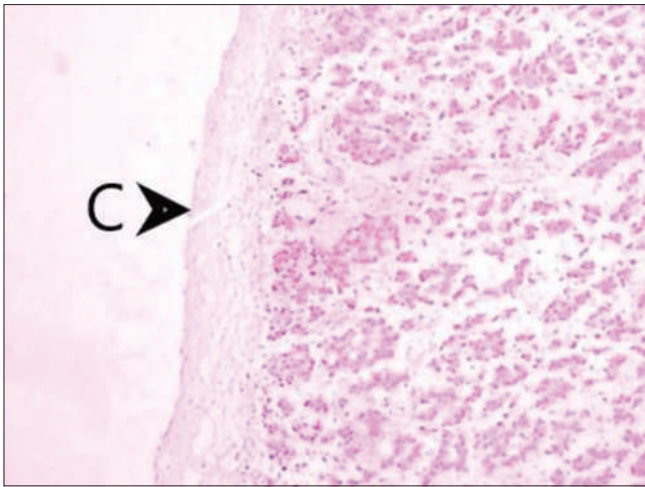
Figure 12: Photomicrograph of 26 weeks human fetal liver showing thick fibrous capsule (C) (H and E, ×10)
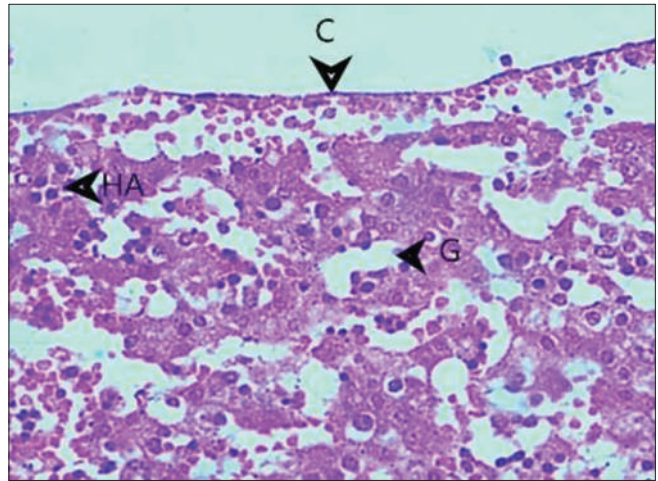
Figure 13: Photomicrograph of 23 weeks human fetal liver showing capsule (C) of endothelial cells (E), HA, and glycogen granules (G) (H and E, ×40). HA: Hematopoietic activity

Figure 14: Photomicrograph of 23 weeks of human fetal liver showing PT consisting of with a large PV, developing BD lined by cuboidal cells and hepatic arteriole (A), lymphatic (L). Portal triad is surrounded by thick fibrous CT and extends into IS, hepatocytic cords are separated by sinusoids (S) (H and E, ×20). PV: Portal venule, BD: Bile ductile, CT: Connective tissue, IS: Interlobular septum, PT: Portal triad

Figure 15: Photomicrograph of 24 weeks of human fetal liver showing PT with a large PV, developing BD lined by cuboidal cells and hepatic arteriole (A) and lymphatics (L), fibrous CT extending into IS and sinusoids (S) (H and E, ×10). PT: Portal triad, PV: Portal venule, BD: Bile ductile, CT: Connective tissue, IS: Interlobular septum

large, circular, and well-defined with radiating pattern cords of hepatocytes separated by hepatic sinusoids filled with blood cells [Figures 18 and 19]. The focal hematopoietic activity sharply declined. The hepatic parenchyma was well-defined in the form of thick anastomosing plates of hepatocytes [Figure 20]. IS, well-formed PT, with a large oval PV, internally lined by a flat layer of endothelial cells, hepatic arteriole, lymphatic, and a bile ductule lined by cuboidal cells [Figure 21]. All these structures were enclosed in a sheath of thick fibrous CT and limited by a limiting plate of hepatocytes [Figure 21]. The stellate cells were present in sinusoids and near the limiting plate. The portal lobule was clearly seen with PT in between and CV at corners [Figure 22].

In Group E, the classical architecture of the hepatic lobule, portal lobule, and hepatic parenchyma with CV, PV, and hepatic sinusoids was clearly visible. [Figures 23-25] The KC and stellate cells were more in number [Figure 26]. The thickness of the capsule increased from Group A to E [Figures 25 and 27]. The hematopoietic activity was observed to become scanty [Figure 28].

Discussion

Elias[9] explained that the mammalian liver is made up of one-cell thick cribriform sheets or plates that form an anastomosis with one another, enclosing gaps between them containing the sinusoids.

Himabindu *et al*.[10] observed mesenchymal cells entrapped between the anastomosing cords of hepatocytes, compact sinusoids, and hematopoietic activity at 10 weeks. At
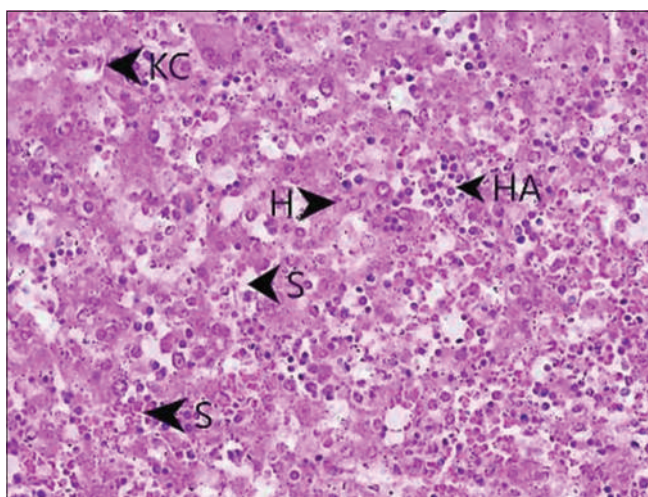
Figure 16: A photomicrograph of 23 weeks human fetal liver showing hepatocytes (H), HA, sinusoids (S), KC (H and E, ×40). HA: Hematopoietic activity, KC: Kupffer cells
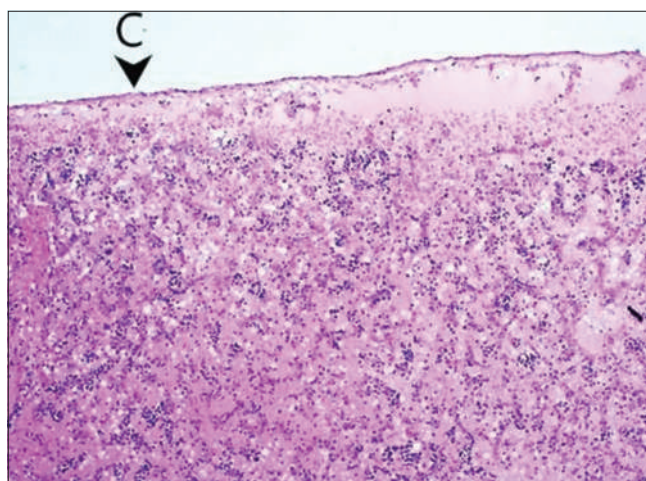
Figure 17: Photomicrograph of 28 weeks human fetal liver showing capsule (C) (H and E, ×10)
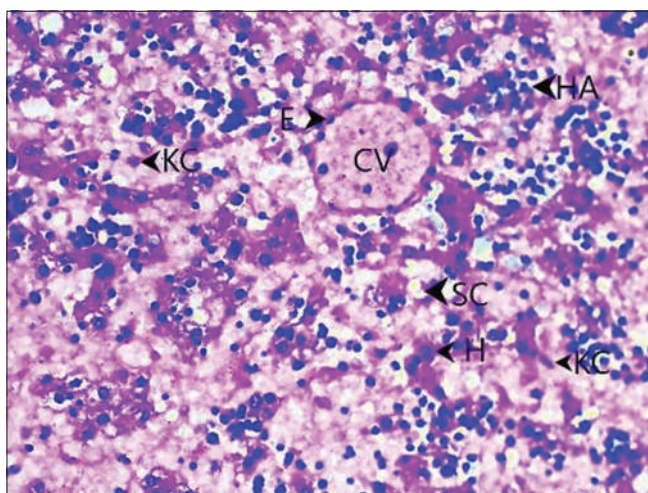
Figure 18: Photomicrograph of 28 weeks fetal liver showing well-defined CV lined by endothelium (E), hepatocytes (H) separated by sinusoids (S), SC, KC, and HA (H and E, ×40). CV: Central vein, SC: Stellate cells, KC: Kupffer cells, HA: Hematopoietic activity
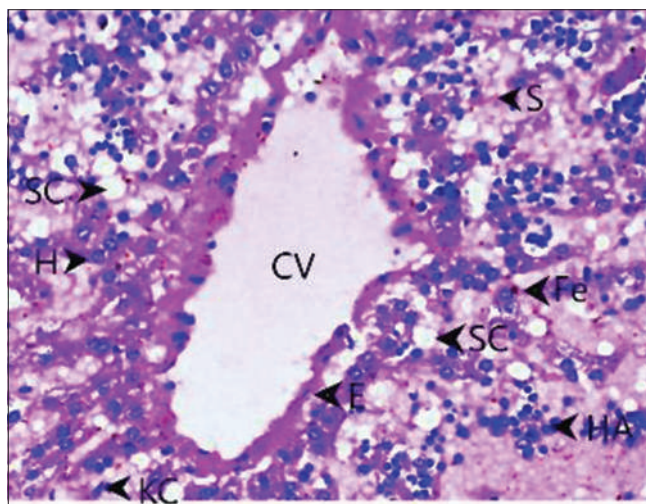
Figure 19: Photomicrograph of 28 weeks fetal liver showing CV lined by endothelium (E), hepatocytes (H) separated by sinusoids (S), excessive SC, KC, iron deposition (Fe) and HA, (H and E, ×40). CV: Central vein, SC: Stellate cells, KC: Kupffer cells, HA: Hematopoietic activity

12 weeks, CVs with radiating cords of the hepatic lamella, PT surrounded by thick CT were seen. Till 24 weeks, hematopoietic activity was dominant which became focal in 26 weeks. In 34 weeks, hepatic lobule and portal lobule were clearly distinguished, hematopoietic activity was highly reduced and large white round spaces of glycogen vacuoles increased. In a full-term liver, the glycogen storage was more.

Subhaana *et al.*[11] observed mesenchymal cells forming the hepatic parenchyma in Group A (12–16 weeks). In Group B (17–20 weeks), the CV and PT were surrounded by thick CT. In Group C (21–24 weeks), dominant hematopoietic activity in hepatic sinusoids was observed and the radiating pattern of hepatocytes from the CV was clearly demarcated. In Group D (25–28 weeks), the hematopoietic activity became focal. Simultaneously, areas in hepatic parenchyma show glycogen deposition in Group E. In Group F (33–36 weeks),

glycogen deposition increased, hematopoietic activity was reduced with clear demarcation of hepatic and portal lobule.

Hashmi *et al.*[12] observed CT elements around PT, capsule, and blood vessels from 12 weeks. CV appeared at 16–17 weeks, PT appeared at 18 weeks, and hepatic lobule in 28 weeks. Classical signs of liver lobule were visible in 22 weeks. From 12 to 36 weeks, a gradual decline in hematopoietic activity was seen.

As per Hamilton *et al.*[13], the hematopoietic activity begins in 6–7 weeks and reaches its peak at 24 weeks of fetal life.

Zamboni *et al.*[14] (1965) confirmed that erythropoiesis started in 7–9 weeks of intrauterine life, and it was fully established in 3rd month of intrauterine life.

Sahoo *et al.*[15] (2017) in 6–8 weeks, observed hepatocytes, CV, and hepatic sinusoids. In 10 weeks, CV with radiating cords of hepatocytes and PTs was seen. In 12 weeks, KC and
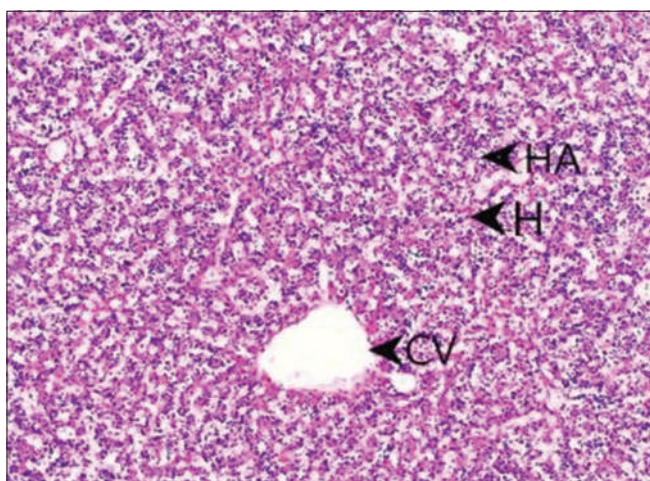
Figure 20: Photomicrograph of 31 weeks fetal liver showing well-defined CV, radiating cords of hepatocytes (H), sinusoids (S), and HA (H and E, ×40). CV: Central vein, HA: Hematopoietic activity
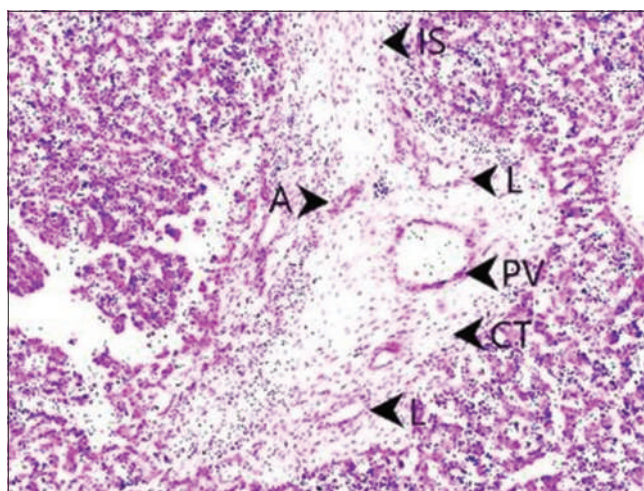
Figure 21: Photomicrograph of 31 weeks of human fetal liver showing PT with a large PV, developing BD lined by cuboidal cells and hepatic arteriole (A), lymphatics (L). Portal triad is surrounded by thick fibrous CT extending into IS (H and E, ×20). PV: Portal venule, BD: Bile ductile, PT: Portal triad, CT: Connective tissue, IS: Interlobular septum
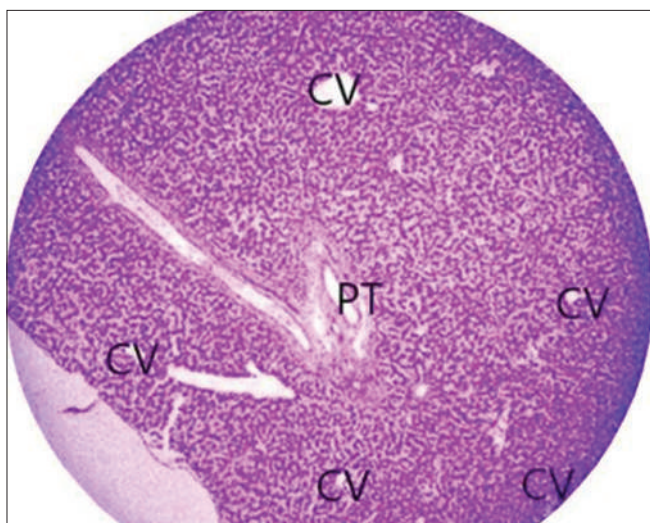
Figure 22: Photomicrograph of 31 weeks fetal liver showing portal lobule, with a centrally placed PT, and corners by CV (H and E, ×4). PT: Portal triad, CV: Centrally vein
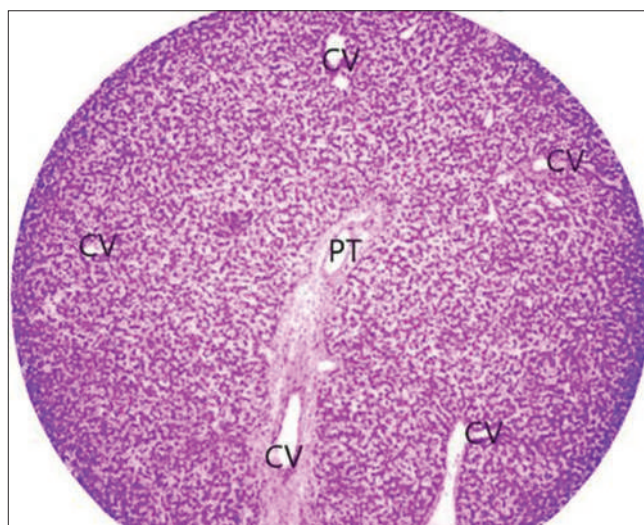
Figure 23: Photomicrograph of 32 weeks human fetal liver showing capsule (C) and PT, CV (H and E, ×10). PT: Portal triad, CV: Central vein

formation of hepatic lobule were observed and their number increases with advanced GA. KC with reticular fibers appeared in 20 weeks. In 24 weeks, the PT and CV were surrounded by thick fibrous CT. In 36 weeks, hepatocytes were binucleated.

Jaiswal, *et al.*[16] (2015) observed ill-defined hepatocytes at C/RL (Caudate/ right lobe ratio) 6.5 cm. The hepatic lobular pattern was seen at caudate-right lobe ratio (C/RL) 8.5 cm, KC at 6.5 cm, PT, CV, hepatic sinusoids, and hematopoietic activity appears occasionally at CRL 5–10 cm. Identifiable structures of PT, i.e., PV, bile ductule and hepatic arteriole were visible at CRL 10–15 cm. Well-defined oval-to-polygonal-shaped hepatocytes with abundant granular eosinophilic cytoplasm and large round nuclei with diffused chromatin were visible at CRL 28 cm.

In the present study, the range of crown-rump length of the studied samples is 10.5–40.4 cm (12–36 weeks).

At 10.5 cm, ill-defined hepatocytes, CV, PT, hepatic sinusoids, KC in sinusoids, and hematopoietic activity were observed. Hepatocytes were well-defined at CRL 19 cm, clusters of stellate cells at 19 cm, and PT was well-defined and surrounded by thick fibrous CT at CRL 19 cm. Hematopoietic activity increased up to CRL 22 cm.

Ansari *et al.*[17] at 12 weeks observed a thin fibrous capsule, irregular clumps of hepatic parenchyma, and hematopoietic activity. At 17–18 weeks, CV and PT were visible, and with advancement in GA, its size increased. At places, clumps of hepatocytes are seen, however, bile ductule was present occasionally. Hepatic sinusoids lined by the endothelium are seen in 15–16 weeks. At 22 weeks, radiating cords of hepatocytes, vacuoles of glycogen, and
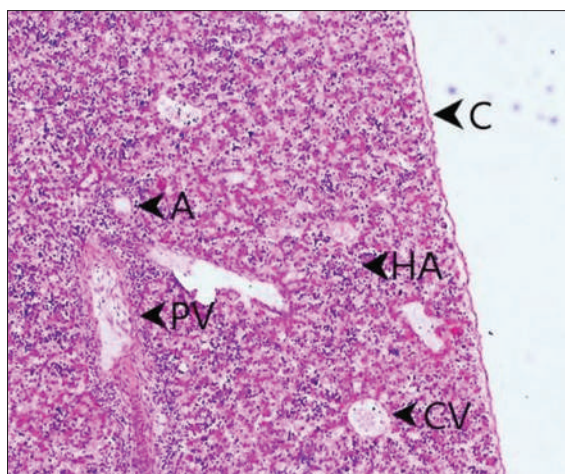
Figure 24: Photomicrograph of 34 weeks of human fetal liver showing portal triad with a large PV, developing BD lined by cuboidal cells and hepatic arteriole (A), CT (H and E, ×20). PV: Portal venule, BD: Bile ductile, CT: Connective tissue
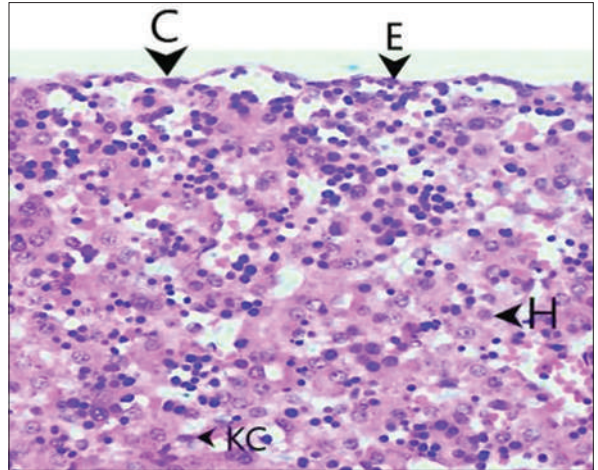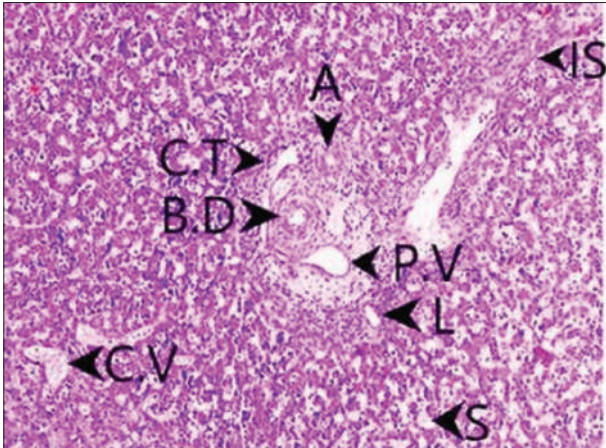

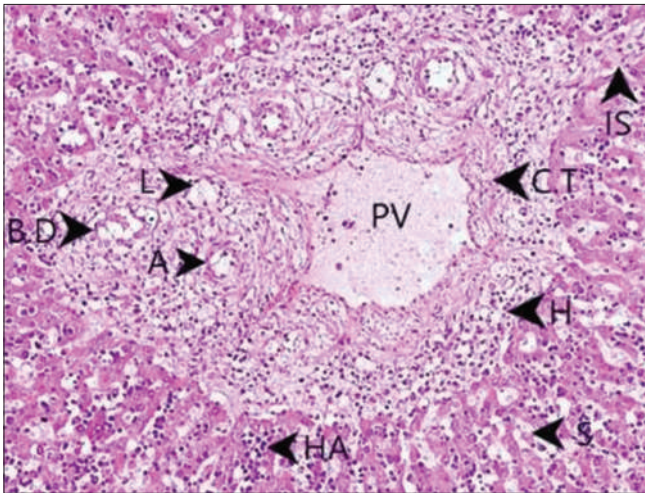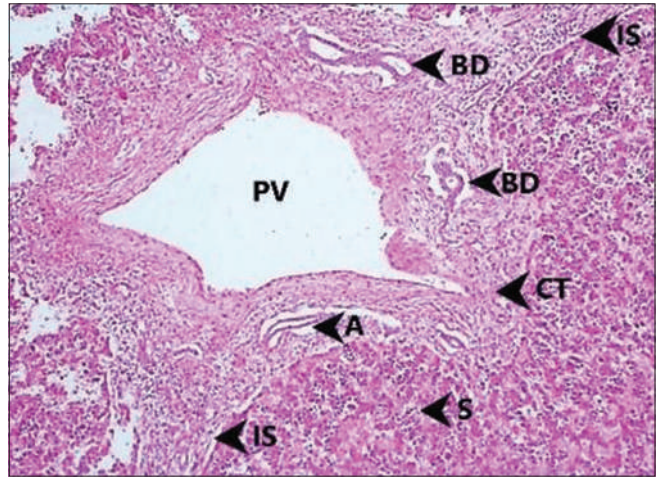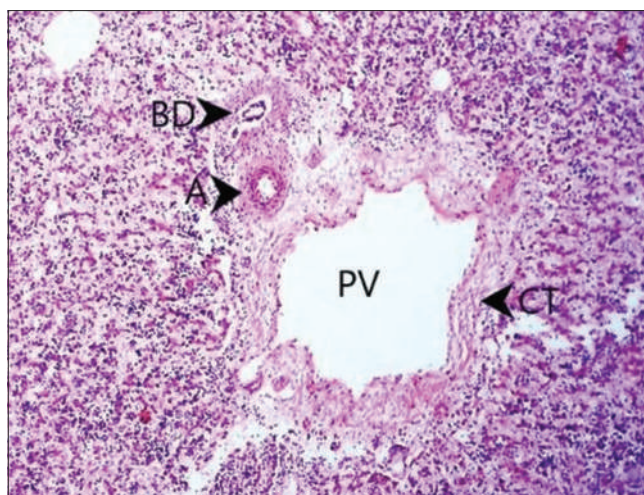Figure 25: Photomicrograph of 35 weeks human fetal liver showing capsule (C), flat endothelial cells (E), hepatocytes (H), and KC (H and E, ×40). KC: Kupffer cells
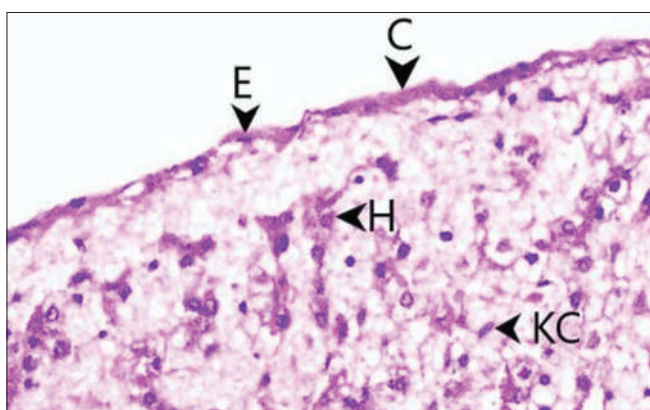
Figure 26: Photomicrograph of 36 weeks fetal liver showing well-defined CV lined by endothelium (E), presence of blood-filled sinusoids (S), hepatocytes (H), separated by sinusoids (S), and HA (H and E, ×10). CV: Central vein, HA: Hematopoietic activity
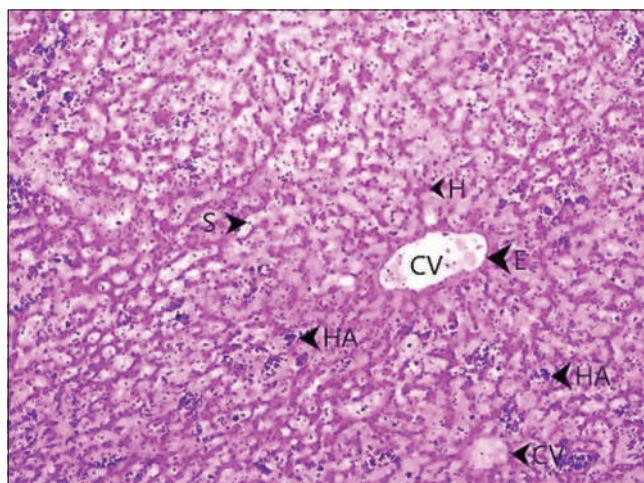
Figure 27: Photomicrograph of 36 weeks human fetal liver showing capsule (C), endothelial cells (E), sinusoids (S), hepatocytes (H), HA, KC, and PT (H and E, ×20). HA: Hematopoietic activity, KC: Kupffer cells, PT: Portal triad

KC, sharp, distinct PT and hepatic lobular architecture were visible. It became more defined in 23–27 weeks. At 28–36 weeks, hematopoiesis decreases after 34 weeks of gestation. Gradual decline in hematopoiesis is seen from 12 to 36 weeks whereas thickening of capsule increases. CT is present around the PT and blood vessels except for the CV.

Mall[18] explained that the hepatic lobule and liver lobule should not be structural units of liver parenchyma and it does not follow the growth pattern of the liver in prenatal life because it constantly mixes with nearby lobules.

The findings of the current study were in accord with the previous research. In our study, in Group A, hepatic sinusoids were lined by endothelial cells, KC, and glycogenated nuclei were present. Clusters of stellate cells and classical signs of hepatic and portal lobule appeared in Group B (17–21 weeks); it disappeared in

Group C (22–26 weeks) and then reorganized in Group D (27–31 weeks). However, glycogen vacuoles were predominantly seen. Hepatic lobule and portal lobule were sharply defined in Group E. In hepatic sinusoids, hematopoietic activity was seen at places. Hematopoietic activity was maximum till 21 weeks and then it decreased, becoming scanty and focal till 32 weeks. Furthermore, a sample of 34 weeks showed high hematopoietic activity and then declines after 36 weeks. Fibrous CT was seen enclosing the structures of PT, blood vessels, and CV in 15 weeks and higher. The capsule was lined by endothelial linings, and it thickens with advanced GA. In 15 weeks, the PT and CV appeared, and it became circular and sharply defined. At 24 weeks, white specks of glycogen granules started appearing and they were more in number around 36 weeks.
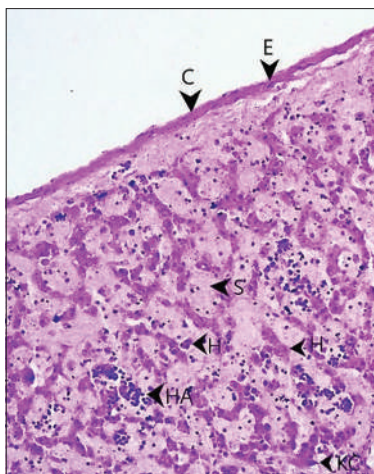
Figure 28: Photomicrograph of 32 weeks fetal liver showing well-defined CV lined by endothelium (E), presence of blood-filled sinusoids (S), and HA (H and E, ×40). CV: Central vein, HA: Hematopoietic activity

Conclusion

Change in general fetal morphometric parameters and liver parameters except biparietal diameter is directly proportional to the change in GA. The knowledge of morphological and histological features and normal limits of dimensions of the liver with respect to GA is a reliable reference help to prevent misdiagnosis of various pathological conditions of the liver such as cirrhosis, hepatomegaly, fetal anemia, intrauterine growth retardation, and congenital anomalies. Certain morphological changes, especially in needle biopsy specimen are slight but of immense importance, so pathologists must be aware of the histology of normal liver to point out these variations. Such type of studies can be used to recognize the evolving cell cultures used in various regenerative therapies of liver diseases.

References

1. Giancotti A, Monti M, Nevi L, Safarikia S, D'Ambrosio V, Brunelli R, *et al.* Functions and the emerging role of the foetal liver into regenerative medicine. Cells 2019;8:914.
2. Ross MH, Pawlina W. Histology: A Text and Atlas: With Correlated Cell and Molecular Biology. 6th ed. Philadelphia, PA: Lippincott Williams and Wilkins, Wolters Kluwer; 2006. p. 974.
3. Hamabe Y, Hirose A, Yamada S, Uwabe C, Okada T, Togashi K, *et al.* Morphology and morphometry of fetal liver at 16-26 weeks of gestation by magnetic resonance imaging: Comparison with embryonic liver at Carnegie stage 23. Hepatol Res 2013;43:639-47.
4. Lewis K, Yoshimoto M, Takebe T. Fetal liver hematopoiesis: From development to delivery. Stem Cell Res Ther 2021;12:139.
5. Standring S. Gray's Anatomy: The Anatomical Basis of Clinical Practice. 41st ed. New York, NY: Elsevier Limited; 2016. p. 1562.
6. Human Tissue Authority. Code of Practice and Standards; 2017. Available from: https://content.hta.gov.uk/sites/default/files/2020-11/Code%20E.pdf. [Last accessed on 2020 Aug 05].
7. Bancroft JD, Gamble M, editors. Theory and practice of histological techniques. Elsevier health sciences; 2008.
8. Feldman AT, Wolfe D. Tissue Processing and Hematoxylin and Eosin Staining in Histopathology. New York: Humana Press; 2014. p. 31-43.
9. Elias H. A re-examination of the structure of the mammalian liver; parenchymal architecture. Am J Anat 1949;84:311-33.
10. Himabindu A, Rao BN. Histogenesis of liver in human fetuses. Int J Appl Med Basic Sci 2015;5:132-9.
11. Subhaana CF, Talapala V, Seethamsetty S. Histogenesis of human fetal liver from 12 weeks to 36 weeks of gestation. Int J Res Med Sci 2020;8:931.
12. Hashmi IC, Wankhede HA. Morphology and histogenesis of developing human liver. Int J Anat Physiol Biochem 2015;2:6-11.
13. Hamilton WJ, Boyd JD, Mossman HW. Human Embryology: Prenatal Development of Form and Function. 4th ed. Cambridge, Baltimore: W. Heffer and Sons Ltd., The Williams and Wilkins Company; 1972. p. 646.
14. Zamboni L. Electron microscopic studies of blood embryogenesis in humans. I. The ultrastructure of the fetal liver. J Ultrastruct Res 1965;12:509-24.
15. Sahoo S, Haldar A, Giri SK. Histogenesis of human fetal liver of various weeks of gestation. Int J Med Health Res 2017;3:101-5.
16. Jaiswal A, Sinha DN, Singh AK. A study on histology of fetal liver. Natl J Clin Anat 2015;4:26-9.
17. Ansari MM, Ovhal AG, Rao SS, Ansari MM. Histogenesis of developing human liver in Marathwada region of Maharashtra. Indian J Clin Anat Physiol 2016;3:309-17.
18. Mall FP. A study of the structural unit of the liver. Am J Anat 1906;5:227-308.

Morphometric Evaluation of the Human Corpus Callosum using Magnetic Resonance Imaging: Sex Difference and Relationship to Age and Intracranial Size

Işik Tuncer,

Department of Anatomy, Medical Faculty, Aksaray University, Aksaray, Turkey

Abstract

Introduction: The objective of this study was to determine the normal values of corpus callosum (CC) subregions in healthy adult individuals in our population using magnetic resonance imaging (MRI) and to reveal gender differences during normal aging. **Material and Methods:** We performed the measurements of certain CC dimensions in 104 (44 males and 60 females) individuals. MRI imaging device was used for the measurements. The subregions of CC were measured with the midsagittal images. After the measurements of CC and its sections' (rostrum [R], genus [G], anterior body, posterior body, isthmus [I], and splenium [S]), length (L), width (W), and area (A) were carried out, the intracranial volume (ICV) and intracranial area (ICA) values were calculated. The Student's *t*-test and Pearson correlation test were used for statistical analysis. **Results:** Morphometric data of length, width, area, ICV, and ICA were collected. No significant difference was identified in CC morphometry by age among the patients ($P > 0.05$). Indicating longer diameters in males, the differences between the genders were significant ($P < 0.05$). Moreover, the mean of R-L, G-A, and G-W measurements was found significant between the age groups ($P < 0.001$). **Conclusion:** Sexual dimorphism in the CC is not a simple artifact of sex differences in brain size and may reflect differences in connectivity necessitated by differences in brain sizes.

Keywords: *Adult, age, corpus callosum, gender*

Introduction

Corpus callosum (CC) is the main transverse commissure that connects the cerebral hemispheres, and is composed of subregions such as genu, rostrum, trunk, and splenium.[1,2] It plays a critical role in the transmission of sensory, motor, and cognitive information between homologous areas in the hemispheres.[3,4] In addition, its susceptibility to certain toxins such as alcohol and certain white matter diseases such as multiple sclerosis is also significant and should not be ignored.[2,5]

CC develops between 8 and 20 weeks of gestation. At 11–12-week postconceptional age, interhemispheric crossing fibers start to transverse the massa commisuralis in the genu region. In addition, the rostrum develops at 18–20-week postconceptional age. Thus, the leading fibers of the future CC cross the midline in the 60–80-mm fetus (12–13-week postconceptional age) embryologically, and are effectively adult

like in the 140–60-mm fetus (18–20-week postconceptional age). It has been stressed that agenesis of CC or absent rostrum may be rare variations. While magnetic resonance imaging (MRI) is used for other purposes, absent rostrum is usually found by chance.[6,7]

In 1982, a sexual dimorphism of the human CC was described.[8] The authors found the female splenium to be more bulbous than its male counterpart. They postulated a morphologic substrate for previously described differences in visuospatial skills between males and females. However, their results could not be replicated by other research groups, either on autopsy brains[9,10] or on magnetic resonance (MR) scans.[11-16]

Accurate measurement of the size of this structure and its subregions in healthy men and women across the adult age range can estimate the normative aging process and sex differences and provide age and sex norms against which to compare patient groups. Current results indicate that brain

Access this article online

Website: https://journals.lww.com/joai

DOI:
10.4103/jasi.jasi_185_21

Quick Response Code:

How to cite this article: Tuncer I. Morphometric evaluation of the human corpus callosum using magnetic resonance imaging: Sex difference and relationship to age and intracranial size. J Anat Soc India 2023;72:114-21.

white matter volume including the CC expands greatly during childhood continuing into late adolescence and possibly beyond,[17,18] and its growth is singularly critical in determining maximum intracranial volume (ICV).[19] Once maturation is complete, however, cortical white matter volume remains relatively stable at least through the seventh decade[19,20] and others have found aging effects in elderly samples, especially those exceeding age 55 years.[21] Weis *et al*. reported aging effects in younger decades, but this group comprised headache clinic patients with negative MRI clinical report. Of these MRI studies, some have shown greater vulnerability to aging in anterior than posterior regions of the CC, particularly marked in women, while others find the greater vulnerability of men compared to women in the older decades.[22]

CC changes in schizophrenia were reported in several studies. An increase in the average width of the callosal trunk was found in chronic schizophrenics compared to a healthy group.[23] A replication analysis revealed that, compared to subjects with late-onset schizophrenia and patients with neurological or other psychiatric diagnoses, the mean CC midsection of 21 early-onset chronic schizophrenic brains had a significantly greater thickness.[24] In another replication analysis,[25] a significant increase in mean callosal thickness in the middle and anterior parts of the callosal body was observed, but not in the posterior parts. It was also found that increased callosal thickness in schizophrenia was associated with gender, and schizophrenic women had a highly significant increase in middle and anterior callosal thickness compared to control women. However, in another study,[26] patients with schizophrenia were identified to have significantly longer corpus callosum, but changes in the midsagittal profile area of the CC were not detected.

This study aims to report the normal values of CC subregions using MRI in healthy adult females and males in our population and to reveal the gender differences, if any.

Material and Methods

The research method used in this study was approved by our institutional review board and by the ethics committee (2019/1957). This study was conducted in Necmettin Erbakan University, Meram Faculty of Medicine, Department of Anatomy, in 2017. Measurements were made in Necmettin Erbakan University, Meram Faculty of Medicine, Department of Radiology. Before the MRI examination, written informed consent was received from all individuals. In this study, a retrospective cerebral MRI evaluation of 104 (43 males and 61 females) individuals over a 1-year period between October 2016 and October 2017 was used. The individuals with neurological symptoms, intracranial lesions on MRI, history of neurological disease, current or past psychiatric illness, alcoholism, or drug use problems were excluded from the study.

Morphometric measurements of the CC and section's length (L) (CCL, RL, GL, AL, PL, IL, and SL), width (W) (CCW, RW, GW, AW, PW, IW, and SW), area (A) (CCA, RA, AL, AW, AA, PA, and IA) [Figures 1 and 2].

A 1.5-T MRI system (Siemens; Avanto, Erlangen, Germany) was used for MRI procedures. A circularly polarized matrix coil was used for radiofrequency reception of the MRI signal. The brain MRI protocol contains axial T2-weighted turbo spin echo (SE) (TR/TE, 4500/118 ms; slice thickness, 6 mm; gap, 1.5 mm) and sagittal T1-weighted SE (TR/TE, 450/11 ms; slice thickness, 5 mm; gap, 1.5 mm).

The calculation of ICV was carried out through modeling the head as an oblate spheroid. x-, y-, and z-axes were represented by the distance between inner skull margins on three brain slices emerged from the spoiled gradient recalled echo sequence, which was the basis of these calculations. The length of the x-axis was specified as left. The right extreme was specified from an axial slice at the AC-PC line level. From the midsagittal slice mentioned above, the length of the y-axis was specified as the anterior and posterior extreme and the z-axis length was specified as the superior parietal lobe/dura margin and the inferior temporal lobe/dura margin from a coronal slice at the anterior commissure. Then, the voxel count was turned into a volume (cc) measure (ICV = 4/3π. x/2. y/2. z/2). Similarly, the midsagittal ICA was predicted from the midsagittal slice (ICA = π. y/2. z/2).

Statistical analysis

The data were analyzed using SPSS 20.0 (IBM Inc., Chicago, IL, USA) software program. Descriptive statistics were presented using frequencies and percentages for categorical variables, mean ± standard deviation (SD) for numerical variables, and percentile values. The Kolmogorov–Smirnov method was used to identify the normality of the continuous variables, Student's *t*-test was used for two independent samples, and the analysis of variance was used for several independent samples. Pearson correlation coefficients were calculated between measurements and gestational age. $P < 0.05$ was regarded to be significant as a 5% type I error.

Results

The study consisted of 104 individuals. The ages of the participants range from 20 to 80, and their mean age was 46.60 ± 16.36. 59.8% ($n = 61$) of the participants were female and 63.7% ($n = 65$) were over 40 years old. The study was conducted at two age groups: under and over 40 years. The measurements of CC were compared according to age groups and gender. The age of females was slightly higher (47.32 ± 15.85 years) than males (46.38 ± 17.98 years). RL value was found to be significantly higher in females ($P = 0.020$) while GA value was found higher in males. Intracranial area and volume

measurements were found to be higher in males and differences were significant ($P = 0.015$) [Table 1].

The measurement values of CC were compared according to age groups [Table 2]. The RL value was found to be significantly higher in women ($P < 0.001$). GW and GA ($P = 0.001$) values were higher in men. AW ($P = 0.042$) and AA ($P = 0.035$) values were significantly higher in men. Y and Z measurement results were higher in men. Although ICA and volume measurements were higher in men, the difference was statistically significant.

Males under 40 years generally had high results in the comparison of males according to age groups. GW was 16.70 ± 1.71 mm on men under 40 years and 14.49 ± 2.55 mm on men over 40 years ($P = 0.007$). GA was found 141.80 ± 20.48 mm in men under 40 years, and likely to decrease in men over 40 years as 115.36 ± 26.55 mm ($P = 0.003$). Intracranial area and volume were found significantly high on males under 40 years [Table 3 and Figures 3, 4].

Minimum and maximum values for each measurement were determined and added in the table. By contrast,
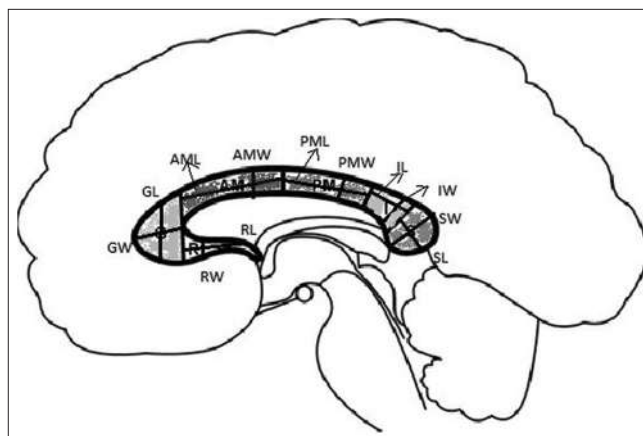
Figure 1: The schematic view of the corpus callosum showing the dimensions of the measured length (L), width (W), and area (A). The major corpus callosum subregions obtained from Witelson *et al.* (1989) (the rostrum [R], genu [G], anterior midbody [AM], posterior midbody [PM], isthmus [I], and splenium [S])

Table 1: Measurements of corpus callosum according to sex

	Mean±SD		P
	Male (*n*=43)	Female (*n*=61)	
CCL	67.82±3.99	69.43±13.49	0.472
CCW	17.39±3.72	17.38±2.31	0.985
CCA	637.38±105.33	622.97±89.13	0.467
RL	4.41±1.15	5.11±1.79	0.020*
RW	4.46±1.08	4.42±1.03	0.854
RA	15.67±6.01	16.85±6.77	0.377
GL	9.72±1.44	9.3±1.79	0.216
GW	15.28±2.5	15.34±2.22	0.914
GA	124.85±27.46	117.75±27.66	0.214
AL	10.23±1.03	10.12±1.02	0.510
AW	5.82±1.3	5.65±1.04	0.461
AA	66.61±15.71	68.74±13.48	0.469
PL	10.46±1.06	10.56±1.09	0.671
PW	5.92±1.34	5.58±0.88	0.116
PA	69.34±13.9	66.79±12.44	0.338
IL	9.94±1.16	9.97±1.16	0.904
IW	6.53±1.88	6.72±2.27	0.654
IA	73.07±17.1	70.41±12.65	0.370
SL	11.51±2.16	11.19±1.6	0.394
SW	18.77±3.43	18.23±2.35	0.346
SA	185.83±38.4	175.96±35.37	0.187
ICA	12440.12±2458.97	11754.46±1796.37	0.109
ICV	1144954.18±244807.72	1035063.26±164815.07	0.015*

*Significant at 0.05 level according to Student's *t*-test.
CCL: Corpus callosum length, CCW: Corpus callosum width, CCA: Corpus callosum area, RL: Rostrum length, RW: Rostrum width, RA: Rostrum area, GL: Genus length, GW: Genus width, GA: Genus area, AL: Anterior length, AW: Anterior width, AA: Anterior area, PL: Posterior length, PW: Posterior width, PA: Posterior area, IL: Isthmus length, IW: Isthmus width, IA: Isthmus area, SL: Splenium length, SW: Splenium width, SA: Splenium area, ICA: Intracranial area, ICV: Intracranial volume

Figure 2: The readological image of the corpus callosum showing the measured lengths and subregions
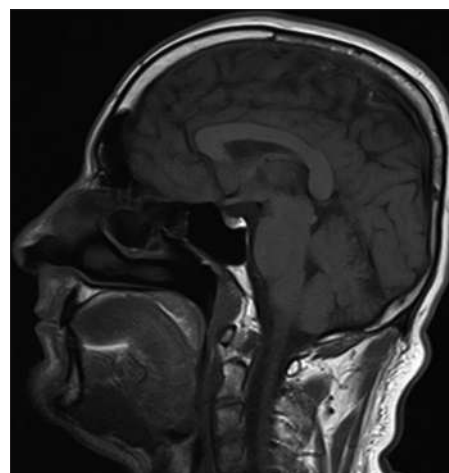
Figure 3: The radiological image of the corpus callosum of a man under 40 years

the CC values of the females under 40 years were lower. RL value was significantly higher in females over 40 years ($P < 0.001$). While those under 40 years had significantly higher GA and AW values, IL values were higher in females over 40 years ($P = 0.016$) and SA values were higher in females over 40 years [Table 4 and Figures 5, 6].

The correlation between the participants' measurements and age was examined. All males had negative significant correlations. The highest correlation was between GA and age ($r = -0.663$; $P < 0.001$) and the lowest was between ICA and age ($r = -0.316$; $P = 0.044$). There was a positive and significant correlation between RL and age in females ($r = 0.456$; $P < 0.001$), and there was a positive and low significant correlation between IL, SW, and age. There was also a negative and significant correlation between GA and AW both in females and males [Table 5].

Discussion

There was a considerable sexual dimorphism in total cross-sectional areas of the CC in this quantitative MRI
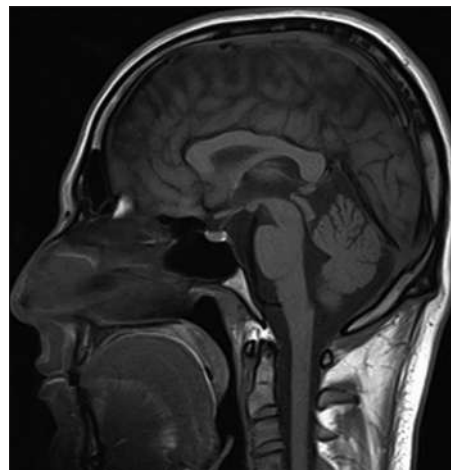
Figure 4: The radiological image of the corpus callosum of a man over 40 years
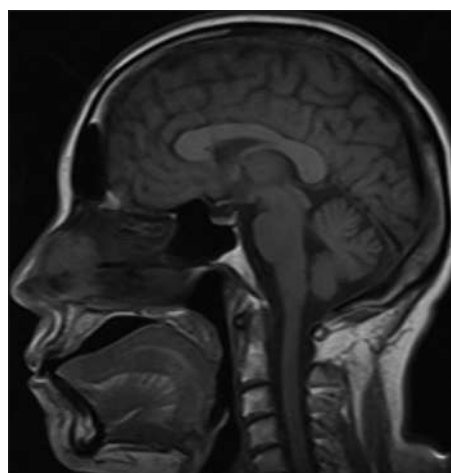
Figure 5: The radiological image of the corpus callosum of a man under 40 years

Table 2: Measurements of corpus callosum according to age groups

	Mean±SD		P
	<40 years (n=37)	>40 years (n=65)	
CCL	69.68±17.12	68.3±4.2	0.543
CCW	17.35±3.44	17.4±2.62	0.939
CCA	643.55±81.17	620.13±102.55	0.243
RL	4.11±1.01	5.24±1.73	<0.001*
RW	4.56±0.95	4.37±1.1	0.376
RA	15.68±5.75	16.79±6.87	0.417
GL	9.69±1.29	9.34±1.85	0.314
GW	16.31±2.04	14.75±2.3	0.001*
GA	132.51±21.45	113.72±28.62	0.001*
AL	10.12±1.02	10.56±1.04	0.312
AW	5.99±0.78	5.57±1.29	0.076
AA	71.44±10.07	65.9±16.02	0.063
PL	10.36±1.03	10.61±1.1	0.258
PW	5.82±1.07	5.66±1.11	0.486
PA	69.44±14.28	66.93±12.33	0.357
IL	9.76±0.95	10.07±1.24	0.202
IW	6.99±1.62	6.45±2.33	0.221
IA	74.5±15.84	69.82±13.71	0.124
SL	11.09±1.18	11.44±2.12	0.364
SW	18.25±2.81	18.56±2.86	0.600
SA	174.99±33.11	182.73±38.61	0.314
ICA	12446.14±2571.15	11803.87±1779.95	0.143
ICV	1128204.61±257546.3	1052793.1±169591.82	0.080

*Significant at 0.05 level according to Student's t-test.
CCL: Corpus callosum length, CCW: Corpus callosum width, CCA: Corpus callosum area, RL: Rostrum length, RW: Rostrum width, RA: Rostrum area, GL: Genus length, GW: Genus width, GA: Genus area, AL: Anterior length, AW: Anterior width, AA: Anterior area, PL: Posterior length, PW: Posterior width, PA: Posterior area, IL: Isthmus length, IW: Isthmus width, IA: Isthmus area, SL: Splenium length, SW: Splenium width, SA: Splenium area, ICA: Intracranial area, ICV: Intracranial volume

Figure 6: The radiological image of the corpus callosum of a woman over 40 years

Table 3: Measurements of corpus callosum on male patients according to age groups

Male	Mean±SD		*P*	Minimum-maximum
	<40 years (*n*=15)	>40 years (*n*=26)		
CCL	67.44±4.28	68.04±3.89	0.655	58.2-77.2
CCW	17.96±5.11	17.07±2.74	0.478	4-24.5
CCA	676.05±101.98	615.72±102.82	0.086	470-875
RL	4.25±1.13	4.50±1.17	0.527	2.6-7.6
RW	4.84±0.97	4.25±1.11	0.107	2.2-7.1
RA	16.70±6.37	15.09±5.85	0.429	5.5-37.7
GL	10.15±1.07	9.48±1.58	0.170	6.3-12.8
GW	16.70±1.71	14.49±2.55	0.007*	10-21
GA	141.80±20.48	115.36±26.55	0.003*	68-175
AL	10.43±0.86	10.58±1.12	0.510	8.3-13.48
AW	6.03±0.96	5.71±1.47	0.456	3.2-9.3
AA	71.98±12.53	63.52±16.73	0.097	27.9-104.3
PL	10.35±0.94	10.53±1.14	0.620	8.5-13.4
PW	6.17±1.14	5.78±1.44	0.371	3.1-9.3
PA	73.25±13.59	67.09±13.82	0.175	40-103.3
IL	10.15±1.07	9.82±1.22	0.398	7.5-12.6
IW	6.96±1.93	6.28±1.85	0.268	2-10.8
IA	79.19±18.65	69.55±15.41	0.082	44-117
SL	11.06±1.22	11.77±2.54	0.320	8.6-22
SW	19.34±3.43	18.44±3.45	0.426	10-26
SA	188.72±39.33	184.17±38.54	0.719	117-260
ICA	13767.60±1582.32	11674.26±2570.03	0.007*	10542.18-15912.26
ICV	1282008.83±186946.7	1065884.19±241961.35	0.005*	903688.86-1591226.4

*Significant at 0.05 level according to student's *t*-test. CCL: Corpus callosum length, CCW: Corpus callosum width, CCA: Corpus callosum area, RL: Rostrum length, RW: Rostrum width, RA: Rostrum area, GL: Genus length, GW: Genus width, GA: Genus area, AL: Anterior length, AW: Anterior width, AA: Anterior area, PL: Posterior length, PW: Posterior width, PA: Posterior area, IL: Isthmus length, IW: Isthmus width, IA: Isthmus area, SL: Splenium length, SW: Splenium width, SA: Splenium area, ICA: Intracranial area, ICV: Intracranial volume, SD: Standard Deviation

study. Since there was a powerful correlation between callosal sizes and overall brain size also demonstrated sexual dimorphism, we used several statistical modalities to eliminate these differences. IC size was used to predict a volume or an area in the study sample including males and females (covariation or calculation of standardized residuals) and to normalize the somatic size differences controlled for maximally reached brain size differences more sufficiently in males than females. The sex difference was observed due to inexistent correlation between the residuals and estimations of brain size in males, but not in females, which granted male advantage in corpus callosal size. If residualized modality was independently applied to both sexes, the size variation would be considered according to sex; however, it would prevent valid comparisons between the groups since both groups would have a mean of 0 and SD of 1.[5]

Witelson completely measured the midsagittal area of the CC in seven subdivisions in a sample of 50 brains acquired from autopsies. The researcher regarded two factors while examining callosal size: sex and hand preference, which was classified as consistent-right-hand (CRH) preference versus non (n)-CRH preference. The group of n-CRH had a larger overall callosal area, and the greatest difference occurred in the posterior body segments, especially the isthmus.[27]

Weber *et al*. analyzed the effect of mesial temporal lobe epilepsy (TLE) on CC thickness in a large sample of well-described participants (*n* = 96) and healthy control group (*n* = 28). They examined the differential effects on callosal structures according to the hemisphere and age of epilepsy onset. Epilepsy was generally determined to be associated with a decreased thickness in posterior callosal regions. Patients with an initial onset and especially those with left onset also had a smaller callosal thickness in more anterior and midbody regions. Their findings might reflect nonspecific as well as specific effects of TLE on CC development and interhemispheric connectivity.[28]

O'Dwyer *et al*. compared volume and diffusivity measures of the CC in participants with TLE and frontal lobe epilepsy (FLE) with those who were healthy.[29] They measured the volumes (cm³) of Witelson regions and the entire CC through high-resolution T1-weighted scans of 18 people in the control group and 44 patients. The CC of patients with TLE and FLE, which were adjusted in line

Female	Mean±SD		P	Minimum-maximum
	<40 years (n=15)	>40 years (n=26)		
CCL	71.10±21.72	68.46±4.44	0.470	60-167.6
CCW	16.96±1.79	17.62±2.55	0.293	10.6-21.3
CCA	622.86±58.23	623.03±103.65	0.994	400-975
RL	4.01±0.94	5.74±1.88	<0.001*	1.8-10.7
RW	4.39±0.92	4.44±1.1	0.842	1.8-6.5
RA	15.03±5.37	17.90±7.33	0.114	4.4-35
GL	9.40±1.35	9.24±2.02	0.748	6.1-12.9
GW	16.06±2.23	14.92±2.13	0.053	10.8-21.1
GA	126.59±20.32	112.63±30.2	0.037*	51-177.6
AL	10.22±1.03	10.35±0.52	0.268	7.6-12.8
AW	5.97±0.64	5.48±1.18	0.040*	3-8.6
AA	71.06±8.21	67.48±15.56	0.331	39-116.5
PL	10.36±1.11	10.66±1.08	0.303	7.8-13.1
PW	5.57±0.97	5.58±0.83	0.957	3.5-7.9
PA	66.73±14.46	66.83±11.41	0.977	35.6-96.4
IL	9.49±0.77	10.23±1.25	0.016*	7-12.9
IW	7.01±1.42	6.56±2.62	0.474	3.5-20.1
IA	71.15±12.93	70.01±12.65	0.742	44-101
SL	11.11±1.18	11.23±1.8	0.800	7.8-15.6
SW	17.47±2.03	18.64±2.44	0.086	14-24
SA	165.19±24.35	181.77±39.13	0.048*	105.6-285.6
ICA	11502.24±2751.57	11890.28±985.58	0.430	9825.42-14546.05
ICV	1018344.45±247383.9	1044065.7±98631.42	0.569	863324.16-1250960.3

Table 4: Measurements of corpus callosum on female patients according to age groups

*Significant at 0.05 level according to Student's *t*-test. CCL: Corpus callosum length, CCW: Corpus callosum width, CCA: Corpus callosum area, RL: Rostrum length, RW: Rostrum width, RA: Rostrum area, GL: Genus length, GW: Genus width, GA: Genus area, AL: Anterior length, AW: Anterior width, AA: Anterior area, PL: Posterior length, PW: Posterior width, PA: Posterior area, IL: Isthmus length, IW: Isthmus width, IA: Isthmus area, SL: Splenium length, SW: Splenium width, SA: Splenium area, ICA: Intracranial area, ICV: Intracranial volume, SD: Standard Deviation

with the total brain volume, was found to be smaller than that of controls. Therefore, atrophy and increased diffusivity in CC subregions, which connect homotopic contralateral cortical regions, were considered to indicate anatomical abnormalities extending beyond the epileptogenic zone in FLE and TLE.[28]

In addition, we found modest evidence for sex differences in relative size of the genu, body, and splenium of the CC. As defined geometrically in this study, the splenium is the smallest region in both sexes. In men, the body was larger than the genu, whereas in women, the genu and body were of similar size. This regional effect was sustained, although only at a trend level, when ratio measures were used. Our analysis, however, did not address shape differences (e.g., bulbosity), especially for the splenium, that have been reported as another dimension of the sexual dimorphism of the CC.

This study confirms several prior reports indicating that the CC area remains stable over the adult age range (at least up to age 76). A recently published study of the CC in elderly healthy twin men (age 68–78) from our laboratory also found no relationship between total CC area and age over that decade.[30] Genetic modeling showed that genetic

effects are stronger than environmental effects for the CC area, providing further evidence in support of the resilience of this structure against the passage of time alone.

It could be clearly demonstrated on MR scans that frontal callosal parts (i.e., rostrum, genu, and anterior parts of the trunk) are involved in normal aging. However, posterior callosal parts (i.e., posterior parts of the trunk and splenium) did not show age-specific changes. The macroscopical finding of the CC shows that frontal and parts of the temporal interhemispheric fiber systems are altered in normal aging. Some results that support this hypothesis already exist. Using stereologic procedures, a decrease in the volume of the frontal lobe could be demonstrated macroscopically.[31] A more exact evaluation of these macroscopic data revealed that mainly the orbital parts of the frontal lobe are changed. Histologic correlates for these macroscopic findings exist. Using variance analysis, we showed that in area 11 (after Brodmann) of the fronto-orbital cortex, neurons of layers 3 and 5 are lost during biologic aging.[32]

The normal development of the CC and its axons after birth were repeatedly examined in cats.[33-35] The CC is formed of very small, densely packed, nonmyelinated

Table 5: According to sex

Pearson correlation (age)	r (P)	
	Male	Female
CCL	0.096 (0.559)	−0.075 (0.569)
CCW	−0.187 (0.253)	0.205 (0.116)
CCA	−0.476 (0.002)*	−0.077 (0.557)
RL	0.072 (0.664)	0.456 (<0.001)*
RW	−0.451 (0.004)*	0.021 (0.874)
RA	−0.193 (0.239)	0.194 (0.137)
GL	−0.442 (0.005)*	−0.143 (0.277)
GW	−0.598 (<0.001)*	−0.191 (0.143)
GA	−0.663 (<0.001)*	−0.279 (0.031)*
AL	0.265 (0.061)	0.182 (0.131)
AW	−0.479 (0.002)*	−0.350 (0.006)*
AA	−0.444 (0.004)*	−0.204 (0.117)
PL	0.285 (0.071)	0.192 (0.141)
PW	−0.454 (0.003)*	−0.105 (0.426)
PA	−0.447 (0.003)*	−0.092 (0.484)
IL	0.026 (0.871)	0.391 (0.002)*
IW	−0.361 (0.020)*	−0.065 (0.622)
IA	−0.429 (0.005)*	−0.216 (0.097)
SL	0.089 (0.580)	0.048 (0.714)
SW	−0.144 (0.370)	0.340 (0.008)*
SA	−0.249 (0.116)	0.235 (0.070)
ICA	−0.316 (0.044)*	0.057 (0.667)
ICV	−0.397 (0.010)*	0.014 (0.916)

*Significant at 0.05 level according to Pearson correlation analysis. CCL: Corpus callosum length, CCW: Corpus callosum width, CCA: Corpus callosum area, RL: Rostrum length, RW: Rostrum width, RA: Rostrum area, GL: Genus length, GW: Genus width, GA: Genus area, AL: Anterior length, AW: Anterior width, AA: Anterior area, PL: Posterior length, PW: Posterior width, PA: Posterior area, IL: Isthmus length, IW: Isthmus width, IA: Isthmus area, SL: Splenium length, SW: Splenium width, SA: Splenium area, ICA: Intracranial area, ICV: Intracranial volume

fibers during birth. Myelination initiates at the 4th postnatal week. The CC is comprised of 60% myelinated axons that exhibit a diameter of 0.6–0.7 mm.[33] The findings of Looney and Elberger suggest that myelination starts and stops earlier in the anterior region of the CC and axons to be continuously lost between the 4th and 150th postnatal days.[35]

Conclusion

Certain differences exist between the averages of some indices of CC of our population and the other populations. Recent gender-specific normative standards for radiological indices of CC in our population are appropriate for routine MRI reading.

Financial support and sponsorship

Nil.

Conflicts of interest

There are no conflicts of interest.

References

1. Williams PL, Bannister LH, Berry MM, Collins P, Dyson M, Dussek JE, et al. Gray's Anatomy: The Anatomical Basis of Medicine and Surgery. 38th ed. New York: Churchill Livingstone; 1995.
2. Georgy BA, Hesselink JR, Jernigan TL. MR imaging of the corpus callosum. AJR Am J Roentgenol 1993;160:949-55.
3. Ota M, Obata T, Akine Y, Ito H, Ikehira H, Asada T, et al. Age-related degeneration of corpus callosum measured with diffusion tensor imaging. Neuroimage 2006;31:1445-52.
4. Hofer S, Frahm J. Topography of the human corpus callosum revisited-comprehensive fiber tractography using diffusion tensor magnetic resonance imaging. Neuroimage 2006;32:989-94.
5. Sullivan EV, Rosenbloom MJ, Desmond JE, Pfefferbaum A. Sex differences in corpus callosum size: Relationship to age and intracranial size. Neurobiol Aging 2001;22:603-11.
6. Griffiths PD, Batty R, Reeves MJ, Connolly DJ. Imaging the corpus callosum, septum pellucidum and fornix in children: Normal anatomy and variations of normality. Neuroradiology 2009;51:337-45.
7. Glenn OA, Goldstein RB, Li KC, Young SJ, Norton ME, Busse RF, et al. Fetal magnetic resonance imaging in the evaluation of fetuses referred for sonographically suspected abnormalities of the corpus callosum. J Ultrasound Med 2005;24:791-804.
8. DeLacoste-Utamsing C, Holloway RL. Sexual dimorphism in the human corpus callosum. Science 1982;216:1431-2.
9. Weber G, Weis S. Morphometric analysis of the human corpus callosum fails to reveal sex-related differences. J Hirnforsch 1986;27:237-40.
10. Demeter S, Ringo JL, Doty RW. Morphometric analysis of the human corpus callosum and anterior commissure. Hum Neurobiol 1988;6:219-26.
11. Bleier R, Houston L, Byne W. Can the corpus callosum predict gender, age, handedness, or cognitive differences? Trends Neurosci 1986;9:391-4.
12. Kertesz A, Polk M, Howell J, Black SE. Cerebral dominance, sex, and callosal size in MRI. Neurology 1987;37:1385-8.
13. Oppenheim JS, Lee BC, Nass R, Gazzaniga MS. No sex-related differences in human corpus callosum based on magnetic resonance imagery. Ann Neurol 1987;21:604-6.
14. Byne W, Bleier R, Houston L. Variations in human corpus callosum do not predict gender: A study using magnetic resonance imaging. Behav Neurosci 1988;102:222-7.
15. Weis S, Weber G, Wenger E, Kimbacher M. The controversy about a sexual dimorphism. Psychol Biol 1988;16:411-5.
16. Weis S, Weber G, Wenger E, Kimbacher M. The controversy about a sexual dimorphism of the human corpus callosum. Int J Neurosci 1989;47:169-73.
17. Aboitiz F, Scheibel AB, Fisher RS, Zaidel E. Fiber composition of the human corpus callosum. Brain Res 1992;598:143-53.
18. Yakovlev PL, Lecours AR. The myelogenetic cycles of regional maturation of the brain. In: Minkowski A, editors. Regional Development of the Brain in Early Life. Oxford: Blackwell Scientific Publications; 1967. p. 3-70.
19. Pfefferbaum A, Mathalon DH, Sullivan EV, Rawles JM, Zipursky RB, Lim KO. A quantitative magnetic resonance imaging study of changes in brain morphology from infancy to late adulthood. Arch Neurol 1994;51:874-87.
20. Raz N, Gunning FM, Head D, Dupuis JH, McQuain J, Briggs SD, et al. Selective aging of the human cerebral cortex observed in vivo: Differential vulnerability of the prefrontal gray

matter. Cereb Cortex 1997;7:268-82.

21. Salat D, Ward A, Kaye JA, Janowsky JS. Sex differences in the corpus callosum with aging. Neurobiol Aging 1997;18:191-7.

22. Weis S, Kimbacher M, Wenger E, Neuhold A. Morphometric analysis of the corpus callosum using MR: Correlation of measurements with aging in healthy individuals. AJNR Am J Neuroradiol 1993;14:637-45.

23. Rosenthal R, Bigelow LB. Quantitative brain measurements in chronic schizophrenia. Br J Psychiatry 1972;121:259-64.

24. Bigelow LB, Nasrallah HA, Rauscher FP. Corpus callosum thickness in chronic schizophrenia. Br J Psychiatry 1983;142:284-7.

25. Mathew RJ, Partain CL, Prakash R, Kulkarni MV, Logan TP, Wilson WH. A study of the septum pellucidum and corpus callosum in schizophrenia with MR imaging. Acta Psychiatr Scand 1985;72:414-21.

26. Nasrallah HA, Andreasen NC, Coffman JA, Olson SC, Dunn VD, Ehrhardt JC, *et al.* A controlled magnetic resonance imaging study of corpus callosum thickness in schizophrenia. Biol Psychiatry 1986;21:274-82.

27. Witelson SF. Hand and sex differences in the isthmus and genu of the human corpus callosum. A postmortem morphological study. Brain 1989;112:799-835.

28. Weber B, Luders E, Faber J, Richter S, Quesada CM, Urbach H, *et al.* Distinct regional atrophy in the corpus callosum of patients with temporal lobe epilepsy. Brain 2007;130:3149-54.

29. O'Dwyer R, Wehner T, LaPresto E, Ping L, Tkach J, Noachtar S, *et al.* Differences in corpus callosum volume and diffusivity between temporal and frontal lobe epilepsy. Epilepsy Behav 2010;19:376-82.

30. Pfefferbaum A, Sullivan EV, Swan GE, Carmelli D. Brain structure in men remains highly heritable in the seventh and eighth decades of life. Neurobiol Aging 2000;21:63-74.

31. Eggers R, Haug H, Fischer D. Preliminary report on macroscopic age changes in the human prosencephalon. A stereologic investigation. J Hirnforsch 1984;25:129-39.

32. Weiss H, Haug U. Trauma, Guilt and Reparation. 1st ed. London, UK: Routledge Publication; 2019.

33. Fleischhauer K, Wartenberg H. Electron microscopic studies of the growth of nerve fibers and of the appearance of myelin shealth in the corpus callosum of the cat. Z Zellforsch Mikrosk Anat 1967;83:568-81.

34. Looney GA, Elberger AJ. Myelination of the corpus callosum in the cat: Time course, topography, and functional implications. J Comp Neurol 1986;248:336-47.

35. Berbel P, Innocenti GM. The development of the corpus callosum in cats: A light- and electron-microscopic study. J Comp Neurol 1988;276:132-56.

To Estimate Age- and Gender-Related Morphometric Change in Cella Media Index of the Lateral Ventricles by Computed Tomography Scan in Adult Human Population of North India

Abstract

Background and Aim: Several histopathological and gross changes are seen in human brain as age increases, causing enlargement of the lateral ventricles. Morphometric measurement and size of the lateral ventricle of the brain are of great importance to identify certain changes and correlate it with clinical significance. This study was designed to provide a normal data of the cella media index (CMI) measurements of the lateral ventricle of the brain and its association between both the genders and its correlation with different age groups of North Indian Population, which will be helpful for diagnosis of cerebral atrophy. **Subjects and Methods:** This study was carried out in the Department of Anatomy and Department of Radiodiagnosis, S. N. Medical College, Agra, Uttar Pradesh. In the present prospective study, computed tomography scans of 200 patients between the age of 18 and 75 years (126 males and 74 females) were done, and measurements of the lateral ventricle of the brain were analyzed statistically. **Results:** In our study, the overall mean CMI was 4.62 ± 0.5 (CMI in male was 4.53 ± 0.41 and mean CMI in female was 4.42 ± 0.28), difference being statistically significant between both genders as $P = 0.04$ ($P \leq 0.05$). In our finding, $r = -0.13$, indicating a mild positive correlation between age and transverse diameter of CMI of the lateral ventricle in North Indian population. **Conclusion:** This study concludes that with increase in age, there is a decrease of cella media ratio/Schiersmann's Index, which is helpful in diagnosis of neurological conditions (e.g. schizophrenia, bipolar disorder, and Alzheimer's disease).

Keywords: *Brain, computed tomography, lateral ventricle, morphometry, ventricular system*

**Jyoti Sharma,
Pradeep Singh,
Anjali Gupta,
Anshu Gupta**

*Department of Anatomy,
S. N. Medical College, Agra,
Uttar Pradesh, India*

Introduction

Anatomists and researchers have always been enthralled to study human brain. Human brain structure is complex and no one is completely aware of its function. Structural changes occur which are normal and expected as age increases. Before any aberrant finding is interpreted, a comprehensive knowledge of normal changes occurring in the brain with increase in age is necessary to be understood as histopathological, and the gross changes are commonly seen as the age increases.[1]

Knowing normal ventricular size will be helpful for clinicians, neurosurgeons, and radiologists in diagnosing cerebral atrophy which may later result in pathological diseases like hydrocephalus schizophrenia, Alzheimer's, dementia, or any other neurological disorders.[2] Sometimes, cortical atrophy and enlargement of

ventricles are major changes that may occur without neurologic deficits.[3]

Computed tomography (CT) scan is preferred as it is noninvasive and no artifacts are produced; hence, with this, measuring ventricles became effortless.[4-6]

This study aimed to determine the association of both the genders and correlation of age with increase or decrease in size of the lateral ventricle of the brain in adult human population of North India using cella media index (CMI) parameter. The latera;l ventricle have two c shaped cavities, one on each side of the cerebral hemisphere. It consists of a central part called body and three extensions: anterior (frontal horn), posterior (occipital horn), and inferior (temporal horn). Each lateral ventricle communicates with the third ventricle with a common interventricular foramen or the foramen of Monro.[7]

How to cite this article: Sharma J, Singh P, Gupta A, Gupta A. To estimate age- and gender-related morphometric change in cella media index of the lateral ventricles by computed tomography scan in adult human population of North India. J Anat Soc India 2023;72:122-5.

The frontal horn is located in front of the interventricular foramen or foramina of Monro in the frontal lobe. It is triangular in shape with boundaries anterior part of the trunk of the corpus callosum as roof, head of the caudate nucleus as head, and the septum pellucidum as medial wall.[7]

The occipital horn of the lateral ventricle extends backward into the occipital lobe with its roof and lateral wall formed by the tapetum, optic radiation, and inferior longitudinal fasciculus; and the bulb of the posterior horn (floor and medial wall) is raised by forceps major and calcar avis.[7]

The temporal horn or inferior horn projecting form the posterior end of the central part runs downward and forward into the temporal lobe and reaches the uncus. In cross section, it is a narrow cavity with boundaries: roof and lateral wall formed by the tapetum, tail of caudate lobe, stria terminalis, amygdaloid body, and floor by hippocampus.[7]

The body of the lateral ventricle communicates with the atrium posteriorly. The roof is formed by the body of the corpus callosum, and the floor is formed by the thalamus. The septum pellucidum and body of the fornix form the superior and inferomedial walls, respectively. The lateral wall is formed by the caudate nucleus and thalamus.[8]

The atrium is a triangular cavity that communicates with the body, temporal horn, and occipital horn.[8]

Subjects and Methods

This cross-sectional study composed of 200 patients (126 males and 74 females) belonging to the age group of 18–75 years, attending the department of radiology for CT scan procedure. It was conducted only after the clearance by the Ethics Committee of our college. These patients were selected randomly over the span of 1½ years from 2020 December to 2022 June. Individuals with a history of drug abuse, trauma, hydrocephalus, cerebral infarct, mass lesions, previous cranial surgeries, and individuals below 18 years of age were not considered for this research. Before undergoing CT procedure, patients fasted for about 4–6 h.

Reports interpreted as normal scans by radiologist were only taken up for this study. Any additional scan was avoided to minimize the exposure of radiation.

Procedure of computed tomography scan

In this study, CT scanner utilized was 64 Slice GE Optima 660 CT scan machine. Exposure factors for the CT scan were set at 140 kvp and 160 mAs, and slice thickness set at 5 mm. With iterative reconstruction algorithm, all CT scans were carried out in axial mode.

Methodology

Procedure was explained to the patient, consent was taken before CT scan, and patient was asked to remove any metallic item (e.g. earrings, hairpin, etc.) or dentures before entering CT scan room.

Patient was asked to lie down on the CT table in supine position, head was centralized, and for its correct positioning, support was provided. To confirm correct positioning of patients, lateral scout image was captured to verify suitable exposure factors [Figure 1].

The orbitomeatal line was drawn; it is defined as the imaginary line drawn from the outer canthus of the eye to the midpoint of the external auditory meatus [Figure 2].

The scans were obtained from the base of the skull considering the lowest tomographic section to the vertex of the skull running parallel to the orbitomeatal line. CT scan total duration was 20–30 s. Without coinciding, 8–10 axial images of the brain were obtained. Patients' CT scan was read by the radiologist, and if they found to have no pathological disease and reported as normal CT, such patients reports were viewed in DICOM Image Software. In the DICOM software, a measurement tool is installed which helps in recording of measurement of any CT image in mm.

For the measurement of CMI, the maximum outer table transverse diameter of the skull or biparietal diameter (BPD) of the skull is measured; then, the maximum width of the lateral ventricles of the brain/cella media (C) is measured in mm [Figure 3]. After recording the measurements, BPD/C is to achieve the final value of CMI for each patients.

Measurements taken

Cella media index/Schiersmann's index

CMI or the Schiersmann's Index is defined as the ratio of maximum outer table transverse diameter of the skull or BPD of the skull (A to B = BPD) to the maximum width of the lateral ventricles of the brain (X to Y = C). Both the measurements are taken at the same level. CMI formula is BPD/C. The normal value of CMI is more than 4 (ranges 4–6). CMI is helpful in assessing cerebral atrophy.[9]

Results

Data analysis of 200 patients was performed using SSPS 16th version Statistical package for socialsciences it is a software produced by ibm corporation. The overall mean and standard deviation were calculated. ANOVA test was carried out between male and female groups for calculating "*P*" value. "*r*" value was achieved by performing the Pearson's correlation between different age groups and CMI readings.

Of 200 patients, 126 were male and 74 female [Table 1]. In different age group, CMI, i.e. (BPD/C), p value was found significant as $p < 0.05$* signifying that there is statistical difference in the size of CMI in different age groups of North Indian Population [Table 2].

Table 1: Different age group distribution age and gender wise

Age group (years)	Male, *n* (%)	Female, *n* (%)	Total, *n* (%)
18-30	33 (26.19)	21 (31.34)	54 (27.00)
31-40	24 (19.05)	23 (34.33)	47 (23.50)
41-50	28 (22.22)	12 (17.91)	40 (20.00)
51-60	16 (12.70)	12 (17.91)	28 (14.00)
61-75	25 (19.84)	6 (8.96)	31 (15.50)
Total	126 (100.00)	74 (110.45)	200 (100.00)

Table 2: Different age group distribution of parameters biparietal diameter, C and biparietal diameter/C

Age group (years)	*n*	Mean±SD		
		BPD	C	BPD/C
18-30	54	111.44±6.97	24.74±3.07	4.56±0.47
31-40	47	111.00±7.03	24.41±2.99	4.60±0.47
41-50	40	111.75±7.17	24.84±3.08	4.55±0.45
51-60	28	110.82±7.18	24.22±3.44	4.64±0.52
61-75	31	109.52±5.71	25.56±2.51	4.31±0.36
F		0.538	0.925	2.517
P		0.70 (NS)	0.45 (NS)	0.04*
r		−0.07	0.07	−0.13

*Significant value is <0.05, BPD: Biparietal diameter, SD: Standard deviation, NS: Not significant

Table 3: Gender-wise distribution of parameters biparietal diameter, C and biparietal diameter/C

Sex	*n*	Mean±SD		
		BPD	C	BPD/C
Male	126	112.18±5.77	24.77±2.12	4.53±0.41
Female	74	110.33±6.83	24.97±2.89	4.42±0.28
Overall data	200	111.02±6.85	24.74±3.03	4.54±0.46
t		−2.04	0.56	−2.04
P		0.04*	0.57 (NS)	0.04*

*Significant at *P*<0.05, NS at *P*>0.05. NS: Not significant, BPD: Biparietal diameter, SD: Standard deviation

CMI (BPD/C) in relation to both the genders is also found to be significant as $P < 0.05*$ stating that there is a considerable difference between both the genders [Table 3].

In correlation of CMI (BPD/C) with increase in age, the Pearson's correlation coefficient (r) showed a mild positive correlation, indicating with increase in age, there is atrophy of CMI as r = −0.13 [Table 2].

The mean CMI value of male was 4.53 ± 0.41 and female was 4.42 ± 0.28, indicating males have larger skull size than females [Table 3].

Discussion

In our study, the mean of CMI was 4.62 ± 0.51, which is similar to Robert Chrzan's study; the mean was 4.61 (2.83–8.11, SD 1.03) for 70–99 years of age.[10] However, in Goldstein's study, the mean CMI was 3.86 (1/0.259),
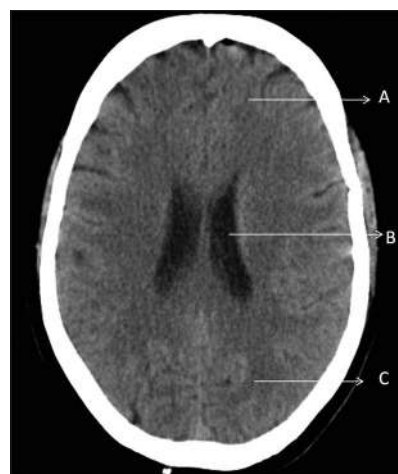
Figure 1: Axial CT image of the brain (Slice Number – 64.3 coi). Taken at the caudate nucleus/mid ventricular level showing body of the lateral ventricle of the brain (at this level, the cella media index measurement is taken). A: Frontal lobe of the brain, B: Body of the lateral ventricle, C: Occipital lobe of the lateral ventricle. CT: Computed tomography
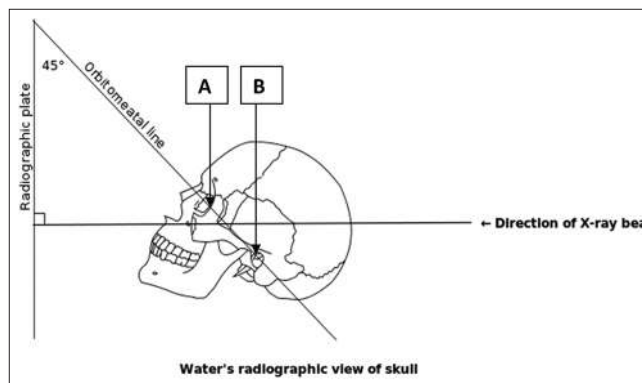
Figure 2: Orbitomeatal line. A: Outer canthus of the eye, B: External auditory meatus
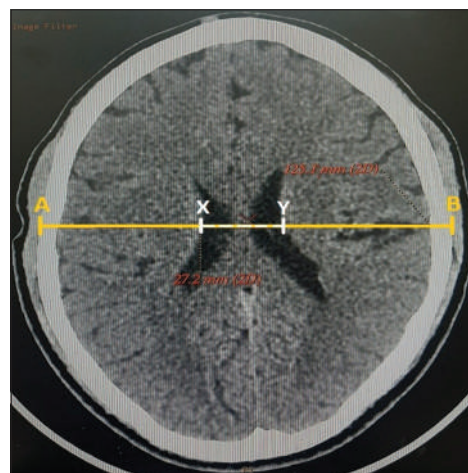
Figure 3: Axial CT image of the brain at the mid-ventricular or caudate nucleus level showing body of the lateral ventricle of the brain. (A-B): Maximum outer table transverse diameter of the skull/biparietal diameter (BPD), (X-Y): Maximum width of the lateral ventricle of the brain cella media index (C). CT: Computed tomography

which is close to the value of 3.92 (1/0.255) in the control group.[11]

According to Mondorf *et al.*,[12] if CMI is usually >4.1, it is normal; if CMI is between 4.0 and 3.6, it indicates mild hydrocephalus; if CMI is 3.5–3.0, it indicates moderate hydrocephalus; and <2.9 indicates severe hydrocephalus; while according to Goyal *et al.*'s study,[13] if the CMI is between 3.5 and 2.3, it indicates mild hydrocephalus; if the CMI is between 2.4 and 1.6, it indicates moderate hydrocephalus; and if the CMI is between 1.9 and 1.2, it indicates severe hydrocephalus.

While in our study, if the CMI is between <4 and 3.0, suggests mild hydrocephalus or ventriculomegaly; if the CMI is between 3 and 2, suggests moderate hydrocephalus or ventriculomegaly; and if the CMI is <2, suggests severe hydrocephalus or ventriculomegaly. While if the CMI is more than 6, it may indicate Alzheimer's, schizophrenia, and bipolar disorders.

In our study, the *P* value of CMI in correlation with both the genders is found significant as $P < 0.05$ indicating that there is a significant difference between males and females.

In our study, the *P* value of CMI in correlation with age is also found significant as $P < 0.05$ indicating that with increase in age, there is a significant difference in the size of CMI, which is found to be similar to Robert Crzhan's study.

In Robert Crzhan's study, the *P* value of CMI in correlation with age was 0.0001, interpreting a strong change in the size of CMI with increase in age as $P < 0.05$. Because of incorporation of centenarians' age group (70–99 years) in Crzhan's study, the *P* value was < 0.001.[10]

The Pearson's correlation coefficient (*r*) of CMI analyzed in our study in relation to increase in age was $r = -0.13$, indicating that with increase in age, there is a mild atrophy in the transverse diameter of the lateral ventricle of the brain which was similar to Crzhan[10] and Goldenstein's study.[11] The Pearson's correlation in Crzhan's study was $r = -0.36$, showing mild atrophy with increase in age.[10]

CMI will be useful to radiologist and psychiatrist as CMI gives a value which will be beneficial to detect ventriculomegaly, hydrocephalus, Alzheimer's, schizophrenia, or any other pathological disorders.

Conclusion

With this study, it has been concluded that with increase in age, there is a significant atrophy of transverse diameter of the lateral ventricle of the brain, and a statistically significant difference is present between both the genders in relation to BPD. If the CMI is found to be <4, it may indicate early diagnosis of obstructive hydrocephalus and ventriculomegaly. If the CMI is more than 6, it may indicate Alzheimer's, schizophrenia, and bipolar disorders. Hence, CMI marker will be helpful in early diagnosis of neurological lesions by the clinicians and radiologists.

Conflicts of interest

The authors declare that they have no conflict of interest.

References

1. Schochet SS Jr. Neuropathology of aging. Neurol Clin 1998;16:569-80.
2. Srijit D, Shipra P. Anatomical study of anomalous posterior horn of lateral ventricle of brain and its clinical significance. Bratisl Lek Listy 2007;108:422-4.
3. Barrett L, Drayer B, Shin C. High-resolution computed tomography in multiple sclerosis. Ann Neurol 1985;17:33-8.
4. Anik Y, Demirci A, Anik I, Etus V, Arslan A. Apparent diffusion coefficient and cerebrospinal fluid flow measurements in patients with hydrocephalus. J Comput Assist Tomogr 2008;32:392-6.
5. Hashimoto M, Ishikawa M, Mori E, Kuwana N, Study of INPH on neurological improvement (SINPHONI). Diagnosis of idiopathic normal pressure hydrocephalus is supported by MRI-based scheme: A prospective cohort study. Cerebrospinal Fluid Res 2010;7:18.
6. Moore DW, Kovanlikaya I, Heier LA, Raj A, Huang C, Chu KW, *et al*. A pilot study of quantitative MRI measurements of ventricular volume and cortical atrophy for the differential diagnosis of normal pressure hydrocephalus. Neurol Res Int 2012;2012:718150.
7. Gupta D. Neuroanatomy. In: Prabhakar H, editor. Essentials of Neuroanesthesia. Ch. 1. Newdelhi: Academic Press; 2017. p. 3-40.
8. Scelsi CL, Rahim TA, Morris JA, Kramer GJ, Gilbert BC, Forseen SE. The lateral ventricles: A detailed review of anatomy, development, and anatomic variations. AJNR Am J Neuroradiol 2020;41:566-72.
9. Keats TE, Sistrom C. Atlas of Radiologic Measurement. United States: Mosby; 2001
10. Chrzan R, Gleń A, Bryll A, Urbanik A. Computed tomography assessment of brain atrophy in centenarians. Int J Environ Res Public Health 2019;16:3659.
11. Goldstein SJ, Wekstein DR, Kirkpatrick C, Lee C, Markesbery WR. Imaging the centenarian brain. A computed tomographic study. J Am Geriatr Soc 1985;33:579-84.
12. Mondorf Y, Gaab MR, Oertel J. The course of the cella media index according to schiersmann after ETV in different causes for obstructive hydrocephalus. General Society of Neurosurgery 2009.
13. Goyal S, Goyal S, Yadav P, Mishra S. CT evaluation of various linear indices in children with clinically suspected hydrocephalus. J Evol Med Dent Sci 2017;6:3078-82.

Anatomical and Morphological Variations in the tendons Constituting the Pes Anserinus of Knee with its Clinical Significance: A Human Cadaveric Study

Abstract

Context: Pes anserinus (PA) includes conjoined tendinous insertion of the sartorius, gracilis, and semitendinosus muscles. Each tendon can have individual insertions attached nearly in a linear arrangement. The presence of accessory tendons, bands, and structures constituting in forming PA shows high variability and has been reported clinical importance in harvesting PA graft and tendon reconstruction procedure. **Aim:** The present study aimed to macroscopically observe anatomical and morphological variations in the structures constituting in the insertion of the PA tendon and establish its clinical significance. **Subjects and Methods:** A total of ninety cadaveric lower limbs including both sexes dissected to observe variations in the structures forming PA at the anteromedial surface of the upper part of the tibia. **Statistical Analysis Used:** The descriptive statistical analysis was done. **Results:** PA was constituted of sartorius, gracilis, and semitendinosus tendons in all the specimens. The most common pattern observed was monotendinous-sartorius, gracilis, and semitendinosus in 67 (74.44%) limbs. The semimembranosus and tibial collateral ligament participation was observed in 5 (5.55%) and 2 (2.22%) limbs, respectively. The accessory band of sartorius and semitendinosus was observed in 2 (2.22%) and 14 (15.55%) limbs, respectively. **Conclusions:** PA in the medial side of the knee is a common injury site. The presence of any accessory structures or bands within can handicap graft harvesting since the gracilis and semitendinosus tendons are routinely harvested for the reconstruction procedure. Furthermore, present anatomical knowledge can be helpful to surgeons for preoperative radiological examination and to avoid complications during transplant graft surgeries of the knee.

Keywords: *Anserine bursitis, anterior cruciate ligament reconstruction, gracilis tendon, guy ropes, hamstring graft, knee joint, pes anserinus, sartorius tendon, semitendinosus tendon*

Meghana Harshadbahi Joshi, Minal K Ravat[1], Vasant H Vaniya[2]

Department of Anatomy, Dr. Kiran C. Patel Medical College and Research Institute, VNSGU, Bharuch, Surat, [1]Department of Anatomy, GMERS Gotri Medical College, [2]Department of Anatomy, Government Medical College, Baroda, The M. S. University, Vadodara, Gujarat, India

Introduction

Pes anserinus (PA) in Latin means "goose foot." The PA is formed by the tendinous insertion of sartorius (S), gracilis (G), and semitendinosus (ST) muscles in the anterior to posterior aspect on the anteromedial surface of the upper part of the tibia, lying superficial to the tibial collateral ligament.[1] The radiating arrangement of insertion pattern of tendons of PA resembles to the goosefoot, hence the name PA. It is also known as guy ropes. The muscles of PA arise from the three different compartments of thigh and have a common tendinous insertion on the anteromedial aspect of tibia separated by a complicated anserine bursa.[2]

- Sartorius is a long, narrow, and ribbon-like muscle of anterior compartment of thigh. It runs obliquely extending from the hip bone to the leg on tibia below the knee. It arises from the anterior superior iliac spine and upper half of the notch below the spine and is inserted on the anteromedial aspect of the tibia, forming a most superficial component of PA

- Gracilis is a long, slender, and most superficial muscle of medial (adductor) compartment of the thigh. The muscle lies on the medial aspect of the thigh and extends from the hip bone above to the tibia bone below the knee. It arises from the anterior surface of the body of pubis from its lower half, inferior pubic ramus and ramus of ischium and it inserts on the anteromedial aspect of the tibia; where it lies between sartorius and semitendinosus muscle and forming a component of PA

Access this article online

Website: https://journals.lww.com/joai

DOI: 10.4103/jasi.jasi_41_22

Quick Response Code:

How to cite this article: Joshi MH, Ravat MK, Vaniya VH. Anatomical and morphological variations in the tendons constituting the pes anserinus of knee with its clinical significance: A human cadaveric study. J Anat Soc India 2023;72:126-30.

- Semitendinosus is a fusiform muscle of the posterior compartment of thigh. It arises from the posteromedial impression of ischial tuberosity and inserts on the anteromedial aspect of the tibia, forming a component of PA.[1]

The anatomical knowledge and relationship of the structures in the medial aspect of the knee and the tendons forming PA is essential for the accurate diagnosis and for the development of improved surgical and operative procedures in the various pathologies related to the knee.[3] The lack of morphological and anatomical knowledge of the PA tendon can lead to damage to the infrapatellar branch of the saphenous nerve, tibial collateral ligament, and difficulty in identifying their insertion pattern in knee surgeries.[4] Overuse, acute trauma, iatrogenic disorders, and tumors are all common causes of PA damage. An incorrect incision can result in complications such as cutting the main tendon, insufficient graft length, tibial nerve injury, decreased normal glide, and muscle stiffness.[5] Currently, steroid injection in the anserine bursa is a method to treat bursitis that can provide pain relief. The accuracy of anserine bursa injection with ultrasound guidance is markedly higher compared to the blind injection.[6] However, in clinical practice, surgeons are frequently confronted with situations that necessitate blind injections, despite the fact that ultrasound-guided injections are highly preferred. Understanding and identifying morphological variations of the PA based on anatomical knowledge would be very useful in the case of a blind injection.[7,8] Hence, understanding the tendon constituent of PA and the arrangement of the accessory bands is a prerequisite for a favorable clinical outcome. As a result, the goal of this study is to macroscopically review and focus on the anatomical and morphological variants of the structures constituting the insertion of PA, and to compare them to previously documented studies in an attempt to provide baseline anatomical information for PA.

Subjects and Methods

This was an observational study carried out in 90 (62 males and 28 females) properly embalmed and formalin-fixed lower limbs of adult cadavers dissected from the cadaveric laboratory of the Anatomy Department. The study was done after obtaining approval from the Institutional Ethics Committee for Human Research. All the available specimens were included in the study that did not have any visible external abnormalities in their lower limb. The specimens previously operated in the lower limb knee region, which may prevent the cadaveric analysis of knee, were excluded from this study. While doing the dissection in the various specimens in knee region, we observed different variations in the insertion pattern of tendons on the anteromedial aspect of the knee including sartorius (S), gracilis (G), and semitendinosus (ST). Various patterns of PA formation including monotendinous-sartorius, gracilis, semitendinosus (S/G/ST pattern), monotendinous-sartorius, Gracilis, semitendinosus, semimembranosus (S/G/ST/SM pattern),

sartorius, gracilis, semitendinosus, semimembranosus, tibial collateral ligament (S/G/ST/SM/ TCL pattern), S/G/ST/aST pattern, S/G/ST/aS pattern, S/G/ ST/aS/aST pattern, S/G/ST/aST/abST pattern were observed. Therefore, the aim was made to evaluate the tendinous insertion of PA, in detail showing total number of specimens with parentage of individual pattern involved in constituent of PA and various individual structures in numbers and percentage contributing in forming PA. For this, an incision was made on the skin at the anteromedial aspect of the knee. Initially, the skin was reflected, and fat and superficial fascia along the medial aspect of the knee was cleaned carefully. Upon dissection, PA tendons including sartorius, gracilis, and semitendinosus muscle were exposed carefully to identify for any anatomical and morphological variations. The insertion site of all the specimens was macroscopically observed by the principal investigator. The data were analyzed for several variations in the disposition of the tendons of muscles, ligaments, and accessory band taking participation in the constitution of each PA, and considered for the computation. The findings were documented, recorded, and photographed. The obtained data were analyzed using descriptive statistics analysis.

Results

Several variations were observed for PA. In the present study, no muscle of PA was found to be absent in any specimen of lower limb. Various structures were observed involving in forming PA and thus forming various patterns of PA. The data are enlisted in detail in Table 1 showing total number of specimens with parentage of various patterns involved in constituent of PA. Furthermore, the data is also presented in graph showing various individual structures in numbers and percentage contributing in forming PA.

Various patterns involved in constituent of pes anserinus

The most common and most constituent in PA was observed with S/G/ST pattern.

The other variant was observed as participation from the semimembranosus muscle S/G/ST/SM pattern, tibial

Table 1: Various pattern involved in constituent of insertion of pes anserinus in total number of specimens and parentage

Pes anserinus pattern formed by	Pattern present in total number of specimens	Percentage (%)
Monotendinous S/G/ST pattern	67	74.44
Monotendinous S/G/ST/SM pattern	5	5.55
S/G/ST/SM/TCL pattern	2	2.22
S/G/ST/aST pattern	12	13.33
S/G/ST/aS pattern	2	2.22
S/G/ST/aS/aST pattern	1	1.11
S/G/ST/aST/abST pattern	1	1.11

S: Sartorius, G: Gracilis, ST: Semitendinosus, SM: Semimembranosus, TCL: Tibial collateral ligament, aS: Accessory band of S, aST: Accessory band of ST, abST: Another band of ST

collateral ligament (S/G/ST/SM/TCL pattern), accessory band of sartorius S/G/ST/aS pattern, and various accessory bands of semitendinosus muscle S/G/ST/aST pattern or S/G/ST/aST/abST pattern.

The participation of accessory band of semitendinosus as S/G/ST/aST pattern was observed as a most frequent variation. Figure 1 and Table 1 shows different patterns involved in constituent of insertion of PA in total number of specimens and in parentage.

Individual structures contributing in the formation of pes anserinus

In the present study, sartorius, gracilis, and semitendinosus were observed to take participation in forming the PA in all the specimens ($n = 90$, 100%). The other variant was observed as participation from the semimembranosus muscle ($n = 7$, 7.77%), tibial collateral ligament ($n = 2$,

2.22%), accessory band of sartorius ($n = 2$, 2.22%), accessory bands of semitendinosus muscle ($n = 2$, 2.22%), and another (ab) accessory bands of semitendinosus muscle ($n = 1$, 1.11%), as depicted in Graph 1.

Discussion

Studies on the anatomical variation of PA are rare in the literature. It serves as an additional secondary valgus constraint, strengthening the medial knee supporting structures. In the present scenario, the arthroscopic ACL reconstruction using semitendinosus and gracilis tendons is a popular technique for the treatment of ACL-deficient knees. Ten embalmed adult human cadaveric limbs were dissected for the gracilis and semitendinosus tendons by Candal-Couto JJ.[3] Bands were seen between tendons, connecting them to the popliteal fascia, sartorius, gastrocnemius, pretibial, and superficial fascia, as the author noted that the accessory bands of the PA exhibit a high degree of diversity. Similarly, Mochizuki *et al.*[5] dissected nine legs of five adult cadavers and observed a superficial longitudinal fibrous bundle on the superficial surface of the sartorius and a deep longitudinal fibrous bundle on the aponeurotic membrane covering the tendon of the gracilis muscle. The fascia covering the medial head of the gastrocnemius and fascia cruris, and a minor tendinous extension from the semimembranosus muscle, were joined with aponeurotic membrane from the semitendinosus tendon and tibial collateral ligament. In the study done by Kijkunasathian *et al.*,[6] The proximal site of PA insertion in the Thai population was determined by measuring the distance between the tibial tuberosity and the PA tendon insertion in 85 cadavers. When performing reconstructive surgery on tendons or administering steroid injections to treat anserine bursitis, these structures are crucial from a clinical standpoint. 46.8% of individuals with knee osteoarthritis have a clinical diagnosis of anserine bursitis. In contrast, radiographic evidence of knee osteoarthritis was seen in 83.3% of individuals with anserine bursitis or tendinitis.[9] Patients with pes anserine bursitis will typically appear with
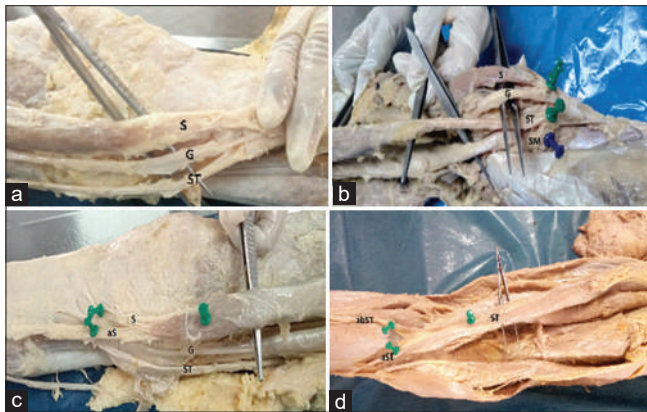
Figure 1: (a) Most frequent constituent of pes anserinus with monotendinous tendons of sartorius (S), gracilis (G), and semitendinosus (ST), muscle forming (S/G/ST) pattern. (b) Tendon of semimembranosus muscle (SM) taking participation in the constituent of pes anserinus forming S/G/ST/SM pattern. (c) Accessory band of sartorius tendon taking participation in the constituent of pes anserinus forming S/G/ST/Sa pattern. (d) Accessory bands of semitendinosus taking participation in the constituent of pes anserinus forming S/G/ST/aST/abST pattern

	Sartotius	Gracilis	Semitendinosus	Semimembranosus	Tibial collateral ligament	accessory band of sartorius	accessory band of semitendinosus	ab accessory band of semitendinosus
N= number of specimens	90	90	90	7	2	2	14	1
Percentage(%)	100%	100%	100%	7.77%	2.22%	2.22%	15.55%	1.11%
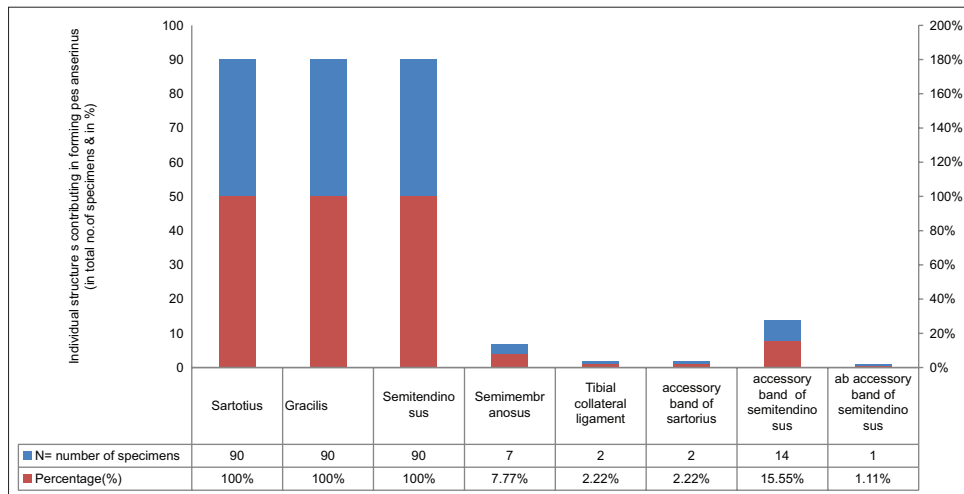
Graph 1: Various individual structures contributing in forming pes anserinus in total number of specimens and in percentage

pain and swelling in the medial aspect of the knee, which may cause the clinician to accurately diagnose them as having differential knee pathology.[10] Furthermore, the diagnostic imaging and minimally invasive surgical approaches of PA are significantly variable.[11,12] The literature suggests that investigation evaluation for the boundary of anserine bursa with the recommended injection site and shape on the insertion area of PA, with the aim of improving clinical practice in uncommon problems like snapping pes syndrome, is highly significant.[12] The ligament restoration and reconstruction surgeries are also used to treat a variety of traumatic injuries, most frequently to the knee and ankle joints. The hamstring tendons are one of the most commonly used grafts in anterior cruciate ligament (ACL) reconstruction of the knee, either as an autograft or allograft. For tendocalcaneus repair, repair of a ruptured patellar tendon, and restoration of the ACL, orthopedic surgeons frequently use knee flexor tendons like the semitendinosus and gracilis.[13,14] The hamstring tendon grafts when compared to patellar-bone-tendon-bone grafts allow harvesting through a minimal skin incision, minimal donor site morbidity, and less extensor mechanism dysfunction or functional deficits. However, during a surgical procedure, concrete landmarks are required to navigate the incision site and identify the appropriate tendons for grafting. The knowledge of surface landmark and anatomical and morphological variants of pes anserine is a prerequisite for orthopedic surgeons while harvesting the anserine graft to minimize various complications like extra care must be taken with the use of the tendon stripper if one is to avoid cutting the main tendon.[12-14] Therefore, the goal of the current study was to provide the most significant information regarding the proper recognition of the numerous variations in tendons and structures that constitute the PA in terms of their insertion type. This similar type of study was carried by various other authors and their results compared with the result of the present study elicited in Table 2.

In order to determine the shape of the PA, Lee *et al.*[12] dissected 86 limbs. They found that the sartorius was placed into the superficial layer, the gracilis was inserted into the deep layer on the medial surface of the tibia, and the semitendinosus was inserted into the deep layer. Ashaolu *et al.*[14] evaluated morphological framework of the PA in Nigerian cadavers and observed the insertion was also joined to the part of tibia close to the tibia tuberosity (90%) and to the fascia

cruris (10%). Additionally, the author noted that accessory bands of the sartorius, gracilis, or semitendinosus were a part of the PA in 95% of cases, but the combined occurrence of the monotendinous sartorius, gracilis, and semitendinosus tendons was only reported in 5% of cases. Cidambi *et al.*[15] performed an MRI study to identify the frequency and characteristics of anomalous PA tendon morphology in an adolescent population undergoing knee ACL reconstruction surgery. The author concluded that the accessory muscle and tendon could be an aberrant strip of the semimembranosus tendon, an anomalous tendon and muscle belly of the gracilis, or a thickening and separation of the sartorius tendon.

In the study done by Lukasz *et al.*,[16] the PA was present and composed of the sartorius, gracilis, and semitendinosus tendons. The existence of accessory bands allowed the author for the differentiation of six different types of PA. Further, the author observed the commonest pattern involving in PA formation was monotendinous sartorius, gracilis and semitendinosus (S/G/ST pattern) in 54 limbs (52.9%). Additionally, three types of insertion were noted (short, band-shaped, and fan-shaped). The mean length between the insertion and the origin of the accessory bands to the fascia of the gastrocnemius muscle was 63.5 mm.

In the study conducted by Murlimanju *et al.*,[18] it was found that 48 lower limbs (90.6%) had PA formed by the gracilis, semitendinosus, and sartorius tendons. It was found that 5 lower limbs (9.4%) had a divergent pattern of PA morphology, whereas 7 (13.2%) had early convergence and 41 (77.4%) had convergent type. Semimembranosus muscle was taking in the formation of PA in 3 lower limbs (5.7%). The PA was inserting into the fascia cruris and not tibia in 8 specimens (15.1%). However, the insertion occurred at both the tibia and fascia cruris in 10 cases (18.9%). In 15.1% of cases, the insertion was limited to the fascia cruris and not the tibia. The semitendinosus was giving an extra slip, which was attaching to the medial condyle of tibia in 7 cases (13.2%). It was giving slip to medial collateral ligament in 2 cases (3.8%) and ligamentum patellae in 1 case (1.9%). The PA formed by the combination of monotendinous sartorius, gracilis, and semitendinosus (S/G/ST pattern) was reported to be the most commonly observed pattern forming PA in the current study. However, such pattern was observed highest in Cidambi *et al.*[16] The present study results were similar to the results observed by the authors Cidambi *et al.*[16] and Murlimanju *et al.*[18] In the present

Table 2: Author-wise comparison of morphological variants of tendons of pes anserinus

Author's name	Year of study	Number of samples	Pes anserinus formed by S/G/ST (%)	Pes anserinus formed by S/G/ST/SM (%)	Other variants (%)
Ashaolu *et al.*[14]	2015	20	1 (5)	25%	70%
Cidambi *et al.*[15]	2016	123	97.60	-	2.40%
Olewnik *et al.*[16]	2019	102	54 (52.9)	-	47.10%
Munhoz *et al.*[17]	2018	7	-	-	-
Murlimanju *et al.*[18]	2019	53	48 (90.60)	3 (5.70)	3.70%
Present study	2021	90	67 (74.44)	5 (5.55)	18 (19.99)

S: Sartorius, G: Gracilis, ST: Semitendinosus, SM: Semimembranosus

study, the author observed that the PA was also formed with combined occurrence of monotendinous sartorius, gracilis, semitendinosus, and semimembranosus tendon (S/G/ST/SM pattern) in 5 (5.55%) specimens, the data were measured almost similar with Murlimanju *et al*.[18] but the value was very less compared to the study done by Ashaolu *et al*.[14]

Further, various study showed a greater distance for the vincula of the gracilis compared to the semitendinosus for the insertion of PA.[19,20] The variations observed in the present study that the tibial collateral ligament, accessory band of sartorius and accessory bands of semitendinosus, and accessory band of gracilis were taking participation in the formation of the PA. The participation of accessory band of semitendinosus (S/G/ST/aST pattern) was observed as a most frequent variation in 12 (13.33%) specimens, and the tibial collateral ligament was in 2 (2.22%). The sartorius, gracilis, semitendinosus, and accessory band of sartorius was observed in 2 (2.22%) specimens.

The sartorius, gracilis, semitendinosus, accessory band of sartorius, and accessory band of semitendinosus (S, G, ST, aS, aST pattern) was observed in 1 (1.11%) specimen. The sartorius, gracilis, semitendinosus, accessory band of sartorius, accessory band of semitendinosus, and another accessory band of semitendinosus (S/G/ST/aS/aST/ abST Pattern) was observed in 1 (1.11%); these types of variations were not commonly seen. In addition, no accessory band of gracilis was observed in the present study and no classification of the PA has been drawn up.

Conclusions

The present study confirms and highlights the several variants of the PA. Based on these findings, it can be concluded that PA was formed by sartorius, gracilis, semitendinosus, semimembranosus tendons, their accessory tendon bands, and tibial collateral ligament. The knowledge of such anatomical variants is significant in planning and performing various surgical procedures by orthopedic surgeons and plastic surgeons. Furthermore, the improved preoperative radiological investigations of PA may aid operating surgeons in avoiding iatrogenic injuries, premature tendon grafts, and subsequent difficulties during the graft harvesting procedure and reconstructive knee surgeries.

Conflicts of interest

There are no conflicts of interest.

References

1. Standring S. Gray's Anatomy: The Anatomical Basis of Clinical Practice. 41st ed. New York: Elsevier; p. 1361-6.
2. Amatuzzi MM, Cocco LF, Di Dio LJ, Gotfryd AO. Surgical anatomy of the variations of the arrangement of the tendons of the muscles of the pes anserinus in male adults. Ital J Anat Embryol 2002;107:29-35.
3. Candal-Couto JJ, Deehan DJ. The accessory bands of gracilis and semitendinosus: An anatomical study. Knee 2003;10:325-8.
4. Gnanadesigan N, Smith RL. Knee pain: Osteoarthritis or anserine bursitis? J Am Med Dir Assoc 2003;4:164-6.
5. Mochizuki T, Akita K, Muneta T, Sato T. Pes anserinus: Layered supportive structure on the medial side of the knee. Clin Anat 2004;17:50-4.
6. Kijkunasathian C, Limitlaohaphan C, Saengpetch N, Saitongdee P, Woratanarat P. The location of pes anserinus insertion in Thai people. J Med Assoc Thai 2009;92 Suppl 6:S189-92.
7. Oliveira VM, Tatsuo A, Cury RD, Avakian R Jr., Aires DJ, De Camargo OP, *et al*. Study of the gracile and semitendinosus muscles insertion. Anat Acta Ortop Bras 2006;14:7-10.
8. Clapp A, Trecek J, Joyce M, Sundaram M. Pes anserine bursitis. Orthopedics 2008;31:306, 407-8.
9. Helfenstein M Jr., Kuromoto J. Anserine syndrome. Rev Bras Reumatol 2010;50:313-27.
10. Finnoff JT, Nutz DJ, Henning PT, Hollman JH, Smith J. Accuracy of ultrasound-guided versus unguided pes anserinus bursa injections. PM R 2010;2:732-9.
11. Charalambous CP, Kwaees TA. Anatomical considerations in hamstring tendon harvesting for anterior cruciate ligament reconstruction. Muscles Ligaments Tendons J 2012;2:253-7.
12. Lee JH, Kim KJ, Jeong YG, Lee NS, Han SY, Lee CG, *et al.* Pes anserinus and anserine bursa: Anatomical study. Anat Cell Biol 2014;47:127-31.
13. Meghana HJ., Vasant HV; Morphometric study of patella and patellar ligament of knee with its clinical significance. MedPulse International Journal of Anatomy. October 2021; 20(1): 44-49.
14. Ashaolu JO, Osinuga TS, Ukwenya VO, Makinde EO, Adekanmbi AJ. Pes anserinus structural framework and constituting tendons are grossly aberrant in Nigerian population. Anat Res Int 2015;2015:483186.
15. Cidambi KR, Pennock AT, Dwek JR, Edmonds EW. Avoiding anomalous tendon harvest at the pes anserinus insertion. J Knee Surg 2016;29:80-3.
16. Olewnik Ł, Gonera B, Podgórski M, Polguj M, Jezierski H, Topol M. A proposal for a new classification of pes anserinus morphology. Knee Surg Sports Traumatol Arthrosc 2019;27:2984-93.
17. Munhoz MA, Cunha FB, Mestriner G. Anatomical and morphometric study of the pes anserine tendons in the knee. JCDR 2018;12:RC05-7.
18. Murlimanju BV, Vadgaonkar R, Ganesh C, Prameela MD, Tonse M, Pai MM, *et al.* Morphological variants of pes anserinus in South India. Muscles Ligaments Tendons J 2019;9:372-8.
19. Curtis BR, Huang BK, Pathria MN, Resnick DL, Smitaman E. Pes Anserinus: Anatomy and Pathology of Native and Harvested Tendons. AJR Am J Roentgenol 2019;213:1107-16.
20. Olewnik Ł, Podgórski M, Polguj M. An unusual insertion of an accessory band of the semitendinosus tendon: Case report and review of the literature. Folia Morphol (Warsz) 2020;79:645-8.

A Morphological Study of Cadaveric Liver

Abstract

Background: Liver is anatomically divided into right, left, quadrate, and caudate lobes. Functionally, it is divided into four portal sectors by four branches of portal vein. Three hepatic veins lie between these sectors as intersectoral veins and these intersectoral plains are called portal fissures. Minor fissures like umbilical fissure, venous fissure, and Rouviere's sulcus are visible clefts on the visceral surface of the liver. Morphological variations in size, shape, lobes, and fissures are frequently found during routine dissection. This study is focused mostly on the surgical anatomy of lobes and fissures relevant for hepatic surgery. **Materials and Methods:** This was a cross-sectional descriptive study conducted on 50 formalin-preserved specimens of liver. The details of morphological features of lobes and fissures were examined and compared with the findings of previous studies. **Results:** Out of 50 liver specimens studied, in 8% of cases left lobe and quadrate lobe and in 12% of cases caudate lobe were hypoplastic. Accessory liver lobes were found in 12% of cases, most of which were small except 2 cases of large tongue shaped projections of accessory lobes attached to the left lobe and 2 on the right lobe. Diaphragmatic sulci were found in 12% of cases and Rouviere's sulcus in 64% of cases. Accessory fissures were also found in quadrate and caudate lobes in 24% and 22% of cases, respectively. Pons hepatis was found in 20% of cases. **Conclusion:** Awareness about prevalence of morphological variations of liver can help avoiding errors in diagnosis and unwanted complications during surgery.

Keywords: *Accessory hepatic lobes, diaphragmatic sulcus, pons hepatis, Rouviere's sulcus*

Mamata Sar,
Sabita Singh,
Sarita Behera,
Dibya Prabha Bara[1],
Jeneeta Baa,
Srikanta Kumar Mishra,
Arpita Soy[1]

Department of Anatomy, VSS Institute of Medical Science and Research, Burla, [1]Department of Anatomy BBMCH, Balangir, Odisha, India

Introduction

Morphologically, liver is divided into right, left, caudate, and quadrate lobes by the peritoneal ligamentous attachments. Functionally, the liver is divided into four portal sectors. Each portal sector is supplied by one of the four major branches of portal vein. Right lobe is divided into anterior and posterior sectors and left lobe into medial and lateral sectors. The three hepatic veins run in the intersectoral plains. They form three major fissures called main, right, and left portal fissures, corresponding to the position of middle, right, and left hepatic vein. These fissures are deeply situated and normally not visible on the surface. The main portal fissure is also called Cantle's line which divides the liver into right and left hemiliver. This line joins the fossa for gall bladder to inferior vena caval sulcus. The left portal fissure divides the left hemiliver into left medial and left lateral sectors. The right portal fissure divides the right hemiliver into right posterior and right anterior sectors. There are three visible clefts, found on the visceral surface, namely umbilical fissure, venous fissure and fissure of Gan's (Rouviere's sulcus). Knowledge of these hepatic fissures is essential for hepatic surgery. Umbilical fissure contains umbilical portion of left branch of portal vein through which portal vein is accessed during surgery for cholangiocarcinoma of porta hepatis. This fissure also contains terminal branch of left hepatic artery and segmental branch of left hepatic duct. Knowledge on the arrangement of duct, artery, and vein in this fissure is of importance during splitting of liver in transplantation surgery. The fissure of Gan's (Rouviere's sulcus) lies on the visceral surface of the right lobe of liver posterior to the fossa for gallbladder. It marks the site of the division of portal pedicle to the right posterior sector. It is found in over 80% of normal livers and is a useful landmark for laparoscopic cholecystectomy. Accessory fissures are rare, though diaphragmatic sulci are seen on the superior surface of the right lobe in approximately 40% of livers.[1] With this background, the present study was conducted to describe

Access this article online

Website: https://journals.lww.com/joai

DOI: 10.4103/jasi.jasi_177_21

Quick Response Code:

How to cite this article: Sar M, Singh S, Behera S, Bara DP, Baa J, Mishra SK, *et al.* A morphological study of cadaveric liver. J Anat Soc India 2023;72:131-4.

the detailed morphology of lobes, fissures and sulci of cadaveric livers focusing mainly on variations of lobes and fissures as these variations bear considerable surgical and radiological importance.

Materials and Methods

After getting the institutional ethics committee approval, this cross-sectional descriptive study was conducted on 50 formalin-fixed livers available in the department of anatomy in our institute. Livers with gross pathological changes, like fibrosis and distortion of external architecture, were excluded from our study. The details of the various morphological features such as shape, size, surfaces, borders, lobes, and fissures were thoroughly examined. Any variations in their morphology were noted and compared with the findings of previous studies on liver morphology.

Results and Observations

Out of 50 liver specimens examined, lobar hypoplasia was found in 11 cases. Multiple lobes were affected in 3 livers. They were left lobe with caudate lobe hypoplasia in 2 specimens and left lobe with quadrate lobe hypoplasia in 1. Isolated hypoplastic left lobe, caudate, and quadrate lobes were found in 1, 4, and 3 livers, respectively. Right lobe hypoplasia was not found in this study [Table 1 and Figure 1a and b].

Accessory lobes were observed in 7 cases. A large accessory lobe projecting from the left lobe was found in 2 livers. A large tongue-shaped accessory lobe called Riedel's lobe was found on the inferior surface of right lobe in one liver. Others were small accessory lobes on the inferior surface of liver, 1 each on the left lobe, right lobe, caudate, and quadrate lobe [Table 1 and Figure 2a and b].

The most common accessory fissure found in this study was Rouviere's sulcus. It was present in 32 (64%) livers, out of which 60% were in continuity with the porta hepatitis (open type) and only 4% were closed or fused type. Other accessory fissures were diaphragmatic sulcus present on the diaphragmatic surface as multiple grooves of variable depth in 6 (12%) of cases. In addition to this, accessory fissures of various size and depth were also found in the caudate lobe 11 (22%), quadrate lobe 12 (24%), and left lobe 1 (2%) [Table 2 and Figure 3a and b].

Table 1: Variations in lobe

Morphological change	Lobes	Number of specimens (%)
Hypoplasia	Left	3 (6)
	Right	0
	Quadrate	5 (10)
	Caudate	5 (10)
Accessory lobes	Left	3 (6)
	Right	2 (4)
	Quadrate	1 (2)
	Caudate	1 (2)

Discussion

Hypoplasia of liver lobes usually goes undetected as they do not normally cause any clinical problem. They are incidentally detected while investigating for other diseases or during cadaveric dissection. Left lobe hypoplasia is more frequently reported than right. In most of the reports hypoplasia of one lobe was associated with compensatory increase in the size of other lobes. The branches of portal vein and hepatic artery to the hypoplastic liver lobe were reduced in caliber. There is also displacement of adjacent viscera. Most commonly gallbladder is found to be in ectopic position. Swarup *et al.* reported a case of hypoplastic right lobe where there was compensatory hypertrophy of left lobe and the right branch of portal vein was reduced in its calibre.[2] Ormeci *et al.* and Kanwal and Akhtar reported cases of hypoplastic left hepatic lobe in contrast enhanced computed tomography, where they found compensatory hyperplasia of right lobe and ectopic position of gall bladder. Both have reported reduction in size of portal venous branch to the left lobe.[3,4] Sakuraoka *et al.* reported a case of large right liver lobe (Riedel's lobe) combined with an atrophic left lateral segment in a donor
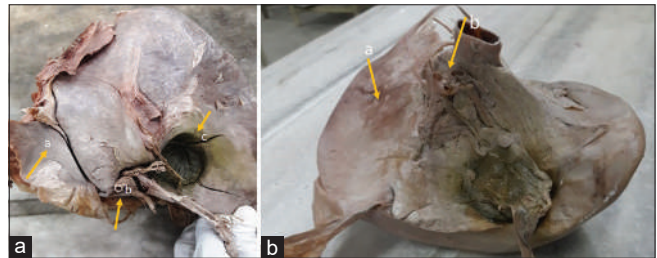
Figure 1: (a) Hypoplastic Left and Quadrate Lobes: a - Hypoplastic left lobe, b - rudimentary quadrate lobe c- Displaced gall bladder. (b) Hypoplastic left and caudate lobe: a - Hypoplastic left lobe b - Hypoplastic caudate lobe

Figure 2: (a) Accessory lobe attached to the left lobe. (b) Accessory lobe attached to Right lobe (Riedel's lobe)
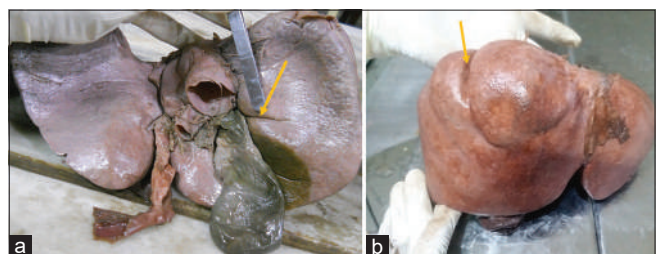
Figure 3: (a) Rouviere's Sulcus (Open type). (b) Diaphragmatic sulcus

Table 2: Accessory fissures	
Accessory fissures	**Number of specimens (%)**
Left lobe	1 (2)
Right lobe (Rouviere's sulcus)	32 (64)
Quadrate lobe	12 (24)
Caudate lobe	11 (22)
Diaphragmatic sulcus	6 (12)

liver for transplantation surgery.[5] In the present study, we didn't observe compensatory hyperplasia of other lobes in any of the cases of hypoplastic lobe, rather the overall size of livers was reduced due to hypoplasia of any lobe. Abnormal position of gallbladder was found in 2 cases of hypoplastic lobes. The portal vein and hepatic artery could not be traced beyond the porta hepatis through dissection. Hence, their caliber could not be measured in the present study. Aktan *et al*. in their study on liver lobe anomalies in 54 cadavers have reported absence of left lobe in one case (1.85%), absence of quadrate lobe in 2 (3.70) and that of caudate lobe in 4 (7.41%) cases.[6] In the present study, complete absence of lobe was not observed in any liver, though a very much rudimentary liver tissue was found in some livers.

Accessory liver lobes appear due to excessive development of the liver tissue. They normally do not cause any clinical problem. Sometimes, the accessory lobe may undergo torsion if it is a pedunculated one. Accessory liver lobes are sometimes confused to be tumors of liver. There are also reports of hepatocellular carcinoma occurring in accessory lobe. Nayak reported accessory lobes in five out of 55 livers studied (9.09%). These accessory lobes were small and were situated in the vicinity of the porta hepatis, caudate, and quadrate lobes.[7] In most cases, the accessory lobes are found on the inferior surface. Riedel's lobe is an accessory lobe, corresponding to hypertrophy of segment V and VI. Glenisson *et al*. have reviewed the prevalence of Riedel's lobe, mainly from radiologic series, that ranged from 3.3% to 14.5% in different literatures.[8] In the present study, large accessory lobe attached to the left lobe were found in 2 cases 1 of which was pedunculated. Riedel's lobe, which is described as the most common type of accessory lobe, was found only in one case.

Accessory fissures are produced because of invagination of visceral peritoneum deep into the liver parenchyma. They are found on any surface of liver and often detected incidentally during autopsy, cadaveric dissection, investigations for other diseases or during surgery. These fissures communicate freely with the peritoneal sac. Therefore, ascitic fluid, blood, or pus from the peritoneal sac may collect in these fissures and confuse them with a hepatic cyst, abscess, or hematoma. Malignant cells may be seeded into these fissures and mimic hepatocellular carcinoma.[9]

Small accessory fissures of various length and depth were found in our study on the visceral surface of all the lobes.

Rouviere's sulcus, which is a deep cleft on the visceral surface of right lobe, behind the fossa for gall bladder is utilized as a reference point or landmark in laparoscopic cholecystectomy, because this is the plain of main bile duct. Any dissection below this plain may pose danger to the bile duct. When the cleft is open throughout and the hepatic pedicle is visible through this, it is called open type. When the cleft is open only at its lateral part and the hepatic pedicle is not visible, it is called fused type or closed type. During laparoscopic cholecystectomy, this sulcus opens widely due to the pressure of CO_2 insufflation and is clearly seen with the help of digital endoscopic cameras. Singh and Prasad have studied the detailed anatomy of Rouviere's sulcus during laparoscopic surgery and reported presence of this sulcus in 71% of cases out of which 60% were open and 11% were closed type.[10] Dahmane *et al*. have studied the anatomy of Rouviere's sulcus in 40 autopsy liver specimens. The frequency of this sulcus was 82% out of which open and fused types were 70% and 12%, respectively.[11] In the present study, Rouviere's sulcus was found in 64% of cases (60% open and 4% closed) which is consistent with the result of Singh and Prasad.

Diaphragmatic sulci correspond to the portal fissures and mark the course of underlying Hepatic Veins. Macchi *et al*. have reported presence of diaphragmatic sulci in 40% of autopsy specimen. They were single in 53% and multiple in rest of the cases. Using corrosion casts they have demonstrated that the topography of the diaphragmatic sulci corresponds to the course of the right and middle hepatic Veins. According to them, there exists a weak zone between adjacent portal territories, along the course of hepatic veins which get indented by the pressure of ribs and muscles of the diaphragm.[12] According to Auh *et al*., its prevalence increases in older age groups. In their study, diaphragmatic indentations were found in 14% of patients below 60 years of age, while it increased to 71% in patients over 80 years of age.[9] Joshi *et al*. reported prominent diaphragmatic sulci on the anterosuperior surface in 6% of the livers.[13] In the present study, accessory fissures were found on the diaphragmatic surface in the form of multiple diaphragmatic sulci of variable depth in 12% of livers and that running through the Cantle's line, which corresponds to the middle hepatic vein was the deepest and most prominent among them.

Conclusion

A large variety of morphological variations with varying degrees of frequency affecting the anatomy of liver were found in this study. Awareness on these deviations from normal anatomy can help the radiologists to prevent errors in diagnosis. A prior knowledge on these variations can also help the surgeons in planning the surgical procedures accordingly and thereby avoiding any undesirable complications.

Financial support and sponsorship

Conflicts of interest

There are no conflicts of interest.

References

1. Rosen CB. Liver. In: Standring S, editor. Gray's Anatomy: The Anatomical Basis of Clinical Practice. 42nd ed. London: Elsevier; 2021. p. 1207.
2. Swarup MS, Bhatt S, Tandon A, Mandal S. Segmental hypoplasia of liver: The importance of radiologic recognition and reporting despite masterly inactivity. Egypt J Radiol Nucl Med 2018;49:1-3.
3. Ormeci T, Erdogan ST, Ormeci A, Aygun C. A rare congenital liver anomaly: Hypoplasia of left hepatic lobe. J Pak Med Assoc 2016;66:1662-4.
4. Kanwal R 3rd, Akhtar S. Left hepatic lobe agenesis with ectopic gallbladder. Cureus 2021;13:e16131.
5. Sakuraoka Y, Seth R, Boteon AP, Perrin M, Isaac J, Subash G, *et al.* Large Riedel's lobe and atrophic left liver in a donor – Accept for transplant or call off? World J Transplant 2020;10:129-37.
6. Aktan ZA, Suvas R, Pinar Y, Arslan O. Lobe and segment anomalies of the liver. J Anat Soc India 2001;50:15-6.
7. Nayak SB. A study on the anomalies of liver in the South Indian cadavers. Int J Morphol 2013;31:658-61.
8. Glenisson M, Salloum C, Lim C, Lacaze L, Malek A, Enriquez A, *et al.* Accessory liver lobes: Anatomical description and clinical implications. J Visc Surg 2014;151:451-5.
9. Auh YH, Lim JH, Kim KW, Lee DH, Lee MG, Cho KS. Loculated fluid collections in hepatic fissures and recesses: CT appearance and potential pitfalls. Radiographics 1994;14:529-40.
10. Singh M, Prasad N. The anatomy of Rouviere's sulcus as seen during laparoscopic cholecystectomy: A proposed classification. J Minim Access Surg 2017;13:89-95.
11. Dahmane R, Morjane A, Starc A. Anatomy and surgical relevance of Rouviere's sulcus. ScientificWorldJournal 2013;2013:254287.
12. Macchi V, Feltrin G, Parenti A, De Caro R. Diaphragmatic sulci and portal fissures. J Anat 2003;202:303-8.
13. Joshi SD, Joshi SS, Athavale SA. Some interesting observations on the surface features of the liver and their clinical implications. Singapore Med J 2009;50:715-9.

Role of Vermal Anteroposterior Length and Width in Age Determination of Fetus

Abstract

Background: Early differentiation of the cerebellum during fetal life makes it the center of interest in the field of obstetrics and gynecology. Moreover, the cerebellar vermis develops a little ahead of the hemispheres. Hence, the morphological parameters of the vermis can be a guide to ascertaining gestational age and assessing any anomalies related to posterior cranial fossa development. **Aims and Objectives:** The study was taken up with the objective of building up a timeline for the appearance of folia and important fissures. Moreover, establishing a correlation between the growing fetus and vermal parameters. **Material and Methods:** A total of 60 human fetal fixed cerebella were included in this observational and descriptive type of study. Fetuses affected with any congenital or neurological deficit were excluded. Grouping of the fetuses was done, based on their gestational age in weeks. The first group from 13-17 weeks, the second group from 18-22weeks, the third group from 23-27 weeks, and the fourth group from 28-32 weeks. **Observation:** Time of appearance of folia and fissures were noted. Vernier calipers were used to measure vermal width and anteroposterior length. Statistical tools like IBM SPSS Statistics for Windows, Version 20.0. Armonk, NY: IBM Corp. and one-way analysis of variance were applied to the data obtained. **Conclusion:** A posterolateral fissure appeared at 13 weeks of gestation while folia and other fissures appeared from the 18th week onwards. Both the parameters of vermis showed a linear correlation with gestational age. Such a timeline and correlation shall prove to be helpful in calculating fetal age in the field of forensic studies.

Keywords: *Fetal age, vermal anteroposterior diameter, vermal width*

**Nadia Ahmad,
Deepa Singh[1],
Sunder Lal Jethani[1]**

Department of Anatomy, Manipal TATA Medical College, Manipal Academy of Higher Education, Manipal, Karnataka, [1]Department of Anatomy, Himalayan Institute of Medical Science, Swami Rama Himalayan University, Dehradun, Uttarakhand, India

Introduction

The cerebellum being an important structure of posterior cranial fossa has drawn a lot of attention from researchers. This part of the hindbrain is not only related to balancing, posture, and muscular coordination but also to higher cognitive functions like language and social emotions.[1] Amongst all the structures of brain, cerebellum is the first to differentiate but the last to mature which occurs by the first birthday of a child.

Externally cerebellum presents with two lateral cerebellar hemispheres and an intervening vermis. Numerous transverse fissures divide the surface of cerebellum into several folia. Amongst the numerous transverse fissures, the most conspicuous ones are the horizontal, posterolateral, and fissure prima. Posterolateral fissure is the first fissure to appear externally, appearing as early as 12–13 weeks of intrauterine life.[2] An increase in surface foliation is

seen during second and third trimesters, by this time there is a deepening of major fissures and emergence of secondary fissures.[3] It has been seen that cerebellar volume increases more rapidly than cerebrum from 20th week of gestation to postnatal period.[4] After 17 weeks growth rate of cerebellum exceeds that of cerebrum.[5] Phylogenetically vermis belongs to paleocerebellum that develops in the mid-line during the 9th week of fetal life. This occurs earlier than the embryogenesis of lateral hemispheres, part of the neocerebellum.[6] This early development of vermis forms a significant aspect of the assessment of posterior cranial fossa defects. Abnormalities of vermis arising in the second trimester like COACH and Dandy-Walker syndrome need to be identified. The lower half of the roof of the fourth ventricle remains covered by a thin structure forming its roof and separating it from cisterna magna. Scanning, before 18 weeks of gestation, the roof is formed is present as a thin film-like structure that

Access this article online

Website: https://journals.lww.com/joai

DOI:
10.4103/jasi.jasi_89_22

Quick Response Code:

How to cite this article: Ahmad N, Singh D, Jethani SL. Role of vermal anteroposterior length and width in age determination of fetus. J Anat Soc India 2023;72:135-9.

is difficult to appreciate and may lead to misdiagnosis of agenesis/dysgenesis of the vermis.[7] A biometric evaluation of vermis can help clinicians to assess the integrity of the same.[8] Development of a nomogram to determine the febased on measurements of the cerebellum, the more commonly used ones being maximum transverse diameter and craniocaudal length of the vermis, and estimation of gestational age of the fetus.[9] The present study aimed to observe the appearance of folia and major fissures and establish a timeline. Also, to display a correlation between morphological parameters of vermis like anteroposterior diameter and width of the vermis with gestational age.

Materials and Methods

A descriptive and observational study was carried out on 60 human fetuses. The study spanned a period of 1 year. Ethical clearance was acquired from the institutional ethical committee. Fetuses between 13th and 32 weeks of gestational age were included that were a result of spontaneous abortion. Fetuses with any gross abnormality/ neurological deficit were excluded from the study. Further, the sample was divided into 4 groups:
- Group 1 - gestational age 13th–17th weeks
- Group 2 - gestational age 18th–22nd weeks
- Group 3 - gestational age 23rd–27th weeks
- Group 4 - gestational age 28th–32nd weeks.

Using a midline incision over the head and dorsal aspect of the neck, the scalp was reflected. A cruciate incision was given on the dura mater to expose the cranial cavity. Following this tentorium cerebelli was identified and cleared along with arachnoid mater to expose the cerebral hemispheres and cerebellum. Only the cerebellum was separated and preserved separately. The following observations were made:
i. Presence or absence of folia and major fissures
ii. Width of vermis – the distance between two farthest points on superior vermis
iii. Anteroposterior diameter of vermis-distance from the apex of 4th ventricle to posterior limit of vermis.

Obtained data were analyzed using the statistical software SPSS Statistics for Windows, Version 20.0. Armonk, NY: IBM Corp. and a one-way analysis of variance. Pearson's coefficient of correlation was estimated for gestational age and the morphological parameters. $P < 0.005$ was considered statistically significant. Variables showing the linear relationship in scatter chart and high order correlation coefficient ($r > 0.70$) were considered for regression analysis.

Observation and Results

The presence or absence of folia and major fissures was observed on the surface of the cerebellum and noted Figure 1. Fissures in groups 1 and 4 may be compared Figures 2-5.

Values for vermal width and anteroposterior length were expressed as mean and standard deviations in all
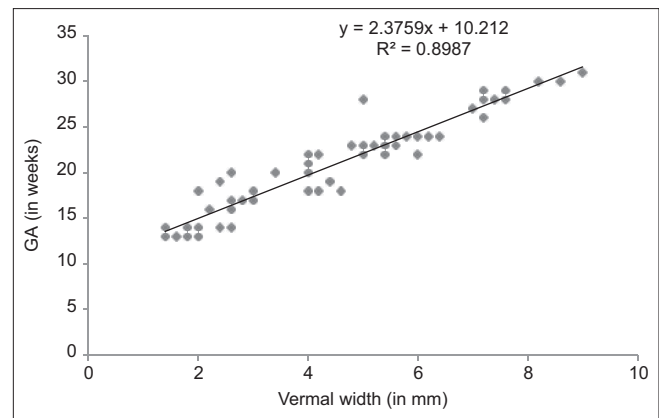
Figure 1: Scatter graph for vermal width and gestational age with regression equation

four groups Figure 6. An increase in vermal width and anteroposterior length was appreciated with increasing gestational age which was statistically significant. Pearson's correlation coefficient was also suggestive of a strong correlation between advancing gestation and the vermal parameters.

Scatter plots were made between vermal parameters and gestational age Figures 7 and 8. Skewed data were expressed as median, maximum, and median with the help of a box and whiskers graph.

Discussion

Vermis begins to develop 30–60 days before cerebellar hemispheres.[10] Its growth is linear throughout pregnancy and thus correlates well with gestational age, biparietal diameter, and head circumference.[11] We found folia in a rudimentary form between the 13th and 17th week, appearing as thin transverse bands separated by shallow groves. Such groves are predecessors of fissure formation. By the 18th week, folia were well identified and by the 28–32nd week well-formed. These findings were similar to observations of Veni *et al.*,[12] Viswasom AA and Jobb observed absence of folial pattern in a 20-week fetus while present in a full-term fetus though they were not as developed as in adults.[13] The formation of folia completes 3 weeks after birth as a result of the proliferation of cells in the external granular layer stated by Mares and Lodin.[14] First fissure to appear in this study was posterolateral at 13 weeks followed by primary at 18 weeks. Liu *et al.* observed primary fissure and posterolateral at 14 and 17 weeks respectively [Figure 7].[15] The primary fissure was reported to be seen at 16 weeks by Ruiz Restrepo *et al.*, [Figure 8].[16] The fact that the blood supply to the cerebellum is unaffected during conditions of fetal distress makes the organ reliable to evaluate gestational age.[17] Based on standardized values of the vermis, vermal anomalies can be detected.[18] An increase was noted by Gezer *et al.*, from 6 mm at 17 weeks to 16 mm at 30 weeks.[19] An magnetic resonance imaging (MRI)-based
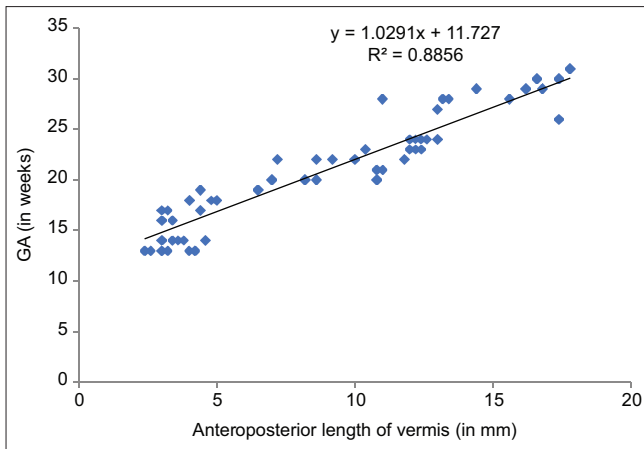
Figure 2: Scatter graph for vermal AP length and gestational age with the regression equation

$$y = 1.0291x + 11.727$$
$$R^2 = 0.8856$$
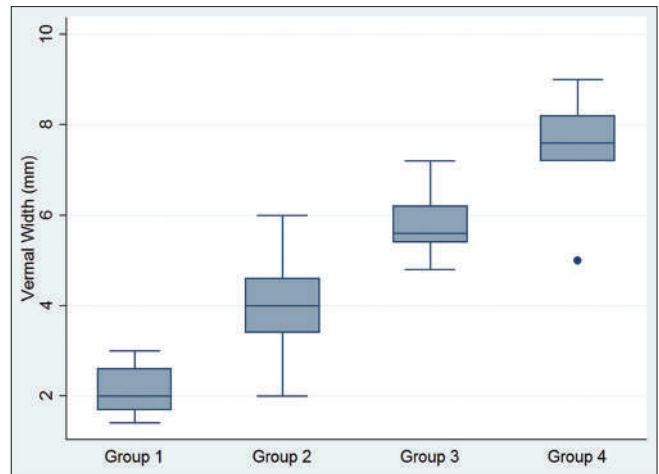
Figure 3: Box plot showing various attributes of vermal width in different groups
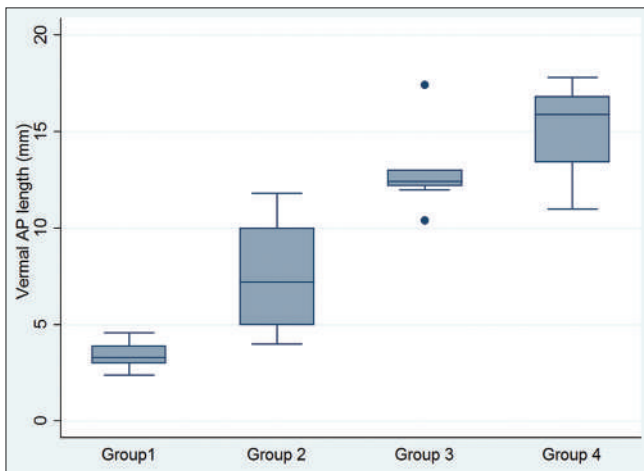
Figure 4: Box plot of various attributes of vermal AP length in different groups
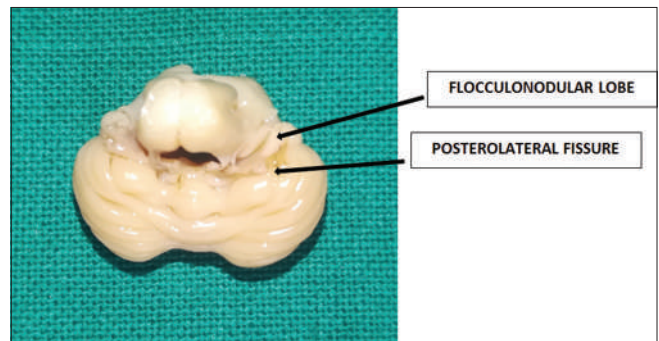
Figure 5: Photomicrograph of Human fetal cerebellum (Group 1) showing the flocculonodular lobe and posterolateral fissure
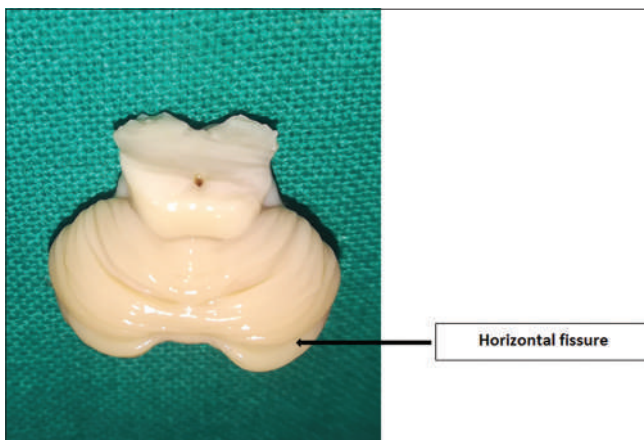
Figure 7: Photomicrograph of Human fetal cerebellum (Group 4) showing flocculonodular lobe and posterolateral fissure

Figure 6: Photomicrograph of Human fetal cerebellum (Group 1) showing appearance of horizontal fissure

study by Ye *et al.* observed the mean to be 11 mm and 15.5 mm in groups with a gestational age of 21–26 and 27–32 weeks respectively.[20] They also stated a positive association between gestational age and AP

diameter of the vermis, $r = 0.7$ ($P < 0.001$). In a study by Katorza *et al.* anteroposterior diameter of vermis at a mean of gestational age, 29.6 week was observed approximately 18, 19, and 16 mm using two-dimensional, three-dimensional, and MRI, respectively.[8] The present study showed the mean to be 15.24 ± 2.18 mm in Group 4. The value was close to the one noted by an MRI study done by Katorza *et al.*,[8] The increase in anteroposterior dimension with advancing pregnancy was linear, well correlated, $r = 0.94$, and statistically significant ($P < 0.001$). Dovjak *et al.* too indicated a
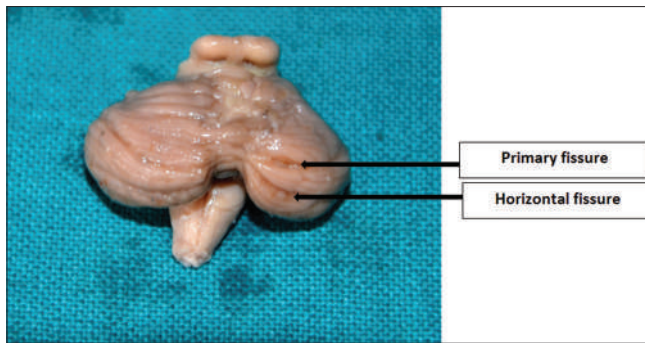
Figure 8: Photomicrograph of Human fetal cerebellum (Group 4) showing horizontal and primary fissure

significant and a strong correlation of the anteroposterior parameter with advancing pregnancy.[21] The width of vermis was taken as a part of vermal measurement since very few authors have mentioned its relevance to gestational age. The parameter was recorded to be 3.95 ± 1.01 mm at 18–22 weeks (Group 2) to 7.54 ± 1.01 mm at 28–32 weeks (Group 4) in this study. Zalel *et al*. noted the vermal width to be ranging from 5 mm at 18–20 weeks to 12.3 mm at 32 weeks.[22] Their mean values were more than ours probably due to the unequal distribution of weeks into groups. Regression analysis was possible, and equations were derived for both parameters as the data was linear. The gestational age of the fetus can be deduced with help of these regression equations proving to be helpful to clinicians and forensic experts in medicolegal cases.

Limitations

A larger size of sample would have been helpful in deriving more accurate regression equations. Tissue when fixed undergoes some amount of shrinkage which may have led to biasing of morphological measurements.

Conclusion

Well-defined fissures appeared earlier than folia. The posterolateral fissure was seen to appear as early as 13 weeks. This was followed by a primary fissure appearing by 18 weeks. At this same time, folia were found to be well-formed. Estimation of vermal parameters can help in identifying congenital abnormality of vermis like Dandy-Walker and COACH syndrome before the birth of the baby. It may also prove to be helpful in the estimation of fetal age, especially when only fixed cerebellar tissue is available to the forensic team. Formulation of regression equations may be used as a tool for age determination in such cases.

Financial support and sponsorship

Nil.

Conflicts of interest

There are no conflicts of interest.

References

1. Koziol LF, Budding DE, Chidekel D. From movement to thought: Executive function, embodied cognition, and the cerebellum. Cerebellum 2012;11:505-25.
2. Rakic P, Sidman RL. Histogenesis of cortical layers in human cerebellum, particularly the lamina dissecans. J Comp Neurol 1970;139:473-500.
3. Lavezzi AM, Ottaviani G, Terni L, Matturri L. Histological and biological developmental characterization of the human cerebellar cortex. Int J Dev Neurosci 2006;24:365-71.
4. Kyriakopoulou V, Vatansever D, Davidson A, Patkee P, Elkommos S, Chew A, *et al.* Normative biometry of the fetal brain using magnetic resonance imaging. Brain Struct Funct 2017;222:2295-307.
5. Xu F, Ge X, Shi Y, Zhang Z, Tang Y, Lin X, *et al.* Morphometric development of the human fetal cerebellum during the early second trimester. Neuroimage 2020;207:116372.
6. Gogtay N, Giedd JN, Lusk L, Hayashi KM, Greenstein D, Vaituzis AC, *et al.* Dynamic mapping of human cortical development during childhood through early adulthood. Proc Natl Acad Sci U S A 2004;101:8174-9.
7. Bromley B, Nadel AS, Pauker S, Estroff JA, Benacerraf BR. Closure of the cerebellar vermis: Evaluation with second trimester US. Radiology 1994;193:761-3.
8. Katorza E, Bertucci E, Perlman S, Taschini S, Ber R, Gilboa Y, *et al.* Development of the fetal vermis: New biometry reference data and comparison of 3 diagnostic Modalities-3D Ultrasound, 2D ultrasound, and MR imaging. AJNR Am J Neuroradiol 2016;37:1359-66.
9. Scott JA, Hamzelou KS, Rajagopalan V, Habas PA, Kim K, Barkovich AJ, *et al.* 3D morphometric analysis of human fetal cerebellar development. Cerebellum 2012;11:761-70.
10. Kollias SS, Ball WS Jr., Prenger EC. Cystic malformations of the posterior fossa: Differential diagnosis clarified through embryologic analysis. Radiographics 1993;13:1211-31.
11. Malinger G, Ginath S, Lerman-Sagie T, Watemberg N, Lev D, Glezerman M. The fetal cerebellar vermis: Normal development as shown by transvaginal ultrasound. Prenat Diagn 2001;21:687-92.
12. Veni SK, Sugavasi R, Devi VS. Histogenesis of human foetal cerebellar cortex. Anat J Afr 2015;4:598-603.
13. Viswasom AA, Jobb A. Age related changes in the Purkinje cells in human cerebellar cortex. J Evol Med Dent Sci 2013;2:5882-90.
14. Mares V, Lodin Z. The cellular kinetics of the developing mouse cerebellum. II. The function of the external granular layer in the process of gyrification. Brain Res 1970;23:343-52.
15. Liu F, Zhang Z, Lin X, Teng G, Meng H, Yu T, *et al.* Development of the human fetal cerebellum in the second trimester: A post mortem magnetic resonance imaging evaluation. J Anat 2011;219:582-8.
16. Ruiz Restrepo JM, Garcia Figueredo D, Cuadrado M, Medrano S, Arcalis N, Conejero A, *et al*. The cerebellum: A review of normal anatomy, pathologic conditions and imaging features. Eur Soc Radiol 2011. p. 1-33. 10.1594/ecr2011/C-0945.
17. Behrman RE, Lees MH, Peterson EN, De Lannoy CW, Seeds AE. Distribution of the circulation in the normal and asphyxiated fetal primate. Am J Obstet Gynecol 1970;108:956-69.
18. Robinson AJ, Blaser S, Toi A, Chitayat D, Halliday W, Pantazi S, *et al.* The fetal cerebellar vermis: Assessment for abnormal development by ultrasonography and magnetic resonance imaging. Ultrasound Q 2007;23:211-23.
19. Gezer C, Ekin A, Sinem Gezer N, Solmaz U, Ozeren M.

Quantitative evaluation of the fetal cerebellar vermis using the median view on two-dimensional ultrasound. Iran J Radiol 2016;13:e34870.

20. Ye J, Rong R, Dou Y, Jiang J, Wang X. Evaluation of the development of the posterior fossa in normal Chinese fetuses by using magnetic resonance imaging. Medicine (Baltimore) 2020;99:e19786.

21. Dovjak GO, Schmidbauer V, Brugger PC, Gruber GM, Diogo M, Glatter S, *et al.* Normal human brainstem development *in vivo*: A quantitative fetal MRI study. Ultrasound Obstet Gynecol 2021;58:254-63.

22. Zalel Y, Seidman DS, Brand N, Lipitz S, Achiron R. The development of the fetal vermis: An *in utero* sonographic evaluation. Ultrasound Obstet Gynecol 2002;19:136-9.

Evaluation of the Ponticulus Posticus with Cone-beam Computed Tomography in a Turkish Population

Abstract

Introduction: The aim of this study was to investigate the incidence of ponticulus posticus (PP) in a sample population with cone-beam computed tomography (CBCT). **Materials and Methods:** The images of 1000 patients who were examined CBCT were analyzed retrospectively. The frequency of PP was evaluated. The presence of complete or partial PP in the atlas was examined on reformed sagittal cross-sectional images. **Results:** It was found that PP was detected in 250 patients (25%). When the prevalence of PP among gender was examined, it was found that 129 (24.2%) of 533 females and 121 (25.9%) of 467 males had PP. Complete PP was detected in 142 patients and partial PP was detected in a total of 151 patients. **Discussion and Conclusion:** In conclusion, PP is a common variation of the atlas. The increase in the frequency of complete PP and the decrease in the frequency of partial PP in older age groups suggested that there may be a correlation between age and PP formation.

Keywords: *Anatomical variation, atlas vertebrae, cone-beam computed tomography, ponticulus posticus*

Suheda Erdem,
Kaan Gündüz¹,
Pelin Kasap²

Department of Maxillofacial Radiology, Faculty of Dentistry, Giresun University, Giresun, Departments of ¹Dentomaxillofacial Radiology and ²Statistics, Faculty of Dentistry, Ondokuz Mayis University, Samsun, Turkey

Introduction

The atlas is divided into two arches by lateral mass. The posterior arch is longer than the anterior arch.

Ponticulus posticus (PP) is a bony bridge between the posterior part of the superior articular process and the posterolateral part of the superior margin of the posterior arch of the atlas.[1,2] PP is a variation of the atlas consisting of a completely or partially calcified bridge [Figure 1a and b]. The PP means "little posterior bridge" in Latin. PP has been mentioned by different names in the literature, including PP, foramen sagittal, foramen atlantoideum posterior, Kimmerle's anomaly, foramen retroarticular superior, canalis vertebralis, retroarticular vertebral artery ring, retroarticular canal, foramen arcuale, and retrocondylar vertebral artery.[1,3,4]

Vertebrobasilar insufficiency, cervical pain syndrome, headache, migraine without aura, the onset of acute hearing loss, and chronic tension-type headaches have been reported associated with PP.[2,5,6] In addition to skeletal anomalies such as frontal bossing and bifid rib in Gorlin–Goltz syndrome, PP formation has also been reported.[7]

Some authors describe PP as a causal element in vertigo, Barre–Lieou syndrome, eye pain, and photophobia. Because PP causes vertebral artery compression, vertebrobasilar circulatory ischemia is provoked. Surgical excision of PP may reduce these signs.[6,8,9]

The structure is seen clearly on plain radiographs of the craniocervical junction in the lateral projection, including the lateral cephalogram. However, radiographic analysis with plain radiographs can evaluate PP in only two dimensions. Cone-beam computed tomography (CBCT) has great advantages over planar skull radiography in visualizing the cervical vertebrae. It enables the depiction of the vertebral column in three planes of space and also has the advantage of having a lower radiation dose and high spatial resolution compared to CT.

The aim of this study was to determine the incidence of PP in the Turkish population. In addition, it was aimed to increase the awareness of clinicians about this variation, which causes various symptoms in the head-and-neck region.

Access this article online

Website: https://journals.lww.com/joai

DOI: 10.4103/jasi.jasi_188_21

Quick Response Code:

How to cite this article: Erdem S, Gündüz K, Kasap P. Evaluation of the ponticulus posticus with cone-beam computed tomography in a Turkish population. J Anat Soc India 2023;72:140-4.

Materials and Methods

Ethics

This study was performed in line with the principles of the Declaration of Helsinki. Approval was granted by the Ethics Committee of University (decision note: 2019/11).

Study design

The participants gave consent for their images to be used in scientific studies. The images of 1000 patients who presented CBCT between the years 2017 and 2018 in the University Faculty of Dentistry Department of Maxillofacial Radiology were analyzed retrospectively. Criteria were set for the inclusion and exclusion of selected images from the study. The criteria for inclusion are that individuals are 18 years old or older. X-ray, scanner, and conical beam-related artifacts that adversely affect the evaluation of CBCT images were determined as criteria for exclusion.

CBCT images were obtained with a dental volumetric imaging system (GALILEOS Comfort Plus, Sirona Dental Systems, Bensheim, Germany) operating at 98 kVp and 15–30 mAs values. CBCT images are generated by a rotation of 204° at 0.3/0.15 mm ≥ isotropic voxel, 14 s scanning time, and 2–6 s expose time. Simultaneous reconstruction was performed with SIRONA Sidexis XG 2.61 imager program with 12-bit grayscale depth, 0.25 mm ≥ isotropic voxels.
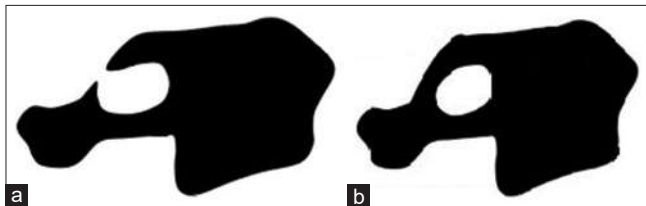
Figure 1: (a) Schematic diagram of a partial PP, (b) Schematic diagram of a complete PP. PP: Ponticulus posticus

All examinations were performed on a 27-inch color Liquid Crystal Display(LCD) screen (The RadiForce MX270W, Eizo Nanao Corporation, Ishikawa, Japan) with a resolution of 3.7 MP, 68 cm, 2560 × 1440. Examination of the CBCT images was performed by a maxillofacial radiologist in a dimly lit room.

One thousand CBCT images were selected consecutively according to inclusion criteria. The selected images were reviewed by a single researcher. The age and gender of the patients were noted based on the CBCT system.

The presence of complete or partial PP in the atlas was examined on reformed sagittal cross-sectional images. The presence of the right and left sides of the PP was also examined. The lack of bone spicule between the posterior arch of the atlas and the upper articular surface was recorded as the absence of PP [Figure 2]. A complete PP was considered a circumferential bony bridge between the posterior arch of the atlas and the superior articular

Figure 2: The white arrow points to the normal atlas: Absent PP on sagittal section CBCT image. PP: Ponticulus. posticus, CBCT: Cone-beam computed tomography

Figure 3: The white arrow points to circumferential bony bridge: Complete PP on sagittal section CBCT image. PP: Ponticulus. posticus, CBCT: Cone-beam computed tomography

Figure 4: The white arrow points to bony spicule: Partial PP on sagittal section CBCT image. PP: Ponticulus. posticus, CBCT: Cone-beam computed tomography

Table 1: Distribution of ponticulus posticus by gender and age groups

	PP		Complete PP		Partial PP	
	n (%)	*P*	*n* (%)	*P*	*n* (%)	*P*
Gender						
Female	129 (24.20)	0.053	58 (10.9)	0.001*	85 (15.9)	0.424
Male	121 (25.9)		84 (18)		56 (14.1)	
Total	250 (25)		142 (14.2)		151 (15.1)	
Age groups						
18–35	67 (23.8)	0.840	32 (11.3)	0.151	46 (16.3)	0.558
36–55	109 (25.7)		60 (14.2)		66 (15.6)	
56	74 (25.2)		50 (17)		39 (13.3)	
Total	250 (25)		142 (14.2)		151 (15.1)	

*Statistically significant level is *P*<0.05. *n*: Number of samples, PP: Ponticulus posticus

facet [Figure 3]. Partial PP describes a bony spicule that forms from the superior articular facet down or from the posterior arch up but does not merge [Figure 4].

All statistical analyses were carried out using IBM SPSS Statistics 21.0 (IBM Corp., Armonk, NY, USA) and MS Excel 2007. Power analysis was used to determine the number of samples. The Chi-square test was used to determine whether there was a statistically significant relationship between age and gender in the presence of PP in all patients.

Results

The patients in the present study ranged from 18 to 88 years with a mean age of 45.24 ± 14.93 years. The mean age of the patients with PP was 45.6 ± 15.37 years. PP, complete PP, and partial PP were examined according to gender and age groups [Table 1]. The number of patients was 1000, including 533 females and 467 males. Although PP was more common in males, no statistically significant relationship was found between gender and PP. However, the prevalence of complete PP was statistically significantly higher in males.

The patients were divided into three age groups. These age groups were 18–35 (282 patients), 36–55 (424 patients), and 56 years and older (294 patients). It was found that while the prevalence of complete PP increased, partial PP prevalence decreased with aging.

In patients with PP, complete/partial and unilateral/bilateral were examined. PP variation was unilateral at 54% and bilateral at 46% [Table 2]. Furthermore, the right and left distributions of complete and partial PP were investigated [Table 3]. As a result of the Chi-square analysis, it can be said that there is a statistically significant relationship between gender and left complete ($P = 0.001$).

Discussion

In the present study, the prevalence of PP was examined in CBCT images. It has been presented that PP is associated with certain conditions such as vertebrobasilar insufficiency, migraine, chronic tension headaches, cervical

Table 2: Distribution of Ponticulus Posticus (PP) by unilateral/bilateral

	PP (%)
Unilateral	
Right Complete-Left Absent	7.6
Left Complete-Right Absent	12.
Right Partial-Left Absent	16.
Left Partial-Right Absent	17.6
Total	54
Bilateral	
Bilateral Complete	19.6
Bilateral Partial	9.2
Right Complete-Left Partial	8.8
Left Complete-Right Partial	8.4
Total	46

pain syndrome, and the onset of acute hearing loss.[2,5,6] It has been reported that there is a correlation between PP and Gorlin–Goltz syndrome.[7] Since PP is associated with many symptoms and diseases, a radiographic examination can help diagnose these diseases.

PP prevalence was reported between 1.3% and 45.9%.[2] In studies conducted in the Turkish population, Bayrakdar *et al.*[10] found the prevalence of PP to be 17.4%. In addition, Şekerci et al. reported the prevalence of PP in the Turkish population as 36.8%. In this study, 1000 CBCT data of Turkish people were examined and PP was found in 25%.

In the present study, although it was more common in males, no statistically significant relationship was found between gender and PP. Similar to the current study, Selby *et al.*[12] and Bayrakdar *et al.*[10] reported a statistically insignificant difference despite male predominance. In other studies reporting male dominance, Geist *et al.*[3] and Sekerci *et al.*[11] stated that this dominance was statistically significant. Some authors stated that the prevalence of PP is higher in females, but the difference is statistically insignificant.[13-15] Mitchell[16] reported for females an incidence of 10.4% and for males an incidence of 6.3% and 10%. Kendrick and Biggs reported in 16.9% of the studied females and 14.6% of the males.[17] The prevalence and

Table 3: Right and left distribution of complete and partial ponticulus posticus

	Right complete PP		Left complete PP		Right partial PP		Left partial PP	
	n (%)	*P*	*n* (%)	*P*	*n* (%)	*P*	*n* (%)	*P*
Female	42 (7.9)	0.186	38 (7.1)	0.001*	47 (8.8)	0.700	54 (10.1)	0.144
Male	48 (10.3)		63 (13.5)		38 (8.1)		35 (7.5)	
Total	90		101		85		89	

*Statistically significant level is *P*<0.05, *n*: Number of samples, PP: Ponticulus posticus

Table 4: The prevalence of ponticulus posticus, distribution by gender, and mean age or age range in previous studies

	PP (%)	Male (%)	Female (%)	Mean age or age ranges
Sharma *et al.*[2]	4.3	5.33	3.76	15
Geist *et al.*[3]	26.2	31	22	<17
Young *et al.*[4]	15.5	NA	NA	NA
Bayrakdar *et al.*[10]	17.4	19.5	16.1	8–81
Sekerci *et al.*[11]	36.8	41.2	33.2	24.8
Selby *et al.*[12]	27.1	30.5	24.7	NA
Chen *et al.*[13]	7	5	9	49.4
Cho[14]	15.5	14	17	45
Hasani *et al.*[15]	20.6	17.1	22.3	35.68
Mitchell[16]	9.8	9.5	10.4	20–80
Kendrick and Biggs[17]	15.8	14.6	16.9	6–17
Paraskevas *et al.*[19]	34.46	35.55	33.72	5–90
Taitz and Nathan[20]	33.7	NA	NA	11–105
Present study	25	25.9	24.2	45.24

NA: Not available, PP: Ponticulus posticus

distribution by gender of PP and mean age or age range in previous studies are illustrated in Table 4.

Another subject of investigation is the relationship between age and PP prevalence. Some authors have said that there is no correlation between aging and PP formation.[11-13,15,18] Contrary to the general view, Bayrakdar *et al.*[10] reported that PP prevalence increased with age. The authors concluded that the incidence of PP did not increase with age. Selby *et al.* have been reported[12] that the PP be forming at mean 9 years of age. Furthermore, the results of the study by Mitchell[16] arose that the PP has a low incidence at different age groups of puberty.

In the present study, when examined complete PP in age groups, it was found that the prevalence increased with aging. This ratio was 17% (50 in 294 patients) in the 56-year and older group with the most common PP prevalence. This was followed by the 36–55-year age group (14.2%) and the 18–35-year age group (11.3%), respectively. There was no statistically significant difference between these groups. The prevalence of complete PP has increased while the prevalence of partial PP has decreased with aging. The peak prevalence of partial PP was in the 18–35-year age group with 16.3%. There were 15.6% in the 36–55-year age group and 13.3% in the 56-year and older age group. Similar to the current study, Paraskevas *et al.*[19] reported

that the ossification process and the incidence of complete PP increased with age, while the incidence of partial PP decreased. These findings suggest that the formation of complete PP occurs following an ossification process of partial PP.[19] These results support the results of Taitz and Nathan[19] who reported that partial PP is more prevalent in the 10-30 age group, and complete PP is more prevalent in the 30-80 age group. Kendrick and Biggs[17] observed two females with unilateral partial PP over a 1- to 2-year period. They reported that a complete unilateral PP had developed during this period. This work supported the idea that partial PP could be a precursor to complete PP.

Various theories about PP formation have been put forward. According to Allen,[21] this condition is a congenital feature. Selby *et al.*[12] claimed it to be a genetic feature. Others, such as Pyo and Lowman[1] and Panjabi and White,[22] have argued that this may be a result of ossification caused by aging. Paraskevas *et al.*[19] and Taitz and Nathan[20] argued that extraneous mechanical factors, for example, the habit of carrying heavy materials in the head, may play a role in the development of atlas anomalies.

Various movements such as flexion, extension, and rotation occur in the atlantoaxial joint. Atlantoaxial instability is extreme movement in the atlantoaxial joint. Balance problems can cause symptoms such as blurred vision, frequent headaches and neck pain, difficulty swallowing, dizziness, fullness in the ears, migraine, suboccipital headache, and tinnitus.[23,24] In the treatment of this atlantoaxial instability, the use of lateral mass screws in the fixation of the atlas has gained popularity.[4,24] However, this treatment comes with important difficulties and life-threatening complications. Placing a C1 lateral mass screw at the classical entry point at the junction of the posterior arch and lateral mass may cause severe bleeding from the epidural plexus and irritation of the C2 nerve root, resulting in occipital neuralgia. Therefore, some surgeons recommend placing the screw upward from the posterior arch.[25] In this new approach, the wide posterior arch of the atlas is the appropriate area for screw placement. It is a practical and useful method for most patients. However, in the presence of PP, screw fixation can be performed on PP, assuming this anomaly as a wide arc, and this condition results in injury to the vertebral artery.[2,4,23]

The neural crest forms the maxilla, mandible, ear bones, hyoid bone, larynx, dentin, cementum, periodontal ligament, alveolar bone, and vertebral column.[26] Studies in adult populations confirm the relationship between PP and

malocclusions, skeletal deviations in both jaws, prenatal observable skull base, and cervical spine abnormalities.[27] It has been suggested that there is a relationship between dental agenesis and PP.[28] It has been reported that the prevalence of cervical spine anomalies is higher in cleft lip and palate patients.[29] The probability of palatal displacement canine increases with the presence of PP.[30]

Conclusion

PP is a common variation of the atlas. The increase in the frequency of complete PP and the decrease in the frequency of partial PP in older age groups suggested that there may be a correlation between age and PP formation. While examining headache, vertigo 170, and cervical pain of unknown cause, clinicians should not ignore this common atlas anomaly besides complications can be prevented during surgical procedures involving the region, with the radiologists reporting this variation.

Financial support and sponsorship

Nil.

Conflicts of interest

There are no conflicts of interest.

References

1. Pyo J, Lowman RM. The ponticulus posticus of the first cervical vertebra. Radiology 1959;72:850-4.
2. Sharma V, Chaudhary D, Mitra R. Prevalence of ponticulus posticus in Indian orthodontic patients. Dentomaxillofac Radiol 2010;39:277-83.
3. Geist JR, Geist SM, Lin LM. A cone beam CT investigation of ponticulus posticus and lateralis in children and adolescents. Dentomaxillofac Radiol 2014;43:20130451.
4. Young JP, Young PH, Ackermann MJ, Anderson PA, Riew KD. The ponticulus posticus: İmplications for screw insertion into the first cervical lateral mass. J Bone Joint Surg Am 2005;87:2495-8.
5. Chitroda PK, Katti G, Baba IA, Najmudin M, Ghali SR, Kalmath B, *et al.* Ponticulus posticus on the posterior arch of atlas, prevalence analysis in symptomatic and asymptomatic patients of gulbarga population. J Clin Diagn Res 2013;7:3044-7.
6. Koutsouraki E, Avdelidi E, Michmizos D, Kapsali SE, Costa V, Baloyannis S. Kimmerle's anomaly as a possible causative factor of chronic tension-type headaches and neurosensory hearing loss: Case report and literature review. Int J Neurosci 2010;120:236-9.
7. Leonardi R, Santarelli A, Barbato E, Ciavarella D, Bolouri S, Härle F, *et al.* Atlanto-occipital ligament calcification: A novel sign in nevoid basal cell carcinoma syndrome. Anticancer Res 2010;30:4265-7.
8. Travan L, Saccheri P, Sabbadini G, Crivellato E. Bilateral arcuate foramen associated with partial defect of the posterior arch of the atlas in a medieval skeleton: Case report and review of the literature. Looking backward to go forward. Surg Radiol Anat 2011;33:495-500.
9. Wight S, Osborne N, Breen AC. Incidence of ponticulus posterior of the atlas in migraine and cervicogenic headache. J Manipulative Physiol Ther 1999;22:15-20.
10. Bayrakdar IS, Miloglu O, Altun O, Gumussoy I, Durna D, Yilmaz AB. Cone beam computed tomography imaging of ponticulus posticus: Prevalence, characteristics, and a review of the literature. Oral Surg Oral Med Oral Pathol Oral Radiol 2014;118:e210-9.
11. Sekerci AE, Soylu E, Arikan MP, Ozcan G, Amuk M, Kocoglu F. Prevalence and morphologic characteristics of ponticulus posticus: Analysis using cone-beam computed tomography. J Chiropr Med 2015;14:153-61.
12. Selby S, Garn SM, Kanareff V. The incidence and familial nature of a bony bridge on the first cervical vertebra. Am J Phys Anthropol 1955;13:129-41.
13. Chen CH, Chen YK, Wang CK. Prevalence of ponticuli posticus among patients referred for dental examinations by cone-beam CT. Spine J 2015;15:1270-6.
14. Cho YJ. Radiological analysis of ponticulus posticus in Koreans. Yonsei Med J 2009;50:45-9.
15. Hasani M, Shahidi S, Rashedi V, Hasani M, Hajiyan K, *et al.* Cone beam CT study of ponticulus posticus: Prevalence, characterictics. Biomed Pharmacol J 2016;9:1067-72.
16. Mitchell J. The incidence and dimensions of the retroarticular canal of the atlas vertebra. Cells Tissues Organs 1998;163:113-20.
17. Kendrıck GS, Bıggs NL. Incidence of the ponticulus posticus of the first cervical vertebra between ages six to seventeen. Anat Rec 1963;145:449-53.
18. Mitchell BS, Humphreys BK, O'Sullivan E. Attachments of the ligamentum nuchae to cervical posterior spinal dura and the lateral part of the occipital bone. J Manipulative Physiol Ther 1998;21:145-8.
19. Paraskevas G, Papaziogas B, Tsonidis C, Kapetanos G. Gross morphology of the bridges over the vertebral artery groove on the atlas. Surg Radiol Anat 2005;27:129-36.
20. Taitz C, Nathan H. Some observations on the posterior and lateral bridge of the atlas. Acta Anat (Basel) 1986;127:212-7.
21. Allen W. The varieties of the atlas in the human subject, and the homologies of its transverse processes. J Anat Physiol 1879;14:18-27.
22. Panjabi M, White A. Clinical Biomechanics of the Spine: Kinematics of the Spine. Philadelphia: JB Lippincott Company; 1990. p. 85-127.
23. Goel A. Screws, facets, and atlantoaxial instability. World Neurosurg 2013;80:514-5.
24. Goel A, Desai KI, Muzumdar DP. Atlantoaxial fixation using plate and screw method: A report of 160 treated patients. Neurosurgery 2002;51:1351-6.
25. Gautschi OP, Payer M, Corniola MV, Smoll NR, Schaller K, Tessitore E. Clinically relevant complications related to posterior atlanto-axial fixation in atlanto-axial instability and their management. Clin Neurol Neurosurg 2014;123:131-5.
26. Dassule HR, McMahon AP. Analysis of epithelial-mesenchymal interactions in the initial morphogenesis of the mammalian tooth. Dev Biol 1998;202:215-27.
27. Sonnesen L, Kjaer I. Cervical column morphology in patients with skeletal open bite. Orthod Craniofac Res 2008;11:17-23.
28. Putrino A, Leonardi RM, Barbato E, Galluccio G. The association between ponticulus posticus and dental agenesis: A retrospective study. Open Dent J 2018;12:510-9.
29. Hoenig JF, Schoener WF. Radiological survey of the cervical spine in cleft lip and palate. Dentomaxillofac Radiol 1992;21:36-9.
30. Haji Ghadimi M, Amini F, Hamedi S, Rakhshan V. Associations among sella turcica bridging, atlas arcuate foramen (ponticulus posticus) development, atlas posterior arch deficiency, and the occurrence of palatally displaced canine impaction. Am J Orthod Dentofacial Orthop 2017;151:513-20.

Neuroanatomy of Stroke: A Computed Tomography-based Topographic Analysis

Abstract

Background: The present study is a computed tomography (CT)-based topographic analysis of cerebral stroke that constitutes the distribution of infarction and hemorrhage with respect to different neuro-anatomical structures. CT scanning is the easily affordable technique in India for the accurate diagnosis of cerebral stroke. **Aim:** The aim of the present study is to evaluate the incidence of brain stroke by CT scan in patients with cerebrovascular accidents. **Subjects and Methods:** Patients with cerebrovascular accidents were subjected to CT scan of the head using GE Revolution ACTs 16 slice multi-detector row CT scanners, slice thickness – 2 mm, 5 mm, and 10 mm and matrix size of 512×512. The incidence of stroke in patients over 20 years of age at SCB Medical College was evaluated during the period 2019–2021. The incidence of stroke was studied according to age, sex, and stroke subtype with arterial involvement. **Results:** The topography of brain infarction was highly variable with all regions of the middle cerebral artery (MCA) territory. There were 190 ischemic and 106 hemorrhagic stroke cases out of 296 patients. The mean age was 55.28 ± 12.73 years. Maximum stroke cases were seen in the age group of 41–60 years and 61–80 years of age. The most common site was basal ganglia 112 (37.83%) and common arterial involvement was MCA 161 (54.4%) with statistical significance ($P < 0.05$). **Conclusions:** The incidence of stroke rises with age and has its peak in the highly productive age group of 40–60 years of age. The findings of the present study will be helpful to young doctors for proper diagnosis and treatment.

Keywords: *Cerebrovascular accident, computed tomography scan, middle cerebral artery territory, stroke*

Sonali Subhadarsini, Aboobacker Sait Shani, Dharma Niranjan Mishra

Department of Anatomy, S. C. B. Medical College, Cuttack, Odisha, India

Introduction

Computed tomography (CT) scan and magnetic resonance imaging (MRI) techniques are utilized to visualize and identify the internal structures of the brain without dissection. The brain is the only organ that makes the humans different from other animals.[1]

The brain is supplied by anterior, middle, and posterior cerebral arteries. The arrangement of arterial communications at the base of the brain forms a unique arterial circle called circle of willis or circulus arteriosus cerebri.[2] Any blockage to these blood vessels leads to cerebrovascular accident commonly known as stroke.

The World Health Organization has defined stroke as "rapidly developing clinical signs of focal or global disturbance of cerebral function, lasting for more than 24 h or leading to death, with no apparent cause other than a vascular origin."[3]

Stroke is the 3rd most common cause of morbidity and mortality in the developed world. Ischemic strokes are contributing 50%–85% of all strokes worldwide and hemorrhagic strokes may be due to subarachnoid hemorrhage or intracerebral hemorrhage accounting for 1%–7% and 7%–27%, respectively, of all strokes worldwide.[4]

As MRI is not as widely available as CT and the scanning times are also longer. Hence, CT remains the most practical and widely available method of imaging the brain.[4]

Stroke is considered as the disease of elderly people, but nowadays, the incidence has increased in young (20%–27%). In the USA, stroke has 11% mortality, while in India, it comprises 4% of medical admissions in major hospitals and 20% of the disease of the central nervous system.[5]

Subjects and Methods

The present study is a retrospective record-based study carried out on 296

Access this article online

Website: https://journals.lww.com/joai

DOI: 10.4103/jasi.jasi_112_22

Quick Response Code:

How to cite this article: Subhadarsini S, Shani AS, Mishra DN. Neuroanatomy of stroke: A computed tomography-based topographic analysis. J Anat Soc India 2023;72:145-50.

stroke patients conducted in the department of anatomy in collaboration with the Department of Medicine and Department of Radiology of SCB Medical College and Hospital, Cuttack from August 2019 to February 2022. Patients clinically diagnosed with stroke were subjected to CT scan of their heads using serial contiguous axial sections of the brain using 0.625 mm in multi-slice spiral scanner with three-dimensional construction by qualified CT radiographers using the standard departmental protocol for brain investigations. CT images and case notes of the patients that underwent cranial CT based on clinical diagnosis were retrieved from the medical records and the relevant data were extracted and analyzed. All the data were collected on the basis of inclusion and exclusion criteria. Inclusion criteria – Patients above 18 years of age with CT confirmed diagnosis of stroke and stroke due to trauma and tumor were excluded from the study. GE Revolution ACTs 128 slices multi-detector row CT scanners with a slice thickness of 0.625–1.25 mm and matrix size of 512×512. Every acquired CT slice is subdivided into a matrix of up to 1024×1024 volume elements (voxels). Each voxel has been traversed during the scan by numerous X-ray photons and the intensity of the transmitted radiation is measured by detectors. From these intensity readings, the density or attenuation value of the tissue at each point in the slice can be calculated. Specific attenuation values are assigned to each individual voxel. The viewed image is then reconstructed as a corresponding matrix of picture elements (pixels). Each pixel is assigned a numerical value (CT number), which is the average of all the attenuation values contained within the corresponding voxel. This number is compared to the attenuation value of water and displayed on a scale of arbitrary units named Hounsfield Units (HU) after Sir Godfrey Hounsfield. This scale assigns water an attenuation value (HU) of 0. The range of CT numbers is 2000 HU wide, although some modern scanners have a greater range of HU up to 4000. Each number represents a shade of gray with +1000 (white) and −1000 (black) at either end of the spectrum.[6] HU measurements: [7] The HU measurement of Bone is +613 HU which ranges from +700 HU to +3000 HU. White matter ~ +24.7 H, Grey matter ~ +35.8 HU, cerebrospinal fluid-ventricle ~ +3.3 HU scalp fat ~ −84.5 HU, Air ~ −966.3 HU and Blood ~ 30–80 HU.

Data analysis

The observed data were entered into the IBM SPSS, Version 28.0. (IBM Corp Armonk, NY) software version for analysis. The percentage, proportion, and standard deviations were observed. The results were presented in text and tables. $P < 0.05$ was considered statistically significant.

Ethical issue

The present study satisfies the criteria of the Institutional Ethics Committee (IEC) S. C. B Medical College Cuttack, 753,007, Orissa, as per the World Medical Association Declaration of Helsinki vide IEC/IRB No. 164 Date. February 07, 2020.

Results

During the study, 296 acute stroke patients were included among the patients admitted to the medicine ward of SCB Medical College and Hospital, Cuttack, who fulfilled the inclusion criteria. All the cases were studied for the pattern of area of the brain affected as per the CT scan findings.

Among 296 stroke patients with the age ranging from 20 to 92 years with a mean age was being 55.28 ± 12.73 years. It was seen that 34 cases that is 11.48% fell in the age group of 20–40 years. The incidence of stroke was maximum in the age group of 41–60 years, which comprised 41.21% of total patients. It was found that 121 patients belonged to the age group of 61–80 years that is 40.87% and 19 patients that is 6.41% belonged to the age group of above 80 years.

The male patients were more in number 194 (65.54%) than female patients 102 (34.45%) and the male: female ratio was 1.9:1. The incidence of male versus female in all the age groups were <0.05 which was statistically significant [Table 1].

In the present study, out of 296 patients, 190 (64.18%) were suffering from ischemic stroke and 106 (35.81%) hemorrhagic stroke, respectively. The age- and sex-wise distribution and percentage were observed. The maximum incidence of stroke was in the age group of 41–60 years group 125 (42.2%) followed by 118 (39.9%) in the age group of 60–80 years, 34 (11.5%) patients in the age group of 20–40 years, and only 19 (6.4%) cases observed more than 80 years of age [Table 2].

Ischemic stroke patients were 190 (64.18%) in the present study. Maximum cases were seen in the age group of 41–60 years 83 (28%) in male 55 (18.6%) and female 28 (9.5%) followed by in the age group of 61–80 years there were 78 (41.05%) male 52 (17.6%) and female 26 (8.8%), 18 cases (6.08%) within the age group of 20–40 years, and in the age group of above 80 years only 11 cases (3.7%) were seen in both male and female patients [Table 2 and Figure 1a].

Hemorrhagic stroke patients were 106 (35.81%) out of 296 in the present study. The maximum incidence of stroke was 42 cases (14.2%), found in the age group of 41–60 years male 29 (9.8%) and female 13 (4.4%) followed by in the age group of 61–80 years. There were 40 cases (13.5%), of which male 27 (9.1%) and female 13 (4.4%), respectively. Other cases belonged to 16 cases (15.09%) in the age group of 20–40 years and in the age group above 80, there were 8 cases (7.54%) with minimal sex difference. So irrespective of gender distribution maximum number of

Table 1: Age and sex distribution in cerebral stroke							
Age group (years)	Male	Mean±SD	Percentage	Female	Mean±SD	Percentage	*P*
20–40	19	30.14±9.35	6.41	15	36.11±6.14	5.06	0.040
41–60	81	47.68±4.01	27.36	41	49.70±4.91	13.85	0.016
61–80	82	71.24±5.76	27.70	39	65.15±3.87	13.18	0.0001
>80	12	84.25±2.55	4.05	7	87.71±3.53	2.36	0.02
Total	194	55.28±12.73	65.54	102	60.79±11.99	34.45	0.0004

SD: Standard deviation

Table 2: Age/sex distribution in ischemic versus hemorrhagic cerebral stroke							
Age (years)	Ischemic stroke (*n*=190)			Hemorrhagic stroke (*n*=106)			Both (*n*=296), *n* (%)
	Male, *n* (%)	Female, *n* (%)	Total, *n* (%)	Male, *n* (%)	Female, *n* (%)	Total, *n* (%)	
20–40	10 (5.26)	8 (4.21)	18 (9.47)	9 (8.5)	7 (6.6)	16 (15.1)	34 (11.5)
41–60	55 (28.95)	28 (14.74)	83 (43.7)	29 (27.36)	13 (12.26)	42 (39.62)	125 (42.2)
61–80	52 (27.37)	26 (13.68)	78 (41.05)	27 (25.47)	13 (12.26)	40 (37.74)	118 (39.9)
>80	7 (3.7)	4 (2.10)	11 (5.8)	5 (4.7)	3 (2.8)	8 (7.5)	19 (6.4)
Total	124 (65)	66 (35)	190 (100)	70 (66)	36 (34)	106 (100)	296 (100)
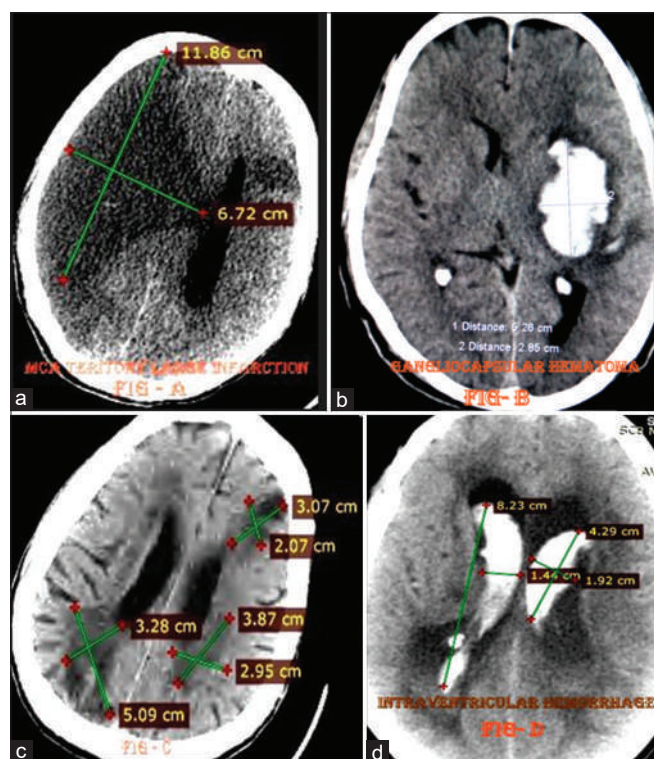
Figure 1: (a) Middle cerebral artery tertiary large infarction. (b) Gangliocapsular hematoma. (c) Anterior cerebral artery and posterior cerebral artery territory infarction. (d) Intra-ventricular hemorrhage

stroke patients were within the age group of 41–60 years 125 (42.2%) cases [Table 2 and Figure 1b].

In this study of 190 ischemic stroke cases both male and female, the most common site of infarction was basal ganglia [Figure 1a] 82 in number (43.15%) followed by parietal lobe 35 (18.42%) and thalamus which was 28 (14.73%) of cases. The affection of frontal lobe stood at 12 (6.31%), occipital lobe was 9 (4.74%), and cerebellum and temporal lobe 8 (4.21%)

each [Figure 1c]. The pontine ischemia was 5 (2.63%) and midbrain 3 (1.6%) contributing lowest incidence in our study.

Out of 106 hemorrhagic cases, the most common site of hemorrhage was basal ganglia and ventricles [Figure 1d] contributing 30 cases (28.30%) each followed by the thalamus in 21 cases (19.81%). Parietal lobe affection was found in 10 cases (9.4%), frontal lobe affection was found in 5 cases (4.71%), and pons and cerebellum each found in 4 cases (3.8%) of the hemorrhagic stroke [Table 3].

The *P* value of ischemic brain stroke 82 (43.2) and hemorrhagic brain stroke 30 (28.3) in both males and females was 0.011, which was <0.05 being statistically significant for basal ganglia. Similar studies were observed for parietal, temporal, and occipital lobes.

Arterial territory involvement in 190 cases of infarction of the brain, 119 (62.6%) cases were seen as the ischemia of middle cerebral artery (MCA), followed by posterior cerebral artery (PCA) territory involvement which was 39 in number (20.5%), anterior cerebral artery (ACA) 17 (8.9%) and vertebrobasilar artery territory involvement was 15 (7.9%) found in the present study.

Out of the 106 cases of cerebral hemorrhage of PCA, territory involvement was 56 (52.8%) cases, followed by MCA territory involvement which was 42 (39.6%), vertebrobasilar artery territory in 5 (4.7%) cases, and ACA territory involvement in 3 (2.8%) [Table 4 and Figure 1c and d].

In the present study, overall, the MCA territory involvement was the most common site of cerebral stroke in 161 (54.4%) cases followed by PCA 95 (32.1%) cases. The ACA and vertebral-basilar artery were contributing to 20 (6.75%) patients each. The MCA, PCA, and ACA territory involvement was $P < 0.05$, which was statistically significant except for vertebral-basilar arteries.

Table 3: Topographic distribution of ischemic and hemorrhagic cerebral stroke in both males and females

Area of brain involved	MI (*n*=124), *n* (%)	FI (*n*=66), *n* (%)	Total number IBS (*n*=190), *n* (%)	MH (*n*=70), *n* (%)	FH (*n*=36), *n* (%)	Total number HBS (*n*=106), *n* (%)	*P* from *Z* score IS: HS
Basal ganglia	55 (29)	27 (14.2)	82 (43.2)	18 (17)	12 (11.3)	30 (28.3)	0.011 (significant)
Thalamus	16 (8.4)	12 (6.3)	28 (14.7)	14 (13.2)	7 (19.4)	21 (19.8)	0.26 (NS)
Mid brain	2 (1.05)	1 (0.5)	3 (1.6)	2 (1.9)	0	2 (1.9)	0.8 (NS)
Pons	4 (2.1)	1 (0.5)	5 (2.6)	2 (1.9)	2 (1.9)	4 (3.8)	0.6 (NS)
Ventricles	0	0	0	23 (21.7)	7 (6.6)	30 (28.3)	<0.0001
Cerebellum	5 (2.6)	3 (1.6)	8 (4.2)	2 (1.9)	2 (1.9)	4 (3.8)	0.8 (NS)
Frontal	10 (5.3)	2 (1.05)	12 (6.3)	3 (2.8)	2 (1.9)	5 (4.7)	0.6 (NS)
Parietal	21 (11)	14 (7.37)	35 (18.4)	6 (5.7)	4 (11.11)	10 (9.4)	0.039 (significant)
Temporal	6 (3.2)	2 (1.05)	8 (4.2)	0	0	0	0.032 (significant)
Occipital	5 (2.6)	4 (2.1)	9 (4.7)	0	0	0	0.022 (significant)
Total	124 (65)	66 (35)	190 (100)	70 (66)	36 (34)	106 (100)	296

MI: Male infarction, FI: Female infarction, MH: Male hemorrhagic, FH: Female Hemorrhagic, IBS: Ischemic brain stroke, HBS: Hemorrhagic brain stroke, NS: Not significant, HS: Hemorrhagic stroke, IS: Ischemic stroke

Table 4: Arterial territory involvement in ischemic versus hemorrhagic cerebral stroke

Arterial territory	Percentage ischemic stroke (*n*=190), *n* (%)	Percentage hemorrhagic stroke (*n*=106), *n* (%)	Total (*n*=296), *n* (%)	*P* from *Z* score
MCA	119 (62.6)	42 (39.6)	161 (54.4)	0.00014
PCA	39 (20.5)	56 (52.8)	95 (32.1)	0.00001
ACA	17 (8.9)	3 (2.8)	20 (6.75)	0.044
Vertebrobasilar system	15 (7.9)	5 (4.7)	20 (6.75)	0.3
Total	190 (100)	106 (100)	100	

MCA: Middle cerebral artery, PCA: Posterior cerebral artery, ACA: Anterior cerebral artery

Discussion

The study conducted for a 2-year period during 2018 and 2019; 187 (0.187%) people in every lakh population suffer strokes in Cuttack, Odisha, per year approximately.[8]

In the present study, 296 stroke patients were studied, the age ranged from 20 to 92 years and mean age with standard deviation was 55.28 ± 12.73 years.[9] The male patients were more in number 194 (65.54%) than female patients 102 (34.45%) and the male: female ratio was 1.9:1.[10,11] The incidence of male versus female in all the age groups was statistically significant $P < 0.05$. The incidence of stroke was maximum in the age group of 41–60 years 125 (42.2%) of total patients.[11]

It was also observed that lesser incidences were seen in the age group of 61–80 years (118; 39.9%) followed by 19 (6.41%) patients over 80 years of age.[12] This gender difference possibly resulted from inherent socio-cultural bias in India, in which female patients are less likely to be admitted to hospitals compared to male patients. Males are also more exposed to tobacco chewing, smoking,

and alcohol intake. This study was comparable to other Indian studies on stroke patients where greater male preponderance was seen. The incidence of male versus female in all the age groups was statistically significant with $P < 0.05$.[13]

In the present observation, 190 (64.18%) out of 296 patients were suffered from ischemic stroke and the maximum incidence stroke was 83 (43.7%) in the age group of 41–60 years age followed by 78 (41.05%) in the age group of 61–80 years. The male patients 124 (65%) were suffering almost twice as much as the female 66 (35%) as described earlier and corroborative with other authors[14] that the highest incidence of ischemic stroke was in the age group of 46–65 years (50%). The maximum stroke cases in the most productive age group of 41–60 were a potential threat to the socioeconomic status of the family and Nation as well. Out of 296 patients, 106 (35.81%) patients suffered from hemorrhagic stroke. The maximum incidence of stroke was 42 (39.62%) cases among hemorrhagic stroke followed by 40 (37.74%) cases in the age group of 61–80 years of age. The male predominance was also observed as 70 (66%) male with 36 (34%) female patients.[15] The most common factor was being early onset of diabetes mellitus and hypertension due to sedentary modern lifestyles in young adults.[12] Atherosclerosis and cardiogenic thrombo-embolism was being the major etiology of cerebral infarction in increasing age. Uncontrolled blood pressure, excessive use of blood thinners (anticoagulants), and rupture of weak vessels (aneurysms) were the common causes of nontraumatic cerebral hemorrhage.[16] In the present study, the most common site of infarction was basal ganglia 82 (43.2%) followed by parietal 35 (18.4%) and thalamus 28 (14.7%). The blood vessels supplying to gangliocapsular region were narrow and tortuous, which was venerable to both hemorrhage and ischemia.[17] Frontal hemorrhage stands at 12 (6.3%) in number and percentage and cerebellum comprises 8 (4.2%). Other areas had minimal contributions such as temporal 8 (4.2%),

occipital 9 (4.7%), pons 5 (2.6%), and midbrain 3 (1.6%), respectively.[18]

In this study, the most common site of hemorrhage was basal ganglia in 30 (28.3%) patients followed by ventricles in 30 (28.3%) and thalamus in 21 (19.8%) cases. Lateral ventricles were common sites of extension of cerebral bleeding around its territory due to atriovenous malformations, microaneurysms, and coagulation disorders. Intra-ventricular bleed was seen in approximately 40% of cases. The volume of hematoma was directly related to the severity of the injury and prognostic outcomes.[19]

Parietal area affection is found in 10 (9.4%), frontal area affection 5 (4.7) found in 5 cases, and pons and cerebellum each found in 4 (3.8%) cases each.[20,21] The parietal lobe and frontal lobe were received its blood supply directly through the main trunk of middle vertebral artery in comparison to thalamus and basal ganglia by striate arteries, accounting lesser incidence stroke so also pons and cerebellum were supplied by several pontine and cerebellar arteries directly derived from the basilar artery.[18]

It was found that out of the 190 cases of infarction of the brain, 119 (62.6%) cases were seen favoring MCA territory involvement, [Figure 1a] followed by PCA territory involvement 39 (20.5%), ACA 17 (8.9%) [Figure 1c] and vertebrobasilar artery 15 (7.9%) territory involvement.[11,21]

It was also studied that out of the 106 cases of cerebral hemorrhage, 56 (52.8%) cases were seen to be favoring PCA territory involvement, followed by MCA territory involvement 42 (39.6%), and vertebro-basilar artery territory 5 (4.7%) and ACA territory involvement 3 (2.8%) of cases.[11,18] Both cerebral ischemia and hemorrhage due to the involvement of MCA, PCA, and ACA territory.[20,21] In the present study, ischemic stroke was seen in the older age group in contrast to hemorrhagic stroke in younger patients. There were significant differences between cerebral ischemia and hemorrhage in relation to the age of the patient and vascular involvement. Ischemic stroke was twice more common as hemorrhagic with statistically significant $P < 0.05$.[22]

Conclusions

Stroke is a huge public health concern because of its high morbidity and disability. The study conducted for a 2 year period during 2018 and 2019, 187 (0.187%) people in every lakh population suffer strokes in Cuttack, Odisha, per year approximately. It is a collection of clinical syndromes resulting from cerebral ischemia to intracranial hemorrhage. In the present study 296 stroke patients were observed with the age range from 21 to 92 years with male predominance almost twice that of females, i.e., 194 (65.54%) male: female patients 102 (34.45%). The occurrence of cerebral stroke rises with age with a double peak incidence between the age group of 41–60 years and 61–80 years of age. The incidence of cerebral infarction

190 (64.18%) which is nearly double than of hemorrhagic stroke 106 (35.81%) in the present study. The most common site of cerebral infarction is basal ganglia followed by parietal lobe and thalamus. In case of hemorrhage, the most common site affected was basal ganglia followed by ventricles, thalamus, and parietal lobe. The most common arterial involvement for cerebral infarction was of MCA and PCA territory where as the reverse in case of a cerebral hemorrhage. In a developing country like India, CT scan is the inexpensive and widely available technique for the diagnosis of acute stroke. Hence, it must be done in all cases whenever feasible for early treatment and better outcome.

Conflicts of interest

There are no conflicts of interest.

References

1. Standring S. Gray's Anatomy. The Anatomical Basis of Clinical Practice. 42nd ed. Elsevier, Amsterdam; 2020. p. 386-7.
2. Singh V. Text Book of Clinical Neuroanatomy. 3rd ed. Elsevier India; 2017. p. 169-76.
3. World Health Organization. International Task Force for Prevention of Coronary Heart Disease and Stroke, Etiology and Epidemiology of Stroke. Geneva, Switzerland: World Health Organization; 1980.
4. Walker BR, Colledge NR, Ralston SH, Penman ID. Davidson's Principles and Practice of Medicine. 22nd ed. Churchill Livingstone/Elsevier, Edinburgh; 2014. p. 1231-47.
5. Park K. Park's Textbook of Preventive and Social Medicine. 25th ed. Bhanot, K. Park; 2019. p. 407-8.
6. Haaga JR, Boll DT. CT and MRI of the Whole Body. 6th ed., Vol. 1. Elsevier Health Sciences, Amsterdam; 2016. p. 310-38.
7. Zimmerman D. Basic Approach to Head CT Interpretation Neuroradiology. BWH (Brigham and Women's Hospital) – 75 Francis Street Boston, Massachusetts, United States; 2022.
8. Behera BP, Maharana DN, Mohanty PS. An observational study of clinic etiological profile of stroke patients in a new tertiary care hospital in North Odisha, India. Int J Res Med Sci 2019;7:3095-102.
9. Behera BP, Mohanty PS. An observational study from a new tertiary care hospital in North Odisha: Clinical and etiological profile of acute ischemic stroke patients. Int J Adv Med 2019;6:1605-10.
10. Ijeh-Tarila KI, Alazigha N, Mbaba AN, Ogolodom MP, Orupabo-Oyan B, Nwazor E, *et al*. Brain computed tomography findings in stroke patients in Port Harcourt: A retrospective hospital-based study. Am J Biomed Sci Res 2020;8:280-4.
11. Sinha R, Karim AR. Role of computed tomography in evaluation of cerebrovascular accidents. Ann Int Med Dent Res 2017;3:35-9.
12. Kaur G, Samar N, Sharma J, Pareek KK, Veerwal R, Kajla P,

et al. A Study of clinico-radiological and socio-demographic profile of patients with stroke in a terttary care hospital of South West Rajasthan. J Assoc Physicians India 2020;68:54-8.

13. Edzie EK, Dzefi-Tettey K, Gorleku P, Amankwa AT, Idun E, Brakohiapa EK, *et al*. Evaluation of the anatomical locations of stroke events from computed tomography scan examinations in a tertiary facility in Ghana. Cureus 2021;13:e14097.

14. Naik M, Rauniyar RK, Sharma UK, Dwivedi S, Karki DB, Samuel JR. Clinico-radiological profile of stroke in Eastern Nepal: A computed tomographic study. Kathmandu Univ Med J (KUMJ) 2006;4:161-6.

15. Ojha PT, Basak S, Aglave V, Yadav J. Incidence of stroke in adults according to age, sex and subtypes in urban Indian population. Neurol Neurosci Rep 2020;3:1-4.

16. Chen RL, Balami JS, Esiri MM, Chen LK, Buchan AM. Ischemic stroke in the elderly: an overview of evidence. Nat Rev Neurol 2010;6:256-65.

17. Mookan SK, Sundaram S, Rajagopalan N. Gangliocapsular bleed with ipsilateral internal carotid artery aplasia. Pol J Radiol 2015;80:398-400.

18. Hwang JC, Cho SJ, Park HK, Chang JC. Sudden migration of a thalamic hemorrhage into the ventricles. J Korean Neurosurg Soc 2010;47:213-6.

19. Vaidya CV, Majmudar DK. A retrospective study of clinical profile of stroke patients from GMERS Medical College and Hospital, Gandhinagar, Gujarat. Int J Clin Trials 2014;1:62-6.

20. Kaur G, Samar N, Sharma J. A Study of Clinico-radiological and socio-demographic profile of patients with stroke in a tertiary care hospital of South West Rajasthan. J Assoc Physicians India 2020;68:55-8.

21. Abdu H, Tadese F, Seyoum G. Comparison of ischemic and hemorrhagic stroke in the medical ward of Dessie Referral Hospital, Northeast Ethiopia: A retrospective study. Neurol Res Int 2021;2021:9996958. doi: 10.1155/2021/9996958.

22. Hossain M, Haque Rimon R, Islam A, Jamil S, Arif Raihan M, Choudhury A, *et al*. The frequency and location of hemorrhage and infarction in stroke patients having hypertension by Computed Tomography (CT) scan. Fortune J Health Sci 2022;5:296-309.

Investigation of Bone Biomechanics in Rats with Traumatic Kidney Injury

Abstract

Objective: Mineral metabolism disorders are common in chronic kidney disease (CKD) and increase the risk of fractures. It has been confirmed by animal models that these changes in bone also cause negative results in the mechanical properties of bone. Although there are many available methods for diagnosing metabolic bone disorders and estimating fracture risk, it has been suggested that biomechanical tests that provide information about bone's structural and material properties are most appropriate, particularly in small rodents with CKD. Therefore, this study aimed to investigate the effects of trauma-induced kidney damage on bone biomechanical properties. **Materials and Methods:** In this study, we used 16 adult Wistar Albino rats, 200–300 g, 4–5 months old. The animals were examined under two groups: kidney control ($n = 9$) and healty kidney control group and kidney damage group ($n = 7$). In the control group, the rats were fixed by laparotomy, and the kidneys were closed without suturing. However, the kidney damage group was approached by suturing. **Results:** When the bone biomechanical properties of the control and kidney-damaged groups were compared, a statistically significant difference was found between the displacement at maximum load, duration, and young's modulus groups ($P < 0.005$). **Conclusion:** The study showed that the bone biomechanical properties of rats with trauma-induced kidney damage changed, and there was an increased fracture risk.

Keywords: *Bone, bone fracture, chronic kidney injury, three point bending*

Asrin Nalbant, Duygu Akin Saygin[1], Arif Aydin[2], Anil Didem Aydin Kabakçi[1]

Department of Anatomy, Faculty of Medicine, Izmir Bakirçay University, Izmir, Departments of [1]Anatomy and [2]Urology, Faculty of Medicine, Necmettin Erbakan University, Konya, Turkey

Introduction

Patients with chronic kidney disease (CKD) have an increased fracture risk. The risk of fractures in patients with CKD is 2–14 times greater than in the general population,[1,2] and the incidence of fractures increases as kidney disease worsens.[3,4] CKD has been defined as a mineral and bone disorder (MBD) by the Global outcomes for kidney disease improvement (KDIGO) working group, but in a broader sense, abnormalities of calcium, phosphorus, parathyroid hormone (PTH) or vitamin D metabolism, bone turnover, mineralization, volume, used to refer to a systemic disorder of mineral and bone metabolism, such as linear growth or strength abnormalities, vascular or other soft tissue calcification.[5] Bone loss occurs in the early course of CKD and worsens as kidney function declines, so at least 50% of patients suffer a fracture at the start of dialysis.[6,7]

Unfortunately, data on the prevention or treatment of fractures in this population are lacking, as abnormal kidney function and hyperparathyroidism are exclusion criteria for nearly all clinical trials of osteoporotic treatments used in the general population.[8,9]

Because of the increased risk of osteoporosis in older people with CKD, it seems essential to establish a rapid strategy to prevent the fragility of bones.[10] Changes in bone remodeling, loss of bone mass, and increased risk of fractures have been observed in patients with CKD compared with those not matched for age.[11,12]

While bone mass is an important determinant, bone's physical and chemical properties also play an important role. Structurally, the mechanical properties of bone depend on several variables.[13,14] Most biomechanical studies in rodent models of CKD have focused on structural and mechanical properties using three-point bending or dynamic mechanical analysis (DMA).[8,15-20] These studies show that bone bending and viscoelastic properties are compromised in animals with CKD.[9] Specifically, DMA shows storage modulus (a measure of stiffness) and tan delta (a measure of energy loss),[16,17] while three-point

How to cite this article: Nalbant A, Saygin DA, Aydin A, Kabakçi AD. Investigation of bone biomechanics in rats with traumatic kidney injury. J Anat Soc India 2023;72:151-7.

bending studies show maximum load, stiffness, and fracture energy.[15]

Some studies have confirmed that CKD-MBD significantly affects cortical bone properties and reduces bone mass and porosity.[9,15,21] Furthermore, the increased risk of fractures in CKD is due to abnormalities in bone quantity and quality.[22] Despite the well-known pathogenesis of CKD-MBD, there is no effective therapeutic strategy for treating these disorders.[23] Various animal models have been used to study CKD, including surgery and dietary and genetic manipulation.[15,19,24]

Despite the many tools used to diagnose bone metabolism and predict fracture risk, dual-energy X-ray absorptiometry (DEXA) is the most commonly applied. This method allows the assessment of bone mass changes characterized by bone mineral density and mineral content.[25] However, some studies have suggested that mass bone measurement by DEXA does not always reflect bone health in the CKD state.[26,27]

Cannata-Andía *et al*.[28] reported that there was no strong correlation between DEXA and bone fractures in patients with CKD. Since the geometric distribution and amount of bone are essential determinants of mechanical strength,[29] skeletal integrity should be evaluated with biomechanical tests in which bones are examined in terms of structure. Therefore, irregular densitometry tests on small rodents with CKD should be complemented with biomechanical tests that accurately reflect bone quality. This method is simple, affordable, and reliable in assessing bone health.[23]

Moreover, these methods are currently used as standards for investigating the effect of a pharmacological intervention or genetic manipulation on bone properties.[30] Apart from this, Fridoni *et al*.[31] used the 3-point bending test to evaluate the effects of pulsed-wave low-level laser therapy on cortical bone in 2 experimental models of osteoporosis in rats.

Although there are numerous methods for assessing bone quality during CKD, biomechanical tests are still few. However, they provide crucial reliable information about structural and mechanical properties (maximum load, stiffness, and fracture energy) and visibility (maximum stress, elastic modulus, and toughness).[23]

The basis for the classification of biomechanical tests is the load direction of various forces, which can vary in five types: compression, tensile, torsion, curvature, or shear. A fair trial can evaluate each of the listed strength types. The three-point bending test is commonly used to assess the biomechanical properties of bone loaded in one direction. A flexural test involving 3-point loaded directions is notable as it imposes particular compressive, tensile, and shear strengths on the specimen. The effect of the applied force, such as the compressive strength on the bone, causes shortening and elongation, while the tensile strength causes contraction and elongation. In contrast, shear strength creates angular distortion.[23]

In this study, it was aimed to evaluate the bone biomechanics of rats with trauma-induced CKD using the three-point bending test.

Materials and Methods

The study used 16 adult Wistar Albino rats, 200–300 g, 4–5 months old. The rats were followed in rooms with a 12/12 h light-dark period, ventilated 15 times per h, a relative humidity of approximately 50% ± 3%, and an average temperature of 22°C. Animal groups were examined under two groups: kidney control (*n* = 9) and kidney damage group (*n* = 7). G*Power analysis of the research was found to be 93%. In the control group, rats were fixed by laparotomy, and the kidneys were closed without suturing. However, the kidney damage group was approached by suturing.

The exact surgical procedure was performed on all animals under anesthesia. Anesthesia and analgesia were administered to all rats by intramuscular route, with alfamine 10% injectable (50 mg/kg) and alfazyne 2% injectable (5 mg/kg) during the procedure. After anesthesia was applied and stabilization was achieved, the lower abdominal area was shaved, and its antiseptic was provided with a 10% povidone-iodine solution. The abdomen was reached by incising the skin, subcutaneous tissue, fat layer, and rectus muscle. After the kidneys were found, primary suturation was performed with a suture on both kidneys' lower and upper poles. A total of 2 sutures were used in each kidney and one in the upper pole, and four different sutures were used in each rat. The same procedures were applied to all rats [Figure 1]. After the process, all rats were given free access to water and food. After the procedure, Enrofloxacin 5 mg/kg was administered subcutaneously to all animals. Rats were housed in standard laboratory conditions and isolated from other rats and possible contaminants.

The femurs of the rats were removed as a whole when the animals were sacrificed at the end of the experiment. The soft tissue around the femur was separated and cleaned. Morphometric measurements of the femur were made (height and weight). After the measurements, a three-point bending test was applied to measure bone biomechanics.

The 3PB test was applied to the experimentally created groups with the BESMAK BMT-100E Universal (Ankara) test device in the study. Femoral diameters were measured before the test. Femur diameters were calculated in mm. In all tests, the loading speed was 2 mm/s, and the distance between the two end supports was adjusted and fixed as 30 mm according to the femur length of the rats. Before starting the tests, a 20N preload was applied to prevent soft tissue gaps on the bone surfaces.

Statistical analysis

Statistical analysis of the data obtained from the study was performed using the Statistical Package for the Social Sciences (Version 21.0, SPSS, Inc., Chicago, IL, USA) program. The Kolmogorov–Smirnov test was applied to check whether the data were normally distributed. Comparisons between groups were made with Student-*t* tests (assumptions confirmed by Shapiro–Wilk and Levene tests). When there were nonnormal distributions or unequal variances, comparisons were made using Wilcoxon ordinal sum and unequal variance tests, respectively. Statistical significance levels were accepted as $P < 0.05$.

Results

At the end of the experiment, the length, weight, and diameters of the femurs of the sacrificed rats were measured. While there was no significant difference between the weight and length measurements of the femurs of the control and kidney-damaged groups ($P > 0.005$), a significant difference was found between the diameters ($P < 0.005$). The values of the morphometric measurements of the experimental groups are shown in Table 1.

The mean and standard deviation values of the biomechanical parameters obtained from the femur samples in the groups are compared in Table 2. There was a statistically significant difference between the displacement at maximum load, duration, and young's modulus groups ($P < 0.05$).

According to the data, the rats with the highest maximum stress and maximum load values were in the control group. The maximum load did not differ significantly between the kidney damage group and the kidney control group ($P > 0.005$). Similarly, there was no significant difference in maximum stress between the kidney-damaged and the kidney control groups ($P > 0.005$). Duration and displacement at maximum load values were higher in the kidney-damaged group than in the control group.

Yield point values were higher in the control group, but there was no significant difference between the groups ($P > 0.005$). Young's modulus was found in the group with the lowest kidney damage, and a significant difference was found between the groups [Table 2].

Discussion

In our study, biomechanical test results of rat femurs belonging to experimentally formed kidney-damaged and control groups were compared. In the literature, evaluation studies on bone biomechanics of chronic kidney injury with three-point bending are limited.

The bending test is commonly used to measure the mechanical properties of whole bones from rodents and other small animals. During the bending test, the entire bone is loaded in bending until it breaks.[32] In general, there are two types of bending tests: 3- and 4-point bending tests. In the first test case, the entire bone is placed on the two supports, and a single-ended loading device is applied to the opposite surface at a point midway between the two supports.[32,33] The main advantage of the three-point bending test is its simplicity; the disadvantage is that it creates high shear stress near the middle section of the bone. However, the four bending tests require equal force at each loading point, which is difficult to achieve in the case of the actual bone test. Therefore, the 3-point bending test is more frequently used to evaluate the biomechanical properties of long bones.[32,34]

Table 1: Morphometric values of rat femurs

Group	Weight (g)	Height (mm)	Diameter (mm)
Kidney control	1.04±0.03	36.76±0.42	4.17±0.05
Kidney injury	1.01±0.03	37.5±0.43	4.46±0.1
P	0.5	0.2	0.02*

*P<0.05. Group averages are given

Figure 1: Primary suturation is applied to the lower and upper poles of the kidney. Arrows indicate sutures

Table 2: Biomechanical values of bones belonging to groups

Group	Maximum load (*n*)	Maximum stress (MPA)	Duration (s)	Displacement maximum load (mm)	Yield point (MPA)	Young's modulus (GPa)
Kidney control	108.91±5.88	88.79±4.93	61.58±2.54	1.68±0.99	83.77±4.68	2.12±0.11
Kidney injury	100.25±6.54	84.04±5.48	75.42±6.99	2.21±0.25	73.74±11.18	1.54±0.2
P	0.53	0.53	0.05*	0.05*	0.3	0.02*

*P<0.05

The biomechanical properties of bones should not be interpreted according to a single parameter, as it may lead to inappropriate results. For example, the bones of rats with osteoporosis are very hard and brittle, resulting in reduced fracture work and increased fracture risk. Conversely, although the bones of young rats are poorly mineralized, they can retain flexibility, increasing to fracture point.[23] Furthermore, bone's structural and material properties must be considered to analyze its biomechanical properties. Maximum parameters such as load, stiffness, and fracture energy are used to describe bones' structural properties and characterize tissue in its intact form. These structural features are used to predict the *in vivo* behavior of tissue.[10] On the other hand, material properties (ultimate stress, elastic modulus, toughness) characterize the material's behavior in forming the texture. However, the results of biomechanical tests may vary depending on the disease analyzed and should be compared with a control group of animals.[23]

According to the load–displacement curve, the slope of the elastic region represents extrinsic stiffness, which is closely related to the mineralization of the bone.[32-34] They also provide information on other biomechanical properties such as the load–displacement curve, maximum load (Fu-force at fracture), work-to-break (area under the W-load–displacement curve), and maximum displacement (dl).[10,33] Each of the above parameters reflects the different properties of the bone, i.e., the maximum load (Fu) reflects the overall integrity of the bone structure, the work to fracture (W) is the amount of energy required to break the bone, and the maximum displacement (dl) is inversely proportional to the fragility of the bone [Graph 1a].[23]

When the load–displacement curve of the study is evaluated, the yield point value of the control group is higher than that of the kidney-damaged group, and it shows that the elastic strain area of the femurs of the rats in the control group is more elevated. Maximum displacement is higher in the kidney-damaged group, indicating greater bone fragility in the kidney-damaged group. However, the breaking point of the experimental group was lower than the control group, although it was not significant. This result shows that the experimental group was broken with less force [Graph 2].

The stress–strain curve, although similar to the load–displacement curve, refers to the material properties of bone. The slope of the curve in the elastic region is called young's modulus (E), which measures the material's intrinsic stiffness. In addition, an area under the stress–strain curve, also called energy absorption or toughness modulus, is a measure of the amount of energy required to cause fracture [Graph 1b].[23,34]

When the stress–strain curve of the study is evaluated, young's modulus is lower in the kidney-damaged group. This result indicates that the intrinsic stiffness of the kidney-damaged group was quiet. At the same time, the energy required for fracture is lower than the control group. The control group's bones absorbed more energy up to the breaking point. In other words, its durability was higher [Graph 3].

Due to the mineral and hormonal abnormalities associated with the loss of kidney function, cellular physiology exhibits a range of abnormalities, from virtually no bone formation to extremely high formation and resorption. As resorption is often predominant, these patients lose bone
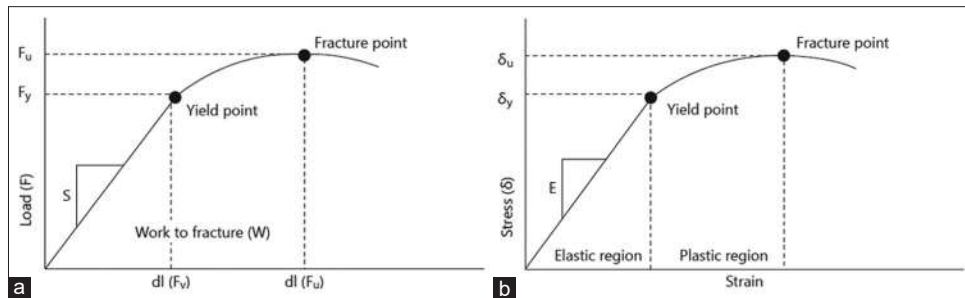
Graph 1: (a) Load–displacement curve, (b) stress–strain curve[23]
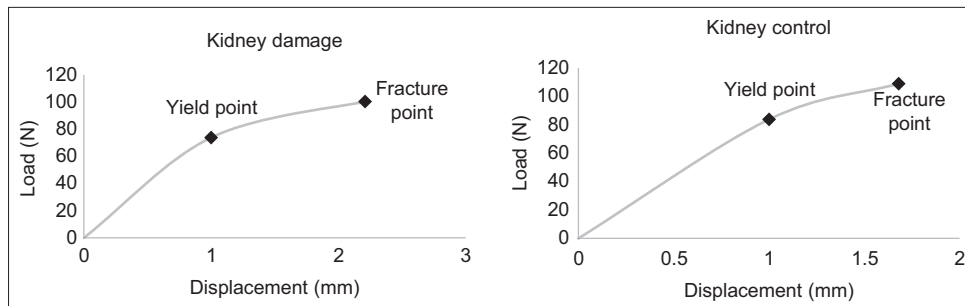
Graph 2: Load–displacement curve of control and kidney-damaged groups
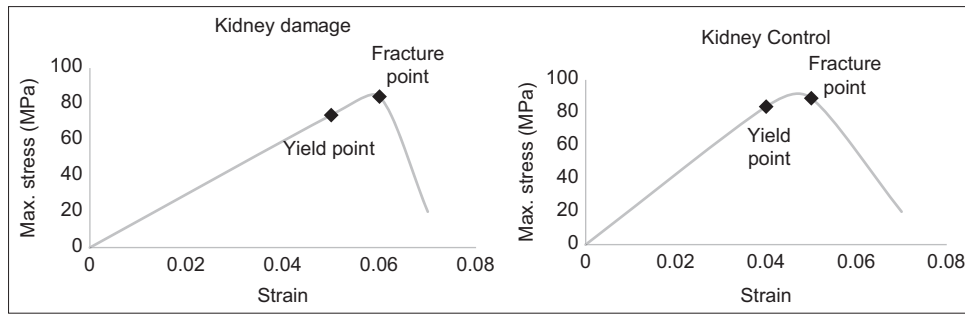
Graph 3: Stress–strain curve of control and kidney-damaged groups

mass and decrease actual bone density, directly reducing the strength of the bone.[35]

There are limited data on biomechanical tests' application in animals with chronic kidney injury. The application of biomechanical testing in experimental animal models of CKD seems reasonable, as this would be an essential step toward expanding knowledge of the existence of CKD-MBD. Moe *et al.*[22] performed a 3-point bending test on the left femur in rats with autosomal dominant polycystic kidney disease associated with the development of CKD. At the end of the study, they observed a decrease in maximum load (Fu) and concluded that bone fragility (W) and hardness increased in these rats compared to normal-aged rats. According to the data obtained from our study, there was no significant difference between the maximum load and maximum stress applied to the rat femurs in the control and experimental groups ($P > 0.005$). In a study on the biomechanical properties of bone in animals, high serum PTH concentration in rats with CKD reduced maximum load, fracture point, stiffness, and maximum stress. At the same time, a slight increase in Young's modulus was observed. In rats with reduced PTH concentration, a slight decrease in maximum load, A slight increase in hardness, maximum stress, and Young's modulus (E) was observed.[9,36] Newman *et al.*[9] stated in their study that they could not find a significant difference between young's modulus in the control group's bones and CKD patients' bones. In this study, it is thought that the lower yield point and the maximum force required for fracture in the experimental group compared to the control group are caused by the increase in the amount of calcium in the bones due to the increase in PTH secretion due to kidney damage, and the decrease in the cortical density with the increase in trabecular density. The increase in diameter in the experimental group can be interpreted as an increase in bone fracture time. However, with the low Young's modulus in the experimental group, it was shown that the endurance of the rat femurs in this group decreased [Graph 4]. Similarly, Jokihaara *et al.*[37] observed changes in bone mass and volumetric bone density in their study. In contrast, another study between rats with CKD induced by 5/6 nephrectomy and healthy controls showed no differences in terms of maximum load, structural stiffness, and maximum
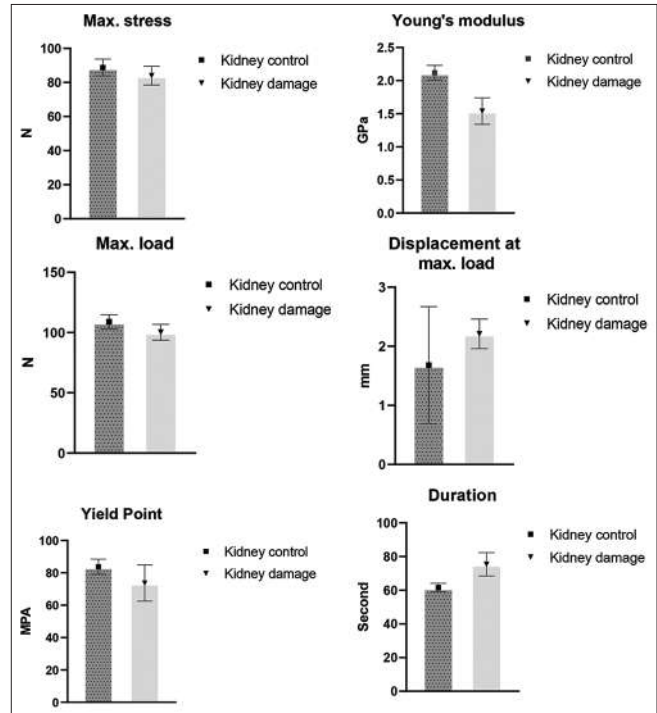
Graph 4: Comparison of the biomechanical properties of the femurs of the control and kidney-damaged groups

force applied to fracture the femoral neck and midshaft. It has been shown that there are no differences in terms of strength. Iwamoto *et al.*[8] showed that using the same animal model CKD, the stiffness decreased, and the fracture increased while the maximum load remained unchanged. When the studies mentioned here are compared with our study, while the maximum load did not change significantly in the experimental group, the hardness decreased, and the fracture increased. There are limited studies describing the effectiveness of biomechanical tests for diagnosing bone conditions in rats with CKD. Accordingly, biomechanical testing should also support all experiments on animals with CKD to assess bone quality.[23] The feature that distinguishes our study from other studies is evaluating the effect of trauma-induced kidney damage on bone. The results of the study show consistency when compared with other studies. At the same time, it has been shown theoretically that the structural properties of the bone will cause changes

in kidney damage. There are limited studies describing the effectiveness of biomechanical tests for diagnosing bone conditions in rats with CKD. Accordingly, biomechanical testing should also support all experiments on animals with CKD to assess bone quality.[23] The feature that distinguishes our study from other studies is evaluating the effect of trauma-induced kidney damage on bone. The results of the study show consistency when compared with other studies. At the same time, it has been shown theoretically that the structural properties of the bone will cause changes in kidney damage.

Limitations

The most important limitation of our study is that the blood values of rats were not checked, and there were no radiographic images of rat femurs. Renewing the study with these data can provide a more straightforward presentation of the changes.

Conclusion

In assessing bone quality in animals with CKD, the use of relevant biomechanical tests (bending and compression testing), which will provide information about the structural and material properties of bone, appears to be the best diagnostic strategy for animals with CKD. This study tried to reveal the negative effect of trauma-induced kidney damage on bone tissue. However, there is a need for new studies to examine the effectiveness of new therapeutic strategies and to use them in different parameters.

Ethics committee approval

Ethics committee approval of the study was approved by Necmettin Erbakan University Experimental Animals Ethics Committee with decision number 2022-016.

Financial support and sponsorship

Nil.

Conflicts of interest

There are no conflicts of interest.

References

1. Nickolas TL, McMahon DJ, Shane E. Relationship between moderate to severe kidney disease and hip fracture in the United States. J Am Soc Nephrol 2006;17:3223-32.
2. Alem AM, Sherrard DJ, Gillen DL, Weiss NS, Beresford SA, Heckbert SR, *et al.* Increased risk of hip fracture among patients with end-stage renal disease. Kidney Int 2000;58:396-9.
3. Naylor KL, McArthur E, Leslie WD, Fraser LA, Jamal SA, Cadarette SM, *et al.* The three-year incidence of fracture in chronic kidney disease. Kidney Int 2014;86:810-8.
4. Jamal SA, Nickolas TL. Bone imaging and fracture risk assessment in kidney disease. Curr Osteoporos Rep 2015;13:166-72.
5. Moe S, Drüeke T, Cunningham J, Goodman W, Martin K, Olgaard K, *et al.* Definition, evaluation, and classification of renal osteodystrophy: A position statement from kidney disease: Improving global outcomes (KDIGO). Kidney Int 2006;69:1945-53.
6. Jamal SA, Gilbert J, Gordon C, Bauer DC. Cortical pQCT measures are associated with fractures in dialysis patients. J Bone Miner Res 2006;21:543-8.
7. Jamal SA, Leiter RE, Jassal V, Hamilton CJ, Bauer DC. Impaired muscle strength is associated with fractures in hemodialysis patients. Osteoporos Int 2006;17:1390-7.
8. Levin A, Bakris GL, Molitch M, Smulders M, Tian J, Williams LA, *et al.* Prevalence of abnormal serum vitamin D, PTH, calcium, and phosphorus in patients with chronic kidney disease: Results of the study to evaluate early kidney disease. Kidney Int 2007;71:31-8.
9. Newman CL, Moe SM, Chen NX, Hammond MA, Wallace JM, Nyman JS, *et al.* Cortical bone mechanical properties are altered in an animal model of progressive chronic kidney disease. PLoS One 2014;9:e99262.
10. Iwamoto J, Seki A, Sato Y, Matsumoto H. Vitamin K(2) improves renal function and increases femoral bone strength in rats with renal insufficiency. Calcif Tissue Int 2012;90:50-9.
11. Cejka D, Patsch JM, Weber M, Diarra D, Riegersperger M, Kikic Z, *et al.* Bone microarchitecture in hemodialysis patients assessed by HR-pQCT. Clin J Am Soc Nephrol 2011;6:2264-71.
12. Nickolas TL, Stein E, Cohen A, Thomas V, Staron RB, McMahon DJ, *et al.* Bone mass and microarchitecture in CKD patients with fracture. J Am Soc Nephrol 2010;21:1371-80.
13. Cole JH, van der Meulen MC. Whole bone mechanics and bone quality. Clin Orthop Relat Res 2011;469:2139-49.
14. Seeman E, Delmas PD. Bone quality – The material and structural basis of bone strength and fragility. N Engl J Med 2006;354:2250-61.
15. Allen MR, Chen NX, Gattone VH 2nd, Chen X, Carr AJ, LeBlanc P, *et al.* Skeletal effects of zoledronic acid in an animal model of chronic kidney disease. Osteoporos Int 2013;24:1471-81.
16. Iwasaki Y, Kazama JJ, Yamato H, Fukagawa M. Changes in chemical composition of cortical bone associated with bone fragility in rat model with chronic kidney disease. Bone 2011;48:1260-7.
17. Iwasaki Y, Kazama JJ, Yamato H, Shimoda H, Fukagawa M. Accumulated uremic toxins attenuate bone mechanical properties in rats with chronic kidney disease. Bone 2013;57:477-83.
18. Jokihaara J, Pörsti I, Pajamäki I, Vuohelainen T, Jolma P, Kööbi P, *et al.* Paricalcitol [19-nor-1,25-(OH) 2D2] in the treatment of experimental renal bone disease. J Bone Miner Res 2006;21:745-51.
19. Moe SM, Radcliffe JS, White KE, Gattone VH 2nd, Seifert MF, Chen X, *et al.* The pathophysiology of early-stage chronic kidney disease-mineral bone disorder (CKD-MBD) and response to phosphate binders in the rat. J Bone Miner Res 2011;26:2672-81.
20. Sabbagh Y, Graciolli FG, O'Brien S, Tang W, dos Reis LM, Ryan S, *et al.* Repression of osteocyte Wnt/β-catenin signaling is an early event in the progression of renal osteodystrophy. J Bone Miner Res 2012;27:1757-72.
21. Nickolas TL, Cremers S, Zhang A, Thomas V, Stein E, Cohen A, *et al.* Discriminants of prevalent fractures in chronic kidney disease. J Am Soc Nephrol 2011;22:1560-72.
22. Moe SM, Chen NX, Newman CL, Gattone VH 2nd, Organ JM, Chen X, *et al.* A comparison of calcium to zoledronic acid for improvement of cortical bone in an animal model of CKD. J Bone Miner Res 2014;29:902-10.
23. Oksztulska-Kolanek E, Znorko B, Michałowska M, Pawlak K. The biomechanical testing for the assessment of bone quality

in an experimental model of chronic kidney disease. Nephron 2016;132:51-8.

24. Mathew S, Lund RJ, Strebeck F, Tustison KS, Geurs T, Hruska KA. Reversal of the adynamic bone disorder and decreased vascular calcification in chronic kidney disease by sevelamer carbonate therapy. J Am Soc Nephrol 2007;18:122-30.

25. Parchi PD, Cervi V, Piolanti N, Ciapini G, Andreani L, Castellini I, *et al.* Densitometric evaluation of periprosthetic bone remodeling. Clin Cases Miner Bone Metab 2014;11:226-31.

26. Cointry GR, Capozza RF, Negri AL, Roldán EJ, Ferretti JL. Biomechanical background for a noninvasive assessment of bone strength and muscle-bone interactions. J Musculoskelet Neuronal Interact 2004;4:1-11.

27. Faulkner KG. Bone matters: Are density increases necessary to reduce fracture risk? J Bone Miner Res 2000;15:183-7.

28. Cannata-Andía JB, Rodriguez García M, Gómez Alonso C. Osteoporosis and adynamic bone in chronic kidney disease. J Nephrol 2013;26:73-80.

29. Kreider JM, Goldstein SA. Trabecular bone mechanical properties in patients with fragility fractures. Clin Orthop Relat Res 2009;467:1955-63.

30. Gallant MA, Brown DM, Organ JM, Allen MR, Burr DB. Reference-point indentation correlates with bone toughness assessed using whole-bone traditional mechanical testing. Bone 2013;53:301-5.

31. Fridoni M, Masteri Farahani R, Nejati H, Salimi M, Gharavi SM, Bayat M, *et al.* Evaluation of the effects of LLLT on biomechanical properties of tibial diaphysis in two rat models of experimental osteoporosis by a three point bending test. Lasers Med Sci 2015;30:1117-25.

32. Turner CH, Burr DB. Basic biomechanical measurements of bone: A tutorial. Bone 1993;14:595-608.

33. Goodyear SR, Aspden RM. Mechanical properties of bone *ex vivo*. Methods Mol Biol 2012;816:555-71.

34. Turner CH, Burr DB. Experimental techniquesfor bone mechanics. In: Cowin SC, editor. Bone Mechanics Hand Book. 2nd edition: CRS Press; 2001.

35. Ott SM. Bone strength: More than just bone density. Kidney Int 2016;89:16-9.

36. Moe SM, Chen NX, Newman CL, Organ JM, Kneissel M, Kramer I, *et al.* Anti-sclerostin antibody treatment in a rat model of progressive renal osteodystrophy. J Bone Miner Res 2015;30:499-509.

37. Jokihaara J, Järvinen TL, Jolma P, Kööbi P, Kalliovalkama J, Tuukkanen J, *et al.* Renal insufficiency-induced bone loss is associated with an increase in bone size and preservation of strength in rat proximal femur. Bone 2006;39:353-60.

Ultrasonographic Analysis of Biparietal Diameter as an Indicator of Gestational Age in North Indian Fetuses

Abstract

Background: Clinical data such as menstrual cycle or uterine size often are not reliable parameter for pregnancy dating. Sonographic measurements of the fetus provide information about gestational age, growth and expected date of delivery. **Aims:** To develop a reference chart to estimate gestational age by ultrasonographic measurement of fetal bi-parietal diameter (BPD) and to find out correlation between two variables. **Material and Methods:** Cross sectional study was conducted on among 750 pregnant women of gestational age of 14-40 weeks, attending the Obstetrics and Gynaecology out-Patient department during one year period. Each fetus was ultrasonographically measured for BPD, the mean was used in subsequent statistical analysis. **Statistical Analysis:** It was done by the software SPSS version 21.0. A p-value < 0.05 considered to be significant. The previously published nomograms were compared by using unpaired t-test. Correlation & regression analysis has been done for BPD and GA. **Results:** Out of total 750 participants, 97.6% females confirmed their pregnancy by urine pregnancy test, 22.9% had dating scan, mean height was 163.004 cm. On ultrasound examination 78% participants had vertex, 7.6% had breech and 14.4% had variable presentation of fetus. Mean BPD increases 3.07 mm per week from 14 to 30 weeks and 1.93 mm per week from 31 to 40 weeks. For establishing a relationship between two variables GA & BPD, the correlation & regression analysis has been done. Sigmoid regression equation was the best for this study. **Conclusions:** Data showing that North Indian fetuses are smaller than European fetuses after 22 weeks gestation.

Keywords: *Gestational age, bi-parietal diameter, ultrasound*

**Archana Singh,
Rakesh Gupta,
Arun Singh[1]**

Departments of Anatomy and [1]Community Medicine, Rohilkhand Medical College and Hospital, Bareilly, Uttar Pradesh, India

Introduction

For managing the normal pregnancy as well as high-risk pregnancy, accurate information on fetal size, growth, and age is important.[1] Menstrual cycle or uterine size often are not reliable parameters for pregnancy dating. The most precise parameter for dating the pregnancy used by obstetricians is ultrasound in early pregnancy.[2]

Fetal biometry is done by ultrasound to measure the various parts of fetal anatomy and their growth. Crown-rump length, fetal bi-parietal diameters (BPD), head circumference, abdominal circumference, and femur length are more commonly measured biometric parameters used to determine gestational age (GA), fetal weight, and growth in different trimesters of pregnancy.[3] Fetal growth in the first 14 weeks occurs by the process of hyperplasia, from 14 to 32 weeks by the

process of hyperplasia and hypertrophy both and thereafter by the process of hypertrophy alone. The genetic growth potential of each fetus reflects in the early size and growth.[4] Uncertain GA has been associated with adverse pregnancy outcome including low birth weight, spontaneous preterm delivery, and perinatal mortality, independent of unfavorable maternal characteristics.[5]

Extensive scanning of the available literature shows that the BPD to be the most important measurement of the fetal head because its value is significantly superior to that of average cranial circumference. Fetal biometry has been shown to be affected by ethnic status, environmental and socioeconomic factors. Therefore biometric curves for one population may over or underestimate the fetal age when used for another population with different demographic characteristics. Many charts and tables for assessing GA have been established since Willocks *et al.*[6] in 1964 on cephalometry, and several standard

How to cite this article: Singh A, Gupta R, Singh A. Ultrasonographic analysis of biparietal diameter as an indicator of gestational age in North Indian fetuses. J Anat Soc India 2023;72:158-68.

charts have been fed into ultrasound machines for ready reference. Fetal anthropometric characteristics vary with ethnicity, social and nutritional status of a population. Therefore this study was undertaken to assess GA with the help of measurement of BPD by ultrasonography in the local population of Rohilkhand region (North India) in U.P. and to compare these values with western nomograms and other Indian studies.

Aims and objectives

To develop a reference chart to estimate GA by ultrasonographic measurement of fetal BPD for North Indian fetuses, to find out the correlation between BPD and GA and its correspondence with the last menstrual period and to compare the BPD for each GA group with available data from other races.

Materials and Methods

A cross-sectional study was conducted among 750 pregnant women of GA of 14–40 weeks residing in the Rohilkhand Region of U.P., India, and attending the Obstetrics and Gynecology Outpatient Department of two Tertiary Care Hospitals in U.P., during 1 year period from December 2014 to November 2015. There were no preselection criteria on the basis of maternal age, parity, or ethnicity. This study was approved by Institutional Ethics Committee (IEC), No. IEC/11/2014. With reference to the study by Quddusa and Chowdhury,[7] sample size was calculated. On the basis of maximum standard deviation (SD), minimum mean (among GA group) of fetal BPD for single GA group. With SD 1.5, type 1 error 5%, with 95% confidence level, the allowable error as 2% of the minimum mean for detecting results with 80% power of study. The sample size for a single GA group was 23, and there were total of 27 GA groups (14–40 weeks) so the sample size was calculated as 611. Only the first ultra-sonographic scan during the second and third trimesters was included in the study (in the case of multiple scans of one study subject) during the study. Pregnant female with multiple gestations, uncertain 1st day of last menstrual period, irregular menstrual cycle, intrauterine growth retardation, major fetal abnormalities on ultrasound examination or history of congenital anomaly, having maternal complications such as hypertension, preeclampsia, abnormal glucose tolerance test, diabetes mellitus, isoimmunization, uterine anomaly, or large fibroids and history of maternal drug, alcohol or tobacco abuse were excluded from the study.

After taking written consent the relevant parameters were recorded in a predesigned pro forma, which included identification data, demographic characteristics, general physical examinations, and obstetrical examination. BPD of each fetus was ultrasonographically measured three times by using model-LOGIQ V5 (Making-GE) ultrasound machine with convex trans-abdominal probe of 3.5 MHz frequency and the mean was used in subsequent statistical analysis. BPD was measured on a trans-axial plane at the level of the thalami where the continuous midline echo is broken by septum pellucidum in the anterior third.

GA was taken as menstrual GA in the exact week. For example 14 weeks 1 day was 14.14 weeks. Actual GA was calculated by the last menstrual period (the date of scanning – last menstrual period). The date of confinement was calculated based on expected duration of pregnancy of 282 days in this population. The gestational group has been so divided that from 13 weeks 4 days up to 14 weeks 3 days has been considered as 14 weeks.

Statistical analysis

All data were tabulated into MS-Excel sheet. All analysis was done by the software Released 2012. IBM SPSS Statistics for Windows, Version 21.0. Armonk, NY: IBM Corp. A $P < 0.05$ is considered to be significant, while the $P < 0.01$ considered being highly significant. The previously published and commonly used nomograms were compared using unpaired *t*-test. For establishing a relationship between two variables (GA and BPD) the correlation and regression analysis has been done. The relationships between the variables were presented graphically in the form of a scattergram. Regression equations are used to express the mathematical relationship between two variables so that the value of on variable (say GA) can be predicted from the knowledge of the other (say BPD). Various regression curves have been fitted on the available data in the search of best-fit curve.

Formulas of various types of regression equations are shown in Table 1.

Results

Mean BPD in the present study increases 3.07 mm per week from 14 to 30 weeks and 1.93 mm per week from 31 to 40 weeks. This shows there is a more rapid growth of BPD initially and slows down gradually in later weeks of GA. However, if we see growth of BPD from 17 to 20 weeks it was 4.24 mm per week, from 20 t o25 weeks it was 2.4 mm per week, from 25 to 30 weeks it was 2.9 mm per week, from 30 to 35 weeks it was 2.08 mm per week and from 35 to 40 weeks growth was 2.24 mm per week [Table 2].

Table 1: Regression equations	
Equation	**Shape**
For the linear regression	$y = a + bx$
For the quadratic regression	$y = a + b.x + cx^2$
For the logarithmic regression	$y = a\ln(b.x)$
For the sigmoid regression	$y = \exp\left(a + \dfrac{b}{x}\right)$

For establishing a relationship between two variables GA and BPD, the correlation and regression analysis have been done. Correlation values vary from −1 to +1. The relationships between GA and BPD are presented graphically and shown in Figure 1.

Regression analysis was done and various equations were derived for each variable (BPD and GA) [Table 3]. The value of GA was predicted from the value of BPD and value of BPD was predicted for each GA by regression equations and values tabulated [Tables 4, 5 and Figures 2-7].

Taking inference from all the observations, sigmoid regression equation was the best for this study, while a simple linear equation can also be used with enough precision. Hence, square regression equation was selected to prepare the BPD (mm) table for every respective GA and compare it with other existing Nomograms of Hadlock *et al*.,[8] Kurtz *et al*.[9] and Shepard and Filly[10] [Table 6 and Figures 8-11]. The square regression equation for estimation of GA of Hadlock *et al*.[8] and the present study was compared [Table 7].

Discussion

The difference in mm of mean BPD measurements for each GA of the present study was compared with mean BPD from that of Hadlock *et al*.[8] No appreciable difference could be found up to 26–27 weeks. There was 1.58 mm average difference between 28 and 29 weeks but after 37 weeks there was 0.75 mm average difference, and after 40 weeks 2.00 mm average difference was found. These differences were statistically significant ($P < 0.05$). Almost the same results were found with BPD table of Shepard and Filly.[10] Statistically significant ($P < 0.05$) differences in mean BPD measurements were observed in GA of 27–35 weeks. Consistent and statistically significant ($P < 0.05$) differences in mean BPD measurements could be observed

Table 2: Mean bi-parietal diameter (mm) and standard deviation for each gestational age

GA in weeks	Sample size	Mean BPD (mm)	SD
14	3	25.67	1.15
16	3	33.17	0.29
17	18	36.56	1.55
18	15	40.65	2.22
19	6	44.4	1.92
20	18	50.12	10.34
21	20	49.51	3.95
22	12	53.2	1.65
23	20	55.03	2.13
24	15	60.37	7.48
25	18	60.88	2.45
26	24	63.33	2.1
27	18	67.31	2.37
28	24	68.48	2.56
29	28	73.64	3.37
30	32	75.37	2.77
31	44	77.56	2.91
32	26	79.21	2.49
33	48	81.59	1.93
34	80	83.95	2.52
35	81	85.78	1.86
36	71	87.86	4.03
37	60	90.75	1.52
38	30	91.66	2.17
39	32	93.05	3
40	4	97	0.24
Total	750	76.06	15.71

GA: Gestational age, BPD: Bi-parietal diameter, SD: Standard deviation

Figure 1: Scattergram showing positive correlation between GA and BPD in this study. GA: Gestational age, BPD: Bi-parietal diameter

Table 3: Various regression equation; estimation of bi-parietal diameter from gestational age and estimation of gestational age from bi-parietal diameter

	Estimation of BPD from GA Y=BPD, X=GA		Estimation of GA from BPD Y=GA, X=BPD	
	Equation	R^2 (%)	Equation	R^2 (%)
Simple linear regression	BPD=2.525GA−3.433	95.10	GA=2.843+0.376×BPD	95.10
Quadratic regression	BPD = −31.434+4.568×GA−0.035×GA^2	95.80	GA=9.008+0.180×BPD+0.001×BPD^2	95.50
Logarithmic regression	BPD=ln (−164.508+70.189×GA)	95.70	GA=10.922×exp (0.014×BPD)	95.70
Sigmoid regression	BPD=exp (5.274−29.087/GA)	96.10	GA = (−29.087)/(ln [BPD] − 5.274)	96.10

GA: Gestational age, BPD: Bi-parietal diameter

Table 4: Predicted values of bi-parietal diameter from gestational age of present study

GA (weeks)	Predicted BPD (mm)		
	Linear equation	Square equation	Sigmoid
10	21.817	10.75	10.65
11	24.342	14.58	13.87
12	26.867	18.34	17.29
13	29.392	22.04	20.83
14	31.917	25.66	24.44
15	34.442	29.21	28.07
16	36.967	32.69	31.69
17	39.492	36.11	35.27
18	42.017	39.45	38.79
19	44.542	42.72	42.23
20	47.067	45.93	45.59
21	49.592	49.06	48.86
22	52.117	52.12	52.03
23	54.642	55.12	55.11
24	57.167	58.04	58.09
25	59.692	60.89	60.98
26	62.217	63.67	63.77
27	64.742	66.39	66.47
28	67.267	69.03	69.07
29	69.792	71.6	71.59
30	72.317	74.11	74.03
31	74.842	76.54	76.38
32	77.367	78.9	78.65
33	79.892	81.2	80.85
34	82.417	83.42	82.97
35	84.942	85.57	85.02
36	87.467	87.65	87.01
37	89.992	89.67	88.93
38	92.517	91.61	90.79
39	95.042	93.48	92.59
40	97.567	95.29	94.33
41	100.092	97.02	96.02
42	102.617	98.68	97.66

GA: Gestational age, BPD: Bi-parietal diameter

Table 5: Predicted values of gestational age from bi-parietal diameter

BPD (mm)	Estimated GA (weeks) - linear equation	Estimated GA (weeks) - quadratic equation	Estimated GA (weeks) - sigmoid equation
25	12.24	14.13	14.15
26	12.62	14.36	14.43
27	13	14.6	14.7
28	13.37	14.83	14.98
29	13.75	15.07	15.26
30	14.12	15.31	15.53
31	14.5	15.55	15.81
32	14.88	15.79	16.09
33	15.25	16.04	16.36
34	15.63	16.28	16.64
35	16	16.53	16.92
36	16.38	16.78	17.21
37	16.76	17.04	17.49
38	17.13	17.29	17.77
39	17.51	17.55	18.06
40	17.88	17.81	18.35
41	18.26	18.07	18.64
42	18.64	18.33	18.93
43	19.01	18.6	19.23
44	19.39	18.86	19.52
45	19.76	19.13	19.82
46	20.14	19.4	20.12
47	20.52	19.68	20.43
48	20.89	19.95	20.73
49	21.27	20.23	21.04
50	21.64	20.51	21.36
51	22.02	20.79	21.67
52	22.4	21.07	21.99
53	22.77	21.36	22.31
54	23.15	21.64	22.64
55	23.52	21.93	22.96
56	23.9	22.22	23.29
57	24.28	22.52	23.63
58	24.65	22.81	23.97
59	25.03	23.11	24.31
60	25.4	23.41	24.66
61	25.78	23.71	25.01
62	26.16	24.01	25.36
63	26.53	24.32	25.72
64	26.91	24.62	26.08
65	27.28	24.93	26.45
66	27.66	25.24	26.82
67	28.04	25.56	27.2
68	28.41	25.87	27.58
69	28.79	26.19	27.97
70	29.16	26.51	28.36
71	29.54	26.83	28.76
72	29.92	27.15	29.16
73	30.29	27.48	29.57
74	30.67	27.8	29.99

with a table of Sabbagha and Hughey[11] among almost all the GA [Table 8].

Campbell,[12] measured BPD by ultrasound in 471 pregnant females and reported an increment of BPD from 20 to 30 weeks of gestation was more rapid (mean - 2.8 mm per week) than in the past 10 weeks (mean - 1.5 mm per week). In the present study, it was 2.65 mm per week from 20 to 30 weeks of gestation, 2.08 mm/week in 30–35 weeks, and 2.24 mm/ week from 35 to 40 weeks of gestation which shows a slight increment in the growth rate of in last weeks of gestation. Mador *et al*.,[13] measured BPD in 13,740 Nigerian pregnant females, the growth rate of BPD was 3.9 mm per week between 13 and 16 weeks of gestation, 3.1 mm per week between 17 and 25 weeks, 2.5 mm per week in between 26 and 29 weeks, 2.1 mm per week in

Contd...

BPD (mm)	Estimated GA (weeks) - linear equation	Estimated GA (weeks) - quadratic equation	Estimated GA (weeks) - sigmoid equation
		Table 5: Contd...	
75	31.04	28.13	30.41
76	31.42	28.46	30.84
77	31.8	28.8	31.27
78	32.17	29.13	31.71
79	32.55	29.47	32.16
80	32.92	29.81	32.61
81	33.3	30.15	33.07
82	33.68	30.49	33.54
83	34.05	30.84	34.01
84	34.43	31.18	34.5
85	34.8	31.53	34.99
86	35.18	31.88	35.49
87	35.56	32.24	35.99
88	35.93	32.59	36.51
89	36.31	32.95	37.04
90	36.68	33.31	37.57
91	37.06	33.67	38.11
92	37.44	34.03	38.67
93	37.81	34.4	39.23
94	38.19	34.76	39.81
95	38.56	35.13	40.39
96	38.94	35.5	40.99
97	39.32	35.88	41.6
98	39.69	36.25	42.21
99	40.07	36.63	42.85
100	40.44	37.01	43.49

GA: Gestational age, BPD: Bi-parietal diameter

Figure 2: Scattergram showing simple quadratic regression equation between GA and BPD. GA: Gestational age, BPD: Bi-parietal diameter
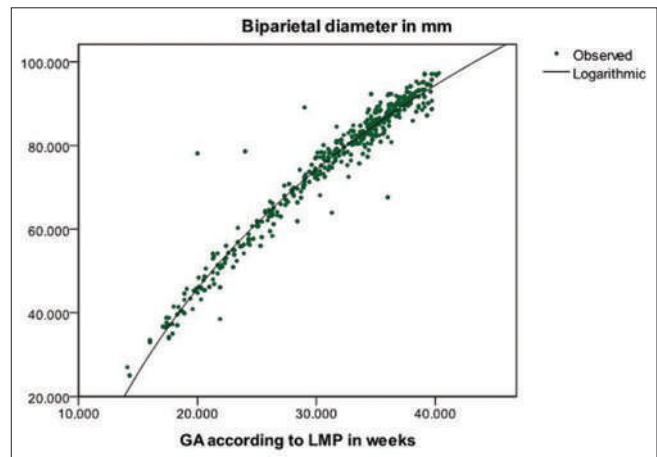
Figure 3: Scattergram showing Logarithmic regression equation between GA and BPD. GA: Gestational age, BPD: Bi-parietal diameter
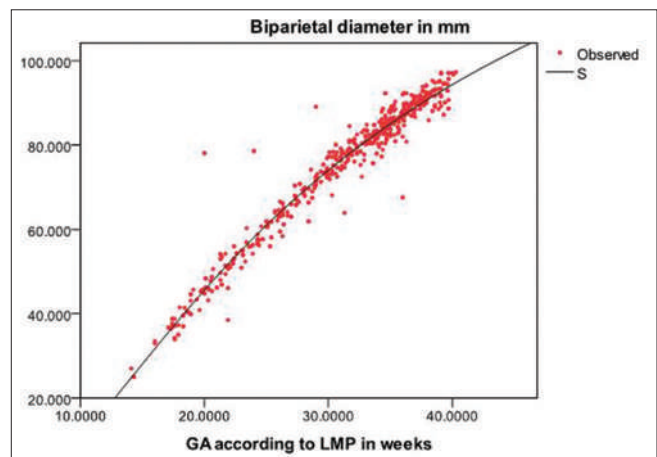
Figure 4: Scattergram showing Sigmoid regression equation between GA and BPD. GA: Gestational age, BPD: Bi-parietal diameter

between 30 and 33 weeks, and 1.6 mm per week between 34 and 42 weeks of gestation, while in present study growth rate was 4.24 mm per week between 17 and 20 weeks of gestation, 3.43 mm per week in between 26 and 29 weeks of gestation, 3.11 mm per week in between 30 and 33 weeks, and 2.24 mm per week in between 35 and 40 weeks of gestation which was higher. Beigi and ZarrinKoub,[14] recorded BPD in 15,693 Dutch females and found a mean weekly increase in the BPD between 12 and 29 weeks of gestation was 3.1 mm per week, between 29 and 36 weeks it was 1.8 mm per week and in between 36 and 40 weeks it was 1.4 mm per week.

Quddusa and Chowdhury[7] reported increment in BPD measurement in Bangladeshi pregnant females was 3 mm per week from 13 to 28 weeks, 2.2 mm per week from 28 to 33 weeks, and thereafter 1 mm per week up to 40 weeks of gestation.

The mean BPD of the present study was compared with other studies[3,15-20] and BPD for particular GA was almost similar to the other Indian studies by Pandey *et al*.[3] and Agrawal *et al*.[15] up to 24–25 weeks of GA. From 25 weeks onward the values of BPD decreases [Table 9].

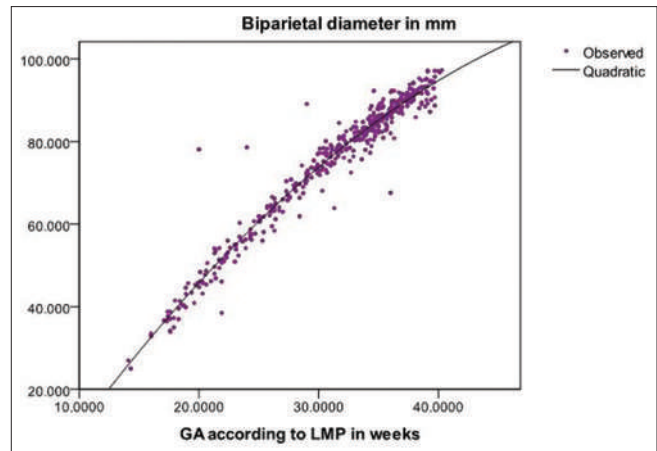In the present study, the mean growth rate of BPD from 14 to 30 weeks was 3.07 mm per week and from 31 to 40 weeks it was 1.93 mm per week, which shows that the growth of BPD is more in the second trimester (12–28 weeks)

GA (weeks)	Estimated BPD of present study (mm) - sigmoid equation	Estimated BPD of present study (mm) - quadratic equation	Mean observed BPD (mm) of present study	Hadlock *et al.*[8]	Kurtz *et al.* (composite)[9]	Shepard and Filly[10]
14	24.44	25.66	25.67	27	27	28
15	28.07	29.21	-	30	31	31
16	31.69	32.69	33.17	33	34	34
17	35.27	36.11	36.56	37	38	37
18	38.79	39.45	40.65	40	41	40
19	42.23	42.72	44.4	43	45	43
20	45.59	45.93	50.12	46	48	46
21	48.86	49.06	49.51	50	51	49
22	52.03	52.12	53.2	53	54	52
23	55.11	55.12	55.03	56	57	55
24	58.09	58.04	60.37	58	60	57
25	60.98	60.89	60.88	61	63	60
26	63.77	63.67	63.33	64	66	63
27	66.47	66.39	67.31	67	69	65
28	69.07	69.03	68.48	70	71	68
29	71.59	71.60	73.64	72	74	71
30	74.03	74.11	75.37	75	76	73
31	76.38	76.54	77.56	77	79	76
32	78.65	78.90	79.21	79	81	78
33	80.85	81.20	81.59	82	83	80
34	82.97	83.42	83.95	84	85	83
35	85.02	85.57	85.78	86	87	85
36	87.01	87.65	87.86	88	89	88
37	88.93	89.67	90.75	90	91	90
38	90.79	91.61	91.66	91	92	92
39	92.59	93.48	93.05	-	-	-
40	94.33	95.29	97.00	-	-	-

Table 6: Comparison between derived bi-parietal diameter (mm) of this study with existing nomograms

GA: Gestational age, BPD: Bi-parietal diameter

Table 7: Comparison of square regression equation of present study with Hadlock *et al.*[8]

Source	Regression equation (square)
Hadlock *et al.*[8]	$GA = 9.54 + 1.482\ BPD + 0.1676\ BPD^2$
This study	$GA = 9.008 + 0.180 \times BPD + 0.001 \times BPD^2$

GA: Gestational age, BPD: Bi-parietal diameter

Figure 5: Scattergrams showing linear regression equations between BPD and GA. GA: Gestational age, BPD: Bi-parietal diameter

which decreases in the third trimester (29–40 weeks) which was almost similar with the study of Ayangade and Okonofua,[16] while the mean BPD of authors Munjanja *et al.*,[17] Campbell *et al.*[18] and Chitty *et al.*[20] were higher than the present study. The mean growth rate of BPD in the present study in the early weeks of gestation 17–20 weeks was 4.24 mm per week and in later weeks of gestation was 2.08 mm per week in 30–35 weeks of GA, which was almost similar with the findings Munjanja,[17] in their study weekly growth rate dropped from 4 mm per week to 0.9 mm per week at 38 weeks. Ayangade and Okonofua.[16] found a definitive decline in the mean BPD growth rate from a mean of 3.6 mm per week at 29th week to 1 mm per week in 39th week [Table 10].

Study data comparison was done with nomogram of Zaidi *et al.*[21] (Pakistan) and significant difference can be seen in

BPD measurement at all GA levels except for 37 weeks. In the comparison with the study of Saksiriwuttho *et al.*[22] significant differences were observed in BPD measurement for most of the GA levels. Consistent and statistically significant ($P < 0.05$) differences in mean BPD measurements could be observed in table of Jeanty *et al.*[23] in approximately 30% of GA. In the comparison with the study A Beigi and ZarrinKoub[14] significant differences were observed in BPD measurement for most of the GA levels [Table 11].

Table 8: Correlation of predicted menstrual age based upon biparietal diameter

GA (weeks)	95% population means lie between		Mean BPD (X)				
	X−t × (SE)	X+t × (SE)	Hadlock *et al.*[8]	Shepard and Filly[10]	Kurtz *et al.*[9]	Sabbagha and Hughey[11]	Present study
14	22.17	29.17	27	28	27	28	25.67
16	32.29	34.05	33	34	34	36	33.17
17	35.77	37.35	37	37	38	39	36.56
18	39.38	41.92	40	40	41	42	40.65
19	42.19	46.61	43	43	45	45	44.4
20	44.83	55.41	46	46	48	48	50.12
21	47.61	51.41	50	49	51	51	49.51
22	52.11	54.29	53	52	54	54	53.2
23	54.01	56.05	56	55	57	58	55.03
24	56.08	64.66	58	57	60	61	60.37
25	59.63	62.13	61	60	63	64	60.88
26	62.42	64.24	64	63	66	67	63.33
27	66.1	68.52	67	65	69	70	67.31
28	67.38	69.58	70	68	71	72	68.48
29	72.31	74.97	72	71	74	75	73.64
30	74.36	76.38	75	73	76	78	75.37
31	76.67	78.45	77	76	79	80	77.56
32	78.18	80.24	79	78	81	82	79.21
33	81.02	82.16	82	80	83	85	81.59
34	83.39	84.51	84	83	85	87	83.95
35	85.37	86.19	86	85	87	88	85.78
36	86.9	88.82	88	88	89	90	87.86
37	90.35	91.15	90	90	91	92	90.75
38	90.84	92.48	91	92	92	93	91.66
39	91.95	94.15	93	95	94	94	93.05
40	96.56	97.44	95	97	95	95	97

GA: Gestational age, BPD: Bi-parietal diameter

Table 9: Comparison of mean bi-parietal diameter (mm) of present study with other study

GA (weeks)	Mean BPD							
	Munjanja *et al.* (Zimbabwe)[17]	Ayangade and Okonofua (Nigeria)[16]	Campbell *et al.*[18]	Kurmanavicius *et al.* (Dutch)[19]	Chitiy *et al.*[20]	Pandey *et al.* (India)[3]	Agrawal (India)[15]	Present study
12	20.9	22	21.2	21	19.7	-	-	-
13	25.1	26.2	21.7	24.9	23.5	-	-	-
14	27.6	27.2	27.8	28.7	27.3	--	-	25.67
15	32.4	30.3	31.4	32.5	31	15.5	31	-
16	35.6	33.9	35.3	36.2	34.7	32.75	32	33.17
17	40.5	36.6	38.7	39.9	38.3	37.25	39	36.56
18	42.6	39.4	41.5	43.5	41.9	40.6	41	40.65
19	47.1	43	46	47	45.4	45.25	46	44.4
20	48.6	46.9	48.2	50.4	48.8	47.66	47	5012
21	51.9	50	51.2	53.8	52.2	55	49	49.51
22	55.8	52.5	54.2	57.1	55.5	56.8	53	53.2
23	58.8	53.8	58.2	60.3	58.7	58	59	55.03
24	61	59.8	61.6	63.4	61.8	61	60	60.37
25	63.9	60.7	64.2	66.5	64.8	62	65	60.88
26	68.1	62.6	65.9	69.4	67.8	65.2	67	63.33
27	71	68.6	70.9	72.2	70.6	65	68	67.31
28	72.5	69.8	75.8	74.9	73.4	71.66	72	68.48
29	76.2	73.8	78.7	77.6	76	74.8	74	73.64
30	77.8	77.1	80.3	80.1	78.6	75	77	75.37

Contd...

GA	Mean BPD							
(weeks)	Munjanja *et al.* (Zimbabwe)[17]	Ayangade and Okonofua (Nigeria)[16]	Campbell *et al.*[18]	Kurmanavicius *et al.* (Dutch)[19]	Chitiy *et al.*[20]	Pandey *et al.* (India)[3]	Agrawal (India)[15]	Present study
31	79.9	79.3	82.2	82.5	81	78.75	79	77.56
32	82.7	81.4	85.7	84.7	83.3	79.2	80	79.21
33	84.4	83.3	86.7	86.9	85.5	83.5	83	81.59
34	86.3	84.7	89.4	88.9	87.6	85	85	83.95
35	88	85.2	91.6	90.8	89.6	82.25	87	85.78
36	88.8	88.7	91.4	92.6	91.5	89.8	89	87.86
37	89.6	89.5	93.5	94.2	93.2	-	90	90.75
38	90.2	90.9	93.5	95.7	94.8	-	-	91.66
39	92	91	96.2	97	96.2	-	94	93.05
40	92	92.8	95.9	98.2	97.5	-		97

GA: Gestational age, BPD: Bi-parietal diameter

Table 10: Growth rate of mean bi-parietal diameter (mm/week) of various studies, at each week interval

Week interval	Munjanja *et al.* (Zimbabe)[17]	Ayangade and Okonofua (Nigeria)[16]	Kurmanavicius *et al.* (Dutch)[19]	Pandey *et al.* (India)[3]	Agrawal (India)[15]	Present study
14–15	4.8	3.1	3.8	-	-	-
15–16	3.2	3.6	3.7	17.25	1	-
16–17	4.9	2.7	3.7	4.5	7	3.39
17–18	2.1	2.8	3.6	3.35	2	4.09
18–19	4.5	3.6	3.5	4.65	5	3.75
19–20	1.5	3.9	3.4	2.41	1	5.72
20–21	3.3	3.1	3.4	7.34	2	0.61
21–22	3.9	2.5	3.3	1.8	4	3.69
22–23	3	1.3	3.1	1.2	6	1.83
23–24	2.2	5.7	3.1	3	1	5.34
24–25	2.9	1.2	3.1	1	5	0.51
25–26	4.2	1.9	2.9	3.2	2	2.45
26–27	2.9	6	2.8	0.2	1	3.98
27–28	1.5	1.2	2.7	6.66	4	1.17
28–29	3.7	4	2.7	3.14	2	5.16
29–30	1.6	3.3	2.5	0.2	3	1.73
30–31	2.1	2.2	2.4	3.75	2	2.19
31–32	2.8	2.1	2.2	0.45	1	1.65
32–33	1.7	1.9	2.2	4.3	3	2.38
33–34	1.9	1.4	2	1.5	2	2.36
34–35	1.7	0.5	1.9	2.25	2	1.83
35–36	0.8	3.5	1.8	2.55	2	2.08
36–37	0.8	0.8	1.6	-	1	2.89
37–38	0.6	1.4	1.5	-	-	0.91
38–39	1.8	0.1	1.3	-	-	1.39
39–40	0.8	1.8	1.2	-	-	3.95

Consistent and statistically significant ($P < 0.05$) differences in mean BPD measurements could be observed in a table of Tinelli *et al.*[24] for all the GA. Several authors have reported no significant differences in BPD of Caucasian and non-Caucasian fetuses in the second trimester. Therefore, ethnicity does not seem to influence fetal age assessment much in the second trimester. The length of the human pregnancy is a matter of discussion. Several Scandinavian studies have addressed this issue.[25] They estimated the median pregnancy length based on the last menstrual period to be 282–284 days. Estimations based on the measurement of the BPD in the second trimester gave a median pregnancy length of 280–281 days. The consensus for our population is 282 days [Table 11].

To the best of our knowledge, a study presenting sonographically derived measurements of fetal growth from a North Indian population and comparing them against

Table 11: Comparison of nomograms of different studies with the present study

GA	Present study		Zaidi *et al.* (X2)[21]				Tinelli *et al.*[24]				Beigi and ZarrinKoub[14]				Jeanty *et al.* (UK) (X2)[23]				Saksiriwuttho *et al.* (Thailand) (X2)[22]			
	n	Mean BPD	*n*	Mean BPD	*t*	*P*	*n*	Mean BPD	*t*	*P*	*n*	Mean BPD	*t*	*P*	*n*	Mean BPD	*t*	*P*	*n*	Mean BPD	*t*	*P*
14	3	25.67	13	33	−8.472	<0.001	5	32	−9.522	<0.001	359	28	−3.493	0.001	40	28	−2.541	0.015	12	28.8	−4.254	0.001
16	3	33.17	15	39.3	−13.75	<0.001	17	38.5	−30.97	<0.001	369	34	−4.466	<0.001	40	36	−3.502	0.001	11	34.9	−1.826	0.093
17	18	36.56	15	44.2	−9.707	<0.001	30	41.7	−14.14	<0.001	395	37	−1.176	0.24	40	39	−2.802	0.007	13	40	−3.278	0.003
18	15	40.65	15	46.2	−6.724	<0.001	14	45	−7.64	<0.001	398	40	1.122	0.262	40	42	−1.582	0.12	16	42	−1.892	0.069
19	6	44.4	15	50.4	−6.295	<0.001	14	48.4	−5.032	<0.001	422	44	0.508	0.612	40	45	−0.539	0.593	20	43.7	0.641	0.528
20	18	50.12	16	51.9	−0.709	<0.001	7	51.7	−0.636	0.531	399	47	1.28	0.201	40	47	1.239	0.22	14	48.9	0.5	0.621
21	20	49.51	15	57.1	−7.035	<0.001	-	55	-	-	409	50	−0.552	0.581	40	49	0.469	0.64	11	50.1	−0.443	0.661
22	12	53.2	14	58.2	−6.093	<0.001	7	58.2	−10.49	<0.001	408	53	0.414	0.679	40	52	1.3	0.2	12	53.3	−0.065	0.949
23	20	55.03	15	63.9	−10.25	<0.001	20	61.5	−13.48	<0.001	417	56	−2.008	0.045	40	57	−2.134	0.037	15	56.5	−1.61	0.117
24	15	60.37	15	65.7	−2.537	0.017	13	64.6	−2.21	0.036	416	60	0.191	0.848	40	60	0.172	0.864	13	59.1	0.64	0.528
25	18	60.88	12	69.6	−12.08	<0.001	13	67.8	−11.87	<0.001	414	63	−3.637	<0.001	40	64	−2.809	0.007	15	65	−2.899	0.007
26	24	63.33	15	70.6	−11.85	<0.001	13	70.8	−17.27	<0.001	431	66	−6.147	<0.001	40	67	−4.803	<0.001	20	63.7	−0.347	0.731
27	18	67.31	13	73.8	−8.663	<0.001	13	73.7	−11.44	<0.001	641	69	−2.999	0.003	40	68	−0.713	0.479	19	67.8	−0.599	0.553
28	24	68.48	13	76	−10.13	<0.001	12	76.6	−15.4	<0.001	598	72	−6.67	<0.001	40	72	−4.291	<0.001	23	71.3	−2.536	0.015
29	28	73.64	13	78.9	−5.71	<0.001	13	79.3	−8.854	<0.001	623	75	−2.12	0.034	40	75	−1.515	0.134	23	73.5	0.141	0.888
30	32	75.37	12	80.8	−5.746	<0.001	43	81.9	−13.29	<0.001	605	77	−3.288	0.001	40	76	−0.788	0.434	26	77.9	−2.871	0.006
31	44	77.56	12	83.1	−5.862	<0.001	22	84.3	−15.38	<0.001	572	79	−3.244	<0.001	40	80	−2.334	0.022	29	79.4	−2.11	0.038
32	26	79.21	15	85.5	−8.85	<0.001	8	86.6	−15.04	<0.001	580	80	−1.6	0.11	40	81	−2.24	0.029	31	81.6	−2.776	0.008
33	48	81.59	15	87.3	−7.37	<0.001	6	88.8	−24.63	<0.001	605	82	−1.417	0.157	40	84	−2.437	0.017	32	82.3	−1.303	0.196
34	80	83.95	16	90.6	−7.426	<0.001	15	90.7	−23.56	<0.001	633	84	−0.167	0.867	40	86	−2.071	0.04	31	84	−0.095	0.925
35	81	85.78	16	91.1	−7.536	<0.001	33	92.5	−31.88	<0.001	635	86	−0.958	0.338	40	88	−2.118	0.036	33	87.5	−3.817	<0.001
36	71	87.86	13	90.8	−3.063	0.003	30	94	−12.85	<0.001	575	88	−0.288	0.773	40	90	−2.014	0.046	31	88.3	−0.705	0.483
37	60	90.75	12	91	−0.347	0.729	18	95.4	−22.64	<0.001	973	90	3.628	<0.001	40	92	−1.195	0.235	29	88.8	3.19	0.002
38	30	91.66	-	-	-	-	30	96.5	−12.07	<0.001	930	91	1.643	0.101	40	93	−1.303	0.197	31	90.3	2.063	0.044
39	32	93.05	-	-	-	-	26	97.3	−8.039	<0.001	910	92	1.97	0.049	40	95	−1.422	0.16	35	91.6	1.787	0.079
40	4	97	-	-	-	-	17	97.9	−6.973	<0.001	1011	93	29.839	<0.001	40	96	0.787	0.436	35	95.3	2.321	0.026

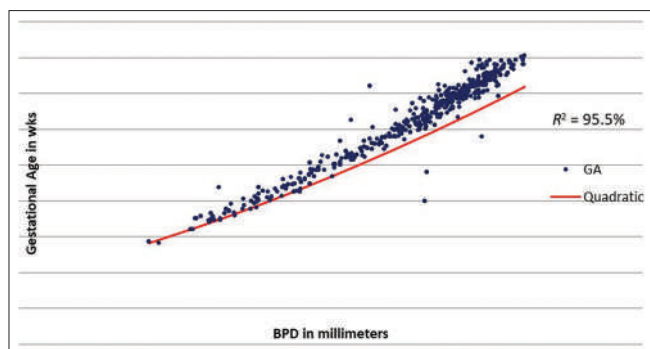GA: Gestational age, BPD: Bi-parietal diameter

Figure 6: Scattergrams showing quadratic regression equations between BPD and GA. GA: Gestational age, BPD: Bi-parietal diameter
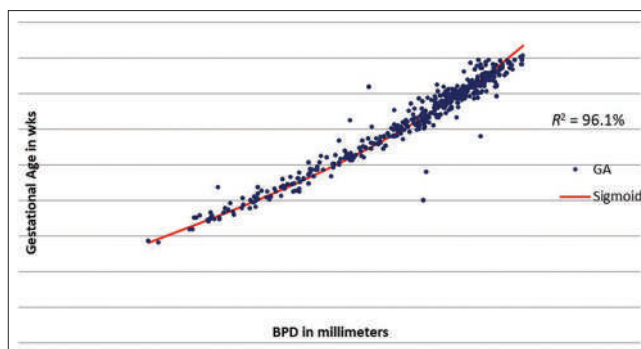

Figure 7: Scattergrams showing sigmoid (s) regression equations between BPD and GA. GA: Gestational age, BPD: Bi-parietal diameter
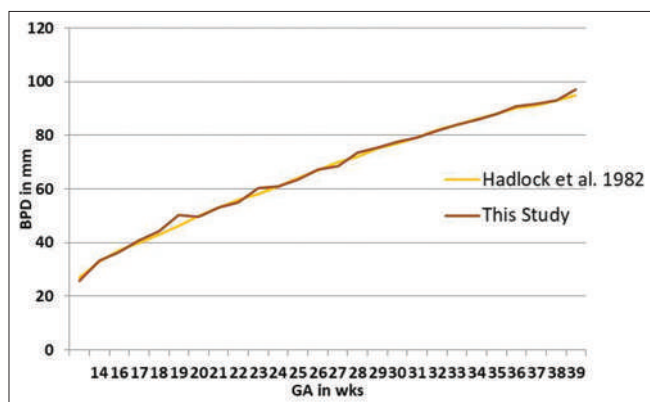

Figure 8: Line Diagram showing comparison of present study with Hadlock *et al.*[8]
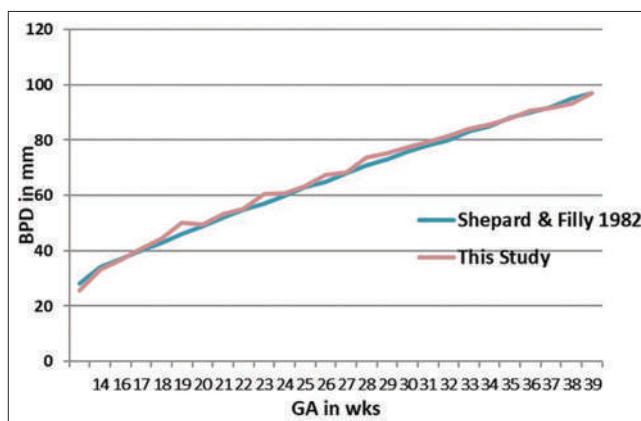

Figure 9: Line Diagram showing comparison of present study with Shepard and Filly[10]
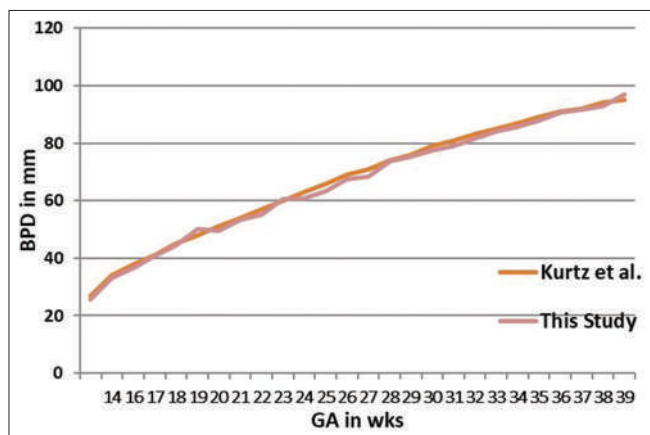

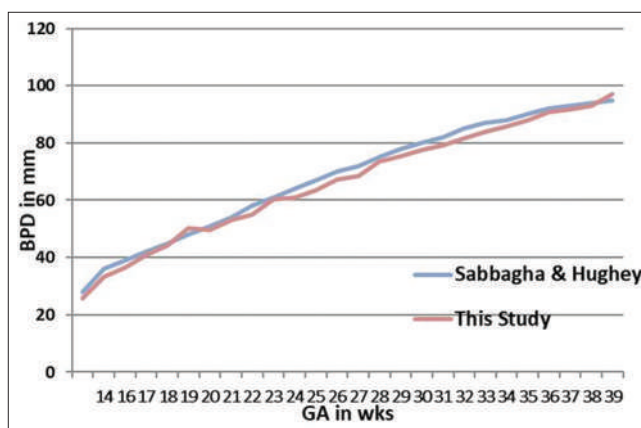**Figure 10: Line Diagram showing Comparison of present study with Kurtz *et al.*[9]**

Figure 11: Line Diagram showing Comparison of present study with Sabbagha and Hughey[11]

a Western population has not been reported previously. Measurements were made according to standardized protocols by 2–3 experienced medical sonologists, ensuring high-quality measurements and minimizing "noise" due to interobserver variation. The study was designed to generate fetal growth reference curves, which are ideally based on cross-sectional data collected evenly throughout the study population. Fetal BPD was significantly smaller than the Western references after 22 weeks' gestation. The BPD became smaller relative to the European population as the pregnancy progressed.

Conclusions

The fetal BPD of the present study was smaller in mixed (rural and urban) North Indian study population than in European and even Pakistani populations, even during mid-pregnancy. This difference increases in the later half of pregnancy and is greatest near the term. Hence, there is a need to have a separate nomogram for the North Indian population. The present study recommended that a square regression correlation is there between the BPD and GA

and best fitted for calculating the BPD from GA or GA from BPD.

Financial support and sponsorship

Nil.

Conflicts of interest

There are no conflicts of interest.

References

1. Sadler TW. ed. Langman's Medical Embryology. 11th ed (South Asian Edition). New Delhi: Wolters Kluwer (India) Pvt Ltd / Lippincott Williams & Wilkins; 2010: pg.95.
2. Kalish RB, Chervenak F. Sonographic determination of gestational age. Ultrasound Rev Obstet Gynecol 2005;4:254-8.
3. Pandey VD, Singh V, Nigam GL, Usmani Y, Yadav Y. Fetal tibial length as a tool for assessment of gestational age – A comparative study in North India. IAIM 2015;2:39-45.
4. Jamdade KP, Amin S, Ferrao SR. Bi-Parietal Diameter (BPD) growth rate between the first and second trimester as a predictor of poor obstetric and neonatal outcome among the Indian population. Int J Clin Trials 2014;1:22-6.
5. Hall MH, Carr-Hill RA. The significance of uncertain gestation for obstetric outcome. Br J Obstet Gynaecol 1985;92:452-60.
6. Willocks J, Donald I, Duggan TC, Day N. Foetal cephalometry by ultrasound. J Obstet Gynaecol Br Commonw 1964;71:11-20.
7. Quddusa S, Chowdhury S. Estimation of gestational age by foetal biparietal diameter in Bangladesh. J Bangladesh Coll Phys Surg 2004;22:53-6.
8. Hadlock FP, Deter RL, Harrist RB, Park SK. Fetal biparietal diameter: A critical re-evaluation of the relation to menstrual age by means of real-time ultrasound. J Ultrasound Med 1982;1:97-104.
9. Kurtz AB, Wapner RJ, Kurtz RJ, Dershaw DD, Rubin CS, Cole-Beuglet C, *et al.* Analysis of biparietal diameter as an accurate indicator of gestational age. J Clin Ultrasound 1980;8:319-26.
10. Shepard M, Filly RA. A standardized plane for biparietal diameter measurement. J Ultrasound Med 1982;1:145-50.
11. Sabbagha RE, Hughey M. Standardization of sonar cephalometry and gestational age. Obstet Gynecol 1978;52:402-6.
12. Campbell S. The prediction of fetal maturity by ultrasonic measurement of the biparietal diameter. J Obstet Gynaecol Br Commonw 1969;76:603-9.
13. Mador ES, Ekwempu CC, Mutihir JT, Adoga GI, Ogunranti JO. Ultrasonographic biometry: Biparietal diameter of Nigerian foetuses. Niger Med J 2011;52:41-4.
14. Beigi A, ZarrinKoub F. Ultrasound assessment of fetal biparietal diameter and femur length during normal pregnancy in Iranian women. Int J Gynaecol Obstet 2000;69:237-42.
15. Agrawal NL. Correlation of gestational age by real time ultra sonographic measurement of fetal Biparietal Diameter (BPD) with existing standard normograms. Indian J Appl Res 2015;5:79-99.
16. Ayangade SO, Okonofua FE. Normal growth of the fetal biparietal diameter in an African population. Int J Gynaecol Obstet 1986;24:35-42.
17. Munjanja S, Masona D, Masvikeni S. Fetal biparietal diameter and head circumference measurements: Results of a longitudinal study in Zimbabwe. Int J Gynecol Obstet 1988;26:223-8.
18. Campbell S, Warsof SL, Little D, Cooper DJ. Routine ultrasound screening for the prediction of gestational age. Obstet Gynecol 1985;65:613-20.
19. Kurmanavicius J, Wright EM, Royston P, Wisser J, Huch R, Huch A, *et al.* Fetal ultrasound biometry: 1. Head reference values. Br J Obstet Gynaecol 1999;106:126-35.
20. Chitty LS, Altman DG, Henderson A, Campbell S. Charts of fetal size: 2. Head measurements. Br J Obstet Gynaecol 1994;101:35-43.
21. Zaidi S, Shehzad K, Omair A. Sonographic foetal measurements in a cohort of population of Karachi, Pakistan. J Pak Med Assoc 2009;59:246-9.
22. Saksiriwuttho P, Ratanasiri T, Komwilaisak R. Fetal biometry charts for normal pregnant women in Northeastern Thailand. J Med Assoc Thai 2007;90:1963-9.
23. Jeanty P, Cousaert E, Hobbins JC, Tack B, Bracken M, Cantraine F. A longitudinal study of fetal head biometry. Am J Perinatol 1984;1:118-28.
24. Tinelli A, Bochicchio MA, Vaira L, Malvasi A. Ultrasonographic fetal growth charts: An informatic approach by quantitative analysis of the impact of ethnicity on diagnoses based on a preliminary report on Salentinian population. Biomed Res Int 2014;2014:386124.
25. Bennini JR, Marussi EF, Barini R, Faro C, Peralta CF. Birth-weight prediction by two- and three-dimensional ultrasound imaging. Ultrasound Obstet Gynecol 2010;35:426-33.

The Stylohyoid Muscle Revisited: Anatomy and Clinical Implications

Abstract

The stylohyoid muscle, one of the four suprahyoid muscles and one of the three styloid muscles, is a small thin muscle running from the styloid process to the hyoid bone. It is intimately related to the styloid process and the styloid ligament. It draws the hyoid bone superiorly and posteriorly along with the posterior belly of the digastric muscle. It functions mainly during swallowing and opening of the mandible. Clinically, it has received much attention for its association with Eagle's syndrome. In this review, anatomic considerations with clinical implications of the stylohyoid muscle will be covered.

Keywords: *Eagle's syndrome, hyoid bone, styloid ligament, styloid process, suprahyoid muscles*

Joo Won Lee[1], Soyeon Kim[1], Larnani Sri[1], Muhammad Akira Takashi Dharma[1], Young-Seok Park[1,2]

[1]*Department of Oral Anatomy and Dental Research Institute, School of Dentistry, Seoul National University,* [2]*Center for Future Dentistry, School of Dentistry, Seoul National University, Seoul, South Korea*

Introduction

The stylohyoid is a slender muscle and one of the four suprahyoid muscles. Sometimes, it is absent or exists as a pair. It lies anterior, medial, and superior to the digastric posterior belly.[1] The muscle also lies medial to the external carotid artery. In the dissection of the upper lateral neck, the stylohyoid is situated lateral to the transverse process of the atlas.[2] Its primary functions are to elevate the hyoid bone during swallowing. This review discusses the diverse features of the stylohyoid muscle published in the literature from the perspective of general anatomy and clinical implications.

General Anatomy

Origin, insertion, and direction

The stylohyoid arises from the posterior or posterolateral surface of the styloid process by a small tendon near its base. The junction between the body of the hyoid bone and the greater cornu is its insertion site. The superior belly of the omohyoid, one of the four infrahyoid muscles, attaches just below there. It passes downward and forward from the origin to the insertion. The intermediate tendon of the digastric muscle is penetrated by the stylohyoid near its insertion[3,4] [Figure 1].

Arterial supply and innervation

The stylohyoid is supplied with arterial blood by several branches of the facial, posterior auricular, and occipital arteries, all of which are large branches of the external carotid artery. The extracranial path of the facial nerve, the stylohyoid branch, innervates the muscle by entering the middle portion of the muscle.[5] The branch often arises with other branches such as the digastric branch.

Relations to adjacent structures

The medial surface of the submandibular gland superficial part is related to the stylohyoid muscle with the digastric posterior belly. The ascending external carotid artery crosses the two muscles and leaves the carotid triangle. After the extradural part of the accessory nerve is crossed by the occipital artery, it descends obliquely, medial to the stylohyoid.[6]

Relations to the anatomic triangle

The carotid triangle is superiorly bordered by the stylohyoid with the digastric posterior belly. Adjacent to the carotid triangle, the digastric triangle is limited posteroinferiorly by the same two muscles. Bademci and Yaşargil[7] newly described the "hypoglossal triangle," which has its superior border as the inferior margin of the stylohyoid muscle.

Stylohyoid ligament

The stylohyoid ligament runs from the styloid process tip to the hyoid bone lesser

How to cite this article: Lee JW, Kim S, Sri L, Dharma MA, Park YS. The stylohyoid muscle revisited: Anatomy and clinical implications. J Anat Soc India 2023;72:169-72.
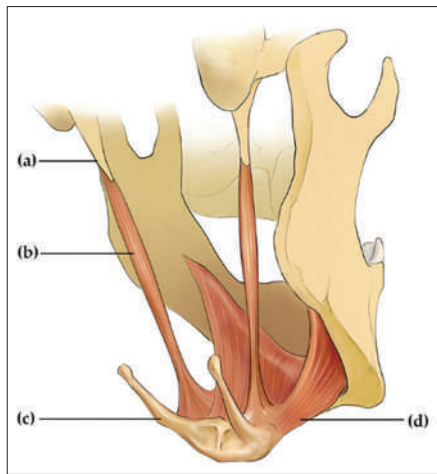
Figure 1: Stylohyoid muscle and adjacent structures. a: Styloid process, b: Stylohyoid muscle, c: Hyoid bone, d: Mylohyoid muscle

cornu. This fibrous cord attaches to the highest fibers of the middle pharyngeal constrictor and is intimately related to the oropharynx lateral wall. The inferior portion of the ligament is overlapped by the hyoglossus muscle. The ligament is derived from the Reichert's cartilage of the second pharyngeal arch and can sometimes be partially or nearly completely calcified.

Styloid process

The styloid process of the temporal bone is a slender pointed bone piece that projects downward and forward from the inferior portion of the temporal bone. The proximal part of the process, the tympanohyal, is ensheathed by the vaginal process. The length of the process is 2.5 cm in average length in a wide range.[6] It is usually straight in form, but sometimes has a curvature. Laterally, the process is covered by the parotid gland. The distal part of the process, the stylohyal, provides attachment to two ligaments and three muscles: the stylohyoid and stylomandibular ligaments, and the styloglossus, stylopharyngeus, and stylohyoid muscles.

Anatomy in variations

As mentioned earlier, the stylohyoid muscle may be absent or exist as a pair. It may also lie just beneath the carotid artery. Sometimes, it is inserted into the mylohyoid or omohyoid. It was reported that a distinct muscle was found in a Chinese cadaver in place of the stylohyoid ligament, which runs from the styloid process to the lesser cornu of the hyoid bone.[8] The accessory stylohyoid muscle was reported in a dissection of a cadaver with an unrepaired complete cleft palate.[9] The unusual insertion of the stylohyoid was reported as covering the hyoid as a collar or a belt. The author suspected this aberration may result in symptoms similar to Eagle's syndrome.[10] Some fibers of the middle pharyngeal constrictor muscles occasionally attach to the stylohyoid.[11]

Several authors reported on the presence of the "tractus angularis" or the "mandibulo-stylohyoid ligament," a strong fascial band from the mandibular angle to the hyoid bone. It was usually described as running from the investing fascia to the digastric posterior belly fascia. Medially, the ligament or fascia covers the stylohyoid with the digastric posterior belly. The position of this ligament is important from the perspective of oral and maxillofacial surgery since it forms part of the separating structures between the submandibular and parotid glands.[12-14] The glossopharyngeal nerve frequently exhibits anastomoses with the facial nerve; the stylohyoid branch is reported to be its main target.[15,16] Interestingly, the stylohyoid branch was reported to innervate the anterior belly of the digastric muscle in association with the mylohyoid nerve.[17,18]

Development

At week 16, the stylohyoid muscle can become visible in relation to the ventral end of Meckel's cartilage from the first pharyngeal arch which follows the curvature of the mandibular process.[19] However, the stylohyoid is a derivative of the second pharyngeal arch, the hyoid arch, with many associated structures such as the styloid process, the stylohyoid ligament, the lesser cornu, and the upper part of the hyoid bone body. The posterior belly of digastric muscles also comes from the arch, which shares facial nerve innervation.[20] In addition, the hyoid arch gives rise to other muscles such as the platysma, buccinators, and facial muscles of expression.

In one anatomic study, it was suggested that the anterior belly of the digastric muscle is formed by combining the most rostral part of the stylohyoid primordium with the caudal part of the anterior digastric primordium, based on the observation that the muscle receives twigs from the facial nerves.[21]

Functions

The stylohyoid draws the hyoid bone upward and backward, elongating the mouth floor. In electrophysiological identification, the stylohyoid with the digastric posterior belly demonstrated activation during jaw opening, oropharyngeal swallowing, and lip pursing.[22] Like other jaw opening muscles, the stylohyoid is designed for velocity and displacement.[23] The stylohyoid with the digastric posterior belly and mylohyoid muscles demonstrated shortening in the initial stage of the swallowing reflex in a computed tomography study.[24] Contraction of the stylohyoid elevates the posterior aspect of the tongue and empties the gutter. This muscle has therefore been studied with other muscles in dysphagia research including physiological cross-sectional area measurement studies.[25,26] The geniohyoid muscle, which draws the hyoid bone upward but forward, partly functions as an antagonist to the stylohyoid.[27]

The patency of the pharyngeal airway is maintained in awake individuals through the combination of several muscles including the stylohyoid, acting to counter the

negative pressure of inspiration. In a study on patients with voice disorders, a shortening or contraction of the stylohyoid and the sternocleidomastoid was reported along with a high held larynx.[28]

Clinical Implications

Surgery

The stylohyoid is occasionally resected for surgical sites at the skull base in cases of malignancies and aneurysms.[29,30] The muscle is sometimes used as a boundary in compartmental tongue surgery.[31]

For the treatment of velopharyngeal incompetence, the pedicled muscle transposition technique can be utilized with the classic Wardill–Kilner operation.[32] The stylohyoid must be considered in the surgical cervicomental improvement of a dysmorphic neck.[33]

Eagle's syndrome

Eagle's syndrome is a rare and poorly understood condition that presents with a variety of symptoms typically including pain in the anterolateral neck.[34] It is also called as stylohyoid complex syndrome. The syndrome is characterized by an elongated styloid process.[35] Although about 4% of the general population exhibits elongated styloid processes, not all of them present with this syndrome.[36] Usually, the syndrome is classified either as Eagle's classic syndrome or Eagle's carotid syndrome.[37] The former is featured by the compression of cranial nerves V, VI, IX, X, and XII, frequently as a result of tonsillectomy or other traumatic events.[34,38] The latter is associated with the compression of the carotid artery by the styloid process and resultant irritation of the sympathetic plexus. When the length exceeds 3 cm, the flexion of the head can lead to the approach of the process tip toward the adjacent neurovascular bundle.[39] Diagnosis is mainly base on imaging modality,[40,41] but sometimes palpation is possible[42] [Figure 2].

Since the stylohyoid ligament is known to be a structure which produces most of the throat pain when injured,[43] it can be included in the differential diagnosis of several other orofacial disturbances such as glossopharyngeal pain, occipital neuralgia, and temporomandibular dysfunction (TMD).[37,44] Interestingly, even though an elongated styloid process was prevalently found in patients with TMD, no relationship has been found between TMD symptoms and measurements of the stylohyoid chain.[45]

The management of Eagle's syndrome is commonly divided into a conservative approach using medicine or more definitive surgical treatment known as a styloidectomy.[46] The extraoral approach is regarded more effective,[47] when cosmetic considerations are not necessary. Literature related to the stylohyoid muscle is mostly on surgical resection with the muscle being calcified in many cases.[48] Uniquely, stylopharyngeal calcification was once reported.[49]
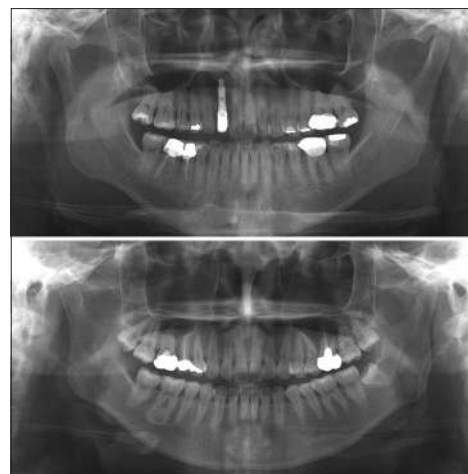

Figure 2: Elongated styloid processes which are frequently observed in routine panoramic radiographs

Conclusion

The anatomical and clinical literature on the stylohyoid muscle was comprehensively reviewed. The muscle has unique anatomic relations to the adjacent structures of the neck and its function in swallowing and mandibular movements are important in the many fields of clinicians as well as the basic scientists. The clinical importance of the muscle has been widely recognized, especially in association with stylohyoid complex syndrome.

Financial support and sponsorship

Conflicts of interest

There are no conflicts of interest.

References

1. Prades JM, Gavid M, Asanau A, Timoshenko AP, Richard C, Martin CH. Surgical anatomy of the styloid muscles and the extracranial glossopharyngeal nerve. Surg Radiol Anat 2014;36:141-6.
2. Sheen TS, Yen KL, Ko JY, Hsu MM. Usefulness of the C1 transverse process as a reference guide in the dissection of the upper lateral neck. Otolaryngol Head Neck Surg 2000;122:284-9.
3. Denk CC, Aldur M, Celik HH, Basar R. A unique anomaly of the fibrous sling of the digastric muscle. Morphologie 1998;82:5-6.
4. Harvey JA, Call Z, Peterson K, Wisco JJ. Weave pattern of accessory heads to the anterior digastric muscle. Surg Radiol Anat 2015;37:1001-4.
5. Seçil Y, Aydogdu I, Ertekin C. Peripheral facial palsy and dysfunction of the oropharynx. J Neurol Neurosurg Psychiatry 2002;72:391-3.
6. Standring S. Gray's Anatomy: The Anatomical Basis of Clinical Practice. Oxford, United Kingdom: Elsevier Limited; 2016.
7. Bademci G, Yaşargil MG. Microsurgical anatomy of the hypoglossal nerve. J Clin Neurosci 2006;13:841-7.
8. Wang CM. An anomalous muscle in place of the stylohyoid

ligament of a Chinese. Anat Rec 1950;107:375-8.

9. Mina MM. Styloid, velar, and pharyngeal muscles in cleft palate. Anatomical findings in elderly cadaver with unrepaired cleft palate. J Otolaryngol 1979;8:179-90.

10. Ozgur Z, Govsa F, Celik S, Ozgur T. An unreported anatomical finding: Unusual insertions of the stylohyoid and digastric muscles. Surg Radiol Anat 2010;32:513-7.

11. Sakamoto Y. Gross anatomical observations of attachments of the middle pharyngeal constrictor. Clin Anat 2014;27:603-9.

12. Jovanovic MS. The mandibulo-stylohyoid ligament (tractus angularis). Surg Radiol Anat 1990;12:91-5.

13. Seward GR. Anatomic surgery for salivary calculi. IV. Calculi in the intraglandular part of the submandibular duct. Oral Surg Oral Med Oral Pathol 1968;25:670-8.

14. Ziarah HA, Atkinson ME. The angular tract: An anatomical structure of surgical significance. Br J Oral Surg 1981;19:116-20.

15. Müller T, Rude J. On a complex anastomosis of the glossopharyngeal nerve in humans. Kaibogaku Zasshi 2000;75:345-8.

16. Salame K, Ouaknine GE, Arensburg B, Rochkind S. Microsurgical anatomy of the facial nerve trunk. Clin Anat 2002;15:93-9.

17. Asami Y, Kawai K, Kanoh T, Koizumi M, Honma S, Tokiyoshi A, *et al.* Double innervation of the anterior belly of the digastric muscle. Anat Sci Int 2006;81:130-3.

18. Kawai K. Anomalous course of the external carotid artery. Anat Sci Int 2016;91:334-40.

19. Wyganowska-Swiatkowska M, Kawala B, Kozanecka A, Kurlej W. Observations on muscular attachments to human developing mandible. Adv Clin Exp Med 2012;21:447-54.

20. Mujuru HA, Marume A, Shumbairerwa S, Ndhlovu A. Agnathia-synotia-microstomia (otocephaly): A case report in an African woman. Cent Afr J Med 2010;56:66-9.

21. Kawai K, Koizumi M, Honma S, Tokiyoshi A, Kodama K. Derivation of the anterior belly of the digastric muscle receiving twigs from the mylohyoid and facial nerves. Ann Anat 2003;185:85-90.

22. Kurt T, Gürgör N, Seçil Y, Yildiz N, Ertekin C. Electrophysiologic identification and evaluation of stylohyoid and posterior digastricus muscle complex. J Electromyogr Kinesiol 2006;16:58-65.

23. Van Eijden TM, Korfage JA, Brugman P. Architecture of the human jaw-closing and jaw-opening muscles. Anat Rec 1997;248:464-74.

24. Okada T, Aoyagi Y, Inamoto Y, Saitoh E, Kagaya H, Shibata S, *et al.* Dynamic change in hyoid muscle length associated with trajectory of hyoid bone during swallowing: Analysis using 320-row area detector computed tomography. J Appl Physiol (1985) 2013;115:1138-45.

25. Pearson WG Jr., Hindson DF, Langmore SE, Zumwalt AC. Evaluating swallowing muscles essential for hyolaryngeal elevation by using muscle functional magnetic resonance imaging. Int J Radiat Oncol Biol Phys 2013;85:735-40.

26. Pearson WG Jr., Langmore SE, Yu LB, Zumwalt AC. Structural analysis of muscles elevating the hyolaryngeal complex. Dysphagia 2012;27:445-51.

27. Pearson WG Jr., Langmore SE, Zumwalt AC. Evaluating the structural properties of suprahyoid muscles and their potential for moving the hyoid. Dysphagia 2011;26:345-51.

28. Rubin JS, Blake E, Mathieson L. Musculoskeletal patterns in patients with voice disorders. J Voice 2007;21:477-84.

29. Otero-Coto E, Orozco M, Lopez Collado M. Giant aneurysm of the high internal carotid artery: Surgical treatment. Surgery 1992;111:348-51.

30. Pellet W, Cannoni M, Pech A. The widened transcochlear approach to jugular foramen tumors. J Neurosurg 1988;69:887-94.

31. Calabrese L, Bruschini R, Giugliano G, Ostuni A, Maffini F, Massaro MA, *et al.* Compartmental tongue surgery: Long term oncologic results in the treatment of tongue cancer. Oral Oncol 2011;47:174-9.

32. Kärcher H, Radner H, Anderhuber F. The pedicled transposition of the digastric and stylohyoid muscles in the treatment of velopharyngeal incompetence. Anatomic basis and clinical application. Acta Anat (Basel) 1992;144:145-51.

33. Guyuron B. Problem neck, hyoid bone, and submental myotomy. Plast Reconstr Surg 1992;90:830-7.

34. Badhey A, Jategaonkar A, Anglin Kovacs AJ, Kadakia S, De Deyn PP, Ducic Y, *et al.* Eagle syndrome: A comprehensive review. Clin Neurol Neurosurg 2017;159:34-8.

35. Fotis D, Mannucci A, Vercellotti G. A possible case of Eagle's syndrome from an Italian ossuary (Chiavari, GE). Cranio 2013;31:61-5.

36. Iwanaga J, Watanabe K, Saga T, Tabira Y, Yamaki KI. Morphometric study of a huge elongated styloid process. Kurume Med J 2017;63:45-8.

37. Fusconi M, Campo F, Pandolfi F, D'Ambrosio F, Greco A, Turchetta R, *et al.* Orofacial pain and stylohyoid complex syndrome. Eur J Pain 2016;20:855-6.

38. Neville BW, Damm DD, Chi AC, Allen CM. Oral and Maxillofacial Pathology. Oxford, United Kingdom: Elsevier; 2015.

39. Fusco DJ, Asteraki S, Spetzler RF. Eagle's syndrome: Embryology, anatomy, and clinical management. Acta Neurochir (Wien) 2012;154:1119-26.

40. Kent DT, Rath TJ, Snyderman C. Conventional and 3-Dimensional computerized tomography in Eagle's syndrome, glossopharyngeal neuralgia, and asymptomatic controls. Otolaryngol Head Neck Surg 2015;153:41-7.

41. Muñoz Herrera A, Pardal Refoyo JL, Ruiz Martín F, Santiago Andrés J, Sánchez del Hoyo A, Ramos Macías A. Diagnostic and clinical evaluation of the stylohyoid apparatus totally or partially ossified. Acta Otorrinolaringol Esp 1990;41:77-81.

42. Loch C, Fehrmann P, Dockhorn HU. Studies on the compression of the external carotid artery in the region of the styloid process of the temporal bone. Laryngorhinootologie 1990;69:260-6.

43. Shankland WE 2nd. Bursitis of the hamular process. Part I: Anatomical and histological evidence. Cranio 1996;14:186-9.

44. Martins WD, Ribas Mde O, Bisinelli J, França BH, Martins G. Eagle's syndrome: Treatment by intraoral bilateral resection of the ossified stylohyoid ligament. A review and report of two cases. Cranio 2013;31:226-31.

45. de Andrade KM, Rodrigues CA, Watanabe PC, Mazzetto MO. Styloid process elongation and calcification in subjects with tmd: Clinical and radiographic aspects. Braz Dent J 2012;23:443-50.

46. Piagkou M, Anagnostopoulou S, Kouladouros K, Piagkos G. Eagle's syndrome: A review of the literature. Clin Anat 2009;22:545-58.

47. Liu SH, Wang Y, Zhang RH, Liu SY, Peng HH. Diagnosis and treatment of 23 cases with stylohyoid syndrome. Shanghai Kou Qiang Yi Xue 2005;14:223-6.

48. Fuat Iondemli, Pavlikhin OG, Akhmed Arslan. Phenomenon of calcification of the stylohyoid ligament. Vestn Otorinolaringol 2004;40-1.

49. Kamil RJ, Gonik NJ, Lee JS, Shifteh K, Smith RV. Transoral resection of stylopharyngeus calcification: A unique manifestation of a stylohyoid complex syndrome. Ann Otol Rhinol Laryngol 2015;124:158-61.

Triorchidism: A Differential Diagnosis of Inguinal Swelling in a 28-Year-Old Male

Abstract

Polyorchidism, more than two testicles, is a rare congenital anomaly of urogenital system. In majority of the cases, supernumerary testis is located intrascrotally. However, testis in the retroperitoneal space is reported rarely. About 50% of cases are detected between 15 and 25 years of age. In this case report, we present a case of triorchidism in a 28-year-old male who came with a complaint of left groin swelling.

Keywords: *Congenital anomaly, groin swelling, inguinal hernia, inguinal swelling, polyorchidism, triorchidism, urogenital*

A. K. Nuveen

Department of Anatomy, Amala Institute of Medical Sciences, Thrissur, Kerala, India

Introduction

Polyorchidism or supernumerary testis is a condition in which a person has more than two testicles. It is a rare congenital anomaly of the urogenital system. The number of cases reported in literature till date is only around two hundred.[1] Triorchidism is the most common presentation which refers to the presence of three testes and it is commonly seen on the left side.[2] The first case of polyorchidism was reported in 1880 by Ashfeld.[3] However, it was during autopsy. The first case found during surgery was in 1895, by Lane.[4] About 50% of cases are detected between 15 and 25 years of age.[5] In about 66% of these cases, the supernumerary testis is located intrascrotally; about 23% in the inguinal canal and 9% in the retroperitoneal space.[6] Majority of these patients are asymptomatic. In this article, we present a case of triorchidism in a 28-year-old male who came with a complaint of left groin swelling.

Case Report

A 28-year-old unmarried male came to the surgery outpatient department with complaints of painless swelling in the left groin region. He noticed the swelling 6 months back which increased in size gradually. There was no history of chronic cough, constipation, or urinary complaints.

On examination, there was a 2 cm × 2 cm swelling in the left inguinal region. The swelling was above and medial to the pubic tubercle without any extension to scrotum. Expansile impulse on cough was present. On doing "three-finger test," the impulse was felt by index finger. The swelling was reducible. Ring occlusion test was positive. External genitalia was normal and testes were palpable in both scrotal sacs. Scrotal ultrasound revealed two normal testes in both the scrota. The diagnosis of left direct inguinal hernia was made and planned for surgery. Intraoperatively, an indirect sac was discovered which contained a globular mass of size 2 cm along with a cord-like structure attached to it [Figure 1]. The vascularity of the mass was independent from that of normal testis. The mass along with its cord-like structure was excised and send for histopathology. Histopathology report revealed it as an atrophic testis [Figure 2a] with rudimentary cord-like structures. There were no features of active spermatogenesis [Figure 2b] or features of malignancy.

Discussion

Polyorchidism is a rare congenital anomaly of the genital system. It is defined as the presence of more than two testes, confirmed by histology. Since the first report, only about 200 cases have been reported in the literature.[1] The most frequent location of supernumerary testes is scrotum. Other locations include the inguinal region and

Access this article online

Website: https://journals.lww.com/joai

DOI:
10.4103/jasi.jasi_23_22

Quick Response Code:

Figure 1: Globular mass of size 2 cm along with its cord-like structure excised

Figure 2: Histopathological analysis of globular mass. (a) Testis and (b) Epididymis

retroperitoneal region. The testis develops from three sources: (1) mesothelium lining the posterior abdominal wall, (2) underling mesenchyme, and (3) primordial germ cells. During the folding of the embryo, the dorsal part of the umbilical vesicle is incorporated into the embryo. At this time, the primordial germ cells migrate along the dorsal mesentery of the hindgut to the gonadal ridges where they get incorporated in the gonadal cords. The gonadal cords differentiate into seminiferous cords, which in turn develop into seminiferous tubules, tubuli recti, and rete testis. The seminiferous tubules are separated by interstitial cells of Leydig, which develop from mesenchyme. The epididymis and vas deferens develop from mesonephric duct. The proximal part of mesonephric duct forms the epididymis and the mesonephric duct distal to epididymis forms the vas deferens. Developmental problems during union or division of the gonadal ridge and mesonephric duct can cause polyorchidism.[7]

There are two embryological theories related to polyorchidism. Longitudinal division of the genital ridge results in the development of two separate testes. Only the lateral mass will be having connection with the developing mesonephric duct which ultimately forms the vas deferens and epididymis. Transverse division of the genital ridge results in a number of anatomical anomalies depending on the level of abnormal division. The most frequent one is a common vas deferens and an epididymis shared by both testicular masses. Division of the mesonephric duct in addition to the division of genital ridge will result in only one testis being connected to the vas deferens. However, both testicular masses will be having separate epididymis. The totally isolated testis usually lacks spermatogenesis.[8,9]

There are certain anomalies associated with polyorchidism. They are undescended testis (40%), inguinal hernia (30%), testicular torsion (15%), hydrocele (9%), and malignancy (6%).[5] The patient in this case had inguinal hernia. According to literature, there is an estimated 6%
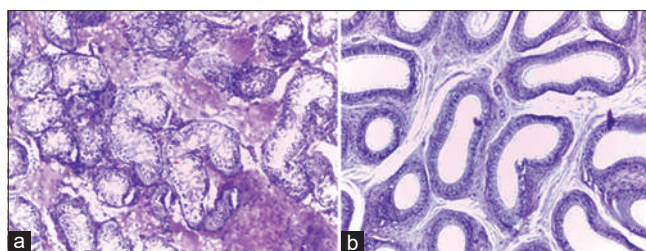
risk of malignancy in cases of polyorchidism. The patient in this case report had no malignancy till surgery. The reported malignancies are seminoma, choriocarcinoma, and teratoma.[10] The literature mentions the risk of malignancy as 6%. However, there is no evidence supporting the idea of a relationship between polyorchidism and malignancy.[11]

Conclusion

Inguinal hernia is the most common differential diagnosis of an inguinal swelling. Most of patients with inguinal swellings will present to a doctor when the swelling becomes symptomatic. The triorchidism is an occasional diagnosis. It has to be considered as a differential diagnosis of inguinal swelling as there is a rare chance of malignancy. Even though the treatment of polyorchidism depends on the site, size, and anatomy of the drainage system of supernumerary testis,[12] it is most commonly treated by orchidectomy.

Declaration of patient consent

The authors certify that they have obtained all appropriate patient consent forms. In the form, the patient has given his consent for his images and other clinical information to be reported in the journal. The patient understands that their name and initials will not be published and due efforts will be made to conceal their identity, but anonymity cannot be guaranteed.

Financial support and sponsorship

Nil.

Conflicts of interest

There are no conflicts of interest.

References

1. Assefa HG, Erge MG, Gebreselassie HA. Triorchidism, a rare genitourinary anomaly: A case series. Res Rep Urol 2021;13:549-52.
2. Bayissa BB, Tesfaye D. Triorchidism; an incidental finding at inguinal hernia repair: A case report. Int J Surg Case Rep 2020;77:813-5.
3. Ashfeld F. Die Missbildungen des Menschen. Leipzig, German: Grunow; 1880.
4. Lane A. A case of supernumery testes. Trans Clin Soc Lond 1895;28:59-60.
5. Spranger R, Gunst M, Kühn M. Polyorchidism: A strange

anomaly with unsuspected properties. J Urol 2002;168:198.

6. Mummed FO, Endris AS, Erge MG. Polyorchidism – An incidental finding during orchidopexy: A case report and review of the literature. Res Rep Urol 2021;13:811-4.

7. Figler TJ, Olson MC, Kinzler GJ. Polyorchidism and rete testis adenoma: Ultrasound and MR findings. Abdom Imaging 1996;21:470-2.

8. Nocks BN. Polyorchidism with normal spermatogenesis and equal sized testes: A theory of embryological development. J Urol 1978;120:638-40.

9. Wilson WA, Littler J. Polyorchidism; a report of two cases with torsion. Br J Surg 1953;41:302-7.

10. Nane I, Ozkan L, Ander H. Inguinal orchiectomy for the extra testis with suspected tumor in a polyorchidic patient: A case report. Int Urol Nephrol 2007;39:557-9.

11. Berger AP, Steiner H, Hoeltl L, Bartsch G, Hobisch A. Occurrence of polyorchidism in a young man. Urology 2002;60:911.

12. Piro E, Abati L, Zocca V, Brugnoni M, D'Alessio A. Triorchidism: Which therapy? Pediatr Med Chir 2017;39:141.

Shifting of Research and Teaching Methodology Training is a Potential Solution for Indian Medical Education

We read your editorial with great interest and appreciate the bold messages it conveys regarding the current research roadblocks in Indian medical institutions and the proposed solutions. Your editorial presents a valid argument about the importance of balancing teaching, research, and patient care in rural medical colleges.[1] However, I believe that it is not only important for rural medical medical colleges but also true for other medical colleges in urban and semi-urban areas. I have worked in various institutions, including an urban medical college in Kolkata, a private medical college in West Bengal, two rural medical colleges in the remotest hilly part of Odisha, and currently working in an institution of national importance in Jharkhand. From my experience, I can deduce that the geographical location of an institution does not determine its resources for research. I have seen well-established research laboratory in a remote college and no research laboratory in a medical college in a metro city. Overall, most Indian medical colleges have limited resources for research.[2] Therefore, the solutions you suggested should apply to all types of medical institutions in India, including rural, urban, government, and private.

I fully agree with your suggestion that teachers who are not inclined to do research should not be forced to do so. However, aside from research, medical teachers were not getting training for teaching mythology previously. That is why the National Medical Commission (NMC) has introduced two courses: one for research methods (i.e., Basic Course in Biomedical Research [BCBR]) and one for teaching methods (i.e., Basic Course in Medical Education). These courses are mandatory for promotion of an assistant professor to associate professor.[3] A large number of medical teachers are senior residents, tutors, and assistant professors. Hence, we suggest that the stakeholders consider shifting these courses to the undergraduate and postgraduate levels as optional courses – research training for undergraduate students and teaching methods for postgraduate students. Those who want to pursue a research carrier after MBBS can receive training in research methodology and interested postgraduates who would like to pursue the teaching profession can enroll for teaching methods course. We have presented proposed course for undergraduate and postgraduate students in Figure 1.

In addition, many graduates opt for teaching job after MBBS. They may be offered training for teaching methodology immediately after joining. This would potentially improve the quality of teaching. Stakeholders should consider shifting the current offline teaching methodology training to online training (like BCBR) for ease of accessibility. Since currently, the Revised Basic Course Workshop of Medical Education is conducted in limited settings, with limited participants, and is not conducted frequently. Moreover, limited seats are offered on priority to the faculties who are waiting for their promotion.

I strongly believe that publication should not be the sole criterion for promotion. Rather, the publication should be used as a preference for promotion when compared to peers. With this in mind, we have proposed a model in which research may be made compulsory for promotion but not research publication.[4] While this model may be challenged, I believe that its tenet will have a long-term positive effect on the quality of publication output from India. Under our model, medical teachers conduct research and store their study results in a centralized repository (which is currently hypothetical and not yet available), and this would be counted as credit for promotion. If authors choose to publish the work, they can also optionally publish their work. This model may encourage research work, even if it involves simple and small projects, without the pressure of publication.

Another issue that is indirectly reflected in your editorial is the scarcity of faculties in peripheral medical colleges. Unfortunately, this is a truth that is commonly manipulated to show regulatory bodies that the minimum required faculties are present. However, the scarcity of faculties is present everywhere, whether it is in a peripheral college or a college in a metro city.[5] The NMC has set minimum criteria for granting permission to medical colleges. However, the concern is often focused on the "minimum" requirement rather than the "optimum" requirement. As a result, teaching in medical colleges in India is often hampered. It is time to ask another question: is there truly a shortage of workforce, or are qualified individuals not being hired?
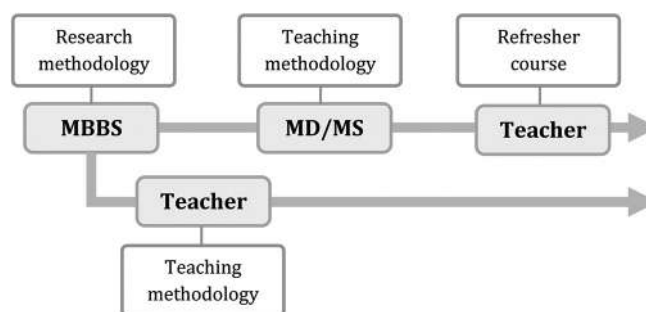

Figure 1: Shifting the research methodology and teaching methodology courses

Disclaimer

Please note that the opinions expressed in this letter are personal and do not reflect or endorsed by the institution or organization.

Financial support and sponsorship

Nil.

Conflicts of interest

There are no conflicts of interest.

Himel Mondal

Department of Physiology, All India Institute of Medical Sciences, Deoghar, Jharkhand, India

Address for correspondence: Dr. Himel Mondal, Department of Physiology, All India Institute of Medical Sciences, Deoghar, Jharkhand, India. E-mail: himelmkcg@gmail.com

References

1. Singh V, Singh R. Teaching should be preferred over research in peripheral medical institutions. J Anat Soc India 2023;72:1.
2. Kapoor A. Quality medical research and publications in India: Time to introspect. Int J Appl Basic Med Res 2019;9:67-8.
3. Mondal H, Mondal S, Behera JK. Roller coaster of publication criteria: What is new in teacher's eligibility qualifications in medical institutions regulations, 2022? Indian J Ophthalmol 2022;70:1845-6.
4. Mondal H, Mondal S. A hypothesis to stop "publish or perish". Med J DY Patil Vidyapeeth 2022;15:809-10.
5. Jain A, Kanchan T, Menezes RG. Shortage of teaching faculty in medical colleges: Some suggestions to overcome the problem. Natl Med J India 2008;21:209.

Access this article online	
Quick Response Code:	**Website:** https://journals.lww.com/joai
	DOI: 10.4103/jasi.jasi_33_23

How to cite this article: Mondal H. Shifting of research and teaching methodology training is a potential solution for Indian medical education. J Anat Soc India 2023;72:176-7.

The Editorial Process

A manuscript will be reviewed for possible publication with the understanding that it is being submitted to Journal of the Anatomical Society of India alone at that point in time and has not been published anywhere, simultaneously submitted, or already accepted for publication elsewhere. The journal expects that authors would authorize one of them to correspond with the Journal for all matters related to the manuscript. All manuscripts received are duly acknowledged. On submission, editors review all submitted manuscripts initially for suitability for formal review. Manuscripts with insufficient originality, serious scientific or technical flaws, or lack of a significant message are rejected before proceeding for formal peer-review. Manuscripts that are unlikely to be of interest to the Journal of the Anatomical Society of India readers are also liable to be rejected at this stage itself.

Manuscripts that are found suitable for publication in Journal of the Anatomical Society of India are sent to two or more expert reviewers. During submission, the contributor is requested to provide names of two or three qualified reviewers who have had experience in the subject of the submitted manuscript, but this is not mandatory. The reviewers should not be affiliated with the same institutes as the contributor/s. However, the selection of these reviewers is at the sole discretion of the editor. The journal follows a double-blind review process, wherein the reviewers and authors are unaware of each other's identity. Every manuscript is also assigned to a member of the editorial team, who based on the comments from the reviewers takes a final decision on the manuscript. The comments and suggestions (acceptance/ rejection/ amendments in manuscript) received from reviewers are conveyed to the corresponding author. If required, the author is requested to provide a point by point response to reviewers' comments and submit a revised version of the manuscript. This process is repeated till reviewers and editors are satisfied with the manuscript.

Manuscripts accepted for publication are copy edited for grammar, punctuation, print style, and format. Page proofs are sent to the corresponding author. The corresponding author is expected to return the corrected proofs within three days. It may not be possible to incorporate corrections received after that period. The whole process of submission of the manuscript to final decision and sending and receiving proofs is completed online. To achieve faster and greater dissemination of knowledge and information, the journal publishes articles online as 'Ahead of Print' immediately on acceptance.

Clinical trial registry

Journal of the Anatomical Society of India favors registration of clinical trials and is a signatory to the Statement on publishing clinical trials in Indian biomedical journals. Journal of the Anatomical Society of India would publish clinical trials that have been registered with a clinical trial registry that allows free online access to public. Registration in the following trial registers is acceptable: http://www.ctri.in/; http://www.actr.org.au/; http://www.clinicaltrials.gov/; http://isrctn.org/; http://www.trialregister.nl/trialreg/index.asp; and http://www.umin.ac.jp/ctr. This is applicable to clinical trials that have begun enrollment of subjects in or after June 2008. Clinical trials that have commenced enrollment of subjects prior to June 2008 would be considered for publication in Journal of the Anatomical Society of India only if they have been registered retrospectively with clinical trial registry that allows unhindered online access to public without charging any fees.

Authorship Criteria

Authorship credit should be based only on substantial contributions to each of the three components mentioned below:

1. Concept and design of study or acquisition of data or analysis and interpretation of data;
2. Drafting the article or revising it critically for important intellectual content; and
3. Final approval of the version to be published.

Participation solely in the acquisition of funding or the collection of data does not justify authorship. General supervision of the research group is not sufficient for authorship. Each contributor should have participated sufficiently in the work to take public responsibility for appropriate portions of the content of the manuscript. The order of naming the contributors should be based on the relative contribution of the contributor towards the study and writing the manuscript. Once submitted the order cannot be changed without written consent of all the contributors. The journal prescribes a maximum number of authors for manuscripts depending upon the type of manuscript, its scope and number of institutions involved (vide infra). The authors should provide a justification, if the number of authors exceeds these limits.

Contribution Details

Contributors should provide a description of contributions made by each of them towards the manuscript. Description should be divided in following categories, as applicable: concept, design, definition of intellectual content, literature search, clinical studies, experimental studies, data acquisition, data analysis, statistical analysis, manuscript preparation, manuscript editing and manuscript review. Authors' contributions will be printed along with the article. One or more author should take responsibility for the integrity of the work as a whole from inception to published article and should be designated as 'guarantor'.

Conflicts of Interest/ Competing Interests

All authors of must disclose any and all conflicts of interest they may have with publication of the manuscript or an institution or product that is mentioned in the manuscript and/or is important to the outcome of the study presented. Authors should also disclose conflict of interest with products that compete with those mentioned in their manuscript.

Submission of Manuscripts

All manuscripts must be submitted on-line through the website https://review.jow.medknow.com/jasi. First time users will have to register at this site. Registration is free but mandatory. Registered authors can keep track of their articles after logging into the site using their user name and password.

• If you experience any problems, please contact the editorial office by e-mail at editor@jasi.org.in

The submitted manuscripts that are not as per the "Instructions to Authors" would be returned to the authors for technical correction, before they undergo editorial/ peer-review. Generally, the manuscript should be submitted in the form of two separate files:

[1] Title Page/First Page File/covering letter:

This file should provide

1. The type of manuscript (original article, case report, review article, Letter to editor, Images, etc.) title of the manuscript, running title, names of all authors/ contributors (with their highest academic degrees, designation and affiliations) and name(s) of department(s) and/ or institution(s) to which the work should be credited, . All information which can reveal your identity should be here. Use text/rtf/doc files. Do not zip the files.
2. The total number of pages, total number of photographs and word counts separately for abstract and for the text (excluding the references, tables and abstract), word counts for introduction + discussion in case of an original article;
3. Source(s) of support in the form of grants, equipment, drugs, or all of these;
4. Acknowledgement, if any. One or more statements should specify 1) contributions that need acknowledging but do not justify authorship, such as general support by a departmental chair; 2) acknowledgments of technical help; and 3) acknowledgments of financial and material support, which should specify the nature of the support. This should be included in the title page of the manuscript and not in the main article file.
5. If the manuscript was presented as part at a meeting, the organization, place, and exact date on which it was read. A full statement to the editor about all submissions and previous reports that might be regarded as

redundant publication of the same or very similar work. Any such work should be referred to specifically, and referenced in the new paper. Copies of such material should be included with the submitted paper, to help the editor decide how to handle the matter.

6. Registration number in case of a clinical trial and where it is registered (name of the registry and its URL)
7. Conflicts of Interest of each author/ contributor. A statement of financial or other relationships that might lead to a conflict of interest, if that information is not included in the manuscript itself or in an authors' form
8. Criteria for inclusion in the authors'/ contributors' list
9. A statement that the manuscript has been read and approved by all the authors, that the requirements for authorship as stated earlier in this document have been met, and that each author believes that the manuscript represents honest work, if that information is not provided in another form (see below); and
10. The name, address, e-mail, and telephone number of the corresponding author, who is responsible for communicating with the other authors about revisions and final approval of the proofs, if that information is not included on the manuscript itself.

[2] Blinded Article file: The main text of the article, beginning from Abstract till References (including tables) should be in this file. The file must not contain any mention of the authors' names or initials or the institution at which the study was done or acknowledgements. Page headers/ running title can include the title but not the authors' names. Manuscripts not in compliance with the Journal's blinding policy will be returned to the corresponding author. Use rtf/doc files. Do not zip the files. **Limit the file size to 1 MB.** Do not incorporate images in the file. If file size is large, graphs can be submitted as images separately without incorporating them in the article file to reduce the size of the file. The pages should be numbered consecutively, beginning with the first page of the blinded article file.

[3] Images: Submit good quality color images. **Each image should be less than 2 MB in size.** Size of the image can be reduced by decreasing the actual height and width of the images (keep up to 1600 x 1200 pixels or 5-6 inches). Images can be submitted as jpeg files. Do not zip the files. Legends for the figures/images should be included at the end of the article file.

[4] The contributors' / copyright transfer form (template provided below) has to be submitted in original with the signatures of all the contributors within two weeks of submission via courier, fax or email as a scanned image. Print ready hard copies of the images (one set) or digital images should be sent to the journal office at the time of submitting revised manuscript. High resolution images (up to 5 MB each) can be sent by email.

Contributors' form / copyright transfer form can be submitted online from the authors' area on https://review.jow.medknow.com/jasi.

Preparation of Manuscripts

Manuscripts must be prepared in accordance with "Uniform requirements for Manuscripts submitted to Biomedical Journals" developed by the International Committee of Medical Journal Editors (October 2008). The uniform requirements and specific requirement of Journal of the Anatomical Society of India are summarized below. Before submitting a manuscript, contributors are requested to check for the latest instructions available. Instructions are also available from the website of the journal (www.jasi.org.in) and from the manuscript submission site https://review.jow.medknow.com/jasi.

Journal of the Anatomical Society of India accepts manuscripts written in American English.

Copies of any permission(s)

It is the responsibility of authors/ contributors to obtain permissions for reproducing any copyrighted material. A copy of the permission obtained must accompany the manuscript. Copies of any and all published articles or other manuscripts in preparation or submitted elsewhere that are related to the manuscript must also accompany the manuscript.

Types of Manuscripts

Original articles:

These include randomized controlled trials, intervention studies, studies of screening and diagnostic test, outcome studies, cost effectiveness analyses, case-control series, and surveys with high response rate. The text of original articles amounting to up to 3000 words (excluding Abstract, references and Tables) should be divided into sections with the headings Abstract, Key-words, Introduction, Material and Methods, Results, Discussion and Conclusion, References, Tables and Figure legends.

An abstract should be in a structured format under following heads: **Introduction, Material and Methods, Results,** and **Discussion and Conclusion.**

Introduction: State the purpose and summarize the rationale for the study or observation.

Material and Methods: It should include and describe the following aspects:

Ethics: When reporting studies on human beings, indicate whether the procedures followed were in accordance with the ethical standards of the responsible committee on human experimentation (institutional or regional) and with the Helsinki Declaration of 1975, as revised in 2000

(available at http://www.wma.net/e/policy/17-c_e.html). For prospective studies involving human participants, authors are expected to mention about approval of (regional/ national/ institutional or independent Ethics Committee or Review Board, obtaining informed consent from adult research participants and obtaining assent for children aged over 7 years participating in the trial. The age beyond which assent would be required could vary as per regional and/ or national guidelines. Ensure confidentiality of subjects by desisting from mentioning participants' names, initials or hospital numbers, especially in illustrative material. When reporting experiments on animals, indicate whether the institution's or a national research council's guide for, or any national law on the care and use of laboratory animals was followed. Evidence for approval by a local Ethics Committee (for both human as well as animal studies) must be supplied by the authors on demand. Animal experimental procedures should be as humane as possible and the details of anesthetics and analgesics used should be clearly stated. The ethical standards of experiments must be in accordance with the guidelines provided by the CPCSEA and World Medical Association Declaration of Helsinki on Ethical Principles for Medical Research Involving Humans for studies involving experimental animals and human beings, respectively). The journal will not consider any paper which is ethically unacceptable. A statement on ethics committee permission and ethical practices must be included in all research articles under the 'Materials and Methods' section.

Study design:

Selection and Description of Participants: Describe your selection of the observational or experimental participants (patients or laboratory animals, including controls) clearly, including eligibility and exclusion criteria and a description of the source population. *Technical information*: Identify the methods, apparatus (give the manufacturer›s name and address in parentheses), and procedures in sufficient detail to allow other workers to reproduce the results. Give references to established methods, including statistical methods (see below); provide references and brief descriptions for methods that have been published but are not well known; describe new or substantially modified methods, give reasons for using them, and evaluate their limitations. Identify precisely all drugs and chemicals used, including generic name(s), dose(s), and route(s) of administration.

Reports of randomized clinical trials should present information on all major study elements, including the protocol, assignment of interventions (methods of randomization, concealment of allocation to treatment groups), and the method of masking (blinding), based on the CONSORT Statement (http://www.consort-statement.org).

Reporting Guidelines for Specific Study Designs

Initiative	Type of Study	Source
CONSORT	Randomized controlled trials	http://www.consort-statement.org
STARD	Studies of diagnostic accuracy	http://www.consort-statement.org/stardstatement.htm
QUOROM	Systematic reviews and meta-analyses	http://www.consort- statement.org/Initiatives/MOOSE/moose.pdf statement.org/Initiatives/MOOSE/moose.pdf
STROBE	Observational studies in epidemiology	http://www.strobe-statement.org
MOOSE	Meta-analyses of observational studies in epidemiology	http://www.consort- statement.org/Initiatives/MOOSE/moose.pdf

Statistics: Whenever possible quantify findings and present them with appropriate indicators of measurement error or uncertainty (such as confidence intervals). Authors should report losses to observation (such as, dropouts from a clinical trial). When data are summarized in the Results section, specify the statistical methods used to analyze them. Avoid non-technical uses of technical terms in statistics, such as 'random' (which implies a randomizing device), 'normal', 'significant', 'correlations', and 'sample'. Define statistical terms, abbreviations, and most symbols. Specify the computer software used. Use upper italics (P 0.048). For all P values include the exact value and not less than 0.05 or 0.001. Mean differences in continuous variables, proportions in categorical variables and relative risks including odds ratios and hazard ratios should be accompanied by their confidence intervals.

Results: Present your results in a logical sequence in the text, tables, and illustrations, giving the main or most important findings first. Do not repeat in the text all the data in the tables or illustrations; emphasize or summarize only important observations. Extra- or supplementary materials and technical detail can be placed in an appendix where it will be accessible but will not interrupt the flow of the text; alternatively, it can be published only in the electronic version of the journal.

When data are summarized in the Results section, give numeric results not only as derivatives (for example, percentages) but also as the absolute numbers from which the derivatives were calculated, and specify the statistical methods used to analyze them. Restrict tables and figures to those needed to explain the argument of the paper and to assess its support. Use graphs as an alternative to tables with many entries; do not duplicate data in graphs and tables. Where scientifically appropriate, analyses of the data by variables such as age and sex should be included.

Discussion: Include summary of *key findings* (primary outcome measures, secondary outcome measures, results as they relate to a prior hypothesis); *Strengths and limitations* of the study (study question, study design, data collection, analysis and interpretation); *Interpretation and implications* in the context of the totality of evidence (is there a systematic review to refer to, if not, could one be reasonably done here and now?, what this study adds to the available evidence, effects on patient care and health policy, possible mechanisms); *Controversies* raised by this study; and *Future research directions* (for this particular research collaboration, underlying mechanisms, clinical research).

Do not repeat in detail data or other material given in the Introduction or the Results section. In particular, contributors should avoid making statements on economic benefits and costs unless their manuscript includes economic data and analyses. Avoid claiming priority and alluding to work that has not been completed. New hypotheses may be stated if needed, however they should be clearly labeled as such. About 30 references can be included. These articles generally should not have more than six authors.

Review Articles:

These are comprehensive review articles on topics related to various fields of Anatomy. The entire manuscript should not exceed 7000 words with no more than 50 references and two authors. Following types of articles can be submitted under this category:

• Newer techniques of dissection and histology

• New methodology in Medical Education

• Review of a current concept

Please note that generally review articles are by invitation only. But unsolicited review articles will be considered for publication on merit basis.

Case reports:

New, interesting and rare cases can be reported. They should be unique, describing a great diagnostic or therapeutic challenge and providing a learning point for the readers. Cases with clinical significance or implications will be given priority. These communications could be of up to 1000 words (excluding Abstract and references) and should have the following headings: Abstract (unstructured), Key-words, Introduction, Case report, Discussion and Conclusion, Reference, Tables and Legends in that order.

The manuscript could be of up to 1000 words (excluding references and abstract) and could be supported with up to 10 references. Case Reports could be authored by up to four authors.

Letter to the Editor:

These should be short and decisive observations. They should preferably be related to articles previously published in the Journal or views expressed in the journal. They should not be preliminary observations that need a later

paper for validation. The letter could have up to 500 words and 5 references. It could be generally authored by not more than four authors.

Book Review: This consists of a critical appraisal of selected books on Anatomy. Potential authors or publishers may submit books, as well as a list of suggested reviewers, to the editorial office. The author/publisher has to pay INR 10,000 per book review.

Other:

Editorial, Guest Editorial, Commentary and Opinion are solicited by the editorial board.

References

References should be *numbered* consecutively in the order in which they are first mentioned in the text (not in alphabetic order). Identify references *in text*, tables, and legends by Arabic numerals in superscript with square bracket after the punctuation *marks. References cited only* in tables or figure legends should be numbered in accordance with the sequence established by the first identification in the text of the particular table or figure. Use the style of the examples below, which are based on the formats used by the NLM *in Index Medicus*. The titles of journals *should be abbreviated* according to the style used in Index Medicus. Use complete name of the journal for non-indexed journals. Avoid using abstracts as references. Information from manuscripts submitted but not accepted should be cited in the text as "unpublished observations" with written permission from the source. Avoid citing a "personal communication" unless it provides essential information not available from a public source, in which case the name of the person and date of communication should be cited in parentheses in the text. The commonly cited types of references are shown here, for other types of references such as newspaper items please refer to ICMJE Guidelines (http://www.icmje.org or http://www.nlm.nih.gov/bsd/uniform_requirements.html).

Articles in Journals

1. Standard journal article (for up to six authors): Parija S C, Ravinder PT, Shariff M. Detection of hydatid antigen in the fluid samples from hydatid cysts by co-agglutination. Trans. R.Soc. Trop. Med. Hyg.1996; 90:255–256.
2. Standard journal article (for more than six authors): List the first six contributors followed by *et al*.

Roddy P, Goiri J, Flevaud L, Palma PP, Morote S, Lima N. *et al*., Field Evaluation of a Rapid Immunochromatographic Assay for Detection of Trypanosoma cruzi Infection by Use of Whole Blood. J. Clin. Microbiol. 2008; 46: 2022-2027.

3. Volume with supplement: Otranto D, Capelli G, Genchi C: Changing distribution patterns of canine vector borne diseases in Italy: leishmaniosis vs. dirofilariosis.

Parasites & Vectors 2009; Suppl 1:S2.

Books and Other Monographs

1. Personal author(s): Parija SC. Textbook of Medical Parasitology. 3rd ed. All India Publishers and Distributors. 2008.
2. Editor(s), compiler(s) as author: Garcia LS, Filarial Nematodes In: Garcia LS (editor) Diagnostic Medical Parasitology ASM press Washington DC 2007: pp 319-356.
3. Chapter in a book: Nesheim M C. Ascariasis and human nutrition. In Ascariasis and its prevention and control, D. W. T. Crompton, M. C. Nesbemi, and Z. S. Pawlowski (eds.). Taylor and Francis,London, U.K.1989, pp. 87–100.

Electronic Sources as reference

Journal article on the Internet: Parija SC, Khairnar K. Detection of excretory *Entamoeba histolytica* DNA in the urine, and detection of *E. histolytica* DNA and lectin antigen in the liver abscess pus for the diagnosis of amoebic liver abscess. *BMC Microbiology* 2007, **7**:41. doi:10.1186/1471-2180-7-41. http://www.biomedcentral.com/1471-2180/7/41

Tables

- Tables should be self-explanatory and should not duplicate textual material.
- Tables with more than 10 columns and 25 rows are not acceptable.
- Number tables, in Arabic numerals, consecutively in the order of their first citation in the text and supply a brief title for each.
- Place explanatory matter in footnotes, not in the heading.
- Explain in footnotes all non-standard abbreviations that are used in each table.
- Obtain permission for all fully borrowed, adapted, and modified tables and provide a credit line in the footnote.
- For footnotes use the following symbols, in this sequence: *, †, ‡, §, ||,¶ , **, ††, ‡‡
- Tables with their legends should be provided at the end of the text after the references. The tables along with their number should be cited at the relevant place in the text

Illustrations (Figures)

- Upload the images in JPEG format. The file size should be within 1024 kb in size while uploading.
- Figures should be numbered consecutively according to the order in which they have been first cited in the text.
- Labels, numbers, and symbols should be clear and of uniform size. The lettering for figures should be large enough to be legible after reduction to fit the width of a printed column.
- Symbols, arrows, or letters used in photomicrographs

should contrast with the background and should be marked neatly with transfer type or by tissue overlay and not by pen.

- Titles and detailed explanations belong in the legends for illustrations not on the illustrations themselves.
- When graphs, scatter-grams or histograms are submitted the numerical data on which they are based should also be supplied.
- The photographs and figures should be trimmed to remove all the unwanted areas.
- If photographs of individuals are used, their pictures must be accompanied by written permission to use the photograph.
- If a figure has been published elsewhere, acknowledge the original source and submit written permission from the copyright holder to reproduce the material. A credit line should appear in the legend for such figures.
- Legends for illustrations: Type or print out legends (maximum 40 words, excluding the credit line) for illustrations using double spacing, with Arabic numerals corresponding to the illustrations. When symbols, arrows, numbers, or letters are used to identify parts of the illustrations, identify and explain each one in the legend. Explain the internal scale (magnification) and identify the method of staining in photomicrographs.
- Final figures for print production: Send sharp, glossy, un-mounted, color photographic prints, with height of 4 inches and width of 6 inches at the time of submitting the revised manuscript. Print outs of digital photographs are not acceptable. If digital images are the only source of images, ensure that the image has minimum resolution of 300 dpi or 1800 x 1600 pixels in TIFF format. Send the images on a CD. Each figure should have a label pasted (avoid use of liquid gum for pasting) on its back indicating the number of the figure, the running title, top of the figure and the legends of the figure. Do not write the contributor/s' name/s. Do not write on the back of figures, scratch, or mark them by using paper clips.
- The Journal reserves the right to crop, rotate, reduce, or enlarge the photographs to an acceptable size.

Protection of Patients' Rights to Privacy

Identifying information should not be published in written descriptions, photographs, sonograms, CT scans, etc., and pedigrees unless the information is essential for scientific purposes and the patient (or parent or guardian, wherever applicable) gives informed consent for publication. Authors should remove patients' names from figures unless they have obtained informed consent from the patients. The journal abides by ICMJE guidelines:

1. Authors, not the journals nor the publisher, need to obtain the patient consent form before the publication and have the form properly archived. The consent forms are not to be uploaded with the cover letter or sent through email to editorial or publisher offices.
2. If the manuscript contains patient images that preclude anonymity, or a description that has obvious indication to the identity of the patient, a statement about obtaining informed patient consent should be indicated in the manuscript.

Sending a revised manuscript

The revised version of the manuscript should be submitted online in a manner similar to that used for submission of the manuscript for the first time. However, there is no need to submit the "First Page" or "Covering Letter" file while submitting a revised version. When submitting a revised manuscript, contributors are requested to include, the 'referees' remarks along with point to point clarification at the beginning in the revised file itself. In addition, they are expected to mark the changes as underlined or colored text in the article.

Reprints and proofs

Journal provides no free printed reprints. Authors can purchase reprints, payment for which should be done at the time of submitting the proofs.

Publication schedule

The journal publishes articles on its website immediately on acceptance and follows a 'continuous publication' schedule. Articles are compiled in issues for 'print on demand' quarterly.

Copyrights

The entire contents of the Journal of the Anatomical Society of India are protected under Indian and international copyrights. The Journal, however, grants to all users a free, irrevocable, worldwide, perpetual right of access to, and a license to copy, use, distribute, perform and display the work publicly and to make and distribute derivative works in any digital medium for any reasonable non-commercial purpose, subject to proper attribution of authorship and ownership of the rights. The journal also grants the right to make small numbers of printed copies for their personal non-commercial use under Creative Commons Attribution-Noncommercial-Share Alike 4.0 Unported License.

Checklist

Covering letter

- Signed by all contributors
- Previous publication / presentations mentioned
- Source of funding mentioned
- Conflicts of interest disclosed

Authors

- Last name and given name provided along with Middle name initials (where applicable)
- Author for correspondence, with e-mail address provided
- Number of contributors restricted as per the instructions
- Identity not revealed in paper except title page (e.g. name of the institute in Methods, citing previous study as 'our study', names on figure labels, name of institute in photographs, etc.)

Presentation and format

- Double spacing
- Margins 2.5 cm from all four sides
- Page numbers included at bottom
- Title page contains all the desired information
- Running title provided (not more than 50 characters)
- Abstract page contains the full title of the manuscript
- Abstract provided (structured abstract of 250 words for original articles, unstructured abstracts of about 150 words for all other manuscripts excluding letters to the Editor)
- Key words provided (three or more)
- Introduction of 75-100 words
- Headings in title case (not ALL CAPITALS)
- The references cited in the text should be after punctuation marks, in superscript with square bracket.
- References according to the journal's instructions, punctuation marks checked

- Send the article file without 'Track Changes'

Language and grammar

- Uniformly American English
- Write the full term for each abbreviation at its first use in the title, abstract, keywords and text separately unless it is a standard unit of measure. Numerals from 1 to 10 spelt out
- Numerals at the beginning of the sentence spelt out
- Check the manuscript for spelling, grammar and punctuation errors
- If a brand name is cited, supply the manufacturer's name and address (city and state/country).
- Species names should be in italics

Tables and figures

- No repetition of data in tables and graphs and in text
- Actual numbers from which graphs drawn, provided
- Figures necessary and of good quality (colour)
- Table and figure numbers in Arabic letters (not Roman)
- Labels pasted on back of the photographs (no names written)
- Figure legends provided (not more than 40 words)
- Patients' privacy maintained (if not permission taken)
- Credit note for borrowed figures/tables provided
- Write the full term for each abbreviation used in the table as a footnote

Journal of
The Anatomical Society of India

Salient Features:

- Publishes research articles related to all aspects of Anatomy and Allied medical/surgical sciences.

- Pre-Publication Peer Review and Post-Publication Peer Review

- Online Manuscript Submission System

- Selection of articles on the basis of MRS system

- Eminent academicians across the globe as the Editorial board members

- Electronic Table of Contents alerts

- Available in both online and print form.